

Role of Myc/Mondo transcriptional network in metabolism and lifespan regulation

Inaugural-Dissertation

zur

Erlangung des Doktorgrades

der Mathematisch-Naturwissenschaftlichen Fakultät

der Universität zu Köln

vorgelegt von

Raymond Alexis Laboy Morales

aus Arecibo, Puerto Rico

Köln, April 2022



Berichterstatter:
(Gutachter)

Prof. Dr. Adam Antebi

Prof. Dr. Filipe Cabreiro

Tag der mündlichen Prüfung: April 28th, 2022

Table of contents

I.	Abbreviations	1
II.	Abstract	4
III.	Introduction	5
	3.1 Aging: A global public health pandemic	5
	3.2 A lesson from model organisms to human aging	6
	3.2.1 <i>C. elegans</i> as a model organism in aging research	6
	3.3 Evolutionary conservation of longevity pathways	7
	3.3.1 Insulin pathway	8
	3.3.2 Dietary restriction and nutrient-sensors: mTORC and AMPK signaling	10
	3.3.3 Mitochondrial longevity	15
	3.3.4 Gonadal longevity	18
	3.3.5 Other pathways and drugs to target aging and age-related diseases	21
	3.3.6 Convergent mechanisms of aging	22
	3.4 Cellular nutrient-sensing pathways and metabolic flexibility	24
	3.4.1 Amino acids	24
	3.4.2 Lipids	25
	3.4.3 Carbohydrates	27
	3.4.4 Metabolic flexibility and organellar communication	28
	3.5 Myc/MondoA family of transcription factors are metabolic sensors	31
	3.5.1 Evolutionary conservation of the transcriptional network	31
	3.5.2 Regulation of MondoA/ChREBP	34
	3.5.3 Mondo proteins as nutrient sensors	36
	3.5.4 MondoA/ChREBP downstream targets	36
	3.5.5 Metabolic disorders associated with MondoA/ChREBP	39
	3.5.6 MML-1/MXL-2 as convergent mechanisms of aging	40
IV.	Research aims	42
V.	Results	43
	Chapter I. Regulation of MML-1 by glucose metabolism	43
	5.1 Glucose metabolism genes regulate MML-1	43
	5.2 The induction of cellular stress pathways does not regulate MML-1 nuclear localization	45
	5.3 Hexokinases as upstream regulators of MML-1 localization and function	46

5.4	Hexokinases are required for germline-removal and reduced mitochondrial function longevity pathways	49
5.5	Hexokinase knockdown increases MML-1 mitochondrial localization	53
5.6	<i>C. elegans</i> hexokinases are differentially expressed	55
5.7	<i>hxx-2</i> regulates MML-1 function through increased PPP	58
5.8	Decreased OGDC function rescues MML-1 nuclear localization in <i>hxx-2i</i>	60
5.9	MML-1 interactome uncovers potential regulators of its function and localization	62
5.10	The mitochondrial pyruvate carrier regulates MML-1	64
5.11	MML-1 colocalizes with peridroplet mitochondria	65
5.12	MML-1 is regulated by the mitochondrial acyl-CoA synthase	68
5.13	Inhibition of mitochondrial β -oxidation rescues MML-1 nuclear localization under <i>hxx-1i</i>	70
5.14	AMPK regulates MML-1 nuclear localization	72
Chapter II.	MML-1/MXL-2 regulation in longevity	75
5.15	MML-1 interactome in the insulin longevity	75
5.16	Insulin signaling and germline MML-1/MXL-2-dependent transcriptomes	76
5.17	Insulin signaling and germline MML-1/MXL-2-dependent metabolomes	81
VI.	Discussion	85
6.1	MML-1 senses multiple steps of glucose metabolism	86
6.2	Hexokinases regulate MML-1 through distinct downstream mechanisms	91
6.3	MML-1 interactome suggests multifaceted communication between organelles and transcription	94
6.4	MML-1 and MXL-2 regulate downstream processes independently	97
6.5	MML-1/MXL-2 transcriptional network rewiring in distinct longevity signals	98
6.6	Scientific advancement and limitations of the study	99
VII.	Future perspectives	101
VIII.	Material and methods	110
8.1	<i>C. elegans</i> husbandry	110
8.1.1	Worm growth and maintenance	110
8.1.2	Genotyping	110
8.1.3	RNAi treatment	111
8.2	<i>C. elegans</i> characterization	111

8.2.1	Demographic analysis	111
8.2.2	Oxygen consumption rate measurements	111
8.2.3	Genome editing	112
8.2.4	Motility assay	112
8.2.5	Body measurements and pharyngeal pumping rates	112
8.3	Molecular biology	113
8.3.1	Molecular cloning	113
8.3.2	RNA extraction	113
8.3.3	RT-qPCR	114
8.3.4	RNA sequencing	114
8.4	Biochemistry	115
8.4.1	Protein extraction and Western blot analysis	115
8.4.2	Immunoprecipitation	116
8.4.3	Proteomics	117
8.4.3.1	LC-MS/MS analysis	117
8.4.3.2	Protein identification and quantification	117
8.4.4	Metabolomics	118
8.4.4.1	Sample preparation	118
8.4.4.2	Untargeted metabolomics and analysis	118
8.4.5	Glucose 6-phosphate and NADP ⁺ /NADPH measurements	119
8.5	Microscopy	120
8.5.1	Staining and preparation of slides	120
8.5.2	Brightfield and fluorescent imaging	120
8.5.3	Confocal Imaging	121
8.6	Statistical analysis	121
8.7	Software	122
IX.	Supplementary tables	123
Supplementary Table 1	Worm strains	123
Supplementary Table 2	Oligonucleotides	125
Supplementary Table 3	Media, buffers, solutions	127
Supplementary Table 4	MML-1 and glucose metabolism RNAi screen	129

Supplementary Table 5	Demographic analysis	131
Supplementary Table 6	MML-1 IP in wildtype and <i>glp-1(e2141)</i>	134
Supplementary Table 7	MML-1 and IP candidates RNAi screen	135
Supplementary Table 8	MML-1 IP in <i>daf-2(e1370)</i>	137
Supplementary Table 9	MML-1/MXL-2-dependent metabolomics in <i>daf-2(e1370)</i>	138
Supplementary Table 10	MML-1/MXL-2-dependent metabolomics in <i>glp-1(e2141)</i>	140
X.	Acknowledgments	144
XI.	Work contributions	145
XII.	References	146
XIII.	Erklärung	199
XIV.	Curriculum vitae	200

I. Abbreviations

2-DG	2-deoxy-glucose
3-BrP	3-bromopyruvate
5MTHF	5-methyltetrahydrofolate
6-AN	6-aminonicotinamide
AA	Antimycin A
ACC	Acetyl-CoA carboxylase
ACN	Acetonitrile
ACSL	Acyl-CoA synthetase
ADP	Adenosine diphosphate
AICAR	5-aminoimidazole-4-carboxamide-1-D-ribo-furanoside
AMP	Adenosine monophosphate
AMPK	AMP-activated protein kinase
ATP	Adenosine triphosphate
bHLH	Basic helix-loop-helix
BSA	Bovine serum albumin
ChoRE	Carbohydrate response element
ChREBP	Carbohydrate-response element-binding protein
CoA	Coenzyme A
CPT	Carnitine palmitoyl transferase
DCD	Dimerization and cytoplasmic localization domain
DEG	Differentially expressed gene
DNA	Deoxyribonucleic acid
DR	Dietary restriction
DTT	Dithiothreitol
E-box	Enhancer box
ER	Endoplasmic reticulum
ETC	Electro transport chain
FA	Formic acid
FAD	Flavin adenine dinucleotide
FAS	Fatty acid synthase
FC	Fold change
FIRKO	Fat-specific insulin receptor knockout
G6P	Glucose 6-phosphate
G6PDH	Glucose 6-phosphate dehydrogenase
GFP	Green fluorescent protein
GLUT	Glucose transporter
GO	Gene ontology

GPDH	Glycerol 3-phosphate dehydrogenase
GRACE	Glucose-response activation conserved element
HAT	Histone acetyltransferase
HDAC	Histone deacetylase
HSL	Hormone sensitive lipase
IP	Immunoprecipitation
IPTG	Isopropyl β -D-1-thiogalactopyranoside
KEGG	Kyoto Encyclopedia of Genes and Genomes
LD	Lipid droplet
LDH	Lactate dehydrogenase
LID	Low-glucose inhibitory domain
MCR	Mondo conserved region
MFRTA	Mitochondria free radical theory of aging
mRNA	Messenger RNA
MS	Mass spectrometry
mTORC	Mechanistic target of rapamycin complex
MUFA	Monounsaturated fatty acid
NAD ⁺ /NADH	Nicotinamide adenine dinucleotide
NADP ⁺ /NADPH	Nicotinamide adenine dinucleotide phosphate
NAFLD	Non-alcoholic fatty liver disease
NASH	Non-alcoholic steatohepatitis
NES	Nuclear export signal
NGM	Nematode growth medium
NLS	Nuclear localization signal
ns	Not significant
OCR	Oxygen consumption rate
OEA	Oleoylethanolamide
OGDC	Oxoglutarate dehydrogenase complex
OGT	O-GlcNAc transferase
OP50	<i>E. coli</i> OP50 strain
PCA	Principle component analysis
PCR	Polymerase chain reaction
PGDH	Phosphogluconate dehydrogenase
PI3K	Phosphatidylinositol 3-kinase
PIP ₂	Phosphatidylinositol 4,5-biphosphate
PIP ₃	Phosphatidylinositol 3,4,5-triphosphate
PK	Pyruvate kinase
PKA	Proteinase kinase A
PPAR	Peroxisome proliferator-activated receptor
PPP	Pentose phosphate pathway

PUFA	Polyunsaturated fatty acid
qPCR	Quantitative PCR
RNA	Ribonucleic acid
RNAi	RNA interference
ROS	Reactive oxygen species
RT	Room temperature
SCS	Succinyl-CoA synthetase
SD	Standard deviation
SDH	Succinate dehydrogenase
SDS	Sodium dodecyl sulfate
SEM	Standard error of the mean
SOD	Superoxide dismutase
TAG	Triacylglycerol
TCA	Tricarboxylic acid
TF	Transcription factor
TOR	Target of rapamycin
tRNA	Transfer RNA
TXNIP	Thioredoxin-interacting protein
UPR	Unfolded protein response

II. Abstract

The transcriptional complex MondoA/Max-like, MML-1/MXL-2, acts as a convergent transcriptional regulatory output of multiple longevity pathways in *C. elegans*. How do these pathways converge on this complex, and what are the upstream signals involved? This work sought to understand the upstream signals that regulate MML-1 localization, transcription, and longevity, using combined genetic, biochemical, omics, and light microscopy approaches. We found that an overall reduction in glucose metabolism decreases MML-1 localization in the nucleus and identified two hexokinase isozymes, *hxx-1* and *hxx-2*, as strong positive regulators of MML-1 function. Upon knockdown, hexokinases reduce MML-1 nuclear localization and cause its redistribution to mitochondria and lipid droplets (LD). Interestingly, although both hexokinases decrease MML-1 nuclear function, we provide evidence that they do so through distinct mechanisms. On the one hand, we found that under *hxx-1* knockdown, there is an increase in fatty acid metabolism, and pharmacological and genetic inhibition of mitochondrial β -oxidation could rescue MML-1 localization. On the other hand, we found that oxoglutarate dehydrogenase complex (OGDC) and the pentose phosphate pathway (PPP) are important for decreasing MML-1 localization and function under *hxx-2* knockdown.

Analysis of the MML-1 interactome in different longevity backgrounds revealed that MML-1 associates with varying proteins from distinct cellular compartments, suggesting a role for MML-1 in integrating diverse organellar signals to the transcriptional response. In particular, we found many mitochondrial proteins, including the mitochondrial pyruvate carrier MPC-1 and the long-chain fatty acid acyl-CoA synthetase ACS-13, which is associated with both mitochondria and lipid droplets. Both candidates showed a degree of cellular co-localization and functional interaction with MML-1, suggesting that these proteins could cooperate with MML-1 in connecting metabolism and transcription.

III. Introduction

3.1 *Aging: A global public health pandemic*

People around the globe are living longer. This trend in the increase of lifespan expectancy started in the 1900s in developed countries and has been followed by low- and middle-income countries over the last decades' (Oeppen & Vaupel, 2002). Some projections estimate that by 2030, all countries will show an increase in the aging population above the age of 65 due to enhanced longevity (Kontis et al., 2017). Improvements in public health have played a significant role in the added years to our lifespan, including the development of antibiotics and vaccines and the increase in sanitary conditions (Burger et al., 2012; Christensen et al., 2009; Rappuoli et al., 2014). However, aging is the major risk factor for predominant killer diseases. These extra years of life often come with a subset of age-associated pathologies, including cardiovascular, neurodegenerative, and musculoskeletal conditions, gastrointestinal disorders, loss of special senses, and decline of the endocrine system. Thus, living longer brings challenges worldwide, including the burden on health services, difficulties with end-of-life care for older people, pressure on caretakers, and economic pressures.

Aging is the progressive decline in functional integrity and homeostasis, culminating in death. In nature, aging is variable and works on different time scales. For example, blue whales can live up to 200 years, while mice live around two years. Other organisms even show negligible senescence, like the cnidarian polyp *Hydra* (Martínez, 1998; Tomczyk et al., 2015). This remarkable variation suggests that aging could have a genetic basis. This idea catalyzed the way researchers study longevity, leading to the breakthrough that aging is malleable, and we can change the rate at which organisms age. Insights into the molecular mechanisms underlying the aging process have emerged from the study of model organisms, which have illuminated environmental, pharmacological, and genetic interventions that affect lifespan on a shorter time scale. Importantly, many of these pathways are conserved throughout the evolutionary spectrum. Even in humans, around 25% of the lifespan is heritable (van den Berg et al., 2019).

The progress made so far offers new possibilities for translating this knowledge into therapeutics to ameliorate age-related diseases and increase the quality of life in old age. Traditionally, medicine has focused on treating each disease individually. Although this has clear benefits, tackling the underlying commonality, age, presents an excellent opportunity to prevent multiple conditions simultaneously, aiming to reduce the morbid period in our last years.

3.2 A lesson from model organisms to human aging

Aging has marked underlying regularities conserved in different organisms (López-Otín et al., 2013). This evolutionary conservation facilitates the studying of the aging process in terms of both time and ethical reasons in model organisms, including the budding yeast *Saccharomyces cerevisiae*, the nematode *Caenorhabditis elegans*, the fruit fly *Drosophila melanogaster*, and vertebrates like the turquoise killifish *Nothobranchius furzeri*, the naked mole-rat *Heterocephalus glaber*, the mice *Mus musculus*, and the rhesus monkey *Macaca mulatta*. All these organisms age at different rates, giving us insights into understanding the causal mechanisms that regulate lifespan.

Model organisms have been pivotal in understanding the molecular pathways of different lifespan-extending paradigms. Especially, the discovery of how nutrient-sensing pathways activate defense mechanisms, rewire metabolism, and extend lifespan facilitated the identification of drugs to target those pathways. Genetic variations in key factors of these signaling pathways have been correlated with long-lived human populations (Taormina et al., 2019; Valenzano et al., 2017), opening the door for the translation of aging research to improve our quality of life.

3.2.1 *C. elegans* as a model organism in aging research

C. elegans is a free-living nematode established as a model organism in the 1970s (Brenner, 1974) and was the first multicellular eukaryote to have its genome sequenced (Consortium, 1998). The adult animal is around 1 mm, and between 83% of its genes have apparent human orthologs (Lai et al., 2000). Its lifespan averages between 3 to 4 weeks and shows signs of aging, including decreased locomotion, immunity, stress resistance, and reproduction. The short life cycle (**Figure 1**), around three days at 20 °C, and lifespan, about 24 days, facilitates the ability to observe and modulate aging in real-time in the laboratory. Researchers have developed genetic and genomic tools for *C. elegans* to study how physiology affects quantifiable phenotypes.

Seminal work from Michael Klass in the '70-the '80s led to the discovery of single-gene mutants in the nematode with increased lifespan (Klass, 1983). Later, Friedman and Johnson followed up this work that led to the discovery of *age-1* mutant worms that lived up to 80% more than wildtype animals (B. Friedman & E. Johnson, 1988). Interestingly, the nematode can enter an alternate metabolic stage in the life cycle named dauer that serves as a long-lived hibernation mode for overwintering, and animals can live up to 6 months (Albert & Riddle, 1988). Work by Kenyon

and colleagues showed that mutation in one of the dauer formation genes, *daf-2*, doubled the lifespan and this longevity dependent on another gene named *daf-16* (C. Kenyon et al., 1993). These works established the idea that genes acting in regulatory cascades could modulate longevity and cemented *C. elegans* as a powerful genetic model to identify novel mechanisms that underlie the connection between metabolism and aging.

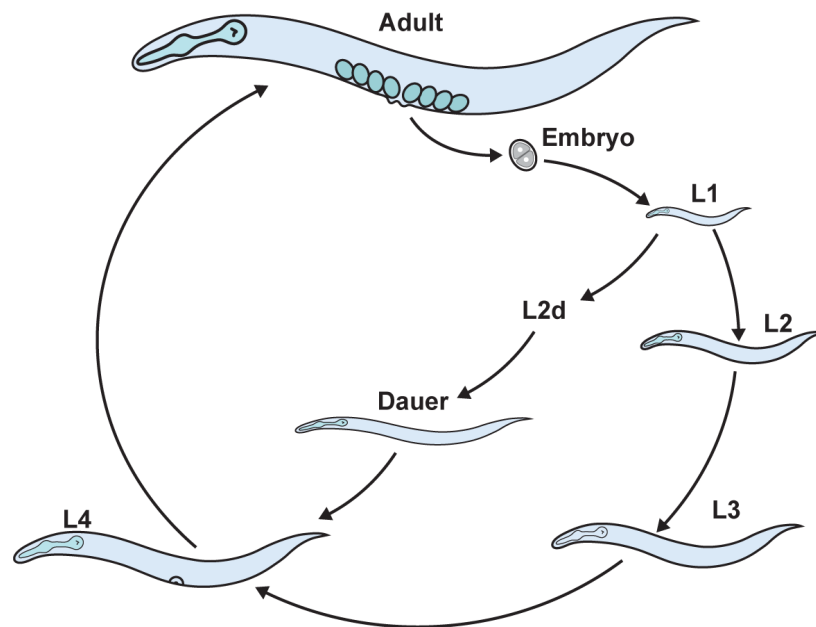


Figure 1. *C. elegans* life cycle. The nematode’s life cycle is composed of 4 larval stages named L1-4. Under different conditions like crowding, starvation, and high temperature, worms can enter an alternate state called dauer which acts as a hibernation-like state. When animals encounter favorable conditions, they can continue developing until adulthood and reproduce—adapted from WormAtlas (L.A. Herndon et al., 2018).

3.3 Evolutionary conservation of longevity pathways

The molecular identity of the first mutations observed to extend lifespan was later reported to be factors involved in the insulin/IGF signaling (Kimura et al., 1997; Ogg & Ruvkun, 1998). This helped to understand how one single gene could affect longevity through endocrine signaling inducing metabolic and developmental changes. These mechanisms were later shown to be conserved throughout the evolutionary spectrum, including in humans, reinforcing the idea that comparative biology is compelling in gerontology (Taormina et al., 2019; Tissenbaum & Guarente, 2002; Valenzano et al., 2017). Since then, several other metabolic pathways have been directly linked to healthspan and longevity in various model systems, including reduced mTOR signaling,

removal of the germline stem cells, dietary interventions, and reduced mitochondrial activity. Interestingly, natural genetic variations in the nutrient-sensing networks discovered in model organisms have been linked to longevity in human populations (Flachsbart et al., 2009; Passtoors et al., 2013).

3.3.1 *Insulin pathway*

Insulin/IGF1 signaling is a nutrient-sensing pathway regulating longevity and healthspan in multiple organisms (C. J. Kenyon, 2010). This pathway matches the metabolism, growth, and reproduction to the nutrient status of the organism. Blunted insulin/IGF signaling extends lifespan, as first discovered in worms (T. E. Johnson, 1990; C. Kenyon et al., 1993), and is conserved in flies (Clancy et al., 2001), and mice (Selman et al., 2008). Interestingly, fat-specific insulin-receptor knockout (FIRKO) mice showed clear improvement in healthspan with preservation of glucose homeostasis and increased lifespan (Blüher et al., 2002, 2003). In humans, natural genetic variants in genes encoding for proteins involved in the insulin/IGF signaling pathway have been associated with longevity in Japanese men (Willcox et al., 2008), Ashkenazi Jewish (Pawlikowska et al., 2009), German (Flachsbart et al., 2009), and Dutch (Spoel et al., 2015) centenarians.

The canonical insulin/IGF signaling in *C. elegans* starts with binding one of the 40 insulin-like peptides to the insulin receptor DAF-2 (Zheng et al., 2019) (**Figure 2**). Upon insulin-like peptide binding, DAF-2 undergoes an autophosphorylation process required for the recruitment of AGE-1. This protein is a homolog of the p110 catalytic subunit of the phosphatidylinositol 3-kinase (PI3K) that catalyzes the conversion of phosphatidylinositol 4,5-biphosphate (PIP₂) into phosphatidylinositol 3,4,5-triphosphate (PIP₃). AGE-1 recruitment to the plasma membrane is assisted by accessory scaffold proteins IST-1 and AAP-1, although they are not required for AGE-1 activity under standard conditions (Wolkow et al., 2002). The lipid phosphatase DAF-18, homolog to the phosphatase and tensin homolog deleted on chromosome 10 (PTEN), counteracts AGE-1 activity by dephosphorylating PIP₃ (Ogg & Ruvkun, 1998). Increased levels of PIP₃ activate PDK-1, a homolog of the 3-phosphoinositide-dependent kinase-1 (PDK), whose downstream targets include AKT-1/2 and SGK-1. These kinases converge in phosphorylating the forkhead-family transcription factor DAF-16 and sequestering it in the cytoplasm through the association with 14-3-3 proteins PAR-5 and FTT-2 (Berdichevsky et al., 2006). Under nutrient depletion or reduced insulin signaling, DAF-16 functions as a pro-longevity factor and translocates

to the nucleus to activate the transcription of genes involved in metabolism and stress resistance (C. J. Kenyon, 2010; Murphy et al., 2003).

Multiple parallel pathways to insulin signaling also converge on DAF-16 to regulate its function. For example, the c-Jun N-terminal kinase JNK-1 phosphorylates DAF-16 and promotes its translocation to the nucleus upon heat stress (Oh et al., 2005). Oxidative stress also regulates DAF-16 through direct phosphorylation by the Ste20-like protein kinase 1 homolog CST-1 (Lehtinen et al., 2006). Upon nutrient deprivation, the AMP-activated kinase (AMPK) phosphorylates DAF-16 at multiple residues (Greer et al., 2007), and DAF-16 regulates the transcription of various subunits of AMPK like *aak-2*, *aakb-1*, *aakg-4*, and *aakg-5*, hence, functioning as a positive feedback loop (Schuster et al., 2010; Tullet et al., 2014). DAF-16 also integrates signals from the reproductive system through the ankyrin-repeat protein KRI-1 and the lipophilic hormone signaling through DAF-9/DAF-12 (Berman & Kenyon, 2006).

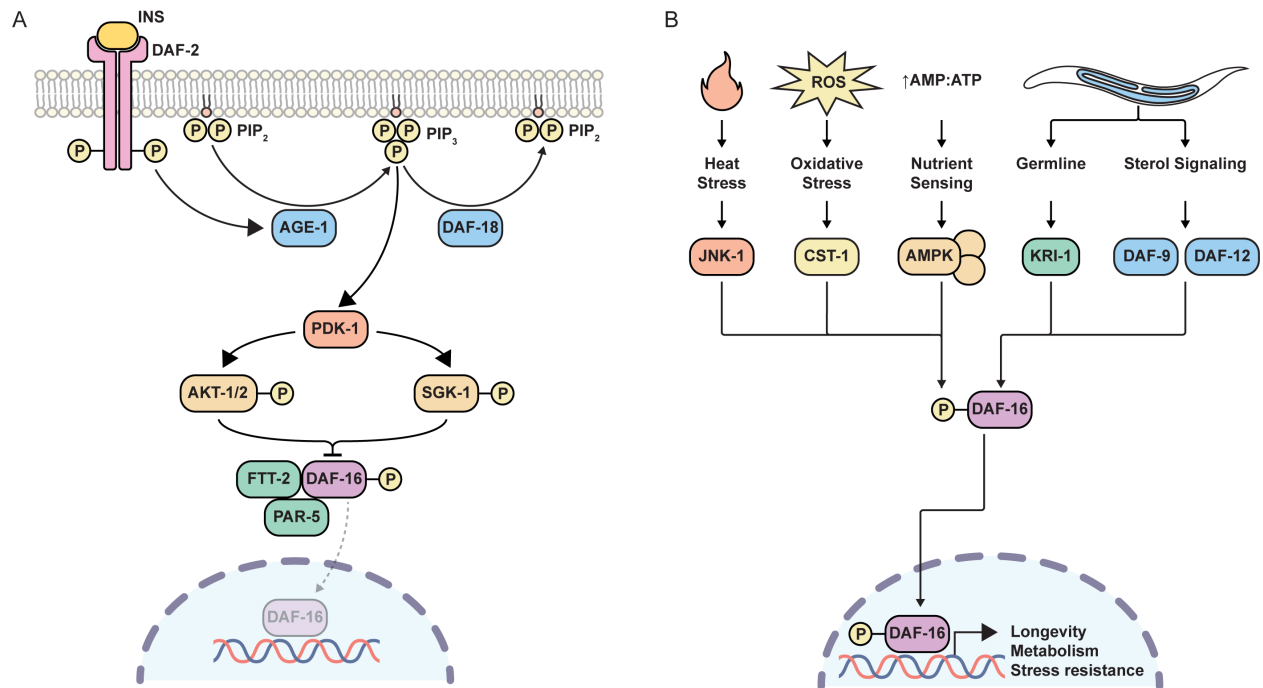


Figure 2. DAF-16 regulation by the canonical insulin/IGF signaling and parallel pathways in *C. elegans*. **A.** Binding insulin-like peptides to the DAF-2 receptor recruits AGE-1, converting PIP₂ to PIP₃. Increased levels of PIP₃ activate downstream kinases, including PDK-1, AKT-1/2, and SGK-1. One of the major outcomes of insulin signaling is the phosphorylation of DAF-16, resulting in the interaction with FTT-2 and PAR-5 and inhibiting its nuclear localization. **B.** DAF-16 is regulated by heat and oxidative stress through the kinases JNK-1 and CST-1. Under nutrient deprivation, an increased AMP/ATP ratio activates AMPK, which directly phosphorylates

DAF-16. Signals from the germline and the sterol signaling converge on DAF-16 to positively regulate its translocation to the nucleus. DAF-16 regulates many downstream genes, including genes associated with longevity, metabolism, and stress resistance. INS, insulin-like peptide; PIP₂, phosphatidylinositol 4,5-bisphosphate; PIP₃, phosphatidylinositol 3,4,5-triphosphate.

Insulin signaling has several implications for the regulation of metabolism. Decreasing insulin signaling in multiple steps has been shown to induce a dauer-constitutive (Daf-c) phenotype in *C. elegans* (Riddle et al., 1981). Mutations in the DAF-2 receptor have been shown to increase the fat content through *de novo* lipogenesis in a DAF-16-dependent manner (O'Rourke et al., 2009; C. L. Perez & Van Gilst, 2008). Indeed, DAF-16 regulates a subset of genes involved in fat metabolism, including fatty acid desaturases, acyl-CoA dehydrogenase, glyoxylate cycle regulators, and autophagy (Lapierre et al., 2011, 2012; Meléndez et al., 2003). Interestingly, increased *de novo* lipogenesis is uncoupled from the longevity conferred by reduced insulin signaling (C. L. Perez & Van Gilst, 2008), thus suggesting that DAF-16 may regulate physiology at different steps independently of its pro-longevity function. It has been shown that DAF-16 also acts in a cell-nonautonomous way to regulate longevity. Neuronal and intestinal rescue of *daf-16* in the *daf-2 daf-16* double mutant increases lifespan (Apfeld & Kenyon, 1998; Libina et al., 2003; Murphy et al., 2003). In *D. melanogaster*, dFOXO expression in the head fat body acts in a systemic way to repress the insulin signaling in the peripheral fat body (Giannakou et al., 2004; Hwangbo et al., 2004), indicating a role of the insulin pathway in the endocrine regulation of longevity.

3.3.2 Dietary restriction and nutrient-sensors: mTORC and AMPK signaling

Dietary restriction (DR) is defined as a reduction of nutrient intake without malnutrition. DR remodels the metabolism to a low-energy state and extends lifespan in the evolutionary spectrum, from yeast and other non-model organisms to primates (Green et al., 2021). The first reports of modulation of lifespan were performed in *Drosophila*, where researchers studied conditions that made insects live longer (Loeb & Northrop, 1916, 1917; Pearl & Parker, 1921). Later in the 1920s, it was reported that flies under alternate fasting had enhanced longevity (Alpatov, 1930; Kopec, 1928). In the 1930s, researchers found that rats with reduced food intake lived beyond those not restricted (McCay et al., 1935). DR has been shown to extend lifespan in rhesus monkeys, and more importantly, it delays the onset of age-related decline and overall

function (Colman et al., 2009; Mattison et al., 2012). Some of the health improvements in primates under DR are sustained physical activity, increased microvascular density in the heart and brain, maintained skeletal muscle mass and immune function, decreased accumulation of iron in the brain, decreased risk of diabetes, cancer, cardiovascular diseases, and brain atrophy. The molecular basis of the benefits of DR lies in the regulation of nutrient sensing and activation of stress response pathways that result in better metabolic efficiency and, ultimately, health and longevity.

Even though DR presents a robust effect on aging and overall health, some detrimental effects of prolonged DR need to be considered when translating these observations into humans. There are physiological defects in growth, reproductive capacity, immunity, thermoregulation, wound repair, bone mass, and physical appearance associated with prolonged DR (Colman et al., 2012; Soare et al., 2011; Jiayi Sun et al., 2020; Tang et al., 2016). There are also sex differences in DR-mediated longevity. In mice, for example, females respond much more to DR than males, while in rats the opposite is true (Swindell, 2012; Tower, 2017). In *D. melanogaster*, DR has a more robust effect on females' lifespan due to an age-dependent deterioration of the gut that males do not undergo (Regan et al., 2016). Hence, understanding the molecular mechanisms underlying how nutrients regulate longevity will help us parse the benefits from undesirable side effects of these interventions.

There are many regimens to induce DR in *C. elegans* that have been shown to extend lifespan. On the one hand, diluting the bacteria either in liquid culture or solid media (Houthoofd et al., 2003; Klass, 1977), dilution of peptone (Hosono et al., 1989), and food deprivation by complete removal of the bacteria (Kaeberlein et al., 2006) increases the nematode's lifespan. On the other hand, genetic mutations that reduce pharyngeal pumping rate decrease food intake (e.g., *eat-2* mutants) have been shown to significantly lengthen lifespan by up to 50% (Avery, 1993; Lakowski & Hekimi, 1998). Interestingly, all these methods share common genetic mechanisms but also extend lifespan through somewhat independent pathways (Greer & Brunet, 2009).

Some DR-mediated regimens are thought to act through mechanisms independent of the insulin signaling pathway because they do not require DAF-16, and there is an additive effect to the *daf-2*-mediated longevity (Houthoofd et al., 2003; Kaeberlein et al., 2006; Lakowski & Hekimi, 1998). Other transcription factors have been implicated in the mechanism for extending longevity by DR. For example, *eat-2* mutants have been shown to require the FoxA transcription factor PHA-4 for the lifespan extension (Panowski et al., 2007). DR was shown to mediate

longevity by activating the Nrf2 transcription factor SKN-1 in ASI neurons, promoting cell non-autonomous signaling in peripheral tissues (Bishop & Guarente, 2007). The heat-shock transcription factor HSF-1 was also shown to induce longevity under bacterial food deprivation (Steinkraus et al., 2008), although *hsf-1* is dispensable for *eat-2*-mediated lifespan extension (Hsu et al., 2003). On the other hand, DR regimens involving limiting food levels on Petri plates do seem to require DAF-16 (Greer et al., 2007). Thus, DR mediates longevity by activating different nutrient-sensing mechanisms that do not work on a linear pathway but rather through a complex network.

Interestingly, multiple cellular nutrient sensors modulate this metabolic and transcriptional rewiring that transduces the signal upon nutrient availability. Among them, the mechanistic target of rapamycin complex (mTORC) functions as a nutrient sensor and integrates amino acid levels and growth factors to modulate metabolism. The mTORC was discovered as a target of the macrolide rapamycin produced by the bacterium *Streptomyces hygroscopicus* (Vézina et al., 1975). When active, the mTORC triggers downstream targets involved in anabolic pathways, including increased protein translation, repression of autophagy, lipogenesis, and nucleotide biogenesis (Laplante & Sabatini, 2012). Furthermore, mTORC mediates many DR effects on health and longevity (Kapahi et al., 2010). Downregulation of mTOR signaling pathways extends lifespan in *C. elegans* and *Drosophila* (S. C. Johnson et al., 2013; Lamming et al., 2013). It also extends the lifespan in mice, with a more robust effect in females (Miller et al., 2014; J. J. Wu et al., 2013), and presents an overall improvement in health during aging, including models of neurodegenerative diseases like Huntington's, Parkinson, and Alzheimer (S. C. Johnson et al., 2013; John H. Lee et al., 2015; Masini et al., 2018; Spilman et al., 2010).

TOR/LET-363 is a serine/threonine kinase and member of the PI3K-related kinase family that functions as the core catalytic subunit of two distinct multiprotein complexes, mTORC1 and mTORC2. These two complexes are formed by specific subunits and phosphorylate different downstream substrates (G. Y. Liu & Sabatini, 2020). The rapamycin-sensitive mTORC1 is regulated by different intracellular and extracellular stimuli, including the availability of amino acids, carbohydrates, oxygen, cholesterol, and the insulin/IGF pathway, whereas the rapamycin-insensitive mTORC2 controls cell proliferation through regulation of the PI3K signaling (G. Y. Liu & Sabatini, 2020). The mTORC1 and mTORC2 are defined by their interacting partners

named DAF-15/Raptor and RICT-1/Rictor, respectively (Jacinto et al., 2004; D. H. Kim et al., 2002; Sarbassov et al., 2004). Inhibition of both complexes extends the lifespan of the nematode. The mTORC1 requires the transcription factors DAF-16, SKN-1, and HSF-1, whereas the mTORC2-mediated longevity requires SKN-1 but not DAF-16 (Robida-Stubbs et al., 2012; Seo et al., 2013).

The mTORC1 controls many aspects of cellular physiology, including translation through regulation of S6 ribosomal protein kinase S6K/RSKS-1, the eukaryotic initiation factor 4E binding protein 4E-BP, and the translation initiation factor eIF4E/IFE-2 (Holz et al., 2005; Tee & Blenis, 2005). Inactivation of *rsks-1* and *ife-2* prolongs lifespan in a PHA-4-dependent and -independent manner, respectively (Sheaffer et al., 2008). mTORC1 is also involved in the regulation of *de novo* lipogenesis and carbohydrate metabolism (e.g., glycolysis and oxidative reactions of the pentose phosphate pathway (PPP)), through S6K, and the transcription factors hypoxia-inducible factor HIF1 α and the sterol regulatory element-binding protein SREBP1/2 (Düvel et al., 2010).

Autophagy is a process conserved throughout evolution where cytosolic and organellar components are engulfed in specialized double-membrane vesicles termed autophagosomes and carried to the lysosome for degradation and turnover. mTORC1 negatively regulates autophagy by directly phosphorylating the core components of the autophagosome formation ATG13 and ULK1 (Ganley et al., 2009; Hosokawa et al., 2009; Jung et al., 2009). The nuclear localization of the transcription factor TFEB/HLH-30, a master regulator of autophagy, is negatively regulated by mTORC1 (Martina et al., 2012; Rocznik-Ferguson et al., 2012; Settembre et al., 2012). In *C. elegans*, mTOR also regulates autophagy through PHA-4, and both autophagy genes and *pha-4* are required for the lifespan extension mediated by decreased mTOR signaling (Hansen et al., 2008; Sheaffer et al., 2008; Tóth et al., 2008). Rapamycin-induced longevity in fruit flies also requires several downstream targets of mTORC1, including protein translation, mediated by S6K and 4E-BP, and autophagy (Bjedov et al., 2010).

The AMPK is a serine/threonine kinase that has a significant role as a metabolic sensor phosphorylating proteins involved in carbohydrate and fat metabolism. AMPK is a heterotrimeric complex composed of subunits α , β , and γ that is activated by an increase in the AMP/ADP:ATP ratio under nutrient deprivation, energy depletion, or stress conditions. This complex mediates the lifespan extension induced by the DR regime through an AMPK-FOXO axis (Burkewitz et al.,

2014; Greer et al., 2007). DR induced by inhibition of glucose metabolism increases lifespan in an *aak-2*-dependent manner (Schulz et al., 2007). AMPK has been shown to extend lifespan by overexpression of the catalytic subunit *aak-2* in *C. elegans* (Apfeld et al., 2004) and AMPK- α in *Drosophila* (Stenesen et al., 2013), modified AMPK- γ subunit (Greer et al., 2007), and expressing a truncated gain-of-function form of *aak-2* containing only the catalytic domain (Mair et al., 2011). In vertebrates, the connection between AMPK and health is conflicting, and both positive and negative implications have been associated with the activation of AMPK (Smith et al., 2020; Woods et al., 2017; X. Yang et al., 2016; Yavari et al., 2016).

AMPK can directly bind adenosine nucleotides to regulate its activity. The γ subunit has the sensing domain for AMP, ADP, or ATP. The binding of AMP activates AMPK through an allosteric regulation that induces phosphorylation by the liver kinase B LKB-1 at residue Thr172 (Gowans et al., 2013; Hawley et al., 2003). This phosphorylation lies in the activation loop of the α subunit kinase domain (Hawley et al., 1996). Other kinases, like the calcium/calmodulin-dependent kinase kinase b CaMKKb (Woods et al., 2005) and the transforming growth factor- β -activated kinase Tak1 (Momcilovic et al., 2006) have been shown to phosphorylate AMPK. However, LKB1 is the most important in the context of nutrient-sensing (Tsou et al., 2011). AMP and ADP binding also inhibit dephosphorylation in Thr172 residue, thus blocking the negative regulation of AMPK by phosphatases (Oakhill et al., 2011; Xiao et al., 2011).

The mTORC1 and the AMPK play antagonistic roles in regulating each other and converge in downstream mechanisms (**Figure 3**). For example, ULK1 is a substrate of both kinase complexes to control autophagy (J. Kim et al., 2011). The tumor suppressor LKB1 phosphorylates and activates the tuberous sclerosis complex TSC2, an important negative regulator of the mTORC1 pathway (Corradetti et al., 2019). AMPK also directly phosphorylates to inhibit and activate mTORC1 and TSC2, respectively, and thus inhibit protein translation (Gwinn et al., 2008; Inoki et al., 2003). On the other hand, S6K phosphorylates AMPK and inhibits its function (Dagon et al., 2012). The complex communication of these two opposing factors is required to regulate cell growth and metabolism and maintain cellular homeostasis.

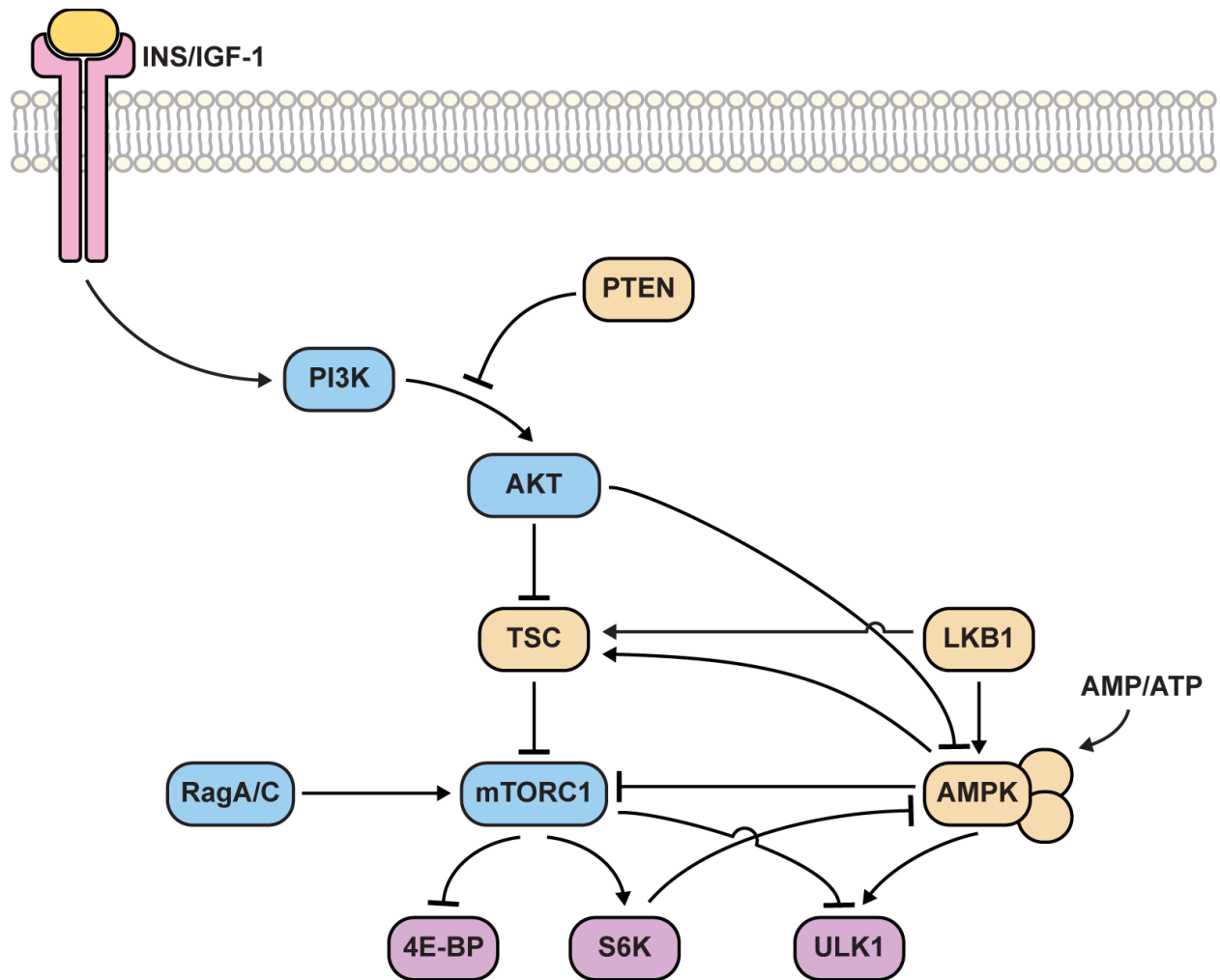


Figure 3. mTORC1 and AMPK function as energy sensors to regulate metabolic flexibility. mTORC1 and AMPK have antagonistic roles. mTORC1 senses nutrient availability, such as high amino acid concentration and growth factors, and activates anabolic pathways. On the other hand, AMPK is activated by low energy status and functions as a pro-longevity factor by activating catabolic pathways and stress response mechanisms. DR has opposite effects on nutrient-sensing complexes, activating AMPK and repressing mTORC1—adapted from (Smith et al., 2020).

3.3.3 Mitochondrial longevity

Mitochondria are organelles involved in a plethora of functions, including energy production (e.g., electron transport chain (ETC) and fatty acid β -oxidation), redox and calcium homeostasis, apoptosis, production of reactive oxygen species (ROS) and precursors for the biosynthesis of molecules, inter-organelle communication, and signaling pathways. This organelle was proposed to be the central node for cellular aging by Denham Hartman, who suggested the mitochondria free radical theory of aging (MFRTA). This theory suggested a direct

connection between ROS production and increased oxidative stress leading to cellular and organismal dysfunction (Harman, 1956). Consistent with this hypothesis, there is a decline in mitochondrial function during aging, and many age-related diseases are associated with increased oxidative damage (Stadtman, 1992). However, multiple observations have challenged the MFRTA. On the one hand, mutations in the superoxide dismutase (SOD), an antioxidant enzyme, reduce the lifespan of yeast, flies, and mice (Duttaroy et al., 2003; Elchuri et al., 2005; Phillips et al., 1989; Wawryn et al., 1999), and overexpression of SOD extends lifespan in flies (Jingtao Sun & Tower, 1999). On the other hand, deletion of *sod-2* in *C. elegans* extends lifespan (Van Raamsdonk & Hekimi, 2009, 2012), and overexpression of additional antioxidant enzymes in *D. melanogaster* did not result in increased longevity (Mockett et al., 2010), thus suggesting that the mitochondria may regulate longevity through mechanisms independent to ROS production.

In *C. elegans*, mutations in the Complex I subunit *nuo-6* and Complex III iron-sulfur protein *isp-1* result in lower oxygen consumption, decreased sensitivity to ROS, and increased lifespan (J. Feng et al., 2001; Wen Yang & Hekimi, 2010). *clk-1* mutants have impaired ubiquinone synthesis that results in defects in the electron transfer between Complex I and III and are long-lived (Lakowski & Hekimi, 1996). However, the connection between the ETC and longevity is more complex. For example, mutations in Complex I subunit *gas-1* (Kayser et al., 2001) and Complex II subunit *mev-1* (S. Honda et al., 1993; Senoo-Matsuda et al., 2001) show rapid accumulation of aging markers and decreased lifespan.

Knockdown of genes that encode for subunits of the ETC and the ATP synthase increase lifespan and alter behavioral rates (Dillin et al., 2002). Dillin and colleagues found increased longevity when worms were fed with the specific RNAi during the transition between L3 and L4 but not during adulthood. This suggested that decreasing mitochondrial activity during development was explicitly important to reprogram metabolism and extend lifespan (Rea et al., 2007). Later it was shown that knockdown of cytochrome c oxidase (Complex IV) subunit *cco-1* in the intestine and neurons was sufficient to extend the lifespan and upregulate the mitochondrial unfolded protein response (UPR^{mt}) in a cell-nonautonomous manner (Durieux et al., 2011). Interestingly, lifespan extension mediated by knockdown of the ETC subunits is independent of DAF-16 and, in combination with *daf-2* mutants, further extends lifespan indicating that they act through different regulatory pathways (Dillin et al., 2002). Conversely, the long-lived mitochondrial mutants *clk-1*, *isp-1*, and *nuo-6* require DAF-16 for the lifespan extension (Senchuk

et al., 2018), thus suggesting that different subunits regulate longevity through independent mechanisms (Figure 4).

The mechanisms by which mitochondria extend lifespan may be evolutionarily conserved. For example, knockdown of ETC complexes I, III, IV, and V extend lifespan in flies (Copeland et al., 2009). Interestingly, the authors also showed that knockdown of Complex I and IV in neurons was enough to increase the lifespan, suggesting that endocrine regulation of mitochondrial longevity may also be conserved. Additionally, heterozygous *mclk1* mice have improved protections against oxidative stress and DNA damage and are long-lived (Xingxing Liu et al., 2005). Knockout mice for the cytochrome c oxidase (Complex IV) assembly factor *Surf1* showed an increased lifespan in both females and males (Dell'Agnello et al., 2007).

Mitochondria mediate lifespan extension through different mechanisms (Figure 4). Reduction of mitochondrial function results in decreased levels of ATP, which activates AMPK function. Consistently, *isp-1* and *clk-1* mutants require AMPK α subunit *aak-2* to extend the lifespan in worms (Curtis et al., 2006). Under reduced mitochondrial function, the vaccinia virus-related nuclear kinase VRK-1 directly phosphorylates AMPK, which is required for the longevity (Park et al., 2020). Lifespan extension mediated by ROS also requires AMPK and the transcription factor HIF-1 (Hwang et al., 2014; S. J. Lee et al., 2010). HIF-1 α is stabilized in *mclk1* heterozygous mice, suggesting that the regulatory mechanism might be conserved (D. Wang et al., 2010). Mitochondrial mutants also require the homeobox transcription factor CEH-23 and a component of the TFIID complex TAF-4 for the longevity (Khan et al., 2013; Walter et al., 2011). It was recently shown that NFYB-1, a conserved histone-like transcription factor, regulates mitochondrial longevity through the lysosomal prosaposin SPP-8 and cardiolipin levels (Tharyan et al., 2020).

Impaired respiration also upregulates the UPR^{mt} stress response. For example, *cco-1* knockdown increases critical effectors of the UPR^{mt}, like the ubiquitin-like UBL-5 and the transcription factor DVE-1, and these are required for the lifespan extension (Durieux et al., 2011). This suggests that increased UPR^{mt} may be required for mitochondrial longevity. The activating transcription factor associated with stress ATSF-1 is responsible for the upregulation of many chaperones that mediate the UPR^{mt} (Fiorese et al., 2016; Nargund et al., 2012). Consistently, *atsf-1* is required for the mitochondrial longevity conferred by *nuo-6* (Z. Wu et al., 2018). However, *atsf-1* is dispensable for the longevity of *cco-1* knockdown and *isp-1* mutants (Bennett et al., 2014),

suggesting that reduced mitochondrial activity extends lifespans through a complex transcriptional network.

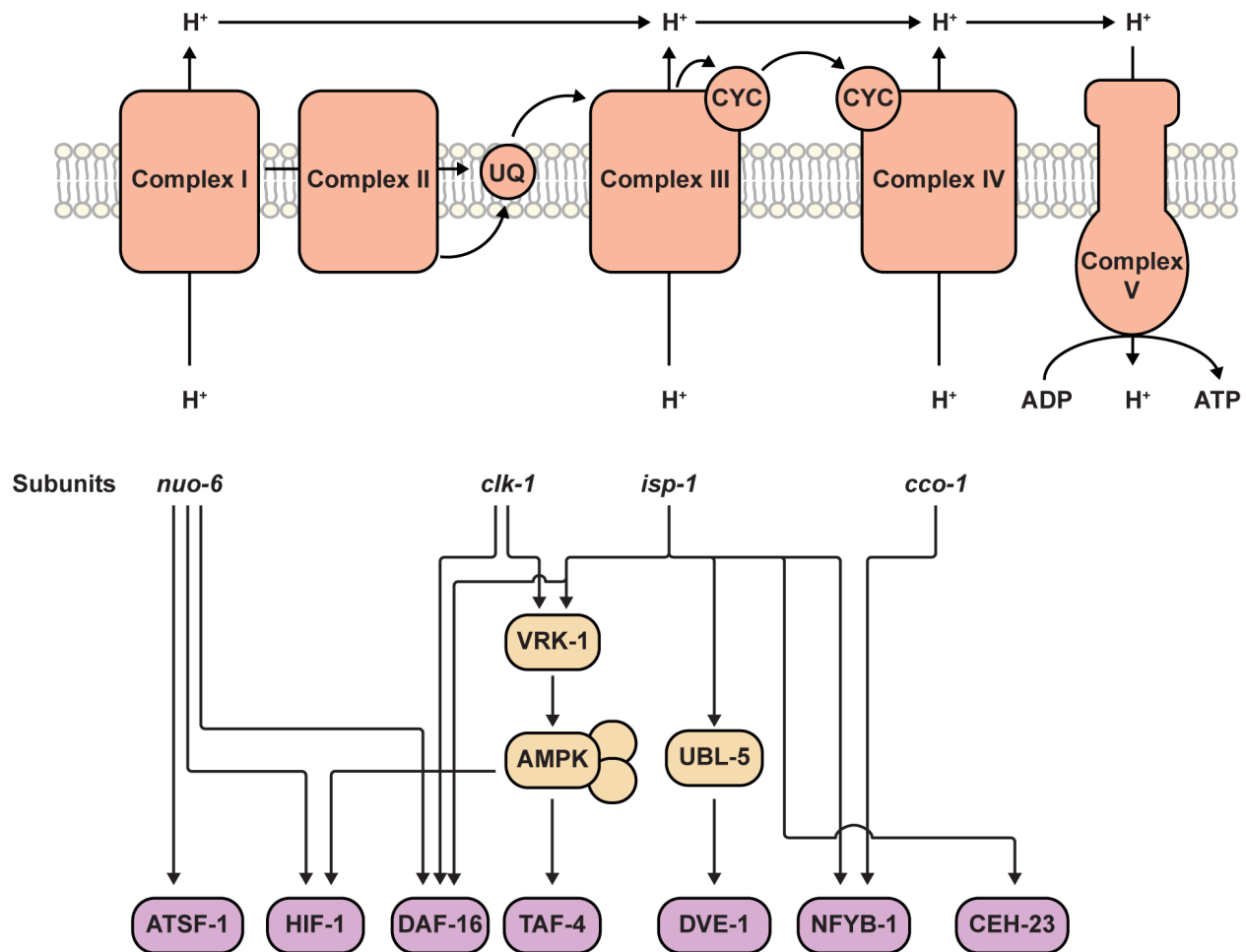


Figure 4. Mitochondrial-induced longevity acts through different effectors. Downregulation of the ETC has been shown to increase longevity in multiple organisms. In the nematode, reduced function by RNAi knockdown or genomic mutations in different subunits extends lifespan, although the downstream targets are not overlapping between all paradigms. Some of the proposed models include high production of ROS that activate the UPR^{mt}, activation of AMPK, and regulation of lysosome-to-mitochondria communication through prosaposin and lipid signaling. These pathways activate several transcription factors that orchestrate a response to reduced mitochondrial function, rewire metabolism, and increase lifespan.

3.3.4 Gonadal longevity

Cues from the reproductive system have been shown to regulate the rate at which organisms age. In *C. elegans*, laser ablation of the gonadal germline-precursor cells extends the lifespan up to 60% in a DAF-16- and DAF-12-dependent manner (Berman & Kenyon, 2006; Hsin

& Kenyon, 1999). The researchers also showed that the lifespan extension was not due to sterility because it required the somatic gonad, suggesting a complex interaction between opposing signals from the germline and somatic gonad. Mutations in the kinase MES-1 and the Notch-1 signaling receptor GLP-1 have been established as genetic models of germline longevity in the nematode (Arantes-Oliveira et al., 2002). These factors influence longevity by suppressing germline stem cells. Interestingly, killing the germline precursor cells also extends lifespan in *D. melanogaster* (Flatt et al., 2008; Sgrò & Partridge, 1999), and ovary transplantation from young mice to post-reproductive females increased the life expectancy by 40% (Cargill et al., 2003; Mason et al., 2009), suggesting that mechanisms associated with the germline and longevity may be evolutionarily conserved.

The germline integrates nutrient signaling to communicate with multiple tissues and remodel metabolism (**Figure 5**). Germline-less *glp-1* mutant animals have high levels of autophagy through increased activity of the transcription factors PHA-4 and DAF-16 in an mTOR-dependent manner (Lapierre et al., 2011). Inhibition of autophagy by knockdown of core components of the autophagic machinery decreased *glp-1* lifespan (Lapierre et al., 2011). Additionally, *glp-1* mutants are associated with increased triglyceride lipase LIPL-4 required for the lifespan extension (M. C. Wang et al., 2008). Increased lipids in *glp-1* activate the transcription factor SKN-1 to upregulate stress defense and metabolic genes required for the longevity (Steinbaugh et al., 2015). Interestingly, the transcription factor NHR-80, homolog to HNF4, plays a synergistic role with DAF-12 to regulate fatty acid desaturases that are required for the longevity of *glp-1* and *mes-1* mutant worms (Goudeau et al., 2011). NHR-49 also plays a crucial role in regulating fatty acid desaturases and β -oxidation required for the lifespan extension (Ratnappan et al., 2014). NHR-49 and NHR-80 integrate signals from the lysosome through the lipid chaperone LBP-8 and oleoylethanolamide (OEA) to communicate to the nucleus and promote longevity (Folick et al., 2015).

The sterol hormone signaling pathway is also required for longevity mediated by the germline. In particular, the nuclear hormone receptor DAF-12 regulates the nuclear localization of DAF-16 in the intestine (Berman & Kenyon, 2006). In this pathway, DAF-9, an ortholog of the cytochrome p450 enzyme, and DAF-36, an ortholog to the Rieske-like oxygenase, are responsible for producing and modifying dafachronic acids. DAF-12 binds dafachronic acids and translocates to the nucleus to activate transcription and inhibit dauer formation (Gerisch et al., 2001).

Consistently, supplementation of dafachronic acids rescues the longevity of germline-less worms that have mutations in the *daf-9* and *daf-36* genes (Gerisch et al., 2007).

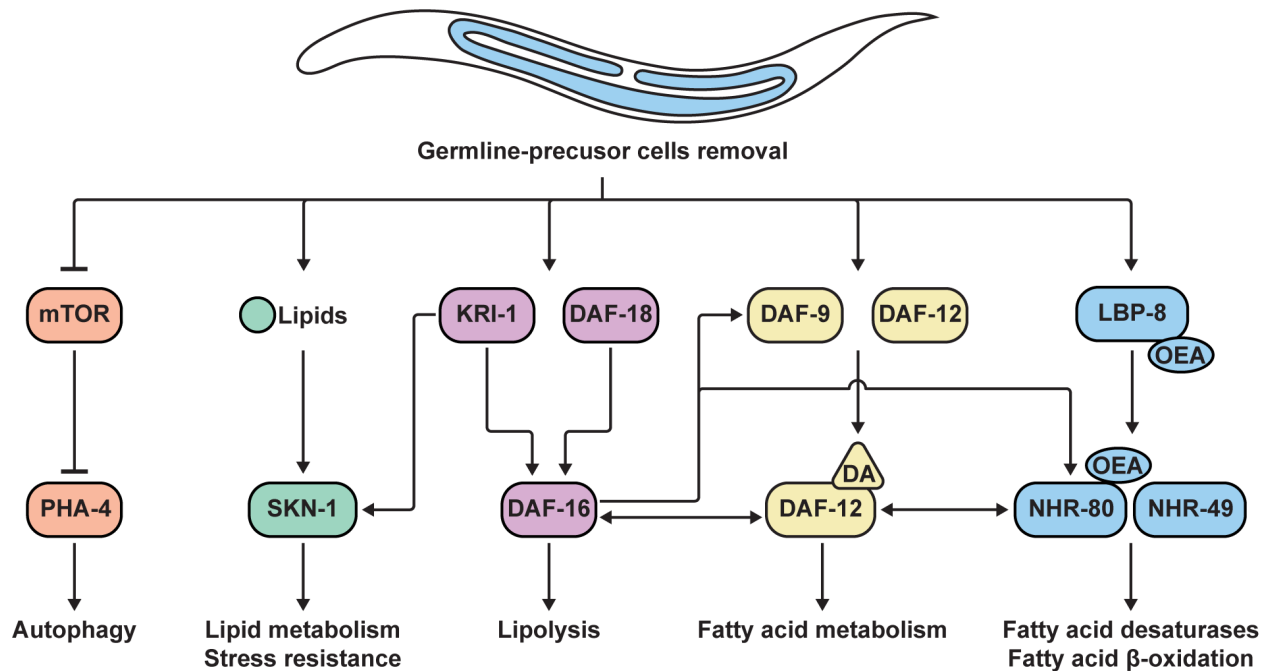


Figure 5. The gonad regulates longevity through multiple effectors. Removal of the gonadal germline-precursor cells by laser ablation or genetic manipulation extends lifespan in *C. elegans* by regulating several transcription factors and pathways. Signals from the somatic germline downregulate mTOR activity, increasing autophagy through PHA-4. Increased lipids stored in the intestine in germline-less worm activate SKN-1, which works in a positive feedback loop and regulate lipid metabolism and stress resistance. Members of the insulin signaling pathway also play an essential role in the germline longevity that converge in the regulation of DAF-16. KRI-1 and DAF-18 are positive regulators of DAF-16 translocation to the nucleus to activate lipolytic genes like *lipl-4* to regulate lifespan. The steroid hormone signaling positively interacts with DAF-16 to regulate fatty acid metabolism. DAF-9 and DAF-36 produce and modify dafachronic acids, the ligands to the hormone receptor DAF-12. This transcription factor is partially required for the nuclear localization of DAF-16 in the intestine upon germline removal. The lysosome-to-nucleus regulation of the germline longevity includes the lipid chaperone LBP-8, which binds OEA, the ligand for NHR-80. NHR-80/NHR-49 translocates to the nucleus and regulates a subset of genes involved in fatty acid desaturation and β -oxidation. OEA, oleoylethanolamide; mTOR, mechanistic target of rapamycin; DA, dafachronic acids.

3.3.5 Other pathways and drugs to target aging and age-related diseases

Understanding the molecular mechanisms underlying the previously mentioned longevity pathways is crucial for future therapeutic approaches to mitigate harmful alterations in cell metabolism and extend healthspan. Multiple drugs have been identified to influence different aspects of age-dependent cellular decline in model organisms. For example, rapamycin, an inhibitor of the mTORC1 pathway, has been shown to extend lifespan across the evolutionary spectrum (Blagosklonny, 2017; Harrison et al., 2009). Interestingly, rapamycin was shown to have a broader effect on a better response during immunization (C. Chen et al., 2009), and pretreatment in the elderly improved the immune response (Mannick et al., 2014). Rapamycin is currently in clinical trials phase 2 to treat aging (ClinicalTrials.gov Identifier: NCT04488601).

Metformin and phenformin are biguanides that indirectly activate AMPK by disrupting mitochondrial function by inhibiting ETC Complex I (H. R. Bridges et al., 2014). This drug is used for the treatment of type 2 diabetes. In *C. elegans*, it has been shown to extend lifespan via AMPK (Onken & Driscoll, 2010) by modulating the folate and methionine metabolism in the *E. coli* used as food source (Cabreiro et al., 2013), thus through a host-microbiome interaction. Chronic treatment with metformin extends the mean lifespan up to 37.8% in female mice (Anisimov et al., 2008). In humans, metformin has been linked with reducing the risk for age-related diseases, including cancer and cardiovascular diseases (Campbell et al., 2017). The Metformin in Longevity Study (MILES) is a clinical trial currently in phase 4, intending to use metformin as an “anti-aging” drug (ClinicalTrials.gov Identifier: NCT02432287).

Resveratrol is a polyphenol shown to increase lifespan in the budding yeast (Howitz et al., 2003), worms, flies (Wood et al., 2004), and mice (Baur et al., 2006), through the NAD-dependent deacetylase Sir2p and its orthologs. This drug induces changes similar to DR, like reduced insulin/IGF signaling and increased AMPK activity in mice, and increases the lifespan of mice fed with a high-fat diet (Baur et al., 2006). Resveratrol improves mitochondrial function and capacity by activating the peroxisome proliferator-activated receptor-gamma coactivator 1 α PGC1 α and protecting mice against diet-induced obesity and insulin resistance (Lagouge et al., 2006). Moreover, nicotinamide adenine dinucleotide (NAD⁺) precursors and boosters have been shown to extend lifespan in model organisms (Belenky et al., 2007; Fang et al., 2014; Mouchiroud et al., 2013; North et al., 2014), and there are several clinical trials for addressing the effects of these

drugs on health (*e.g.*, cognition, immune response, cardiovascular risk) in humans (Rajman et al., 2018).

Trametinib is a small-molecule inhibitor of the Ras-Erk-ETS signaling that has been shown to extend lifespan in *D. melanogaster* (Slack et al., 2015). This drug has been used to treat melanoma and is a highly specific inhibitor of the MEK kinase, inhibiting the activation of Erk by Ras (Yamaguchi et al., 2011). Whether trametinib impacts lifespan or healthspan in mammals remains elusive. However, it ameliorates neuroinflammation (Huang et al., 2020), which is linked to aging and age-related diseases (Franceschi et al., 2018).

Lithium has been used for many decades to treat mood-affecting disorders, including bipolar disorder. Exposure to lithium extended the lifespan of yeast (Sofola-Adesakin et al., 2014) and nematodes (McColl et al., 2008). In flies, lithium extends lifespan independently of the sex through the glycogen synthase kinase GSK-3 and the transcription factor NRF-2 (Castillo-Quan et al., 2016). Interestingly, rapamycin-dependent increase in adiposity is reversed by lithium supplementation (Castillo-Quan et al., 2019), suggesting drug combination may be more effective in tackling aging. Researchers also found that lithium concentration in drinking water inversely correlates with mortality in a Japanese population (Zarse et al., 2011), suggesting possible evolutionary conservation of the lifespan-extending mechanisms induced by lithium. However, lithium supplementation in mice had only mild benefits in males, including better glucose tolerance and motor activity, but it failed to extend lifespan in either sex (Nespital et al., 2021). Thus, increasing our understanding of the molecular mechanisms involved in nutrient sensing will allow us to identify new druggable targets to prevent pathological loss of energy homeostasis and promote healthy aging.

3.3.6 Convergent mechanisms of aging

Most of the work in the aging field has focused on understanding the molecular mechanisms of different specific longevity paradigms. However, many pathways share common effectors that mediate lifespan extension, raising the idea that convergent mechanisms might be at the core of aging. For example, many of the components of insulin signaling are involved in the crosstalk between longevity pathways. Especially, DAF-16 has been shown to mediate the transcriptional response from different inputs, regulating multiple processes, including activation of stress response genes and reprogramming metabolism (C. J. Kenyon, 2010). As described

previously, many longevity pathways also converge in the nutrient sensors AMPK and mTORC. However, in the last decade, many novel convergent mechanisms have been shown to regulate longevity.

The nucleolus is a vital regulation node in multiple longevity pathways, and small nucleoli are cellular hallmarks of longevity. One factor that mediates this is NCL-1, homolog to BRAT/TRIM2, which is required for longevity mediated by DR, reduced mTOR and insulin signaling, reduced mitochondrial function, and germline (Tiku et al., 2017). Many longevity mutants show decreased levels of ribosome biogenesis and the nucleolar marker fibrillarin FIB-1, which are reversed by *ncl-1* loss-of-function. Long-lived mutants were also shown to have smaller nucleoli than wildtype, and *ncl-1* mutants showed an increase in the nucleolar area correlated with the abrogation of the lifespan extension. Interestingly, *ncl-1* overexpression was sufficient to promote longevity (Tiku et al., 2017).

Longevity pathways also converge on metabolic modules like the folate cycle (Annibal et al., 2021). The folate cycle feeds one-carbon groups into the methionine cycle, *de novo* purine synthesis, amino acid metabolism, thymidine production, and NADPH generation. Long-lived mutants show altered levels of folate intermediates, including downregulation of 5-methyltetrahydrofolate (5MTHF) and knockdown of *dhfr-1*, which diminishes the folate pool, extends lifespan in *C. elegans* (Annibal et al., 2021). Interestingly, the authors reported alterations in other metabolites correlated with longevity in multiple pathways, like thiamine, though the downstream mechanisms remain elusive.

The basic helix-loop-helix (bHLH) transcription factor EB TFEB/HLH-30 is required for multiple longevity pathways (Lapierre et al., 2013). This factor is considered a master regulator for lysosomal biogenesis and autophagy, and it has been shown to translocate to the nucleus upon nutrient deprivation in an mTOR-dependent manner (Martina et al., 2012; Roczniak-Ferguson et al., 2012; Settembre et al., 2011, 2012). HLH-30 is also required to mobilize stored fats during fasting (O'Rourke & Ruvkun, 2013), and overexpression of HLH-30 is sufficient to extend lifespan at least in part by inducing autophagy (Lapierre et al., 2013). Consistent with the protective role of autophagy, many conserved longevity pathways have been shown to modulate aging via autophagy, including reduced insulin/IGF signaling (Meléndez et al., 2003), DR (Hansen et al., 2008; Jia & Levine, 2007; Mörck & Pilon, 2006; Tóth et al., 2008), mTOR inhibition (Hansen et al., 2008; Tóth et al., 2008), AMPK overexpression (Egan et al., 2011), and germline removal

(Lapierre et al., 2011). Thus, HLH-30 and autophagy have been established as significant nodes regulating nutrient availability and longevity.

The Myc/Mondo family transcription factors MML-1 and its binding partner MXL-2 were also found to act as pro-longevity factors in which multiple longevity pathways converge (D. W. Johnson et al., 2014; Nakamura et al., 2016). These transcription factors regulate numerous cellular processes, including downregulation of the mTORC1 pathway, regulate carbohydrate and lipid metabolism, and autophagy. Interestingly, the authors showed that MML-1/MXL-2 and HLH-30 commonly regulate some downstream targets and are required for each other's nuclear localization (Nakamura et al., 2016). Thus, understanding the underlying mechanisms that converge in longevity regulation will help us identify new clinical targets to extend health and lifespan.

3.4 Cellular nutrient-sensing pathways and metabolic flexibility

Nutrient sensing is pivotal for activating different pathways in the anabolism and catabolism of macro and micronutrients. During evolution, all organisms have evolved mechanisms to detect nutrients at the cellular level and induce physiological changes in a systemic way. Each class of nutrient is sensed by specific factors that result in the activation of metabolic enzymes accompanied by transcriptional, post-translational, and allosteric regulation. Metabolism is plastic, and communication between different nutrient-sensing pathways is essential to ensure metabolic homeostasis.

Enzymes involved in the metabolism of macronutrients are usually regulated by allosteric inhibition of their downstream metabolite to ensure proper control of the pathway. Post-translational modifications also play a direct role in regulating metabolic enzymes through phosphorylation/dephosphorylation and O-GlcNAcylation. As described previously, transcription factors also play a significant role in the long-term response to nutrients through regulating metabolic genes. Many transcription factors can directly bind metabolites to activate or repress their transcriptional activity. Thus, understanding the molecular mechanisms that regulate these transcription factors is crucial to comprehend their role in physiology and pathology.

3.4.1 Amino acids

Amino acids are the building blocks for proteins. During translation, the ribosome takes transfer RNAs (tRNAs) coupled to specific amino acids to incorporate them into growing

polypeptide chains in a linear sequence determined by the messenger RNA (mRNA). Under amino acid deprivation, there is an increase in uncharged tRNAs that can be sensed by the general control nonderepressible GCN2/GCN-2 resulting in the phosphorylation and inhibition of the eukaryotic translation initiator factor eIF2 α , hence hindering general translation but selectively activating translation of specific mRNA subsets (Berlango et al., 1999; Sonenberg & Hinnebusch, 2009). GCN-2 is a serine/threonine kinase required for the lifespan extension induced by DR regimens and reduced mTOR signaling through the activation of stress genes in a PHA-4-dependent manner in *C. elegans* (Rousakis et al., 2013).

In 2008, two independent groups showed that mTOR plays a crucial role in amino acid sensing mediated by its recruitment at the lysosomal surface by the Rag GTPases (E. Kim et al., 2008; Sancak et al., 2008). The Rags function as heterodimers composed of RagA or RagB associated with RagC or RagD that regulate mTOR through different inputs (G. Y. Liu & Sabatini, 2020). The mitogen-activated protein kinase MAP4K3 physically binds dRagA and dRagC in *D. melanogaster* to activate mTOR upon amino acid availability (Bryk et al., 2010). The folliculin FLCN and folliculin-interacting protein FNIP complex is a potent RagC/D activator sensitive to amino acid levels, thus regulating the mTORC1 signaling (Tsun et al., 2013). The vacuolar protein sorting VPS34 also regulates mTOR upon amino acid availability (Byfield et al., 2005).

On the other hand, particular amino acids regulate the mTOR signaling cascade. For example, Sestrin2 binds leucine to inhibit the Sestrin2-GATOR2 interaction, thus enhancing the mTORC1 activity (Chantranupong et al., 2014; Saxton et al., 2016). Arginine stimulates mTORC1 activity through the lysosomal arginine sensor SLC38A9 and inhibits the CASTOR1-GATOR2 suppressor complex (Chantranupong et al., 2016; Rebsamen et al., 2015; S. Wang et al., 2015). mTORC1 function is also regulated by sensing amino acids in different cellular compartments, activating other downstream effectors (Goberdhan et al., 2016). Thus, the mTOR hub is an essential node for regulating metabolism in response to amino acid availability.

3.4.2 Lipids

Lipids are macromolecules essential in many cellular processes, including structural roles as part of membranes, secondary messengers, and energy reservoirs. The major families of lipids are fatty acids, phospholipids, sphingolipids, and sterol and prenol lipids (Fahy et al., 2009). Triacylglycerols (TAGs) are synthesized by esterification reactions of glycerol with diverse

species of phospholipids. TAGs are stored in specialized compartments, named lipid droplets (LD), and are mobilized upon nutrient deprivation to be degraded by fatty acid oxidation. Phospholipids are also the primary component of cellular membranes due to their amphipathic properties. Sphingolipids (*e.g.*, ceramides, sphingomyelins, and glycosphingolipids) are an integral part of membranes and play an essential role in transducing signaling from multiple pathways. Cholesterol is part of cellular membranes important for their fluidity properties and is a precursor for synthesizing steroid hormones.

Fatty acids are also classified depending on the covalent bonds between the carbons in the hydrocarbon chain. On the one hand, saturated fatty acids have a single bond on each carbon, hence increasing the number of hydrogens per carbon (*e.g.*, palmitate). On the other hand, unsaturated fatty acids have one (monounsaturated fatty acids (MUFAs), *e.g.*, oleic acid) or multiple (polyunsaturated fatty acids (PUFAs), *e.g.*, linoleic acid) double bonds in the hydrocarbon chain.

Cellular sensing of lipids includes multiple nuclear receptors like the peroxisome proliferator-activated receptor (PPAR), the PPAR γ co-activator PGC1 α , the liver X receptor LXR, and the hepatocyte nuclear factor HNF4 α . PPARs are transcription factors that regulate multiple processes upon activation by fatty acids (Varga et al., 2011). Regulation between starvation and fed conditions requires PPAR α to promote gluconeogenesis and lipid trafficking (Atherton et al., 2009), and saturated fats stimulate fatty acid oxidation in a PPAR α -dependent manner (Sampath et al., 2007). In contrast, PPAR γ is regulated by unsaturated fatty acids and modulates a broad spectrum of physiological functions, including adipogenesis, lipid storage, fatty acid and glucose uptake, and inflammation (Barak et al., 1999; Hevener et al., 2007; Vacca et al., 2015). LXR forms a heterodimer with the retinoid X receptor RXR and directly binds oxysterol ligands, thereby controlling processes like lipogenesis, bile acid production, and cholesterol synthesis (Janowski et al., 1996; Sampath et al., 2007). HNF α has been shown to bind linoleic acid directly. However, its transcriptional activity was not affected by binding the ligand (Yuan et al., 2009), suggesting that linoleic acid may play another role like stabilizing the protein. HNF α works with PPARs to orchestrate their functions during feeding and fasting (Martinez-Jimenez et al., 2010). HNF α downstream targets include genes involved in the glucose, fatty acid, and cholesterol metabolism (Mitchell et al., 2002). Other proteins can also sense lipids, like the G-protein-coupled receptor

DPR40, which senses long-chain free fatty acids and induces glucose-dependent insulin secretion (Itoh et al., 2003).

SREBP and the SREBP cleavage-activating protein SCAP are involved in intracellular cholesterol sensing. SREBP-SCAP complex binds cholesterol and thus remains tethered to the endoplasmic reticulum (ER). Under low cholesterol levels, this complex dissociates from the ER and shuttles to the Golgi apparatus. SREBP is processed and releases an N-terminus domain that translocates to the nucleus and functions as a transcription factor regulating genes involved in the cholesterol synthesis (A. J. Brown et al., 2002; M. S. Brown & Goldstein, 1997). Interestingly, SBP-1/SREBP is required to mitigate the effects of a high glucose diet on lifespan by converting saturated fatty acids to unsaturated species in *C. elegans* (D. Lee et al., 2015), thus linking lipid sensing and longevity.

3.4.3 Carbohydrates

Carbohydrates are the primary carbon source across phylogenetic taxa and are essential to sustain life. Glucose is one of the most important monosaccharides in biology as it plays a central role in different pathways. Glucose is stored in long polysaccharides: glycogen in the animal kingdom, amylose and amylopectin in plants. Pentoses such as ribose and deoxyribose are an integral part of nucleotides, the building blocks of RNA and DNA, respectively. Ribose is also important in the biosynthesis of cofactors like adenosine phosphates (AMP/ADP/ATP) and cofactors such as NAD^+ , flavin adenine dinucleotide (FAD), and acetyl-Coenzyme A (acetyl-CoA).

Upon digestion, complex sugars are broken down through different enzymatic reactions to allow the absorption of these nutrients by the cell. Glucose transporters (GLUTs) are responsible for glucose uptake through the plasma membrane (Herman & Kahn, 2006). In mammals, members of the GLUT family are expressed in different tissues and have different affinities to the solutes (Navale & Paranjape, 2016). They are mainly regulated by two opposing hormones, insulin and glucagon, produced in the pancreas (Ojha et al., 2019). Upon high glucose, the β -pancreatic cells secrete insulin to increase glucose metabolism. Insulin binds the insulin receptor eliciting a signaling cascade that results in enhanced glucose uptake through regulation of the GLUTs and other proteins. On the other hand, when glucose levels drop, the α -pancreatic cells secrete

glucagon, an antagonizing hormone to insulin, which stimulates the breakdown of glycogen through glycogenolysis, releasing glucose into the bloodstream.

In *C. elegans*, there is one putative glucose transporter named FGT-1 also capable of transporting other hexoses like mannose, galactose, and fructose (Kitaoka et al., 2013). Interestingly, knockdown of *fgt-1* extends lifespan in the nematode through the insulin signaling pathway (Y. Feng et al., 2013). Consistently, inhibition of the glycolytic enzyme glucose phosphate isomerase *gpi-1* (Hamilton et al., 2005; S. S. Lee et al., 2003) and blockage of glycolysis by supplementation of 2-deoxyglucose (2-DG) (Schulz et al., 2007) also extends lifespan. Hence, glucose sensing directly rewires metabolism and regulates longevity.

Intracellular signaling mechanisms also sense glucose. AMPK functions as one of the primary sensors for energy status, switching between catabolic and anabolic pathways. AMPK regulates carbohydrate metabolism by increasing glucose uptake via increased GLUT4 (Sakamoto & Holman, 2008) and enhancing glycolysis by phosphorylating the 6-phosphofructokinase PFK2 (Marsin et al., 2002). The glycogen synthase is negatively regulated by AMPK, and supplementation of 5-aminoimidazole-4-carboxamide-1-D-ribo-furanoside (AICAR), an AMPK activator, induces its phosphorylation and inhibits glycogenesis (Jørgensen et al., 2004). Additionally, AMPK activation in the liver reduces gluconeogenic genes, including glucose-6-phosphatase and phosphoenolpyruvate carboxykinase, through multiple mechanisms (Koo et al., 2005; Mihaylova et al., 2011). AMPK also regulates lipid metabolism depending on glucose levels. SREBP and the acetyl-CoA carboxylase (ACC) are directly phosphorylated by AMPK, thus inhibiting lipogenesis (Dyck et al., 1999; Y. Li et al., 2011). ACC phosphorylation inhibits the production of malonyl-CoA, a substrate for the fatty acid synthase (FAS) and precursor for *de novo* synthesis of palmitate (Dyck et al., 1999) (**Figure 8**). However, how carbohydrate and fat metabolism impinged on transcriptional regulation for long-term response to metabolic adaption remains largely unknown.

3.4.4 Metabolic flexibility and organellar communication

Cell-autonomous and non-autonomous signals tightly regulate anabolic and catabolic processes depending on the metabolic requirements (**Figure 6**). Anabolic processes are favored when nutrients, like glycogen and fatty acid synthesis and storage, are available to sustain growth. On the other hand, catabolic processes, like fatty acid β -oxidation and glycogenolysis, are activated

upon nutrient deprivation to provide energy and maintain essential functions. Thus, metabolic flexibility is defined as the ability to switch between these different metabolic states. For example, metabolism adaptation during feeding versus fasting or burning carbohydrates versus fats. During aging or metabolic disorders like obesity, there is a loss in the metabolic flexibility (Goodpaster & Sparks, 2017; Kelley & Mandarino, 1990; Kelley & Simoneau, 1994). Hence, fine-tuning mechanisms that participate in nutrient sensing are pivotal in supporting homeostasis, and understanding the molecular mechanisms underlying these processes is fundamental in physiology and the aging field.

Bioenergetic demand is intimately linked to mitochondrial network morphology, which is highly dynamic (**Figure 6**). Mitochondria undergo fusion and fission according to cellular energy demand, and this dynamic process is essential for proper cell function and overall organismal health (Schrepfer & Scorrano, 2016). When nutrients are plentiful, mitochondria are in a more fragmented state. Mitochondria also undergo fission upon cellular stress (S. Wu et al., 2011), and this process is essential for the removal of damaged mitochondria (G. Chen et al., 2020). Upon food deprivation, mitochondrial fusion is enhanced to allow metabolite diffusion and increase respiration efficiency (Rambold et al., 2011). However, many other factors regulating mitochondrial dynamics impinge on cellular and organismal metabolism, including stress (Wai & Langer, 2016).

Dysregulation of mitochondrial dynamics contributes to the pathophysiology of type 2 diabetes, obesity, and aging (Dall & Færgeman, 2019; Zorzano et al., 2009). It has been shown that there is progressive mitochondrial fragmentation in *C. elegans* and mice during aging (H. C. Jiang et al., 2015; Leduc-Gaudet et al., 2015; Sebastián et al., 2016). Consistently with mitochondrial fragmentation as pro-aging, inhibition of fission extends longevity in yeast (Scheckhuber et al., 2007), while the fused mitochondrial network is correlated with longevity in *C. elegans* (Chaudhari & Kipreos, 2017), thus linking mitochondrial dynamics and longevity. However, mitochondrial fragmentation is also essential for the turnover of damaged mitochondria. Indeed, inducing mitochondrial fragmentation and mitophagy, the selective degradation of mitochondria, in adult neurons extends lifespan in *D. melanogaster* (Rana et al., 2013). Recently, it was shown that both mitochondrial fusion and fission are required for the longevity conferred by overexpression of a truncated version of *aak-2* in *C. elegans* (Weir et al., 2017). Therefore, the mitochondrial capacity to remodel and adapt between energetic states and properly regulate

mitochondrial biogenesis and turnover is linked to health and aging. Moreover, identifying molecular mechanisms that can restore whole energy homeostasis will accelerate the development of effective therapeutic strategies for disease and aging.

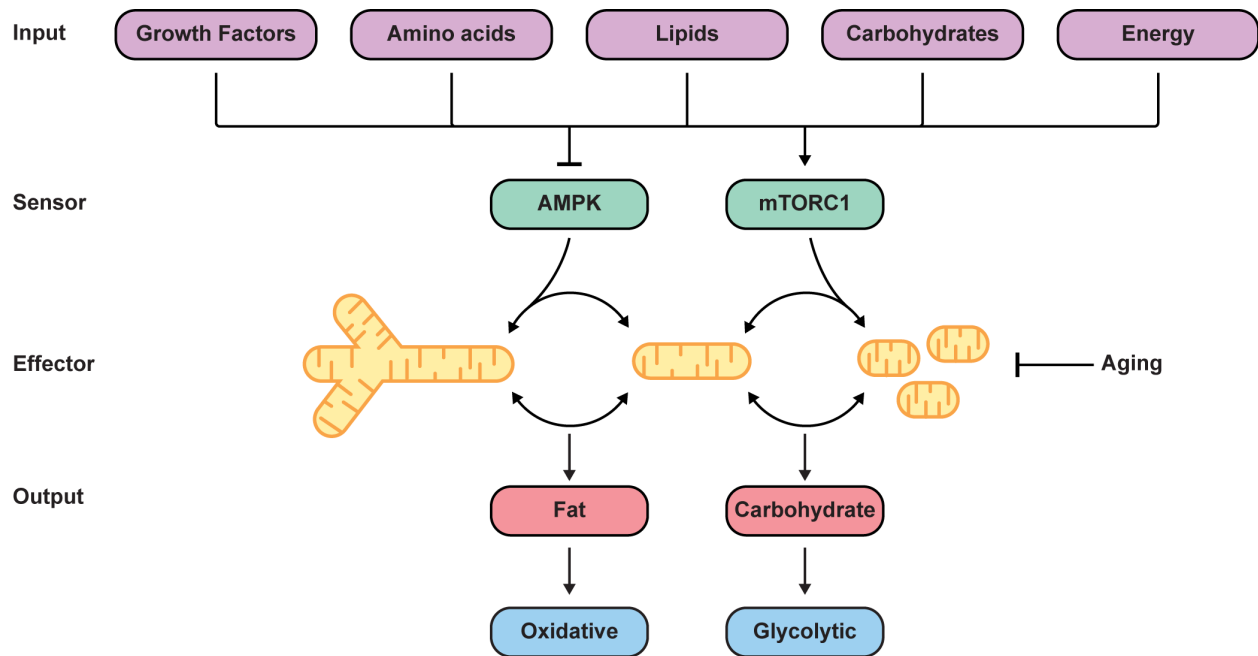


Figure 6. Metabolic flexibility is required for maintaining cellular homeostasis. Under nutrient deprivation, AMPK actively supports mitochondrial fusion and increases fatty acid oxidation. When nutrients are available, mTORC1 is active, resulting in mitochondrial fragmentation and the usage of carbohydrates as an energy source. This metabolic flexibility is lost during pathological conditions and aging and consequentially results in metabolic disorders.

The segregation of different metabolic pathways within organelles ensures metabolic specificity. However, organelles also interact with one another, allowing communication between compartments to maintain cellular homeostasis. For example, mitochondria and ER interaction are important for multiple processes, including lipid trafficking, mitochondrial dynamics, Ca^{2+} signaling, UPR, apoptosis, and autophagosome formation (Rieusset, 2018). Communication between both organelles is essential to maintain proper cellular function. The disruption of mitochondria-ER contact sites has been associated with the progression of neurodegenerative diseases, including Alzheimer's disease, Parkinson's disease, and amyloid lateral sclerosis (Paillusson et al., 2016; E. L. Wilson & Metzakopian, 2021). Mitochondria also physically interact with lysosomes to regulate mitochondrial and lysosomal dynamics, phospholipid exchange,

mitochondrial protein translation, and autophagy (Deus et al., 2020). Interestingly, increased mitochondria-lysosome interaction and blockage of untethering in neurons have been linked to Parkinson's disease pathophysiology (S. Kim et al., 2021).

Mitochondria and LDs are actively associated in tissues with high energetic demands (Boutant et al., 2017). There are two alternative hypotheses to explain the function of the interaction between both organelles. On the one hand, nutrient deprivation favors the mobilization of TAGs stored in LDs, releasing free fatty acids that can be imported to mitochondria for β -oxidation (Granneman et al., 2011; Nguyen et al., 2017; Rambold et al., 2015). On the other hand, the crosstalk between mitochondria and LD supports LD expansion through an increase in TAG synthesis (Benador et al., 2018). In either case, the connection between organelles increases the efficiency of the diffusion of metabolites. Thus, communication between organelles coordinates the adaptation of metabolism to nutrient availability and energetic demands.

3.5. *Myc/MondoA family of transcription factors are metabolic sensors*

3.5.1 *Evolutionary conservation of the transcriptional network*

The evolutionarily conserved Myc superfamily is composed of basic helix-loop-helix leucine zipper (bHLHZip) transcription factors that act as essential regulators of cell growth, proliferation, and metabolic flexibility (Lourenco et al., 2021) (**Figure 7A**). These transcription factors recognize and bind hexanucleotide tandem sequences (CANNTG) in the promoter regions called Enhancer box (E-box) sequences (Massari & Murre, 2000). Of this large family, Myc is one of the most studied because of its implications as a proto-oncogene (Lourenco et al., 2021). On the one hand, proteins of the Myc family work in heterodimeric complexes with Max and Myc:Max complexes activate the transcription of targets that regulate proliferation, apoptosis, and metabolism (Blackwell et al., 1990; Prendergast et al., 1991). On the other hand, members of the Mad family bind to Max and function as transcriptional repressors playing an antagonistic role to Myc:Max complexes (Ayer et al., 1993).

Max-like (Mlx) was first identified as an interactor of Mad1 and Mad4 to function as a transcriptional repressor (Billin et al., 1999). The following year, a new member of the bHLHZip superfamily, MondoA/MLXIP, was described to form a heterodimer with Mlx and activate the transcription of E-box-dependent reporter genes (Billin et al., 2000). Mlx and MondoA were shown to be ubiquitously expressed in adult tissues, although MondoA expression was higher in

skeletal muscle. An independent group later discovered a third member of the family, the carbohydrate-response element-binding protein ChREBP/MondoB/MLXIPL, in the rat liver (Yamashita et al., 2001). They showed that this transcription factor binds to related E-box sequences named carbohydrate response elements (ChoREs), formed by two E-box sequences spaced by five nucleotides present in many lipogenic genes, and mediates a glucose-dependent transcriptional activation of L-type pyruvate kinase L-PK. MondoA was later shown to be activated by glucose and regulate around 75% of the glucose-responsive genes (Stoltzman et al., 2008).

Myc/Mondo members radiated in vertebrates through gene duplication and divergence during the evolution (McFerrin & Atchley, 2011). This is supported by the idea that some members share commonly regulated genes resulting in partial redundancy, but also, they preferentially regulate genes reflecting their tissue expression patterns. Interestingly, MondoA has diverged less from the ancestral gene, suggesting it mediates more ancient functions in glucose metabolism (Singh & Irwin, 2016). In invertebrates, the Myc/Mondo transcriptional network contains fewer players. *D. melanogaster*'s genome contains a single copy of Myc, Max, Mnt, Mondo, and Mlx genes (Gallant et al., 1996; McFerrin & Atchley, 2011; Peyrefitte et al., 2001). The *C. elegans* genome contains one single MondoA/ChREBP ortholog called Myc and Mondo-like MML-1, one Mlx ortholog MXL-2, two Max orthologs MXL-1 and MXL-3, and one Mad ortholog MDL-1 (Billin & Ayer, 2006) (**Figure 7A**). This simplified version of the transcriptional network allows us to understand better the molecular mechanism involved in regulating the signaling cascade that can then be translated to mammalian systems.

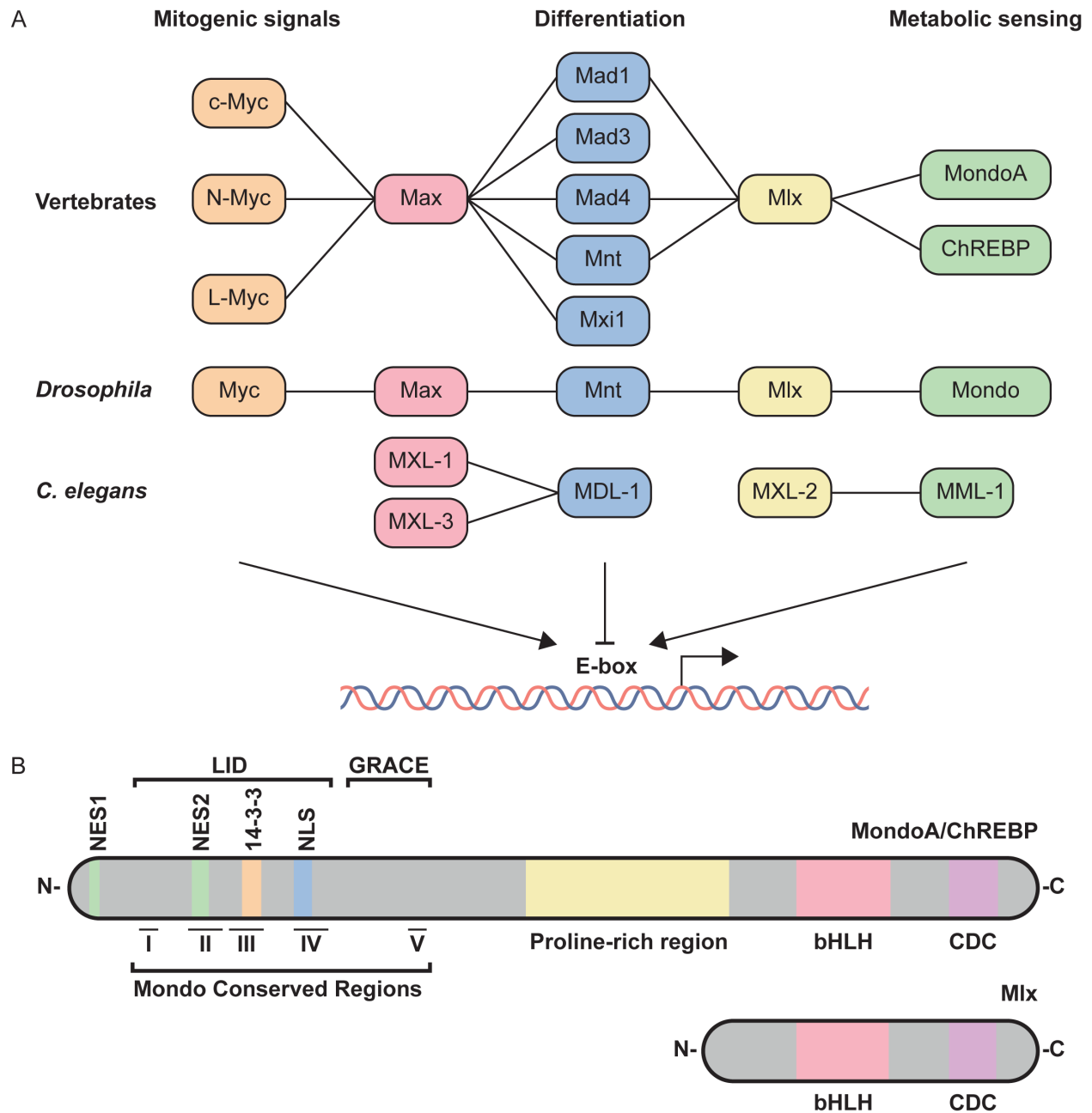


Figure 7. Myc/Mondo superfamily of transcription factors. **A.** Myc/Mondo transcription factors form heterodimers that regulate cell growth and metabolic genes. In vertebrates, members of the Myc family dimerize with Max and function as transcriptional activators. Members of the Mad family can form heterodimers with Max or Mlx forming transcriptional repressor complexes. MondoA and ChREBP bind to Mlx and positively regulate glucose metabolism and *de novo* lipogenesis. In *D. melanogaster* and *C. elegans*, this transcriptional network contains fewer members. **B.** Schematic representation of MondoA/ChREBP and Mlx. The N-terminus region contains the Mondo conserved region (MCR) divided into five subdomains. It also includes two nuclear export signals (NES1 and NES2) that interact with CRM1 (Exportin 1) and the nuclear

localization signal (NLS) that interacts with importin α/β . The 14-3-3 binding site is located in MCRIII. The N-terminus also contains the low-glucose inhibitory domain (LID) and the glucose-response activation conserved element (GRACE) that mediate the glucose-responsiveness of ChREBP and MondoA. The C-terminus contains the basic helix-loop-helix (bHLH) leucine zipper region and the dimerization and cytoplasmic localization domain (DCD) which mediate their heterodimerization and DNA binding. Based on (Havula & Hietakangas, 2012).

3.5.2 Regulation of MondoA/ChREBP

MondoA and ChREBP are large proteins with multiple domains that have a dynamic localization, shuttling between the cytoplasm and the nucleus depending on the glucose concentration (**Figure 7B**). The domain for the glucose-mediated activation of MondoA/ChREBP has been mapped to the N-terminus named glucose-sensing module, or Mondo conserved region (MCR) (Eilers et al., 2002; M. V. Li et al., 2006). The MCR is highly conserved and composed of a low-glucose inhibitory domain (LID) and a glucose-response activation conserved element (GRACE). Under low glucose levels, the LID inhibits the transactivation activity of the GRACE (M. V. Li et al., 2006). Consistently, deletion of LID results in a glucose-independent hyperactivation of ChREBP (Davies et al., 2010). The current model suggests that glucose/G6P directly binds to MondoA/ChREBP and derepresses the GRACE, causing a conformational change that allows its dimerization with Mlx. The C-terminus contains the bHLH domain that binds to the DNA, and the cytoplasmic and dimerization domain (CDC) that mediates the subcellular localization and interaction with Mlx (Eilers et al., 2002). In contrast, Mlx is a much smaller protein lacking the glucose-responsive domain and only contains the bHLH and CDC domains (Billin et al., 1999).

MondoA and ChREBP are also regulated by interaction with other proteins and post-translational modifications. The N-terminus of these transcription factors contain a nuclear localization signal (NLS) and two nuclear export signals (NES1 and NES2) that mediate the interaction with importin α/β and the chromosomal maintenance CMR1, respectively (De Luis et al., 2000; Eilers et al., 2002; Fukasawa et al., 2010; Ge et al., 2011). The MCRIII contains a 14-3-3 binding site that contributes to the cytosolic localization of both MondoA and ChREBP (Eilers et al., 2002; Sakiyama et al., 2008). The heterodimerization with Mlx is required for the nuclear translocation and DNA binding (T. Kawaguchi et al., 2001; Sans et al., 2006). mTORC1 can directly bind and suppress MondoA inhibiting the dimerization with Mlx (Kaadige et al., 2015). Interestingly, nuclear localization is not sufficient to induce the transcriptional activity of

MondoA/ChREBP (Davies et al., 2008; Peterson et al., 2010); thus, additional regulation is required for the expression of the downstream genes. Interestingly, MondoA was shown to localize with the mitochondrial outer membrane through protein-protein interaction and was proposed to serve as an energy sensor connecting mitochondria and the nucleus (Sans et al., 2006). However, the protein(s) involved in MondoA localization with mitochondria have not been identified yet. MondoA/ChREBP and Mlx have also been shown to bind LDs, thus decreasing the glucose-dependent transcriptional response (Mejhert et al., 2020).

Many kinases and phosphatases converge in the regulation of MondoA and ChREBP. The protein kinase A (PKA) and AMPK directly phosphorylate ChREBP and inhibit its function (Kabashima et al., 2003; Takumi Kawaguchi et al., 2002). ChREBP contains two important PKA phosphorylation sites, one in the NLS (S196) and one within the bHLH domain (T666), that inhibit the nuclear translocation and reduce the DNA-binding activity (Kabashima et al., 2003). In response to glucagon, PKA phosphorylates ChREBP and sequesters it in the cytoplasm through interaction with a 14-3-3 protein (T. Kawaguchi et al., 2001). AMP has been shown to directly bind to the ChREBP/14-3-3 heterodimer resulting in the increased affinity of ChREBP for 14-3-3 and stabilization of the heterodimer (Sato et al., 2016). Other PKA-independent phosphorylation sites have been identified to be essential for a glucose-mediated response (Tsatsos & Towle, 2006). However, the upstream kinases for these specific sites have yet to be discovered. Interestingly, the phosphorylation sites implicated in the glucose responsiveness of ChREBP are not conserved in MondoA (Sans et al., 2006). MondoA is a substrate for mTOR phosphorylation at S33, although this does not regulate MondoA transcriptional activity (Yu et al., 2011). Whether other kinases regulate MondoA remain elusive.

ChREBP activity is also regulated by acetylation and *O*-GlcNAcylation. ChREBP interacts with *O*-GlcNAc transferase (OGT) and is *O*-GlcNAcetylated, stabilizing the protein and enhancing its transcriptional activity (Guinez et al., 2011). Recently, *C. elegans* MML-1/Mondo has been suggested to be regulated by *O*-GlcNAcylation (Ceballos et al., 2021), although the function of this post-translational modification is yet to be determined. The histone acetyltransferase (HAT) coactivator p300 and the serine/threonine kinase salt-inducible kinase SIK2 are key upstream regulators of the ChREBP activity (Bricambert et al., 2010). Thus, the regulation of MondoA/ChREBP entails a complex network of metabolite binding, protein-protein interactions,

subcellular localization, and post-translational modifications required to fine-tune metabolic programming.

3.5.3 *Mondo proteins as nutrient sensors*

MondoA/ChREBP are nutrient sensors that orchestrate a transcriptional response to alter metabolism. Their transcriptional activity is regulated by sugars and suppressed by PUFAs (Dentin et al., 2004, 2005). One of the first works that linked nutrient levels to their activity was the observation that AMPK inhibited the DNA-binding activity of ChREBP by phosphorylation of S568 in rat primary hepatocytes, thus repressing the glucose-induced L-PK transcription (Takumi Kawaguchi et al., 2002). Under high glucose concentrations, ChREBP dephosphorylation is favored by phosphatases (PP2A) activity in the cytoplasm and nuclei. In the same work, the researchers suggested that the pentose phosphate intermediate, xylulose 5-phosphate, activates the PPase trimer, which dephosphorylates S196, S568, and T666 and enhances ChREBP transcriptional activity. In 2012, a group challenged the idea that xylulose 5-phosphate mediated this activation and suggested that glucose 6-phosphate (G6P) is the metabolite responsible for inducing ChREBP nuclear translocation and transcriptional activity upon glucose stimulation in hepatocytes (Dentin et al., 2012). Similarly, MondoA is activated by G6P in rat L6 myoblasts (Stoltzman et al., 2008) and other hexose phosphates in HA1ER cells (Stoltzman et al., 2011). Fructose 2,6-biphosphate is also required to recruit ChREBP to the glucose-6-phosphatase and L-PK promoters in hepatocytes (Arden et al., 2012), suggesting that multiple metabolites modulate the activity of these transcription factors. However, whether MondoA or ChREBP senses the nutrients' level by directly binding specific metabolites or through other effectors has yet to be determined.

3.5.4 *MondoA/ChREBP downstream targets*

Glucose is the most important carbohydrate, and its metabolism is coupled to the specific function of the tissue where it is consumed (**Figure 8**). In the liver, glucose is mainly used for *de novo* lipogenesis and subsequent TAG synthesis that are transported and stored in the adipose tissue. ChREBP is primarily expressed in liver and adipose tissue and regulates lipogenic genes. L-PK was the first reported direct target of the ChREBP (Yamashita et al., 2001). Thereafter, many genes are regulated by ChREBP upon glucose stimulation, including genes involved in lipogenic

pathways like the stearoyl-CoA desaturase SCD-1, fatty acid elongase 6 ELOVL6, glycerol 3-phosphate dehydrogenase GPDH, ACC, and FAS (Iizuka et al., 2008; Ishii et al., 2004; Jeong et al., 2011; Pongvarin et al., 2015). Moreover, ChREBP regulates the glucose-induced expression of glucose-6-phosphate dehydrogenase (G6PDH), the rate-limiting enzyme of the PPP (Ma et al., 2006). This enzyme converts G6P to 6-phosphogluconolactone and produces NADPH required for *de novo* lipogenesis and other reactions.

On the other hand, muscle is highly dependent on glucose to sustain muscle contraction and endurance. MondoA is highly expressed in the skeletal muscle and regulates many genes involved in glycolysis, such as hexokinase HKII, lactate dehydrogenase LDH-A, and 6-phospho-2-fructokinase/fructose-2,6-biphosphatase PFKFB3, and transketolase (Billin et al., 2000; Sans et al., 2006) (**Figure 8**). The thioredoxin-interacting protein TXNIP and its paralog ARRDC4 are the best-characterized downstream targets of MondoA. TXNIP belongs to the alpha-arrestin protein family and is an important regulator of redox signaling. High glucose levels upregulate TXNIP expression in a MondoA-dependent manner and functions as a potent negative regulator of glucose uptake (Stoltzman et al., 2008). TXNIP regulates glucose uptake by directly binding to GLUT1 inducing its internalization by clathrin-mediated endocytosis, and reducing GLUT1 mRNA (N. Wu et al., 2013), consequently controlling glucose metabolism through negative feedback.

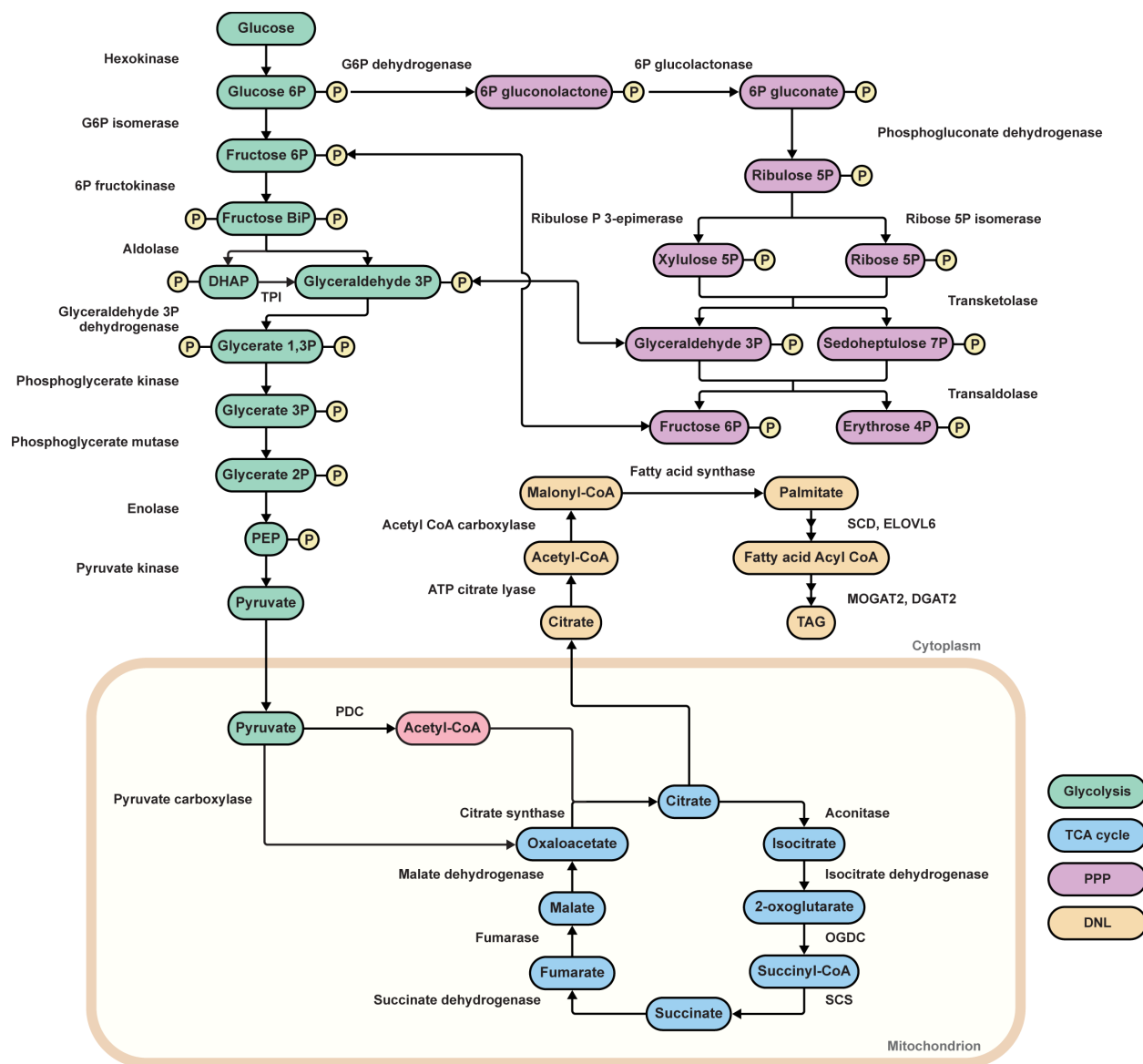


Figure 8. Glucose metabolism and *de novo* lipid biogenesis. Glucose can be oxidized via glycolysis to pyruvate, which can be imported to the mitochondria. Mitochondrial pyruvate can be converted to acetyl-CoA or oxaloacetate to enter the TCA cycle. G6P can also be diverted to other branches like the PPP. In the presence of excess glucose, citrate can be exported to the cytoplasm and be used for *de novo* lipogenesis and TAG synthesis. G6P, glucose 6-phosphate; DHAP, dihydroxyacetone phosphate; TPI, triosephosphate isomerase; PEP, phosphoenolpyruvate; PDC, pyruvate dehydrogenase complex; OGDC, oxoglutarate dehydrogenase complex; SCS, succinyl CoA synthase; SCD, stearoyl-CoA desaturase; ELOVL6, elongation of very-long-chain fatty acids protein 6; MOGAT2, monoacylglycerol *O*-acyltransferase 2; DGAT2, diacylglycerol *O*-acyltransferase homolog 2; DNL, *de novo* lipogenesis.

3.5.5 Metabolic disorders associated with MondoA/ChREBP

Due to their critical role in regulating metabolism, MondoA and ChREBP have been implicated in numerous metabolic disorders in humans, including type 2 diabetes, metabolic syndrome, and cancer. ChREBP knockout mice display various metabolic defects, including reduced liver fatty acid levels and adiposity, hyperglycemia, and increased insulin and glycogen levels (Iizuka et al., 2004). Overexpression of dominant-negative Mlx improved glucose intolerance in diabetes-prone mice with metabolic syndrome (Iizuka et al., 2008). Moreover, ChREBP knockout mice cannot survive on a high-sucrose and -fructose diet (Iizuka et al., 2004). MondoA knockout mice are viable and have average body weight, glucose levels, and plasma lipid profiles; however, they have increased serum lactate and alanine levels and utilize fatty acids for fuel during exercise (Imamura et al., 2014).

ChREBP was initially identified as a gene deleted in William-Beuren Syndrome, a neurodevelopmental disorder characterized by multiple physiological abnormalities, including cardiovascular complications and diabetes (De Luis et al., 2000). Genome-wide screens have identified variations in the ChREBP gene associated with high plasma triglyceride levels, elevated plasma liver enzymes, and increased risk for coronary artery disease (Kathiresan et al., 2008; Kooner et al., 2008; J. Wang et al., 2008). Increased *de novo* lipogenesis by ChREBP- β isoform is linked to metabolic risk markers and obesity (Eissing et al., 2013). However, in adipose tissue, expression levels of ChREBP- β have been found to positively correlate with insulin sensitivity and glucose tolerance in humans, and this factor has been proposed as a therapeutic target for treating type 2 diabetes and obesity (Herman et al., 2012; Kursawe et al., 2013).

Non-alcoholic fatty liver disease (NAFLD) is characterized by excessive TAG accumulation in the liver and is linked with insulin resistance, type 2 diabetes, and obesity (Cheung & Sanyal, 2009; Marchesini et al., 2001). NAFLD is characterized by steatosis and abnormal fat accumulation in hepatocytes. This disease can develop into non-alcoholic steatohepatitis (NASH) and subsequently into cirrhosis and liver cancer (Hassan et al., 2014). ChREBP has been linked to the pathophysiology of NAFLD, leading to hepatic steatosis and insulin resistance (Denechaud et al., 2008). Conversely, increased ChREBP activity has also been shown to dissociate hepatic steatosis from insulin resistance by converting saturated fatty acids to MUFAs, which has beneficial effects on glucose and lipid metabolism (Benhamed et al., 2012). Thus, modulation of ChREBP activity can potentially protect NAFLD patients from developing diabetes.

The obese ob/ob mouse model has been extensively used to study insulin resistance, metabolic disorders, and type 2 diabetes (Genuth, 1969). These mice have mutations that alter leptin production, resulting in excessive eating behavior (Campfield et al., 1996; Friedman et al., 1991). Liver-specific inhibition of ChREBP or knockout in ob/ob mice displays improved metabolic profiles, including reduced lipogenic genes expression, decreased hepatic fatty acid synthesis, improved glucose tolerance, normalization of plasma free fatty acids, and triglyceride levels (Iizuka et al., 2006; Postic et al., 2007).

MondoA and ChREBP have been implicated in metabolic reprogramming in cancer. Tumor cells rely mainly on aerobic glycolysis to sustain the high energy demands for anabolic reactions in a phenomenon called the Warburg effect (Liberti & Locasale, 2016; Warburg, 1925). Increased ChREBP activity in colorectal and hepatic cancer models has been shown to mediate the increase in glycolysis, *de novo* lipogenesis, and nucleotide biosynthesis (Tong et al., 2009). Dysregulation of Myc reprograms cells to promote neoplasia, abnormal growth of cells, dependent on MondoA (Carroll et al., 2015). Indeed, MondoA knockdown induces apoptosis, and Myc/MondoA co-regulated genes correlate with the outcome of diverse cancers. Thus, MondoA and ChREBP are suitable therapeutic targets for treating metabolic disorders and cancer.

3.5.6 MML-1/MXL-2 as convergent mechanisms of aging

MML-1 and MXL-2 were identified in our lab in an RNAi screen looking for suppressors of the germline longevity (Nakamura et al., 2016). Interestingly, both MML-1 and the binding partner MXL-2 were required for lifespan extension mediated by reduced insulin and mTOR signaling and decreased mitochondria activity longevity (D. W. Johnson et al., 2014; Nakamura et al., 2016) (**Figure 9**). MML-1 and HLH-30/TFEB share many downstream targets and processes, including genes involved in amino acid and fatty acid metabolism, autophagy, and longevity. MML-1 downregulates the mTORC1 signaling by suppressing the leucyl tRNA synthetase *lars-1*, an upstream activator of mTORC1. On the other hand, mTORC1 knockdown triggers transcriptional activation of MML-1 and MXL-2, thus suggesting that these transcription factors also work downstream of mTOR. This mechanism is proposed to be evolutionarily conserved as MondoA and ChREBP stimulate TFEB nuclear localization upon starvation in cells (Nakamura et al., 2016). Moreover, MML-1 and MXL-2 have been suggested to regulate the transcription factor NHR-49/PPAR α to promote MUFAs and inhibit mTORC1 signaling (Karalay, unpublished).

However, it is still unknown how these transcription factors integrate multiple upstream signals to regulate longevity.

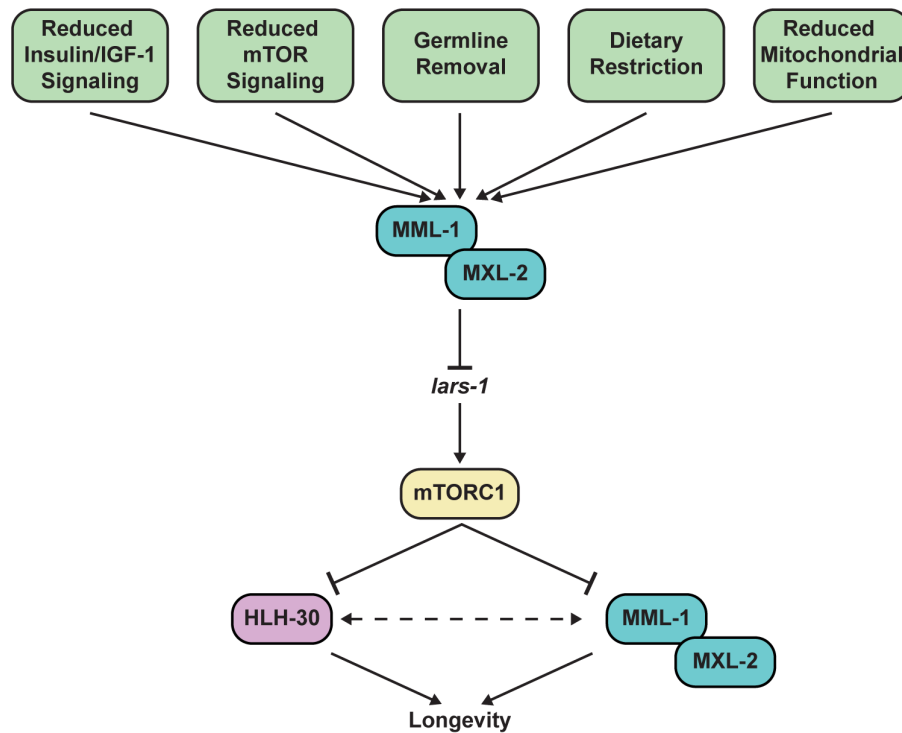


Figure 9. MML-1/MXL-2 are convergent factors that mediate longevity. MML-1/MXL-2 are pro-longevity transcription factors required for the lifespan extension mediated by multiple longevity pathways. When active, MML-1 and MXL-2 downregulate mTORC1 signaling through decreasing *lars-1*. Moreover, mTORC1 negatively regulates MML-1. MML-1 and the transcription factor HLH-30 regulate each other to extend lifespan—adapted from (Nakamura et al., 2016).

IV. Research Aims

As described previously, organisms have developed complex mechanisms to sense nutrient levels and adapt their metabolism accordingly. How do these mechanisms translate the metabolic state to a transcriptional response? MondoA and ChREBP are two main transcription factors that coordinate carbohydrate and lipid metabolism. However, much of the work has been done in specific cell types where metabolic communication between tissues cannot be addressed. Thus, *C. elegans* presents an excellent model organism to study this regulatory network due to the simplified pathway but being a complex multicellular organism. It will also give us insights into how nutrient sensing and transcriptional response translate to health and longevity.

In *C. elegans*, the transcriptional complex formed by MML-1/MXL-2 is part of an integrated helix-loop-helix (HLH) network required for lifespan extension in diverse longevity pathways (D. W. Johnson et al., 2014; Nakamura et al., 2016). Our lab demonstrated many of the downstream signals regulated by these transcription factors, including the mutual regulation with HLH-30 and crosstalk with the mTOR signaling (Nakamura et al., 2016). However, the upstream metabolic signals that regulate MML-1/MXL-2 in complex organism-wide settings and how this translates to longevity are still not well understood. Therefore, this thesis project has two main aims:

1. Determine the upstream signals that regulate MML-1 in *C. elegans*
2. Investigate the role of MML-1/MXL-2 in different longevity backgrounds

V. Results

Chapter I. Regulation of MML-1 by glucose metabolism

5.1 *Glucose metabolism genes regulate MML-1*

MondoA has been reported to respond to glucose 6-phosphate (G6P) and other hexose phosphate sugars in cultured cells (Stoltzman et al., 2008, 2011). Nevertheless, little is known about the regulation of MondoA in a whole-organism-wide setting. Most of the work has focused on the molecular mechanisms downstream of this transcription factor. Hence, we decided to investigate how MML-1 is regulated by glucose metabolism. To address this, we performed a targeted RNA interference (RNAi)-based screen to knock down genes encoding enzymes involved in glucose metabolism. We tested 83 RNAi clones that target glycolysis, pyruvate oxidation and metabolism, tricarboxylic acid (TCA) cycle, pentose phosphate pathway (PPP), hexosamine pathway, gluconeogenesis, glycogenesis, glycogenolysis, and the trehalose pathway. We used an MML-1::GFP reporter line to measure the nuclear localization in the intestine of adult animals as a proxy of its function.

Overall, we found a preponderance of decreased MML-1 nuclear localization when knocking down various genes involved in glucose metabolism (**Figure 10, Supplementary Table 4**). Most of the enzymes involved in glycolysis and knockdown of pyruvate dehydrogenase complex, which links glycolysis to the TCA via acetyl-CoA, decreased accumulation of nuclear MML-1. Interestingly, while most enzymes in the TCA cycle decreased nuclear MML-1, inhibition of the oxoglutarate dehydrogenase complex (OGDC) subunits *ogdh-1* and *dld-1* increased MML-1 nuclear localization. Subsequent steps, including the succinyl-CoA synthetase (SCS) beta subunits *sucg-1* and *suca-1*, and the succinate dehydrogenase (SDH) flavoprotein subunit *sdha-1*, also increased MML-1 nuclear accumulation. SDH functions in both the TCA and electron transport chain (ETC) by oxidizing succinate to fumarate and reducing ubiquinone to ubiquinol, respectively. We also observed that the knockdown of enzymes involved in the oxidative and non-oxidative branches of the PPP, phosphogluconate dehydrogenase (PGDH) *T25B9.9*, and transketolase *tkt-1* genes, respectively, triggered a strong increase in MML-1 nuclear accumulation. Taken together, these data suggest that overall changes in glucose metabolism regulate MML-1 and that this transcription factor may sense the divergence of G6P to different branches of this network.

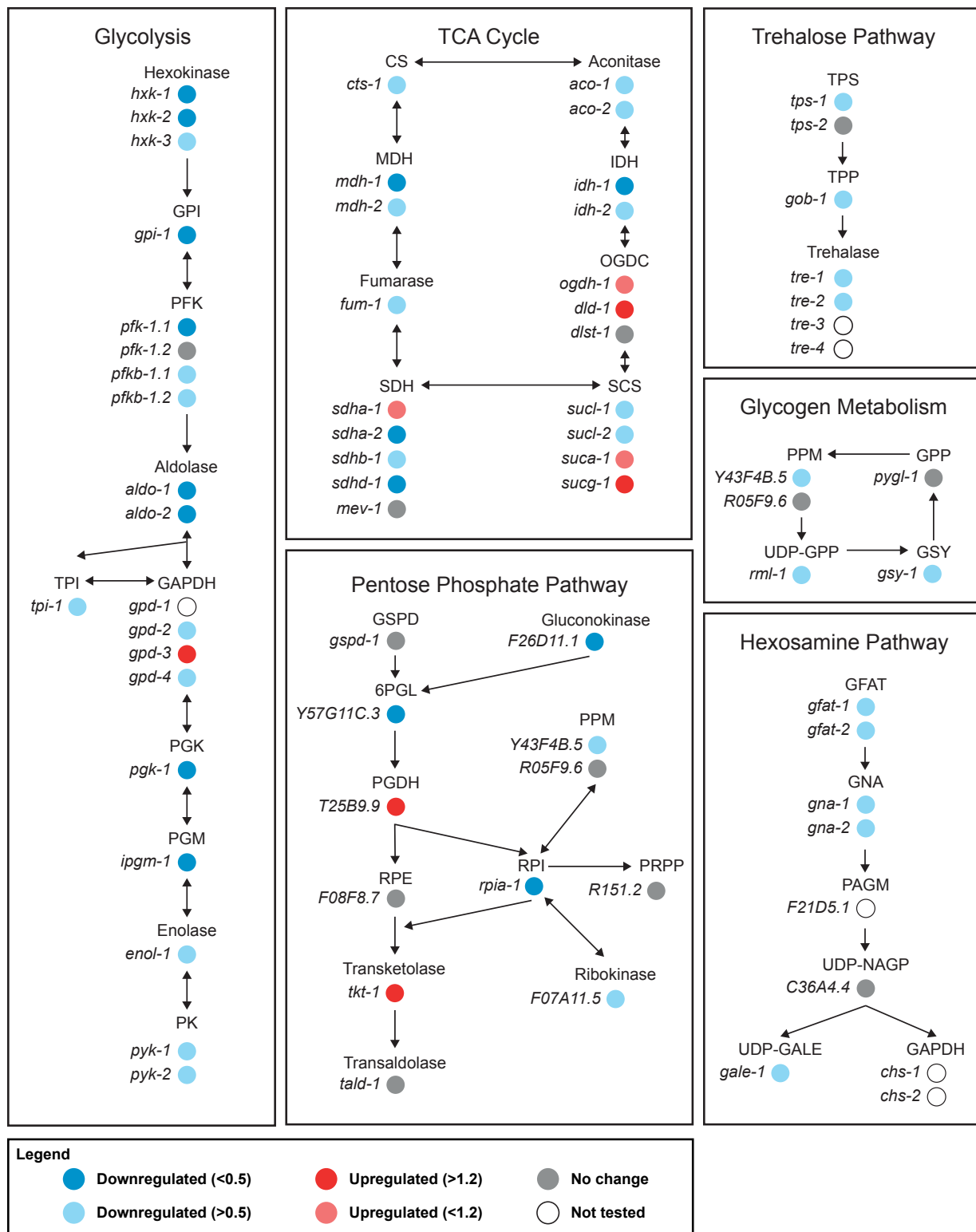


Figure 10. Glucose metabolism genes regulate MML-1 nuclear localization. Worms were grown egg on in the indicated RNAi until day one of adulthood, and MML-1::GFP nuclear localization was measured in the intestine. Circles are color-coded to indicate the increase and decrease of MML-1::GFP nuclear localization by RNAi knockdown of the indicated genes. All

the data were normalized to luciferase RNAi internal control (*luc* RNAi). See **Supplementary Table 4** for statistical analysis and a complete list of genes ($N \geq 2$).

5.2 The induction of cellular stress pathways does not regulate MML-1 nuclear localization

Many of the genes that regulate MML-1 localization are involved in mitochondrial metabolism, such as OGDC and SCS, and inhibition of these complexes could activate stress response pathways. Hence, we assessed whether MML-1 nuclear localization was associated with activation of cellular stress response pathways under conditions where MML-1 nuclear localization was increased or decreased. As readouts, we used transcriptional reporters for cytosolic stress response *hsp-16.2p::GFP*, ER stress response *hsp-4p::GFP*, and mitochondrial stress response *hsp-6p::GFP*. None of the genes that regulate MML-1 nuclear localization affected the expression of *hsp-16.2p::GFP* (**Figure 11A**). *hvk-2i* significantly increased the expression of *hsp-4p::GFP*, while *sucl-1i*, *suca-1i*, and *sucg-1i* showed decreased expression compared to control (**Figure 11B**). As expected, we also saw an increased expression of *hsp-6p::GFP* upon knockdown of mitochondrial components *ogdh-1*, *sucl-1*, and *sucl-2* (**Figure 11C**). However, inducing mitochondrial stress with Antimycin A (AA), a Complex III inhibitor, did not affect MML-1 nuclear localization nor rescue it under *hvk-2i* (**Figure 11D**). Taken together, these data show no consistent correlation between MML-1 nuclear localization and induction of cellular stress responses.

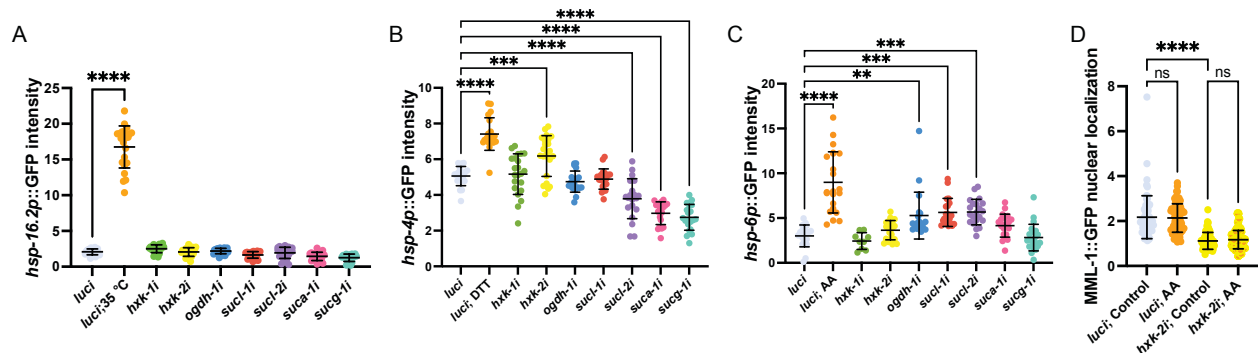


Figure 11. The regulation of cellular stress pathways does not explain MML-1 nuclear localization. A-C. Quantification of *hsp-16.2p::GFP* (A), *hsp-4p::GFP* (B), and *hsp-6p::GFP* (C) transcriptional reporters representing cytosolic heat shock, ER stress, and mitochondrial stress response outputs, respectively, upon knockdown of the specified RNAi. Worms were imaged on day one adult stage. For positive controls, day one adult worms were transferred to 35 °C for 2 h to induce *hsp-16.2p::GFP*. For *hsp-4p::GFP* and *hsp-6p::GFP* induction, worms were grown until

the L4 stage and subjected to dithiothreitol (DTT) 5 mM or Antimycin A (AA) 10 µg/mL for 24 h, respectively. **D.** MML-1::GFP nuclear localization of day one adult worms grown under *hxx-2i*. AA was added at the L4 stage, and nuclear localization was measured after 24 h (N=3). Significance was calculated with a one-way ANOVA test. **A-D** bars represent mean + SD.

5.3 Hexokinases as upstream regulators of MML-1 localization and function

Our screen revealed that hexokinase knockdown had the most potent effect in decreasing MML-1 nuclear localization. This enzyme is involved in the first step of glucose metabolism, phosphorylating glucose to G6P, and is a critical mediator of cellular metabolism (**Figure 12A**). Among the three *C. elegans* hexokinase genes, *hxx-1* and *hxx-2* more strongly affected MML-1 nuclear localization. To confirm this finding, we used an independent MML-1::GFP reporter line (wgIs198 [*mml-1::TY1::EGFP::3xFLAG(92C12)* + *unc-119(+)*]) and again found that MML-1 nuclear accumulation was significantly reduced upon *hxx-1* and *hxx-2* knockdowns (**Figure 12B**). We also saw that *mml-1* mRNA levels were unaffected by *hxx* knockdown, indicating that these hexokinases regulate MML-1 at a post-transcriptional level (**Figure 12C**).

To test the specificity of RNAi knockdown, we tagged each of the three endogenous hexokinase loci with the fluorescent protein mKate2 by CRISPR/Cas9. We used these strains to evaluate the protein levels by Western blot and found that each RNAi was specific (**Figure 12D and E**). As glycolysis is essential during development, we measured the size (area and length) of worms fed with hexokinase RNAi egg on. However, *hxx-1i* and *hxx-2i* displayed no significant change in worm growth, while *hxx-3i* treated animals were somewhat smaller (**Figure 12F and G**). To determine if our observations were due to a change in food intake, we counted pharyngeal pumping rate but found no significant difference compared to control (**Figure 12H**), nor did we see an effect on the motility of worms (**Figure 12I**). Taken together, these data indicate that there is no RNAi cross-reactivity among the hexokinase isozymes and that the effects on MML-1 nuclear localization are not due to a decrease in food consumption.

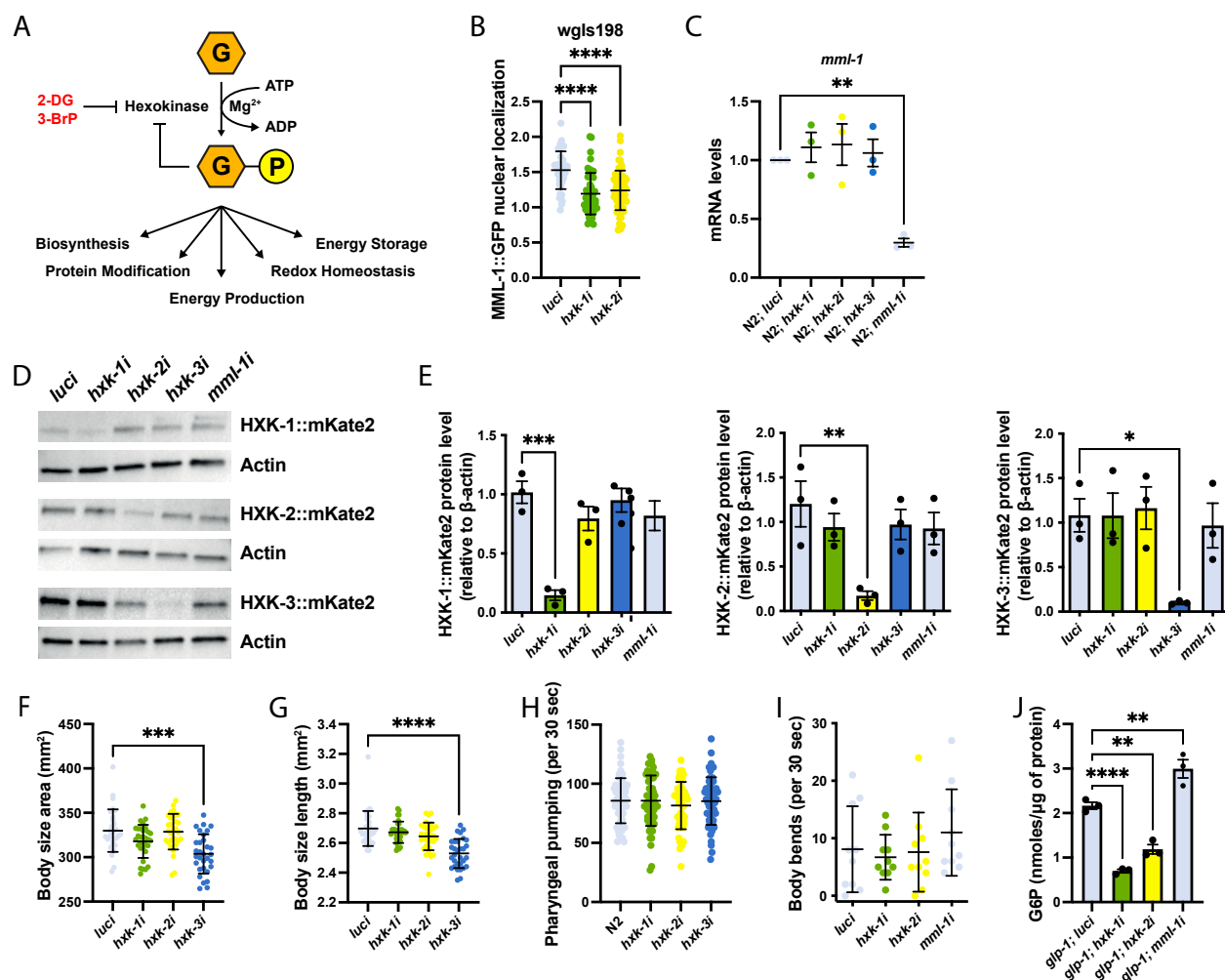


Figure 12. Hexokinase 1 and 2 regulate MML-1 localization. **A.** Hexokinase phosphorylates glucose to glucose 6-phosphate (G6P). G6P can then be diverted to multiple pathways, including being further metabolized in glycolysis for energy production and biosynthesis, used as a substrate for glycosylation/acetylation, stored as glycogen and triacylglycerol (TAG), or for glutathione reduction in redox homeostasis. **B.** MML-1 nuclear localization was quantified in intestinal cells of day one adult worms using the fosmid line *wgl-198* (N=3). **C.** *mml-1* mRNA levels under hexokinase knockdown measured by qPCR analysis (N=3). **D-E.** Representative Western blot (**D**) and densitometry analysis (**E**) of hexokinase basal levels under *hpk-1*, *hpk-2*, *hpk-3*, and *mml-1* (N=3). **F-I.** Measurements of body size area (**F**), length (**G**), and pharyngeal pumping rate (**H**) of day one adult worms grown under hexokinase knockdown (N=3). **I.** Thrashing assay of day one adult worms grown in the indicated RNAi reported as the body bends after transfer to M9 buffer (N=2). Significance was calculated with a one-way ANOVA test. **J.** Quantification of G6P levels relative to total protein in day one adult *glp-1(e2141)* mutants under the indicated RNAi (N=3). Statistical significance was calculated with one-way ANOVA. **C** statistical significance was calculated with a two-tailed *t*-test. **B, F, G, H, and I** bars represent mean + SD. **C, E, and J** bars represent mean + SEM.

Consistent with their biochemical function as hexokinases, we found that *hxx-1* and *hxx-2* knockdown was sufficient to reduce endogenous G6P levels compared to control (**Figure 12J**). To test whether the phosphotransferase activity of hexokinase is responsible for regulating MML-1 nuclear localization, we used two drugs to inhibit hexokinases pharmacologically. 3-Bromopyruvate (3-BrP) is an HKII inhibitor, and 2-deoxy-glucose (2-DG) is an analog of glucose phosphorylated to 2-DG6P but cannot be further metabolized, thus inhibiting hexokinase function. Supplementation of both drugs significantly decreased MML-1 nuclear localization compared to control (**Figure 13A and B**).

Changes in MML-1 nuclear localization would be expected to modulate its transcriptional activity. To test this idea, we next analyzed the expression of downstream targets reportedly linked to gonadal longevity (Nakamura et al., 2016) under hexokinase knockdown. We observed decreased *lgg-2*, *mdl-1*, *swt-1*, and *fat-5* expressions under *hxx-1i* and *hxx-2i*, but not under *hxx-3i* (**Figure 13C**), consistent with decreased MML-1 transcriptional activity. Collectively, these data indicate that hexokinases are upstream regulators of MML-1 nuclear localization and transcriptional function in *C. elegans*.

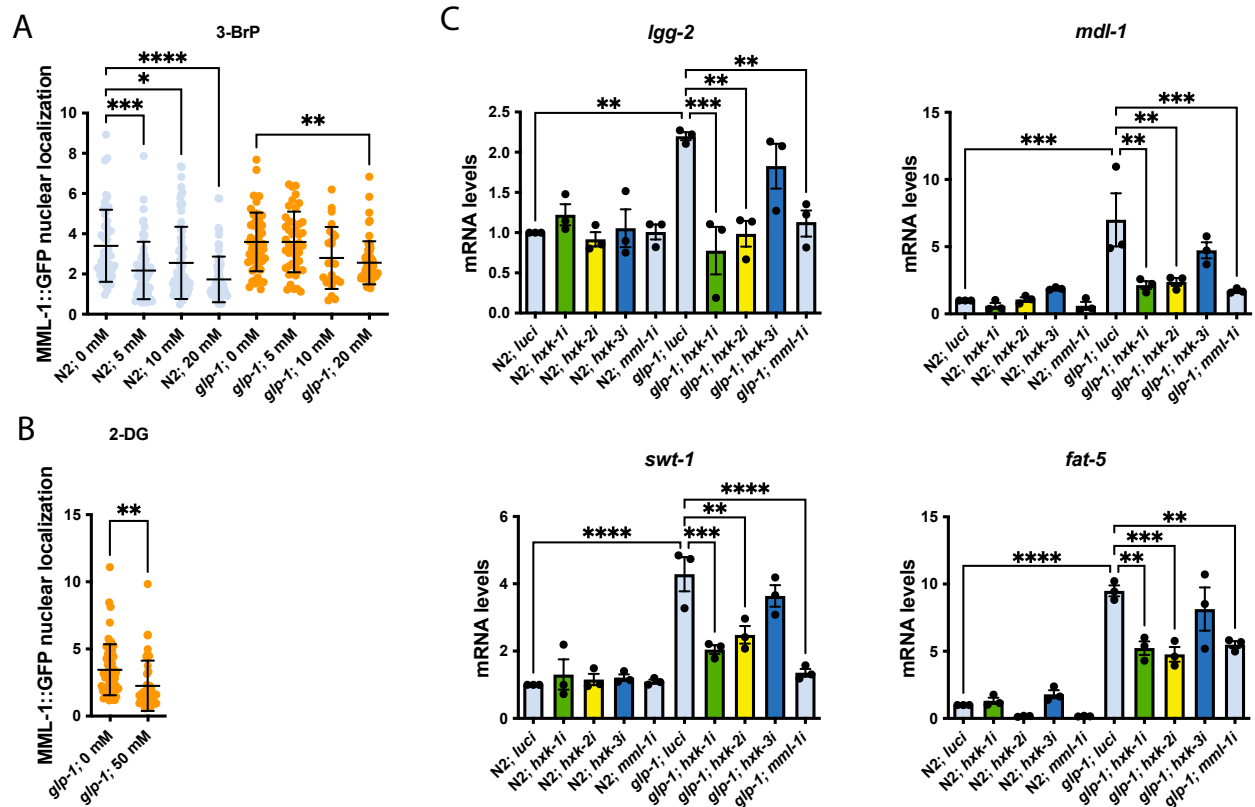


Figure 13. Hexokinases regulate MML-1 transcriptional activity. **A.** MML-1 nuclear localization was quantified in intestinal cells of day one adult N2 and *glp-1(e2141)* worms grown egg on with 5 to 20 mM 3-bromopyruvate (3-BrP) (N=2). Statistical significance was calculated with one-way ANOVA. **B.** MML-1 nuclear localization of day one adult *glp-1(e2141)* worms grown egg on with 50 mM of 2-deoxy-glucose (2-DG) (N=2). Statistical significance was calculated with *t*-test. **C.** Relative mRNA levels of MML-1 downstream targets in young adult worms measured by qPCR (N=3). Statistical significance was calculated with a two-tailed *t*-test. **A** and **B** bars represent mean + SD. **C** bars represent mean + SEM.

5.4 Hexokinases are required for germline-removal and reduced mitochondrial function longevity pathways

Previous studies have demonstrated that MML-1 and MXL-2 are required for the lifespan extension in multiple longevity pathways, including germline-less *glp-1(e2141)*, reduced mitochondrial activity *isp-1(qm150)*, and the insulin signaling hypomorphic mutant *daf-2(e1370)* (Nakamura et al., 2016). Hence, we tested whether hexokinases influenced MML-1 subcellular localization in these longevity models. For this, we crossed the MML-1::GFP reporter line to these genetic backgrounds and measured MML-1 localization in the intestine of day one adult worms (**Figure 14A**). As expected, MML-1 nuclear localization was increased in *glp-1(e2141)* as reported previously (Nakamura et al., 2016) (**Figure 14B**) as well as in *isp-1(qm150)* compared to wildtype (**Figure 14C**). Upon *hxx-1* and *hxx-2* knockdown, MML-1 nuclear localization was decreased in wildtype, *glp-1(e2141)*, and *isp-1(qm150)* longevity models (**Figure 14B and C**). Surprisingly, we found no significant difference in MML-1 localization in *daf-2(e1370)* compared to wildtype, and localization was unaffected by hexokinase knockdown in this mutant (**Figure 14D**). Taken together, these data suggest that *hxx-1* and *hxx-2* are upstream regulators of MML-1 in a pathway-specific manner.

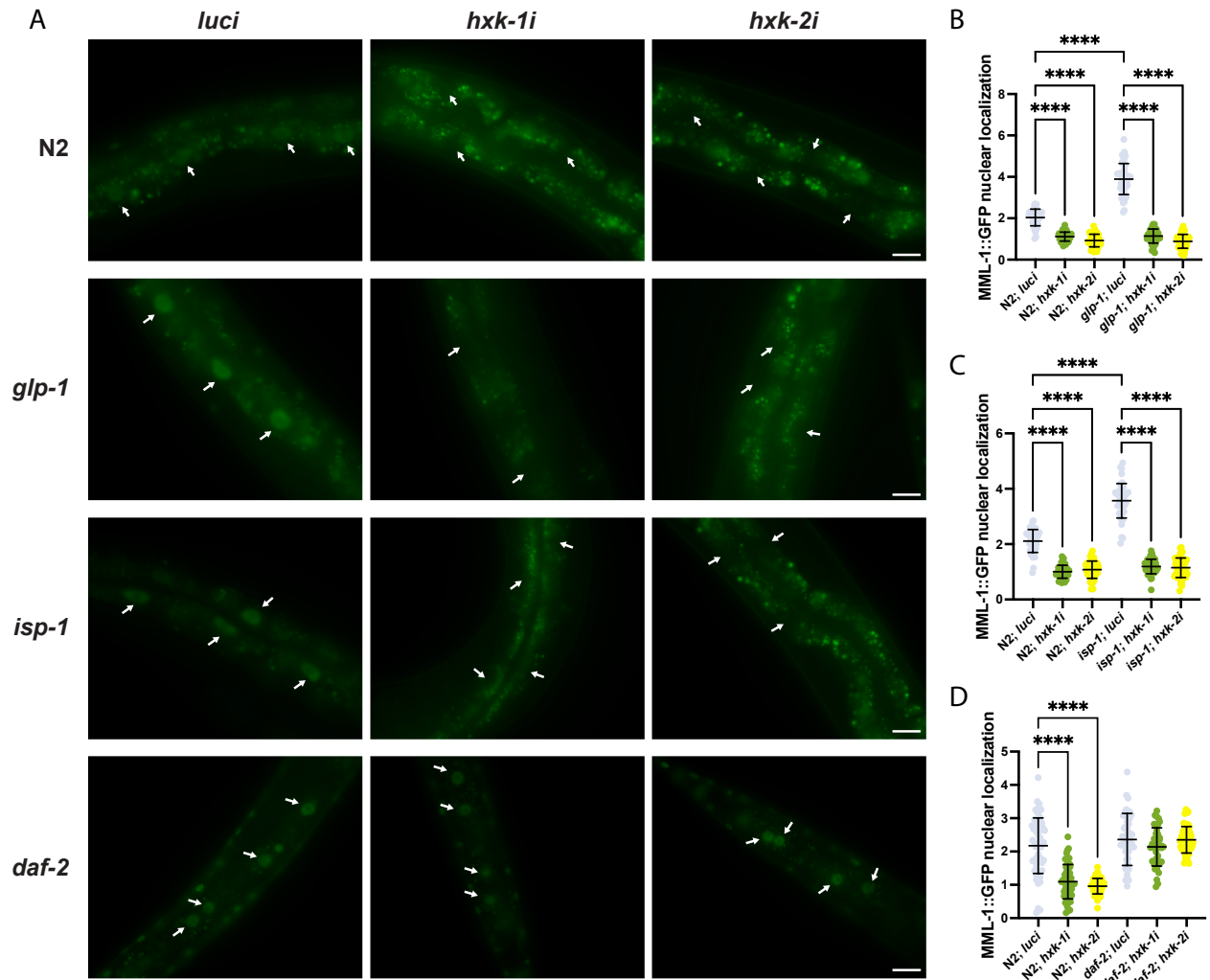


Figure 14. *hxk-1* and *hxk-2* are required for MML-1 nuclear localization in germline and mitochondrial longevity models. **A.** Representative images of MML-1 nuclear localization in wildtype and different longevity backgrounds. MML-1::GFP was quantified in nuclei from intestinal cells (white arrows) in day one adult worms. **B-D.** Quantification of MML-1 nuclear localization in *glp-1(e2141)* (**B**), *isp-1(qm150)* (**C**), and *daf-2(e1370)* (**D**) (N=3). Significance was calculated with a one-way ANOVA test. **A** scale bars represent 20 μ m. **B, C, and D** bars represent mean + SD.

Aside from MML-1 and MXL-2, DAF-16/FOXO and HLH-30/TFEB are other major transcription mediators of metabolism and longevity (Lin et al., 2018). In particular, MML-1 and HLH-30 have been shown to regulate each other's nuclear localization through downregulation of the mTOR signaling (Nakamura et al., 2016). Therefore, we next asked whether the effect of hexokinase was specific to MML-1 or whether it also regulates HLH-30 or DAF-16. We used an HLH-30::GFP reporter in N2 and *glp-1(e2141)* backgrounds and the DAF-16::GFP reporter in N2

and *daf-2(e1370)* backgrounds to monitor the localization of these transcription factors. We observed increased HLH-30 nuclear localization upon *hxxk-2i* in the wildtype background (**Figure 15A and B**). As seen previously, *mml-1i* in the *glp-1(e2141)* background reduced HLH-30::GFP nuclear localization, whereas hexokinase knockdown had no effect (**Figure 15A and B**). DAF-16 nuclear localization was also unaffected by hexokinase knockdown in wildtype or *daf-2(e1370)* (**Figure 15C and D**). Taken together, these data indicate that hexokinases specifically regulate MML-1 nuclear localization in these contexts.

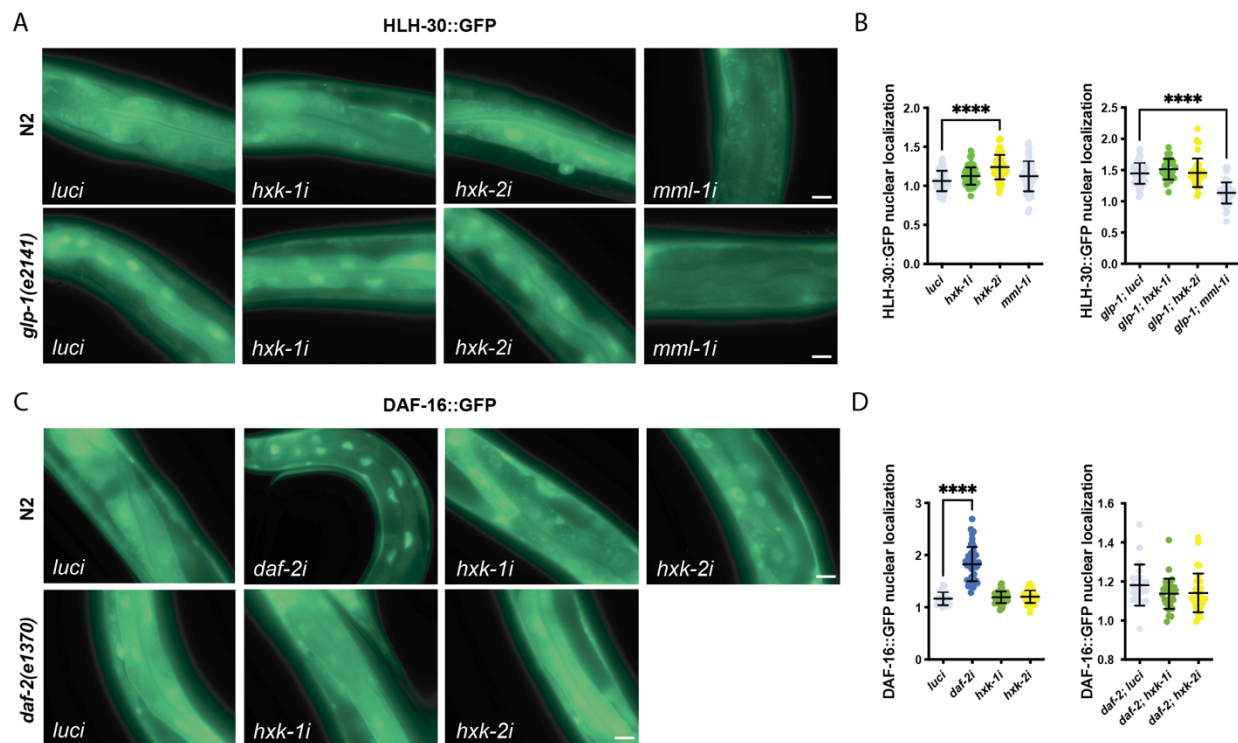


Figure 15. The nuclear localization of HLH-30 and DAF-16 is not affected by hexokinase knockdown. A-B. Representative images (A) and quantification (B) of nuclear localization in intestinal cells of day one adult worms expressing HLH-30::GFP in wildtype and *glp-1(e2141)* under *hxxk-1i*, *hxxk-2i*, and *mml-1i* (N=3). C-D. Representative images (C) and quantification (D) of nuclear localization in intestinal cells of day one adult worms expressing DAF-16::GFP in wildtype and *daf-2(e1370)* under *hxxk-1i*, *hxxk-2i*, and *daf-2i* (N=3). Significance was calculated with a one-way ANOVA test. A and C scale bars represent 20 μ m. B and D bars represent mean + SD.

Since hexokinase knockdown decreases MML-1 nuclear localization in the longevity models, we reasoned that the lifespan might also be abolished. Accordingly, *hxxk-1i* and *hxxk-2i*

significantly decreased *glp-1(e2141)* and *isp-1(qm150)* longevity but had no significant effect on wildtype lifespan (**Figure 16A and B**). Interestingly, *hxx-1* and *hxx-2* knockdown also did not affect *daf-2(e1370)* longevity, even though *mml-1* is required for life span extension in this mutant (**Figure 16C**). This is consistent with our observation that MML-1 nuclear localization is not affected by hexokinase knockdown in the *daf-2(e1370)* mutants. Collectively, these data suggest that *hxx-1* and *hxx-2* are specifically required for MML-1 function in germline and mitochondria longevity pathways.

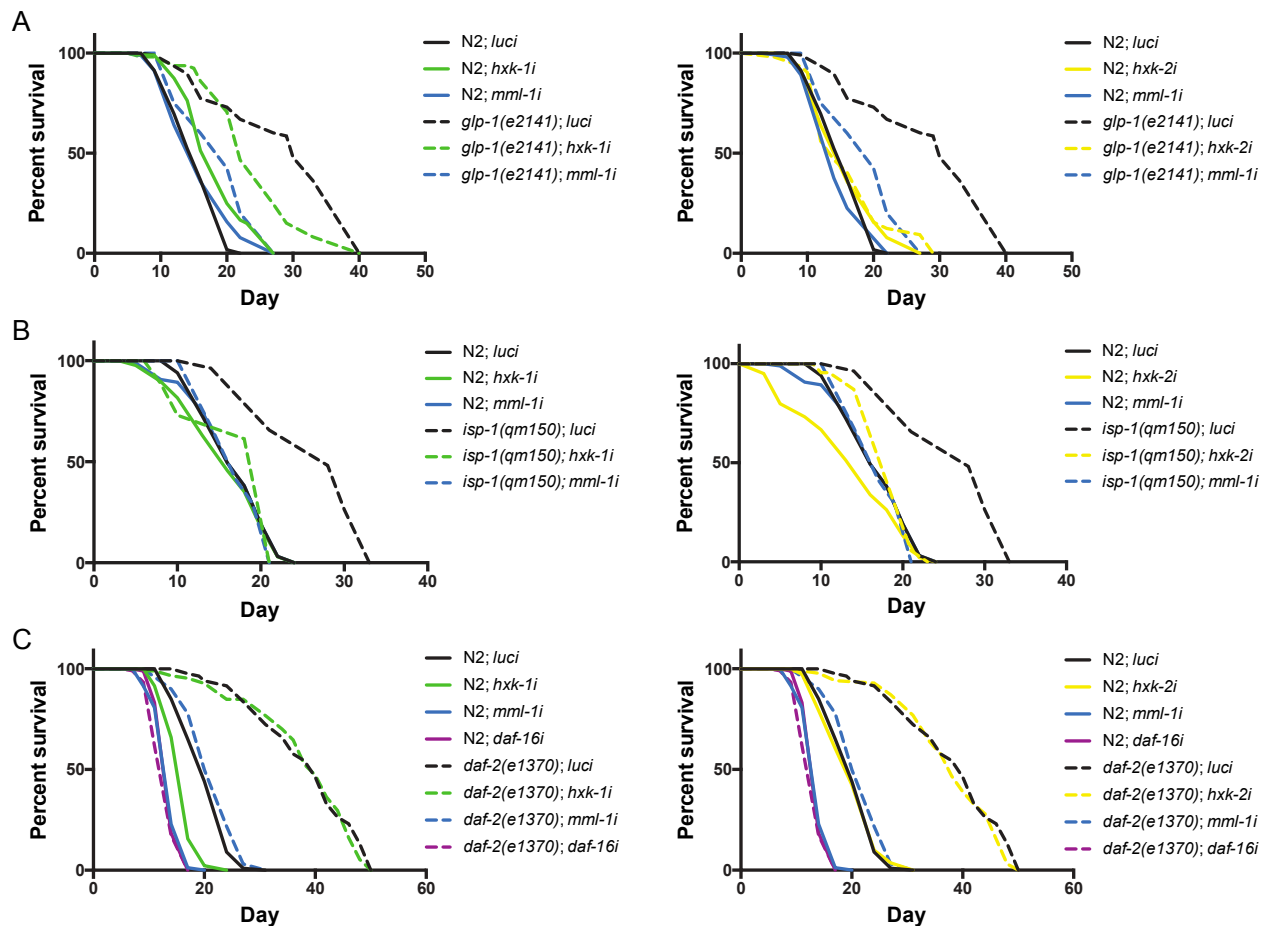


Figure 16. *hxx-1* and *hxx-2* are required to extend lifespan in germline and mitochondrial longevity pathways. A-C. *hxx-1i* and *hxx-2i* suppress the longevity of germline-less *glp-1(e2141)* (A) and reduced mitochondrial function *isp-1(qm150)* (B) mutants but are not required for the longevity of insulin signaling *daf-2(e1370)* mutant (C). Lifespans of *hxx-1i* and *hxx-2i* and each longevity model were performed in the same experiment and plotted separately for clarity; therefore, controls lifespans are shared between plots. See **Supplementary Table 5** for biological replicates and statistical analysis.

5.5 Hexokinase knockdown increases MML-1 mitochondrial localization

Since we saw a decrease in MML-1 nuclear localization upon hexokinase knockdown, we wondered whether MML-1 might re-localize to another subcellular compartment. To test this idea, we crossed the MML-1::GFP reporter strain with two compartmental markers and examined colocalization by confocal microscopy. We first looked at the lysosome/endosome reporter strain LMP-1::mKate2 but saw no evident colocalization in intestinal cells upon *hxx-2* knockdown or control conditions (**Figure 17A, B, and C**). We had previously shown that MML-1 localizes with mitochondria in the hypodermis; however, this subcellular localization in other tissues had not been examined (Nakamura et al., 2016). Hence, we crossed the MML-1::GFP strain with the mitochondrial reporter TOMM-20::mCherry under the intestinal promoter *ges-1* and confirmed that MML-1 localized with mitochondria in the intestine (**Figure 17D and E**). Under normal conditions, around 60-80% of the total MML-1 is nuclear, and 15% co-localizes with mitochondria. Interestingly, MML-1 mitochondrial localization was increased to 62% of total MML-1 upon *hxx-2i* (**Figure 17F**). Taken together, our data indicate that upon *hxx-2* knockdown, MML-1 is excluded from the nucleus and re-localizes to a subset of mitochondria; however, we cannot exclude the possibility that MML-1 interacts with other organelles like the endoplasmic reticulum (ER) and lysosome-related organelles (LRO).

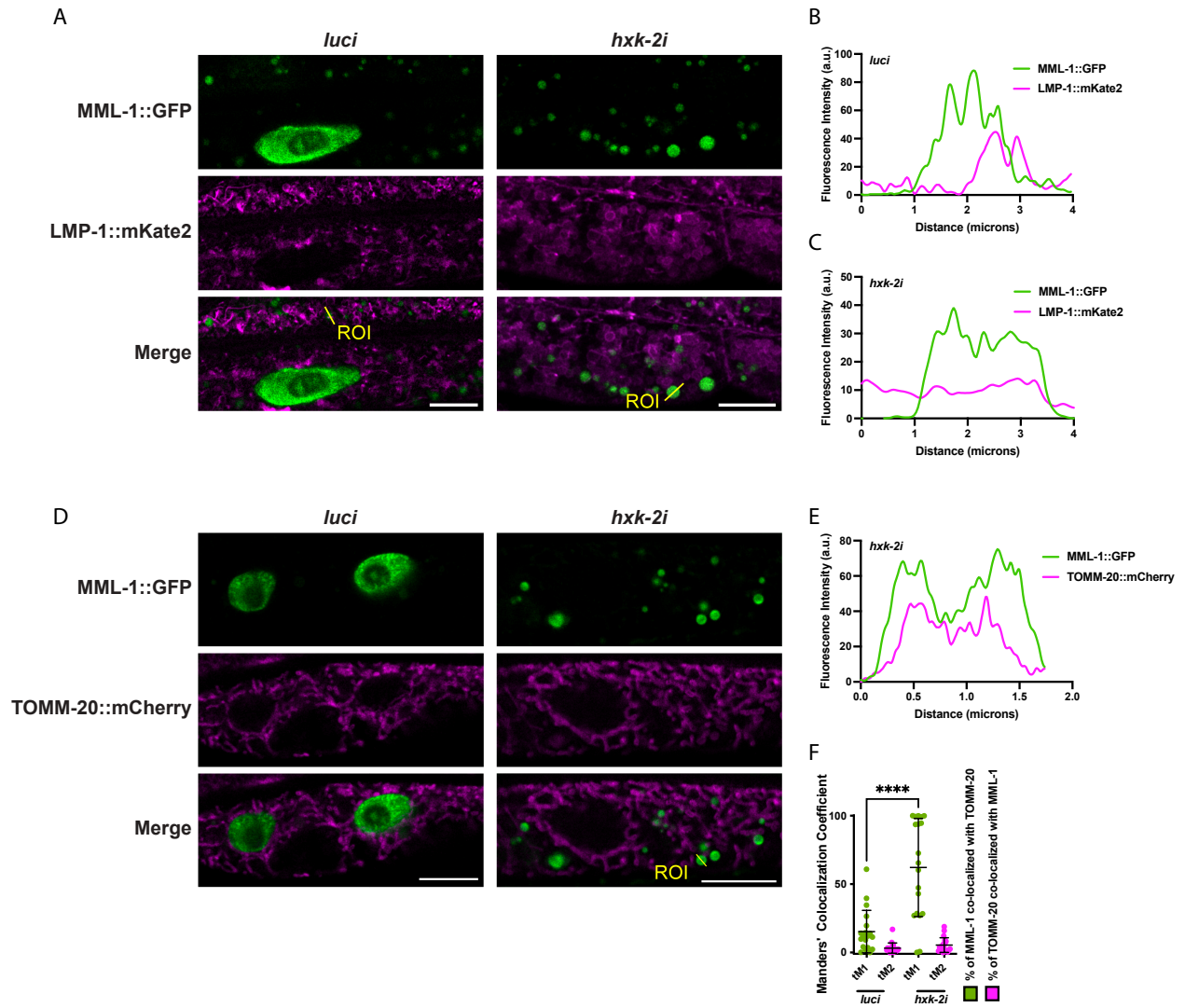


Figure 17. MML-1 localization with intestinal mitochondria is enhanced upon *hxx-2* knockdown. **A.** Representative confocal images of day one adult worms expressing MML-1::GFP and the lysosomal/endosomal protein LMP-1::mKate2 under *luci* and *hxx-2i*. The intensity plot of the ROI from *luci* (**B**) and *hxx-2i* (**C**) images indicates no overlapping signal (n>10 MML-1 positive puncta per worm). **D.** Representative confocal images of day one adult worms expressing MML-1::GFP and the mitochondria reporter *ges-1p::TOMM-20::mCherry* under *luci* and *hxx-2i*. **E.** Intensity plot of the ROI from *hxx-2i* images indicates overlapping signals. **F.** Quantification of MML-1 and TOMM-20 colocalization was measured using the Manders' Colocalization Coefficients tM1 (GFP channel) and tM2 (mCherry channel), which respectively represent the colocalization between the pixels from the GFP channel with the mCherry channel and *vice versa* (N=3). Significance was calculated with *t*-test. **A** and **D** scale bars represent 10 μ m. **F** bars represent mean + SD.

5.6 *C. elegans* hexokinases are differentially expressed

Mammals harbor four hexokinases that differ in tissue expression, subcellular localization, and affinity to glucose and G6P. However, knowledge of the nematode's isozymes is limited. *C. elegans* has three genes encoding for hexokinases: *hxx-1*/F14B4.2, *hxx-2*/H25P06.1, and *hxx-3*/Y77E11A.1. These genes encode for conserved enzymes of around 55 kDa. We used the hexokinase tagged with mKate2 strains to investigate the tissue-specific expression and subcellular localization of the different isozymes by confocal microscopy. We found that HXX-1 was expressed in neurons, the pharynx, the gonadal sheath, and coelomocytes (**Figure 18A**). HXX-2 had a reticular expression in neurons, muscle, intestine, and hypodermis (**Figure 18B**). HXX-3 signal was diffused and highly expressed in the pharynx, muscle, hypodermis, and intestine (**Figure 18C**).

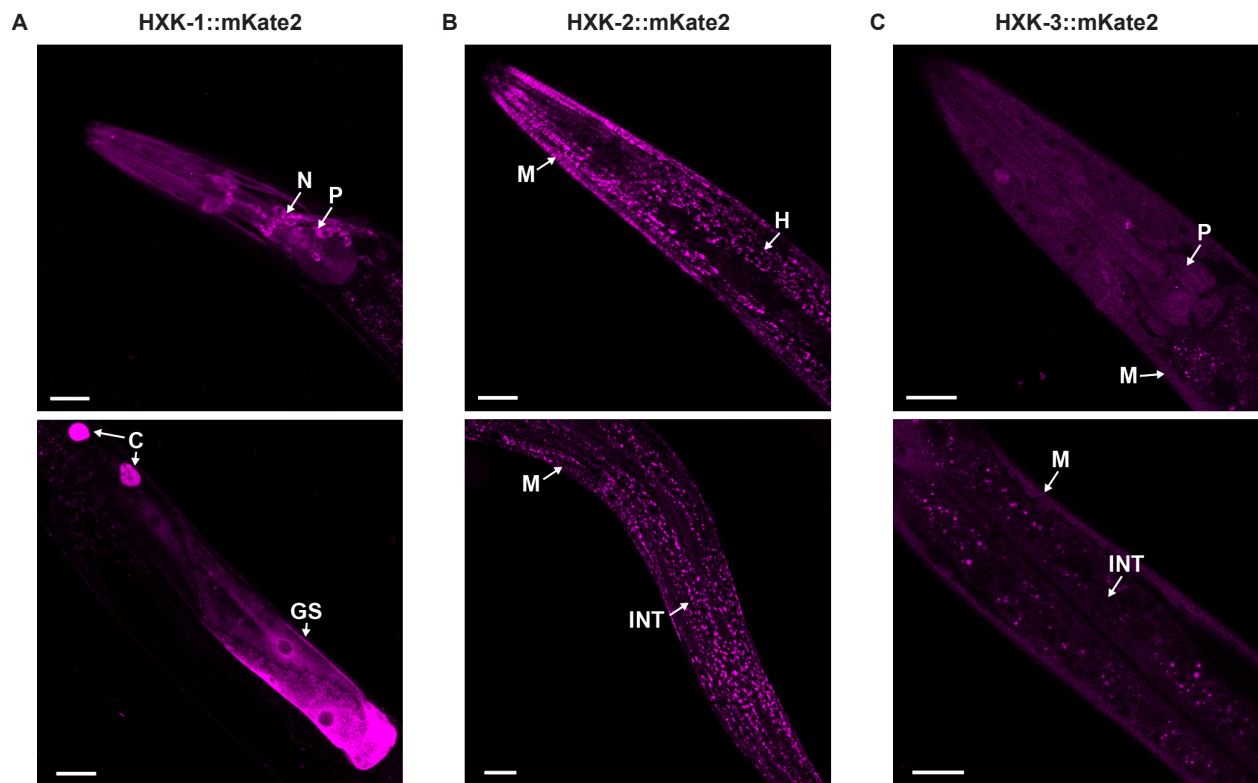


Figure 18. *C. elegans* hexokinases are expressed in different tissues. A-C. Localization of the worm HXX-1 (A), HXX-2 (B), and HXX-3 (C) tagged with the fluorescent protein mKate2. The primary tissues are identified with arrows. Abbreviations: N, neurons; P, pharynx; C, coelomocytes; GS, gonadal sheath; M, muscle; H, hypodermis; INT, intestine. Scale bars represent 20 μm.

Human HKI and HKII have been shown to reversibly bind to mitochondria (Sui & Wilson, 1997). Binding is dependent on an intrinsic hydrophobic N-terminal sequence that is critical for the insertion into the outer mitochondrial membrane (Pastorino et al., 2002), as well as through interactions with the voltage-dependent anion channel VDAC1 (Lindén et al., 1982). Due to the reticular expression pattern, HXK-2 was a plausible candidate to be mitochondrially localized. To further address this idea, we aligned the N-terminus of the *C. elegans* hexokinases with the human HKI and found many hydrophobic residues conserved (**Figure 19A**). Hydrophobicity analysis of these sequences using the Kyte-Doolittle plots (Gasteiger et al., 2005; Kyte & Doolittle, 1982) revealed that HXK-2 had the highest hydrophobic score (2.078) in the first ten amino acids, making it an excellent candidate to be targeted to a membrane (**Figure 19B**). To corroborate this idea, we crossed the HXK-2::mKate2 strain with a mitochondrial reporter that expresses GFP with a mitochondrial targeting sequence under the body wall muscle promoter *myo-3*. Indeed, we found that full-length HXK-2 strongly co-localized with mitochondria (**Figure 19C**). We also generated a *hvk-2* deletion mutation by CRISPR/Cas9 that lacks the first ten amino acids after the initiator methionine and found that mitochondrial localization was abolished entirely (**Figure 19C**). Upon knockdown of *vdac-1*, however, HXK-2 colocalization with mitochondria was retained (**Figure 19D**). As MML-1 also localizes with mitochondria, we decided to test whether HXK-2 and MML-1 co-localize and found overlapping fluorescent signals of both proteins (**Figure 19E and F**). In summary, we found that the three hexokinases are differentially expressed and identified HXK-2 as the worm mitochondrial hexokinase, which co-localizes with MML-1 in this compartment.

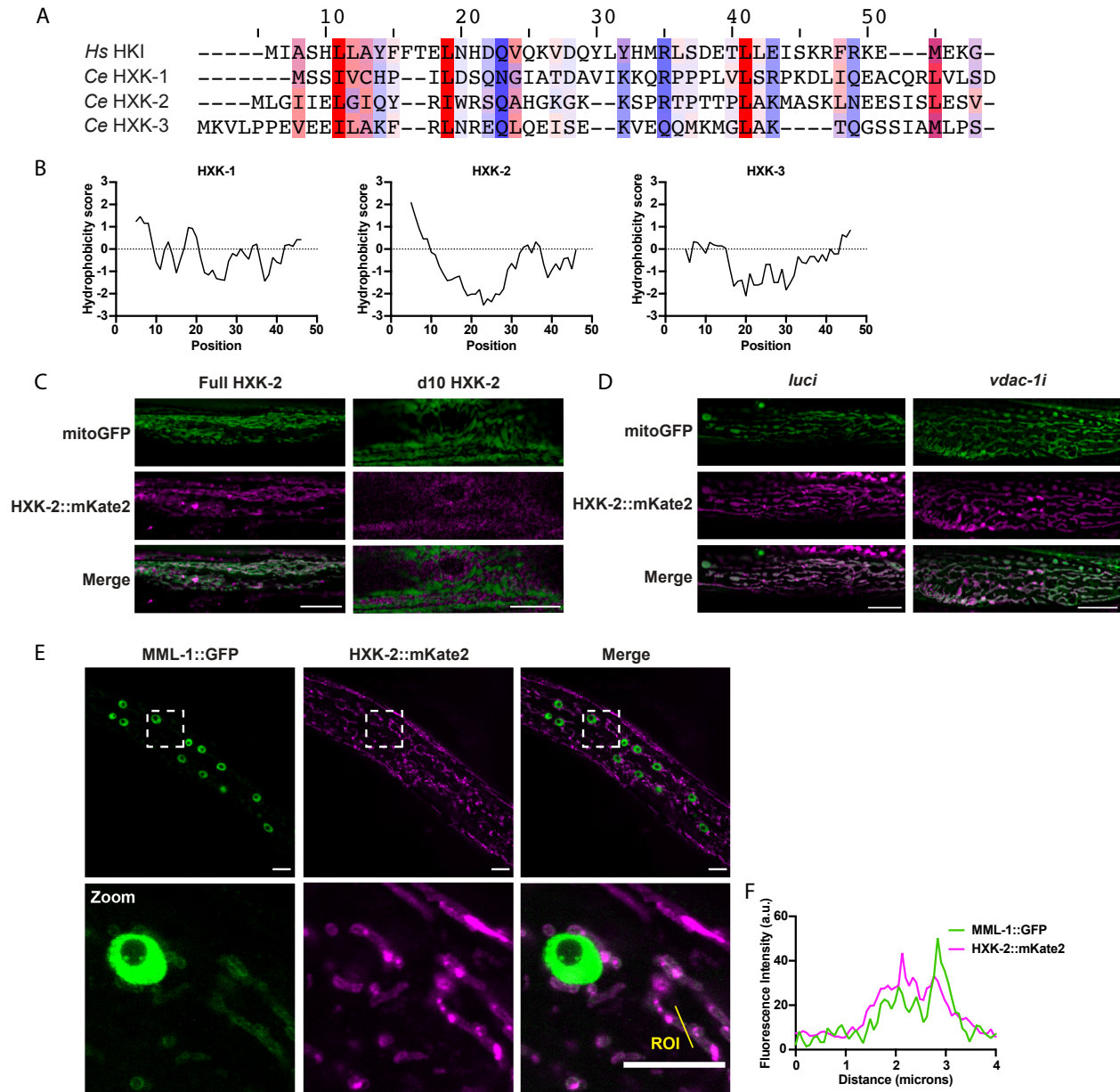


Figure 19. HXK-2 and MML-1 co-localize at the mitochondria. **A.** Sequence of the N-terminus of human (*Hs*) HKI and *C. elegans* (*Ce*) hexokinases. Hydrophobic amino acid residues are highlighted. **B.** Hydropobicity plots of the first 50 amino acids of the nematode's hexokinases using the Kyte & Doolittle scale. Score >1.6 are considered potential membrane-spanning domains. **C.** Colocalization of mitochondrial reporter *myo-3p::mitoGFP* with full-length HXK-2::mKate2 and d10 HXK-2::mKate2 lacking the first ten residues of the N-terminus. **D.** Colocalization of HXK-2::mKate2 with mitochondrial reporter *myo-3p::mitoGFP* under *vdac-1* knockdown. **E.** Representative confocal images of the hypodermis of an L4 worm expressing MML-1::GFP and HXK-2::mKate2. Below is a zoom of the regions marked with the white boxes. The contrast of the MML-1::GFP zoomed images was enhanced for better visualization of the extra-nuclear signal of MML-1. **C, D,** and **E** scale bars represent 10 μ m.

5.7 *hvk-2* regulates MML-1 function through increased PPP

From our RNAi screen above, we also observed increased MML-1 nuclear localization upon the knockdown of two enzymes from the PPP (**Figure 10**). The PPP is a cytosolic metabolic pathway involved in the interconversion of 3 to 7 carbon sugars that generates precursors for the biosynthesis of lipids, amino acids, and nucleotides. It also maintains redox homeostasis through NADPH production (**Figure 20A**). To further address these findings, we tested the effect of pharmacologic inhibition PPP on MML-1 nuclear localization using 6-aminonicotinamide (6-AN), which is a competitive inhibitor of the glucose 6P dehydrogenase (G6DH) and phosphogluconate dehydrogenase (6PGD). These two enzymes generate NADPH in the PPP. In agreement with our previous results, we observed increased MML-1 nuclear localization after supplementation of 1 mM of 6-AN (**Figure 20B**). We also found that *hvk-2i*, but not *hvk-1i*, significantly increased the NADPH levels, suggesting that the PPP could be enhanced in worms lacking the mitochondrial hexokinase (**Figure 20C and D**). Next, we sought to test the epistatic interaction of hexokinase and PPP knockdown on MML-1 nuclear localization. For these experiments, we performed double RNAi of *hvk-1* and *hvk-2* in combination with the 6PGD *T25B9.9*, transketolase *tkt-1*, and transaldolase *tald-1*. Interestingly, knocking down these enzymes rescued MML-1 nuclear localization under *hvk-2i* (**Figure 20F**) but did not rescue the localization under *hvk-1i* (**Figure 20E**). We also found that knocking down PPP enzymes had little effect on G6P levels in control or upon hexokinase double knockdowns, suggesting that PPP uncouples the correlation between the G6P level and MML-1 nuclear localization (**Figure 20G and H**). To evaluate MML-1 function, we measured its transcriptional readouts and found that knocking down the PPP under *hvk-2i* rescued the expression of *lgg-2*, *mdl-1*, *swt-1*, and *fat-5* (**Figure 20J**); however, it had no effect under *hvk-1i* (**Figure 20I**). Taken together, these data suggest that PPP plays a role in inhibiting MML-1 function downstream of *hvk-2*, independent of the G6P levels.

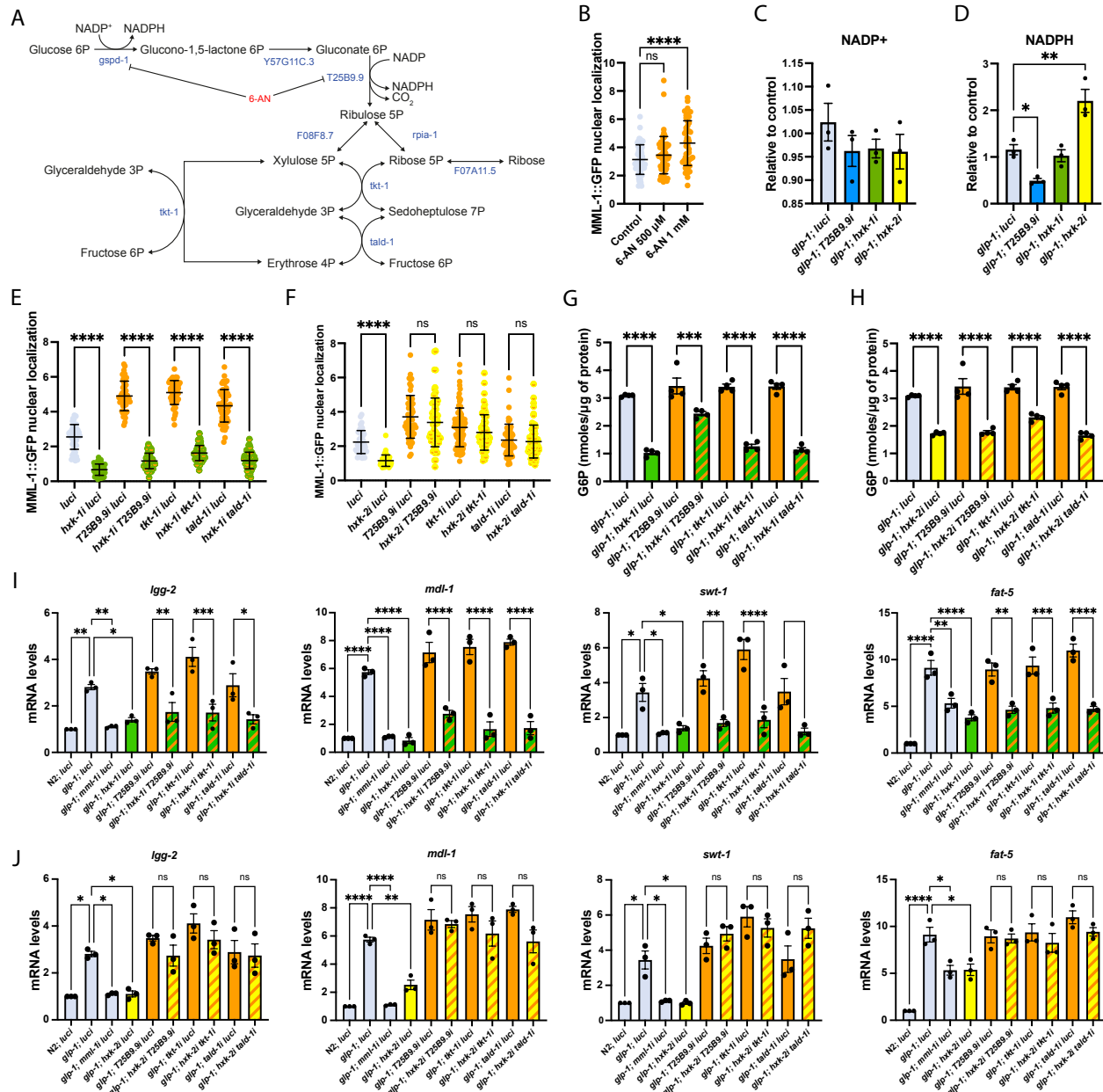


Figure 20. Inhibition of the PPP rescues MML-1 nuclear localization upon *hxx-2* knockdown.

A. The PPP is a cytosolic pathway that metabolizes G6P to produce NADPH, ribose 5-phosphate, and interconverts 3 to 7 carbon sugars. **B.** MML-1 nuclear localization of day one adult worms grew egg on with 500 μ M and 1 mM of 6-AN (N=2). **C-D.** Quantification of NAD⁺ (**C**) and NADPH (**D**) levels in day one adult *glp-1(e2141)* worms grown in the indicated RNAi. Metabolite levels were normalized to total protein concentration (N=3). **E-F.** MML-1 nuclear localization of day one adult worms upon double knockdown of *hxx-1* (**E**) and *hxx-2* (**F**) with enzymes of the PPP (N=3). **G-H.** Quantification of G6P levels relative to total protein measured in day one adult *glp-1(e2141)* worms grown under *hxx-1i* (**G**) and *hxx-2i* (**H**) in combination with enzymes from the PPP (N=4). **I-J.** qPCR analysis of MML-1 downstream targets in young adult worms with

double knockdown of *hxx-1* (I) and *hxx-2* (J) and enzymes from the PPP (N=3). Significance was calculated with a one-way ANOVA test. I and J statistical significance were calculated with a two-tailed *t*-test. B, E, and F bars represent mean + SD. C, D, G, H, I, and J bars represent mean + SEM.

Finally, we asked whether reducing the PPP could impact *glp-1(e2141)* lifespan upon *hxx-2* knockdown. Inhibition of the PPP has been reported to extend lifespan in *C. elegans* by activating the mitochondrial UPR^{mt} (Bennett et al., 2017). As reported previously, we found a significant lifespan extension upon *tkt-1* knockdown in wildtype. Moreover, knockdown of the PPP in the *glp-1(e2141)* background had no additive effect on longevity, suggesting that *glp-1* and *tkt-1* may share common mechanisms in extending lifespan. Consistent with our data above, *hxx-2i* suppressed *glp-1(e2141)* longevity, and knockdown of *T25B9.9* (Figure 21A) and *tkt-1* (Figure 21B) completely rescued the longevity. Collectively, these data indicate that an increase in the PPP under *hxx-2* knockdown suppresses MML-1 function, and reducing the PPP restores longer life.

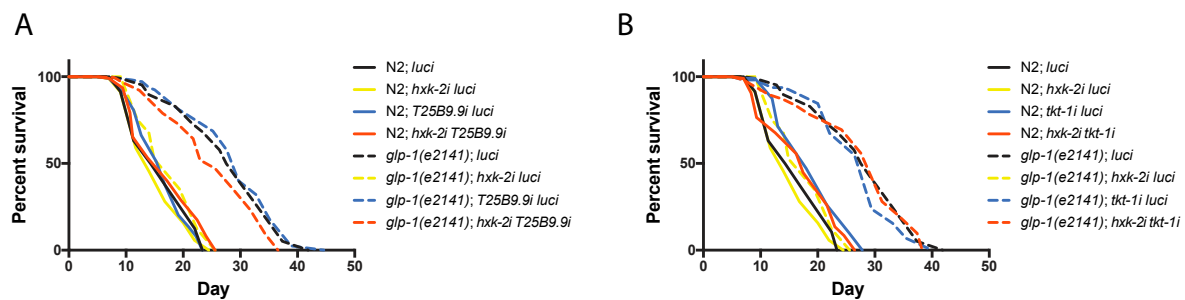


Figure 21. Decreasing the PPP restores *glp-1(e2141)* longevity under *hxx-2* knockdown. A-B. Lifespan analysis of *glp-1(e2141)* with *hxx-2i* and *T25B9.9i* (A) and *tkt-1i* (B) single and double knockdowns. Lifespans were performed in the same experiment and plotted separately for clarity; therefore, controls lifespans are shared between plots (N=2). See **Supplementary Table 5** for statistical analysis.

5.8 Decreased OGDC function rescues MML-1 nuclear localization in *hxx-2i*

In our previous screen, we found that downregulation of two subunits of the OGDC, *ogdh-1* and *dld-1*, increased MML-1 nuclear localization (Figure 10). This TCA cycle complex catalyzes the oxidative decarboxylation of 2-oxoglutarate (α -ketoglutarate) to form succinyl-CoA. It is also a key control point as its substrate 2-oxoglutarate can be integrated from anaplerotic reactions from glutamate deamination. Hence, we wanted to test whether the regulation of MML-1 nuclear localization by hexokinase is epistatic to the OGDC. We performed double RNAi knockdown of

hvk-1 and *hvk-2* with *ogdh-1i*, *dld-1i*, and *dlst-1i*. We found that knockdown of the three components of the OGDC rescued MML-1 nuclear localization under *hvk-2i* (**Figure 22B**) but had no effect under *hvk-1i* (**Figure 22A**). Interestingly, G6P levels were decreased upon *hvk-1i* and *hvk-2i* and remained unchanged in the double knockdown in the *glp-1(e2141)* background (**Figure 22C and D**), again suggesting that we had uncoupled MML-1 nuclear localization from G6P levels. We also measured the expression of MML-1 downstream targets under these conditions and observed rescue of the expression in the double knockdown of the OGDC with *hvk-2i* (**Figure 22F**) but not with *hvk-1i* (**Figure 22E**). Taken together, these data suggest that the OGDC acts downstream of *hvk-2*, but not *hvk-1*, to regulate MML-1 nuclear localization and transcriptional activity, independent of G6P levels.

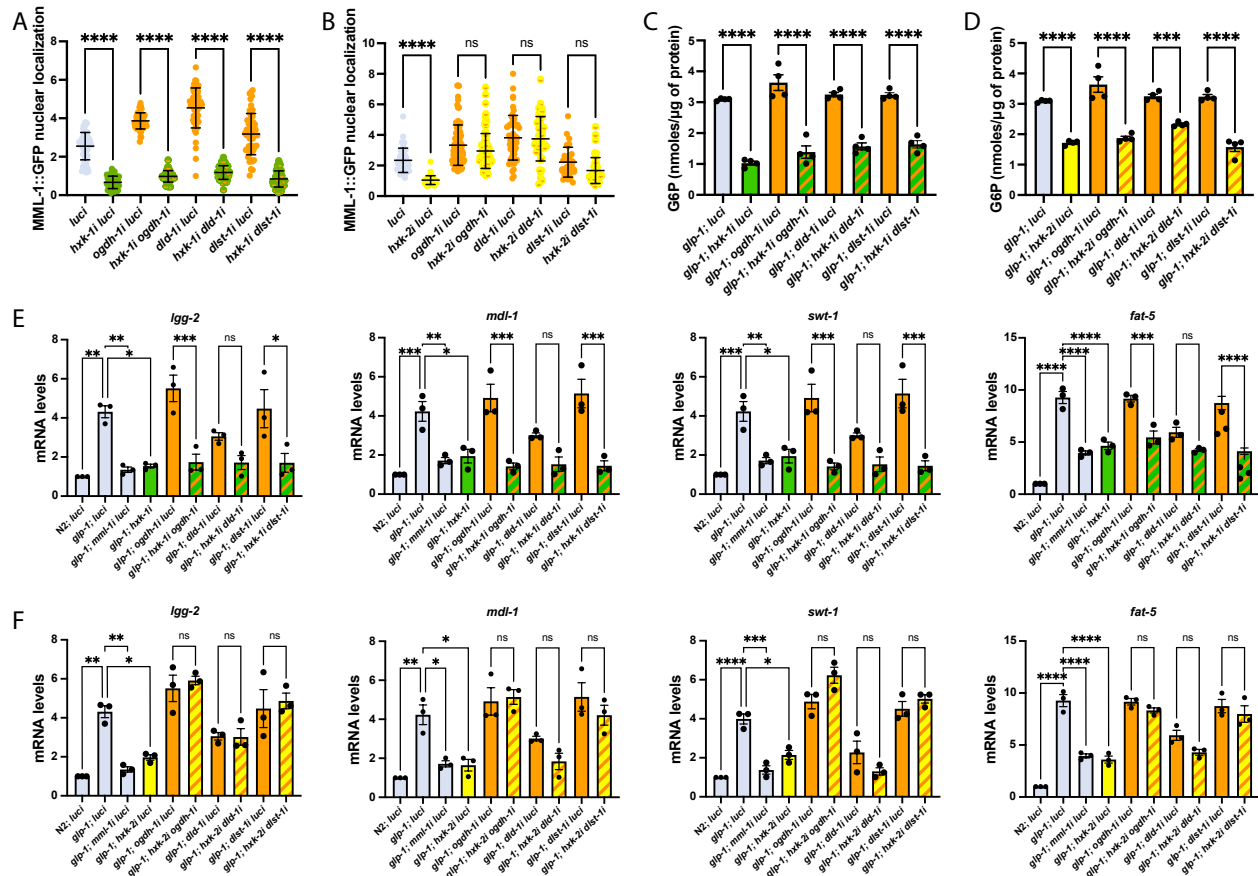


Figure 22. The OGDC complex inhibits MML-1 nuclear localization upon *hvk-2* knockdown. A-B. MML-1 nuclear localization of day one adult worms under *hvk-1i* (A) and *hvk-2i* (B) in combination with components of the OGDC (N=3). C-D. G6P levels relative to total protein measured in day one adult *glp-1(e2141)* worms grown under *hvk-1i* (C) and *hvk-2i* (D) in combination with components of the OGDC (N=4). E-F. qPCR analysis of MML-1 downstream

targets in young adult worms with double knockdown of *hxx-1* (E) and *hxx-2* (F) and components of the OGDC (N=3). Significance was calculated with one-way ANOVA test. E and F statistical significance was calculated with a two-tailed *t*-test. A and B bars represent mean + SD. C, D, E, and F bars represent mean + SEM.

5.9 MML-1 interactome uncovers potential regulators of its function and localization

Given the localization of MML-1 to mitochondria and possibly other organelles, we decided to identify potential MML-1 binding partners to better understand its subcellular distribution. We used CRISPR/Cas9 to tag the endogenous MML-1 locus with a 3xFLAG tag for these experiments. MML-1 was immunoprecipitated from wildtype and *glp-1(e2141)* total protein extracts, and potential interactors were identified by mass spectrometry. We detected ca.1300 to 2000 different proteins from three biological replicates of the different genotypes (Figure 23A) and found differences among the proteins enriched in wildtype compared to *glp-1(e2141)* (Figure 23B). MML-1 was the most abundant protein in the wildtype pulldown and the fifth in the *glp-1(e2141)* background compared to the N2 control (Figure 23C and D, Supplementary Table 6). We detected several proteins in the immunoprecipitation (IP), including MXL-2, an established MML-1 binding partner (Pickett et al., 2007), and vitellogenins VIT-1, VIT-3, and VIT-4, which are highly abundant yolk proteins. Analysis of the top 50 co-enriched candidates in wildtype and *glp-1(e2141)* MML-1 IPs revealed enrichment for nuclear and mitochondrial proteins (Figure 23E). We also found multiple enriched proteins from the ER, two abundant proteins from lipid droplets (LD), and two nucleolar factors.

We combined the proteomic identification of MML-1 potential binding partners with an RNAi screen to investigate whether these interactors regulate MML-1 function. We quantified MML-1 nuclear localization in the intestine of worms grown in RNAi against the top 50 candidates from the wildtype IP (Vonolfen, 2020). Out of the 50 clones, 19 significantly affected MML-1 nuclear localization (Supplementary Table 7). Knockdown of the mitochondrial proteins ACS-13 and AKAP-1, the nucleolar proteins BYN-1 and ZK430.7, and the ER protein UGT-46 significantly increased MML-1 nuclear localization (Figure 23F). These proteins are involved in multiple processes, including fatty acid metabolism, PKA and AMPK signaling pathway, ribosome biogenesis, and xenobiotic metabolism. Knockdown of *mxl-2* decreased MML-1 nuclear localization, consistent with what has been reported with MondoA and Mlx in mammalian cells (Eilers et al., 2002). Interestingly, we also found that knockdown of the mitochondrial pyruvate

carrier *mpc-1* decreased MML-1 nuclear localization comparable to *hxx-1i* and *hxx-2i*. Taken together, these data suggest a more intricate connection between MML-1 and different organelles.

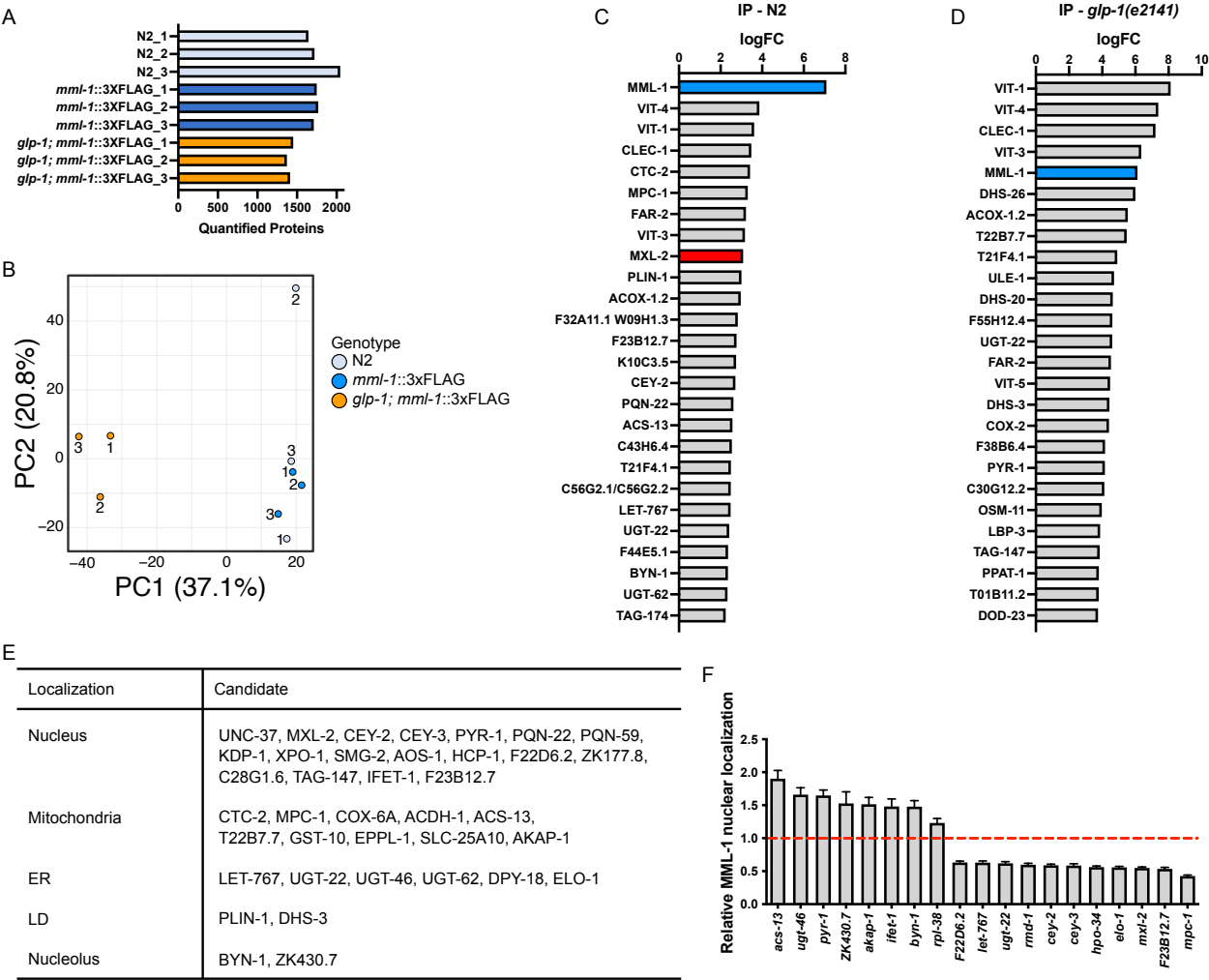


Figure 23. MML-1 interactome is enriched with proteins from multiple organelles. **A.** Quantified proteins in each biological replicate of wildtype, N2; *mml-1::3xFLAG*, and *glp-1; mml-1::3xFLAG*. **B.** PCA analysis with each biological replicate of the genotypes from proteomics. **C-D.** Anti-FLAG immunoprecipitation from whole-worm lysates of animals expressing MML-1::3xFLAG in either wildtype (**C**) or *glp-1(e2141)* (**D**) backgrounds. IP was analyzed by mass spectrometry. The 25 top candidates co-enriched with MML-1 compared to N2 control are shown as log FC, including MML-1 and its established binding partner MXL-2. (**E**) Top candidates co-enriched in MML-1 IP from wildtype and *glp-1(e2141)* grouped by predicted subcellular localization (uniport.org). **F.** MML-1 nuclear localization relative to *luci* control (red line) of day one adult worms grew in the indicated RNAi egg on (see **Supplementary Table 6** for the complete list and statistical analysis). Only the significant candidates are shown (N=3). Significance was calculated with a one-way ANOVA test. **F** bars represent mean + SEM.

5.10 The mitochondrial pyruvate carrier regulates MML-1

We found the mitochondrial pyruvate carrier MPC-1 co-enriched in MML-1 pulldowns. This transporter of the inner mitochondrial membrane connects glycolysis with mitochondrial metabolism by transporting pyruvate to the mitochondrial matrix. Interestingly, we found that knockdown of *mpc-1* strongly decreased MML-1 nuclear localization in wild-type animals and confirmed this in *glp-1(e2141)* mutants (**Figure 24A**). Further, *mpc-1i* suppressed MDL-1, a downstream target of MML-1, nuclear localization under *glp-1(e2141)* (**Figure 24B**), consistent with a decrease in MML-1 nuclear activity. We also saw a significant increase in colocalization between MML-1 and mitochondria upon *mpc-1i* (**Figure 24C**), comparable to *hxx-2* knockdown. Next, we used CRISPR/Cas9 to tag MPC-1 with mKate2 and visualized its expression by confocal microscopy. In presumptive mitochondria, we found MPC-1 expressed in multiple tissues, including hypodermis, intestine, and body wall muscle (**Figure 24D**). We crossed the MPC-1::mKate2 to the MML-1::GFP reporter strain to analyze colocalization. We found overlapping signals from both proteins (**Figure 24E and F**), suggesting the MPC-1 could link MML-1 to the regulation of glucose metabolism.

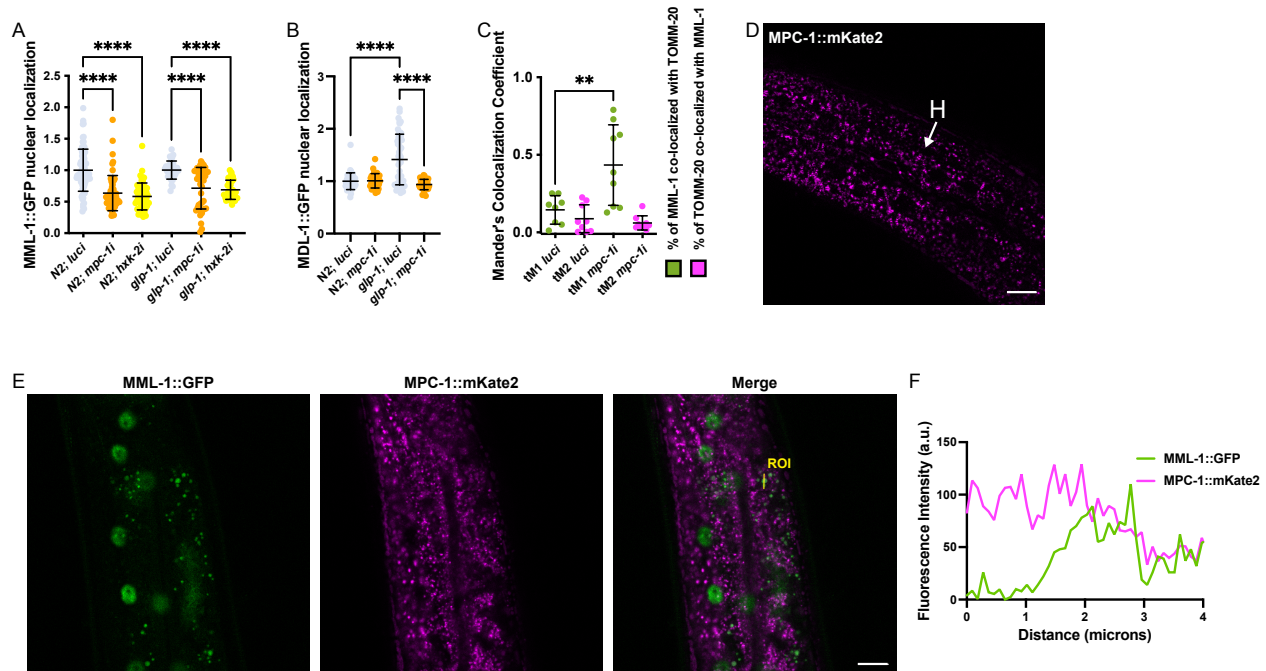


Figure 24. The mitochondria pyruvate carrier MPC-1 regulates MML-1 localization and function. **A.** MML-1 nuclear localization in wildtype and *glp-1(e2141)* day one adult worms grown under the indicated RNAi (N=3). **B.** MDL-1 nuclear localization in day one adult wildtype and *glp-1(e2141)* worms under *luci* control and *mpc-1i* (N=3). **C.** Quantification of MML-1::GFP

and TOMM-20::mCherry colocalization was measured using the Manders' Colocalization Coefficients tM1 (GFP channel) and tM2 (mCherry channel), which respectively represent the colocalization between the pixels from the GFP channel with the mCherry channel and *vice versa* (N=2). **D**. Representative confocal image of MPC-1::mKate2 in day one adult worms in the hypodermis. Abbreviation: H, hypodermis. **E-F**. Representative confocal image of MML-1::GFP and MPC-1::mKate2 colocalization in the hypodermis of day one adult worms. The intensity plot of the ROI from **E**. Significance was calculated with one-way ANOVA test. For **C**, significance was calculated with a *t*-test. **A**, **B**, and **C** bars represent mean + SD. **D** and **E** scale bars represent 10 μ m.

5.11 MML-1 colocalizes with peridroplet mitochondria

Mitochondria and LD dynamically interact in highly active metabolic tissues, and it has been shown that mitochondria associated with LD have specific metabolic behavior compared to cytosolic mitochondria (*e.g.*, different dynamics, motility, and capacity to burn carbohydrates and lipids) (Gordaliza-Alaguero et al., 2019). LDs are organelles involved in multiple roles serving as nutrient reservoirs and participating in signaling pathways. Under nutrient deprivation, the interaction of mitochondria and LD is enhanced to favor fatty acid oxidation (Rambold et al., 2015). Interestingly, PLIN-1 and DHS-3, two of the most abundant LD proteins, were co-enriched in wildtype and *glp-1(e2141)* MML-1 IP, respectively (**Figure 23E**). Hence, we wanted to test whether MML-1 localized to these organelles. First, we sought to establish a way to visualize LD *in vivo* with a fluorescent dye compatible with our markers. LipiBlue has been previously used to visualize LD in mammalian cells (Tatenaka et al., 2019), but has not been confirmed in the worm. To address this, we used DHS-3::GFP and PLIN-1::mCherry reporter strains. We found that LipiBlue stained structures positive with DHS-3 (**Figure 25A and B**) and PLIN-1 (**Figure 25C and D**), indicating that LipiBlue could be used as a reliable method for visualization of LD in *C. elegans*.

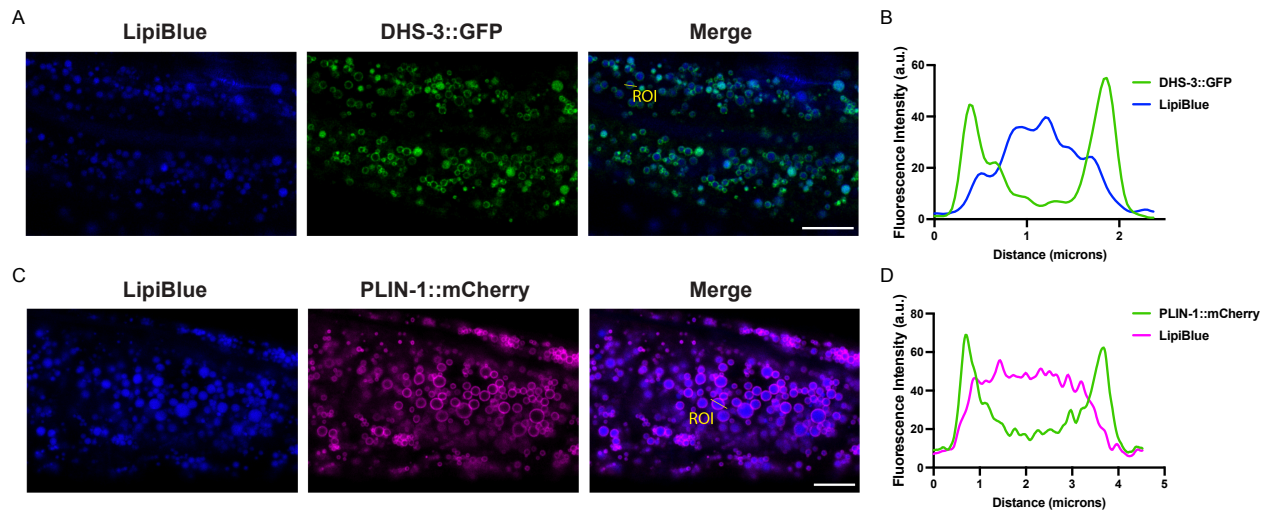


Figure 25. LipiBlue stains LD in *C. elegans*. A-B. Representative images (A) of day one adult worms expressing the LD protein DHS-30::GFP reporter grown with LipiBlue egg on. Intensity plot (B) of the marked ROI from A showing DHS-3::GFP and LipiBlue localization. C-D. Representative images (C) of day one adult worms expressing the PLIN-1::mCherry reporter grown with LipiBlue egg on. Intensity plot (D) of the marked ROI from C showing PLIN-1::mCherry and LipiBlue localization. A and C scale bars represent 10 μ m.

Next, we examined MML-1 in LipiBlue stained animals and saw that it localized with LipiBlue positive structures (Figure 26A and B). Moreover, this colocalization was significantly increased upon *hxx-2* knockdown (Figure 26C). Interestingly, we observed that MML-1 appeared localized to mitochondria associated with LD (Figure 26B). Inhibition of transaldolase and enzymes from the PPP has been shown to activate a fasting-like response by increasing lipolysis and enhancing the breakdown of LDs (Bennett et al., 2017). Therefore, we wondered whether the LD size correlates with MML-1 nuclear localization. For this, we knockdown *hxx-2* and *tkl-1* to decrease and increase MML-1 nuclear localization, respectively. We observed a significant reduction in diameter and the total amount of LDs (Figure 26D and E) upon knockdown of *tkl-1*. Moreover, double knockdown of *hxx-2* and *tkl-1* resulted in smaller and fewer LDs than control (Figure 26D and E). Collectively, these data suggest that MML-1 can localize with a specific subpopulation of mitochondria and that inhibition of the PPP can rescue MML-1 nuclear localization upon *hxx-2i* correlated with decreasing LD size.

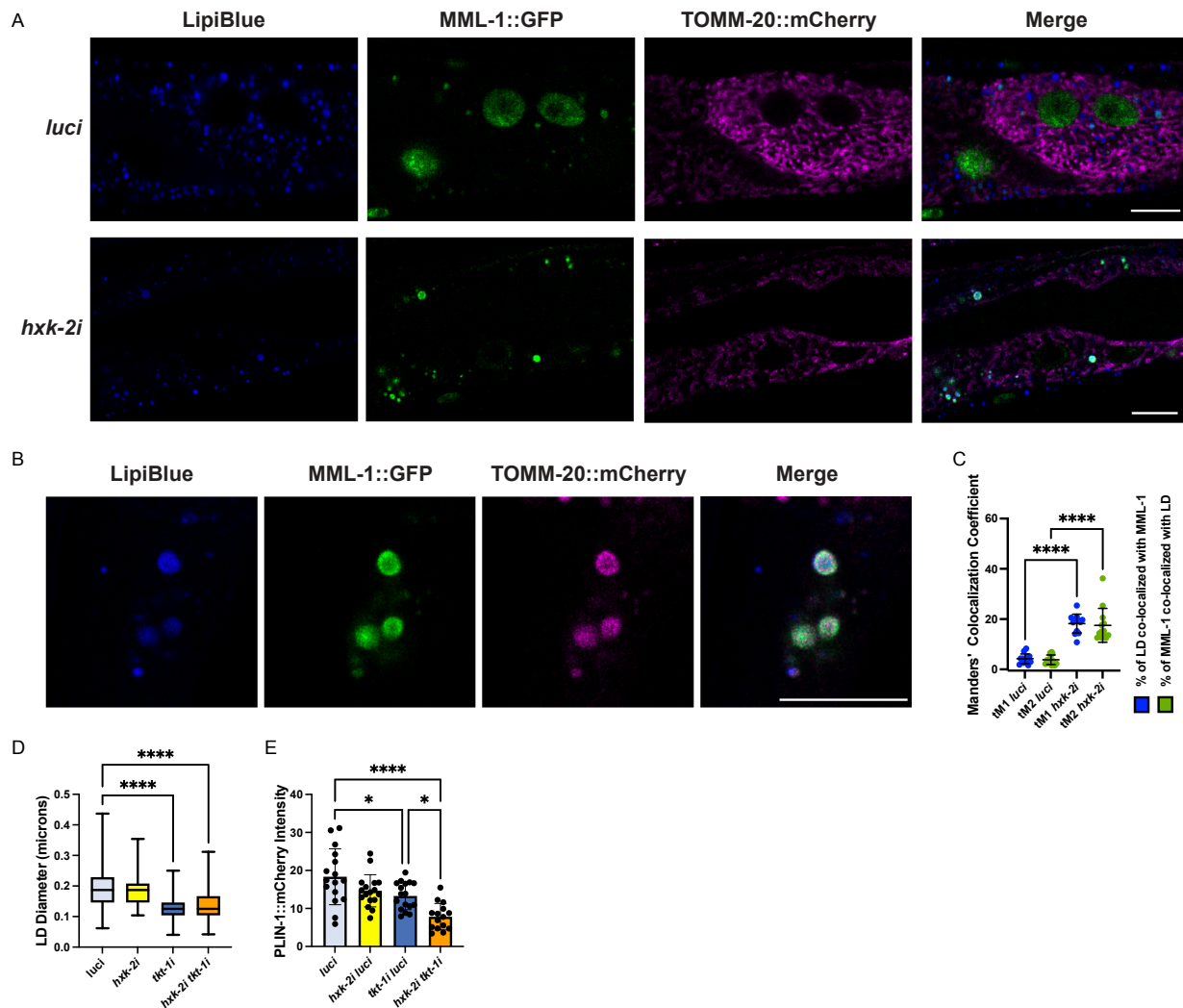


Figure 26. MML-1 localizes with mitochondria associated with LD. A-B. Confocal microscopy of day one adult worms expressing MML-1::GFP and TOMM-20::mCherry stained with LipiBlue under *luci* and *hxx-2i* (A) (N=3). In **B**, the magnified image shows the localization of the three signals. **B.** Quantification of MML-1::GFP and LD colocalization was measured using the Manders' Colocalization Coefficients tM1 (LipiBlue channel) and tM2 (GFP channel), which respectively represent the colocalization between the pixels from the LipiBlue channel with the GFP channel and *vice versa* (N=3). **D.** LD diameter quantified in day one adult worms expressing PLIN-1::mCherry grown under the indicated RNAi. **E.** Expression of PLIN-1::mCherry calculated as intensity per area. Statistical significance was calculated with one-way ANOVA. For **C**, statistical significance was calculated with a *t*-test. **C** and **E** bars represent mean + SD. **A** and **B** scale bars represent 10 μ m.

5.12 MML-1 is regulated by the mitochondrial acyl-CoA synthase

From our pulldown data, we found that mitochondrial proteins were enriched as potential interactors of MML-1. Among them, we found two subunits of the cytochrome c oxidase (Complex IV), CTC-2 and COX-6A, together with other proteins from the mitochondrial inner membrane. Also, we found ACS-13 as an MML-1 potential interactor and observed increased MML-1 nuclear localization upon *acs-13* knockdown in wildtype background (**Figure 23F**). *acs-13* encodes for long-chain fatty acid acyl-CoA synthetase (ACSL). The mitochondrial ACSL1 catalyzes the conversion of long-chain fatty acids to fatty acyl-CoA that can be further oxidized or used for other reactions (*e.g.*, esterification reactions, signal transduction, lipid remodeling) (**Figure 27A**). It has been shown that ACS-13 localizes to mitochondria in *C. elegans* (Ruiz et al., 2019). First, we confirmed that knockdown of *acs-13* also increased MML-1 nuclear localization in the *glp-1(e2141)* longevity model (**Figure 23B**). We used MDL-1 nuclear accumulation as a proxy for MML-1 transcriptional activity. However, we found no difference in MDL-1 nuclear localization upon *acs-13* knockdown in wildtype nor a further increase in *glp-1(e2141)* (**Figure 27C**), indicating that the *acs-13i*-induced increase in MML-1 nuclear localization is not sufficient to affect target gene expression. Whether other MML-1 downstream targets are regulated upon *acs-13* knockdown remains elusive.

Next, we tested whether *acs-13* and *mml-1* colocalize. To do so, we used CRISPR/Cas9 to tag *acs-13* with the fluorescent protein mKate2 and crossed this strain with the MML-1::GFP reporter line. We observed that our CRISPR line displayed an ACS-13 reticular signal similar to mitochondria and found ACS-13 expressed in multiple tissues, including germline, muscle, intestine, and hypodermis (**Figure 27D**). We found that MML-1 colocalized with ACS-13 at mitochondria in the hypodermis of L4 stage animals (**Figure 27E**). Surprisingly, the MML-1 signal appeared inside the mitochondria based on MML-1 fluorescent signals bounded by ACS-13 (**Figure 27F**). However, this observation needs further validation since neither MML-1 nor MondoA have been reported to reside within mitochondria. We also found MML-1 associated with ACS-13 in the intestine (**Figure 27G and H**). Taken together, these data suggest ACS-13 as a potential MML-1 interactor in the mitochondria outer membrane that might integrate signals from fatty acid metabolism to MML-1 transcriptional regulation.

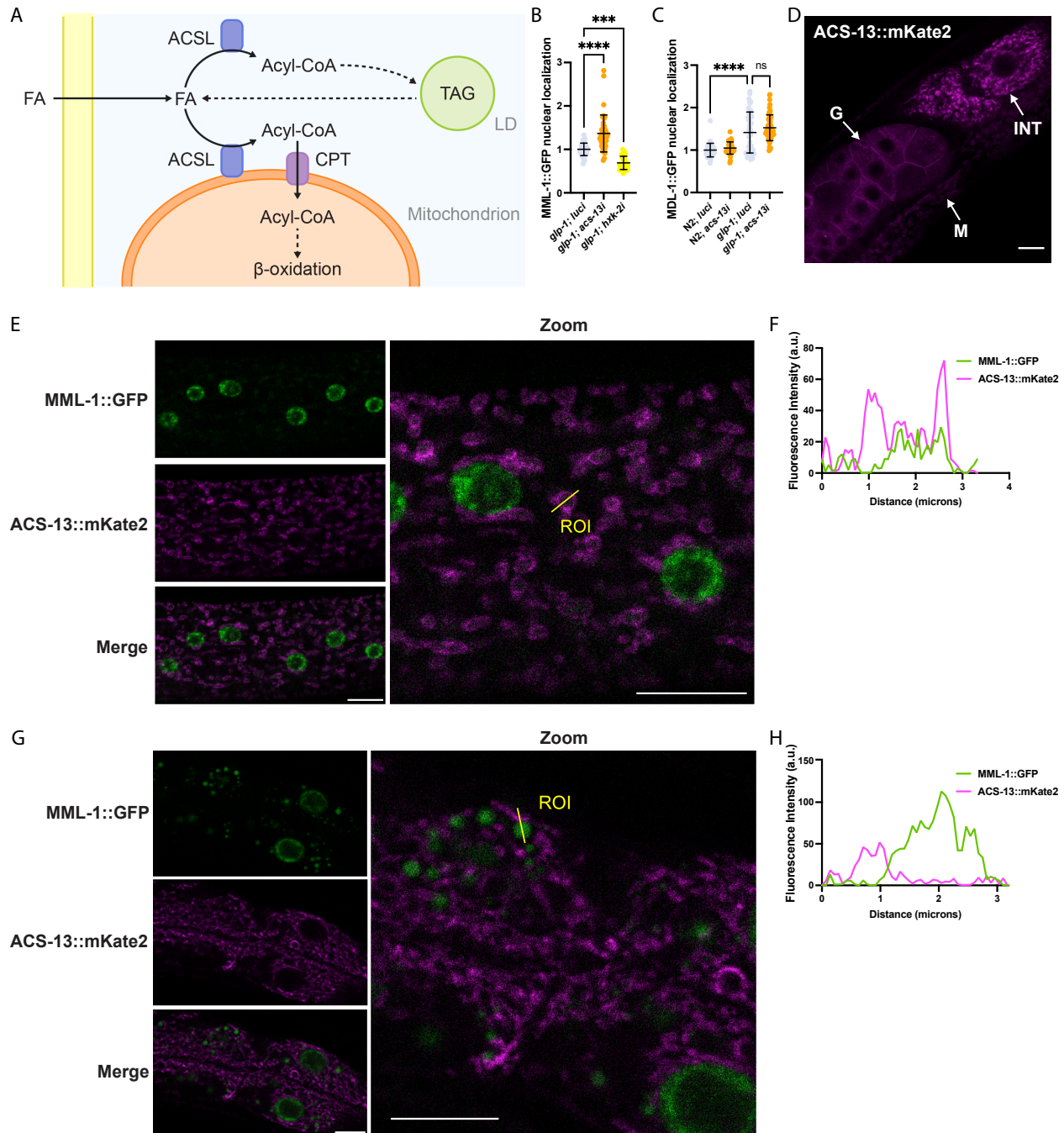


Figure 27. ACS-13 and MML-1 colocalize at the mitochondria and regulates its nuclear localization. **A.** Long fatty acids (FA) are converted to fatty acyl-CoA by the acyl-CoA synthetase (ACSL). This acyl-CoA can be imported into the mitochondria by the carnitine palmitoyltransferase (CPT) to be further metabolized through β -oxidation or can be used for other reactions, including being converted to triacylglycerol (TAG) and stored in lipid droplets (LD). Under nutrient deprivation, TAGs are released from the LD by hydrolases to be processed into free fatty acids and used to maintain metabolic homeostasis. **B.** MML-1 nuclear localization in day one adult *glp-1(e2141)* worms grown under the indicated RNAi (N=3). **C.** MDL-1 nuclear

localization in wildtype and *glp-1(e2141)* day one adult worms under *luci* control and *acs-13i* (N=3). **D.** Representative confocal image of ACS-13::mKate2 in day one adult worms the germline, intestine, and body wall muscle. Abbreviations: G, germline; M, muscle; INT, intestine. **E-F.** Representative confocal images of MML-1::GFP and ACS-13::mKate2 colocalization in the hypodermis of L4 stage worms. Intensity plot of the ROI from **E.** **G-H.** Representative confocal image of MML-1::GFP and ACS-13::mKate2 colocalization in the intestine of day one adult worms. The intensity plot of the ROI from **G.** Statistical significance was calculated with one-way ANOVA. **B** and **C** bars represent mean + SD. **D, E,** and **G** scale bars represent 10 μ m.

5.13 Inhibition of mitochondrial β -oxidation rescues MML-1 nuclear localization under *hxx-1i*

Hexokinase downregulation might be expected to cause a reduction in the reliance on glycolysis and an increase in fatty acid metabolism as fuel for cellular maintenance. Mitochondrial β -oxidation is an important step in generating acetyl-CoA that enters the TCA cycle through the catabolism of fatty acids to produce energy (**Figure 28A**). Hence, we wanted to investigate whether decreasing fatty acid oxidation could affect MML-1 nuclear localization upon hexokinase knockdown. First, we measured the neutral lipid content by feeding the worms with the labeled fatty acid C1-BODIPY-C12 and found increased total lipid storage under hexokinase knockdown in the wildtype and *glp-1(e2141)* backgrounds (**Figure 27B**).

Next, we measured the oxygen consumption rate (OCR) upon hexokinase knockdown with and without Etomoxir, a mitochondrial β -oxidation inhibitor that acts on the carnitine palmitoyltransferase (CPT). Changes in OCR in the presence of Etomoxir are a correlative measure of β -oxidation of fatty acids in the mitochondria (Ramachandran et al., 2019). We found no difference in basal OCR in our conditions in the wildtype background (**Figure 27C**). *glp-1(e2141)* animals showed decreased basal OCR compared to wildtype, whereas *hxx-1* and *mml-1* knockdown significantly increased the basal OCR (**Figure 27C**). Interestingly, we saw a greater percentage of OCR reduction upon the addition of Etomoxir under *hxx-1* knockdown in wildtype and under *hxx-1*, *hxx-2*, and *mml-1* knockdown in *glp-1(e2141)* (**Figure 27D**), indicating higher mitochondrial β -oxidation levels. We confirmed this result using the transcriptional reporter *acs-2p::GFP*, which encodes a mitochondrial acyl-CoA synthase induced and required for fatty acid β -oxidation (Van Gilst et al., 2005). We found increased *acs-2p::GFP* upon *hxx-1* and *hxx-2* knockdown (**Figure 27E**).

We next wondered whether this increase in fatty acid oxidation was responsible for decreased MML-1 nuclear localization. First, we performed a double knockdown of *hxx-1* and

hvk-2 combined with *cpt-1i* and *acs-2i*. We found that MML-1 nuclear localization was rescued upon *acs-2i* under *hvk-1* knockdown; however, *cpt-1i* did not rescue MML-1 nuclear localization (**Figure 27F**). Neither *cpt-1i* nor *acs-2i* rescued the MML-1 nuclear localization under *hvk-2* knockdown (**Figure 27F**). We also pharmacologically inhibited fatty acid oxidation by supplementing Etomoxir and again saw the rescue of MML-1 nuclear localization under *hvk-1* knockdown, but no effect upon *hvk-2* or *mpc-1* knockdown (**Figure 27G**). These data indicate that *hvk-1* regulates MML-1 by increasing mitochondrial β -oxidation and reveal that the two hexokinases might regulate MML-1 nuclear localization through independent pathways.

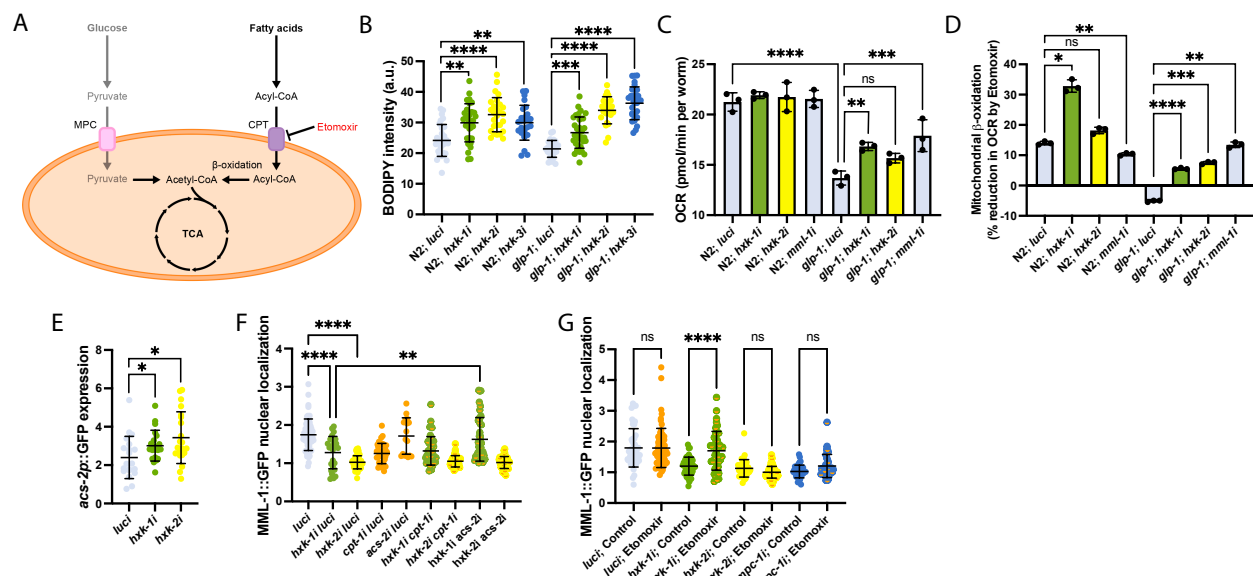


Figure 28. Mitochondrial β -oxidation inhibits MML-1 nuclear localization upon *hvk-1* knockdown. **A.** When glycolysis is reduced, cells rely on fatty acids for energy production. Free fatty acids are activated to acyl-CoA and transported to the mitochondria through the carnitine palmitoyltransferase (CPT) in the mitochondrial outer membrane. The acyl-CoA is then metabolized by β -oxidation to generate acetyl-CoA that can enter the TCA cycle to produce energy. **B.** Worms were grown with C1-BODIPY-C12 egg on and measured on day one of adulthood (N=3). **C-D.** The oxygen consumption rate (OCR) was measured with the Seahorse XF96 Analyzer for basal OCR (**C**) and after the addition of the mitochondrial β -oxidation inhibitor (**D**), shown as the percentage of decreased OCR after the injection of etomoxir (N=3). **E.** Quantification of day one adult worms expressing the transcriptional reporter *acs-2p::GFP* under hexokinase knockdown (N=3). **F.** MML-1 nuclear localization of day one adult worms grown with double knockdown of *hvk-1* and *hvk-2* combined with *cpt-1i* and *acs-2i* (N=3). **G.** MML-1 nuclear localization of day one adult worms grown in different RNAi conditions with or without supplementation of etomoxir 100 μ M egg on (N=3). Statistical significance was calculated with

one-way ANOVA. **B**, **E**, **F**, and **G** bars represent mean + SD. **C** and **D** scale bars represent mean + SEM.

5.14 AMPK regulates MML-1 nuclear localization

We have previously shown that mTOR is a negative regulator of MML-1/MXL-2 complex and that decreasing mTORC1 by knocking down core components of the complex could rescue the nuclear localization of HLH-30 in the *glp-1(e2141) mml-1(ok849)* mutant strain (Nakamura et al., 2016). To test whether hexokinase knockdown increases mTORC1 activity, hence repressing MML-1 nuclear localization, we tagged the leucyl-tRNA synthetase *lars-1* with mKate2 by CRISPR/Cas9. LARS-1 is a positive effector of mTORC1 signaling, regulating Rag GTPases in yeast and mammalian cells (Bonfils et al., 2012; Han et al., 2012). We used this reporter as a proxy for mTORC1 activity and found a significant increase in LARS-1 intensity under *hxx-2i* compared to wildtype. As seen previously, LARS-1 expression was reduced in the *glp-1(e2141)* background; however, *hxx-1i* or *hxx-2i* had no further effect (**Figure 29A**). To validate these findings, we inhibited mTORC1 with the drug Torin-1 (**Figure 29B**) and by knocking down *let-363*/TOR (**Figure 29C**) under *hxx-2i* but saw no rescue of MML-1 nuclear localization. Taken together, these data suggest that *hxx-2i* inhibition of MML-1 nuclear localization is downstream or independent of mTOR and that other mechanisms might be at work.

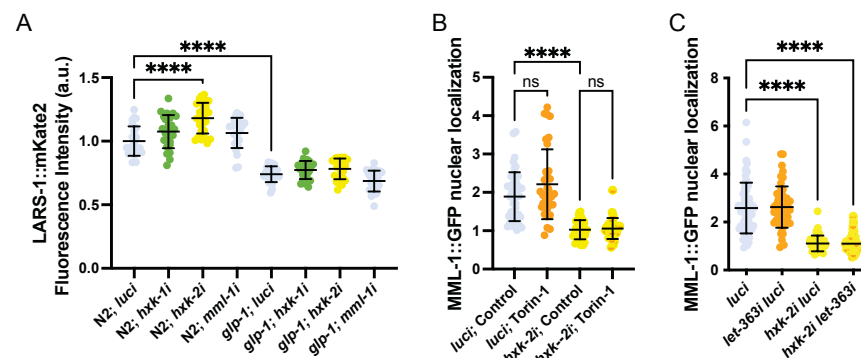


Figure 29. mTOR inhibition does not rescue MML-1 nuclear localization upon *hxx-2* knockdown. **A.** Quantification of LARS-1::mKate2 in day one wildtype and *glp-1(e2141)* adult worms grown in different RNAi (N=2). **B.** MML-1 nuclear localization of day one wildtype adult worms grown with mTOR inhibitor Torin-1 10 μ M egg on (N=2). **C.** MML-1 nuclear localization of day one wildtype worms with *hxx-2* and *let-363* double knockdown (N=2). Statistical significance was calculated with one-way ANOVA. **A**, **B**, and **C** bars represent mean + SD.

Another key metabolic enzyme involved in metabolic adaption is the AMP-activated protein kinase (AMPK). Under low ATP levels, AMPK is activated and phosphorylates substrates to activate catabolic processes and stress responses. Hence, we wished to test whether AMPK was involved in metabolic reprogramming regulating MML-1. First, we measured AMPK activity by detecting the phosphorylation levels of the α catalytic subunit at Thr172, which resides in the activation loop and is required to activate the AMPK (Hardie et al., 2012). This phosphorylation site is conserved in the AMPK α subunits AAK-1 and AAK-2 of *C. elegans* as Thr243 (Apfeld et al., 2004; Y. Zhang et al., 2019) (**Figure 30A**). To confirm the specificity of the antibody, we used the *aak-1(tm1944)* and *aak-2(ok524)* null mutants and found that the antibody only recognized AAK-2 phosphorylation (**Figure 30B and C**). Next, we measured AMPK phosphorylation upon hexokinase knockdown and found no difference in wildtype or the *glp-1(e2141)* backgrounds (**Figure 30B and C**).

We next tested whether AMPK activity impacts MML-1 nuclear localization. Surprisingly, we observed increased MML-1 nuclear localization upon knockout of *aak-1* and *aak-2* (**Figure 30D and E**). As AAK-1 and AAK-2 have partially overlapping functions, we confirmed this finding with the *aak-1(tm1944) aak-2(ok524)* double mutant (**Figure 30F**). Finally, we tested whether AMPK α knockout could rescue the nuclear localization upon *hxx-2* knockdown and found that in the *aak-1(tm1944) aak-2(ok524)* mutant with *hxx-2i*, MML-1 nuclear localization was restored to wildtype levels. Collectively, these data implicate AMPK in the metabolic reprogramming regulating MML-1 function.

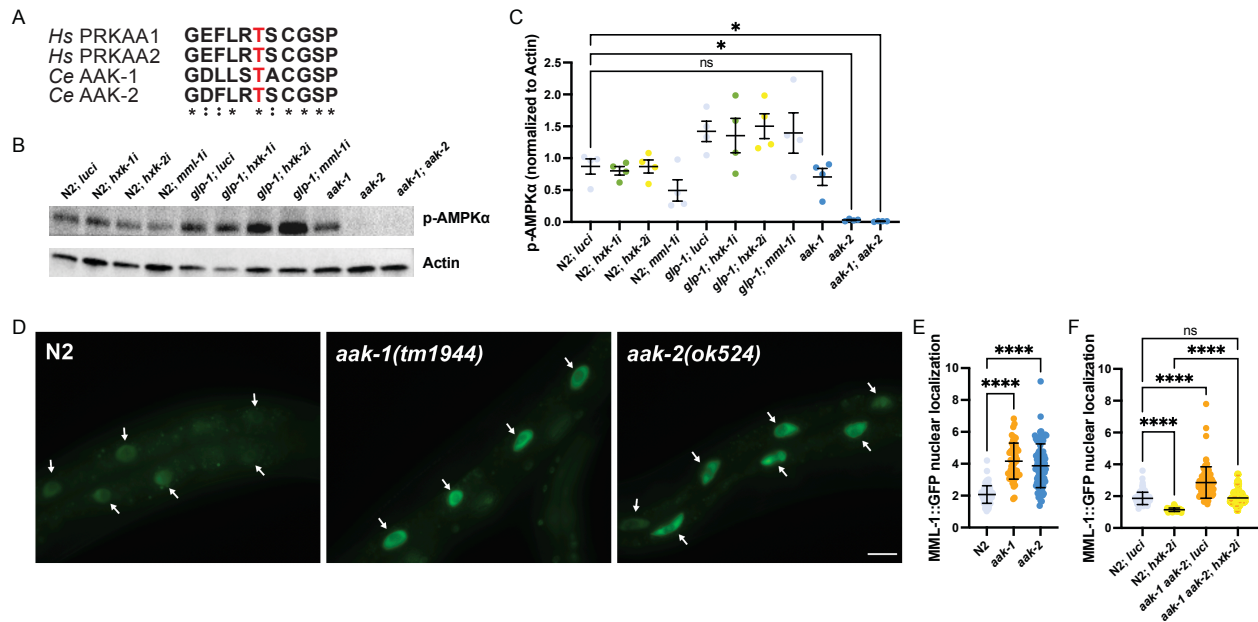


Figure 30. *hsk-2i* decreases MML-1 nuclear localization in an AMPK-dependent manner. A. Sequence of the two AMPKα subunits from humans (*Hs*) and worms (*Ce*). LKB1 phosphorylation sites Thr172 are highlighted in red. **B-C.** Representative immunoblot and quantification of AMPKα phosphorylation in day one adult wildtype N2 and *glp-1(e2141)* worms upon hexokinase knockdown. Actin levels were used as a loading control (N=4). **D-E.** Representative images (**D**) and quantification (**E**) of MML-1::GFP reporter nuclear localization in the AMPKα knockout strains *aak-1(tm1944)* and *aak-2(ok524)*. **F.** Quantification of MML-1::GFP nuclear localization in wildtype N2 and *aak-1(tm1944) aak-2(ok524)* double mutant upon *hsk-2* knockdown (N=3). **D** scale bar represents 20 μm. Statistical significance was calculated with one-way ANOVA. **C** bars represent mean + SEM. **E** and **F** bars represent mean + SD.

Chapter II. MML-1/MXL-2 regulation in longevity

5.15 *MML-1 interactome in the insulin longevity*

To gain insights into MML-1 regulation and function in insulin longevity, we immunoprecipitated MML-1::3xFLAG from *daf-2(e1370)* animals and identified potential binding partners by mass spectrometry. We detected between 287 and 727 proteins in the different biological replicates (**Figure 31A**) and the genotypes clustered together (**Figure 31B**). MML-1 was the second most enriched protein compared to control *daf-2(e1370)* worms without the 3xFLAG tag (**Figure 31C, Supplementary Table 8**). The most abundant protein co-enriched with MML-1 was ACER-1, an acetyl-CoA hydrolase/transferase that regulates histone acetylation levels (Gao et al., 2015). From the top 25 candidates (**Figure 31C**), some of the co-enriched candidates are proteins involved in maintaining redox homeostasis, including the catalase CTL-1, the glutathione S-transferase GST-1, the methionine sulfoxide reductase MSR-1, and the thioredoxin-dependent peroxide reductase PRDX-3. Other proteins were involved in carbohydrate and lipid metabolism, like the cytosolic ATP-dependent citrate synthase ACLY-1, the pyruvate kinase PYK-1, the ATP synthase subunit ATP-1, the G6PDH GSPD-1, and the electron transfer flavoprotein subunit alpha F27D4.1. Surprisingly, compared to the top enriched proteins from the immunoprecipitation of MML-1 in wildtype and *glp-1*, we found no overlap in the potential interactors. Collectively, these data suggest that MML-1 may interact with different proteins depending on the genetic context and offers a possibility for studying novel functions of MML-1 in the reduced insulin signaling-mediated longevity.

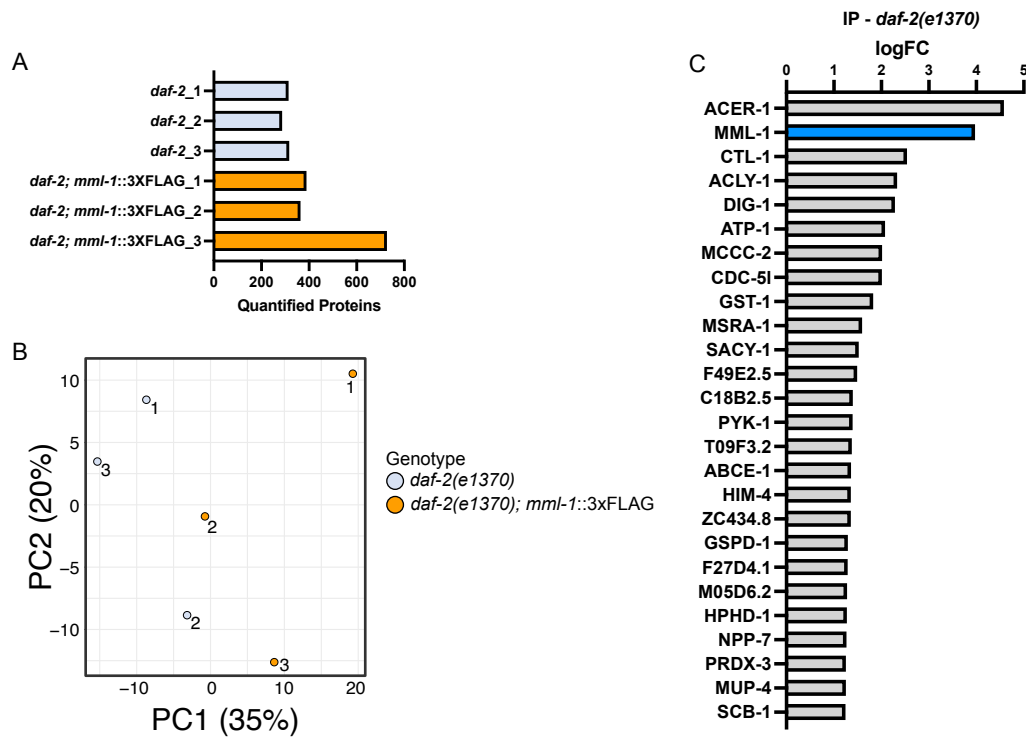


Figure 31. MML-1 interactome in the reduced insulin signaling longevity. **A.** Quantified proteins in each biological replicate of *daf-2(e1370)* and *daf-2(e1370); mml-1::3xFLAG* (N=3). **B.** PCA analysis with each biological replicate of the genotypes from proteomics. **C.** Anti-FLAG immunoprecipitation from whole-worm lysates of animals expressing MML-1::3xFLAG in *daf-2(e1370)* background. IP was analyzed by mass spectrometry to identify peptides. The 25 top candidates co-enriched with MML-1 compared to *daf-2(e1370)* control are shown as log FC, including MML-1.

5.16 Insulin signaling and germline MML-1/MXL-2-dependent transcriptomes

As mentioned previously, MML-1/MXL-2 are required for the lifespan extension of multiple longevity pathways. Our data also suggest that MML-1 regulation may be specific to the longevity context. Hence, we used a combination of genome-wide expression analysis and metabolomics to determine the MML-1/MXL-2-dependent effects in the context of insulin and germline longevity. First, we measured the differential expression of genes (DEGs) by RNAseq from wildtype, *daf-2(e1370)*, *mml-1(ok849)*, *mxl-2(tm1516)*, and the double mutants with *daf-2(e1370)*. The PCA analysis of these data showed clustering between the biological replicates and differentiation between genotypes (**Figure 32A**). *mml-1(ok849)* and *mxl-2(tm1516)* loss-of-function mutants resulted in the regulation of multiple genes in wildtype and *daf-2(e1370)*. However, the *mml-1(ok849)* mutant had a more substantial effect on the transcriptome of

daf-2(e1370), while the *mxl-2(tm1516)* mutant had a more substantial impact in wildtype (**Figure 32B**). Comparison between *mml-1(ok849)* and *mxl-2(tm1516)* transcriptomes in the *daf-2(e1370)* background revealed a small number of genes (67 DEGs) commonly regulated by both transcription factors.

Gene ontology (GO) analysis of *daf-2(e1370) mml-1(ok849)* versus *daf-2(e1370)* transcriptomes revealed enrichment in genes implicated in cell and nervous system development, reproduction, and locomotion (**Figure 32C**). Kyoto Encyclopedia of Genes and Genomes (KEGG) pathway analysis revealed an enrichment of genes implicated in the proteasome, nitrogen, amino acid, and amino sugar metabolism (**Figure 32D**). By comparison, *mxl-2*-dependent changes on the *daf-2(e1370)* transcriptome were widely different from *mml-1(ok849)*. There was an overrepresentation of DEGs involved in metabolic processes such as carboxylic acid, glucuronate, uronic acid, flavonoid, and other organic acids (**Figure 32E**). From the KEGG pathway analysis, the *mxl-2*-dependent transcriptome was enriched with genes involved in the carbon and nitrogen metabolism, fatty acid degradation, and amino acid metabolism (**Figure 32F**). Taken together, these data suggest that MML-1 and MXL-2 might work in independent transcriptional cascades in the insulin longevity pathway.

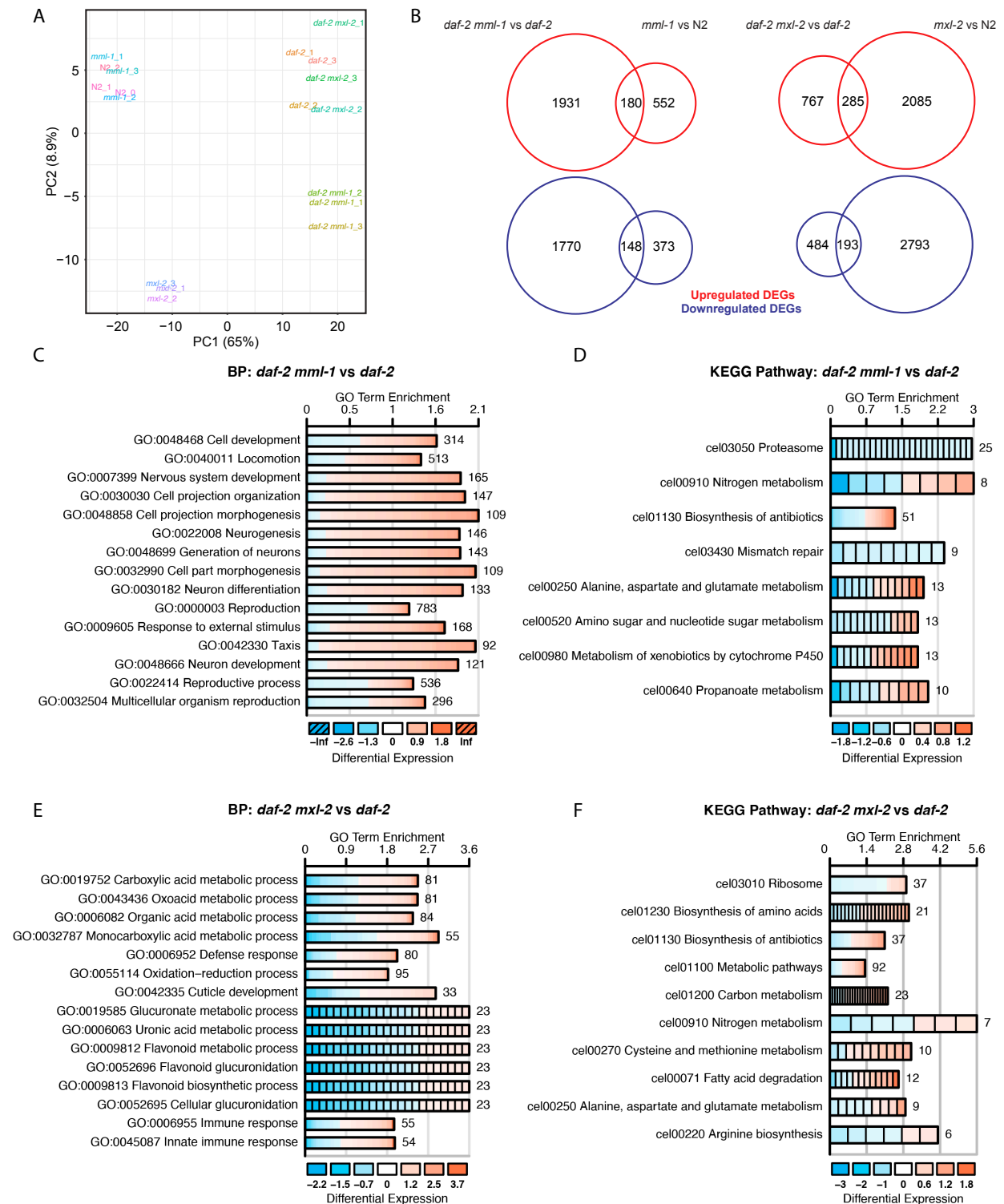


Figure 32. Transcriptome analysis reveals differences between MML-1 and MXL-2 regulated genes in the insulin signaling pathway. A. PCA analysis with each biological replicate of the genotypes from the transcriptomics. **B.** Venn diagrams with the number of DEGs up- and downregulated identified through RNAseq from *daf-2(e1370) mml-1(ok849)* versus *daf-2(e1370)*, *mml-1(ok849)* versus N2, *daf-2(e1370) mxl-2(tm1516)* versus *daf-2(e1370)*, and *mxl-2(tm1516)*

versus N2. **C-D.** GO term enrichment analysis of *daf-2(e1370) mml-1(ok849)* versus *daf-2(e1370)* transcriptome using DAVID analysis for biological process (BP) (**C**) and KEGG pathway (**D**). **E-F.** GO term enrichment analysis of *daf-2(e1370) mxl-2(tm1516)* versus *daf-2(e1370)* transcriptome using DAVID for biological process (BP) (**E**) and KEGG pathway (**F**). The GO enrichments are represented by the log FC (color-coded), and the numbers of genes in each category are shown on the right of each bar.

To better understand the function of MML-1/MXL-2 in two distinct longevity contexts, we compared the *mml-1*- and *mxl-2*-dependent transcriptomes in the *daf-2(e1370)* background with our previous data of these transcription factors in the *glp-1(e2141)* background (Nakamura et al., 2016). First, we compared the significant DEGs represented in both transcriptomes and found that MML-1 and MXL-2 regulate a subset of genes differently in both longevity models (**Figure 33A and B**). A closer analysis of these transcriptomic data shows that MML-1 similarly regulates 438 genes (216 upregulated and 222 downregulated), and 229 genes were regulated oppositely by MML-1 in the double mutants compared to the single mutant (**Figure 33C**). Interestingly, we found that MML-1 had a more substantial effect in regulating genes in *daf-2(e1370)* than in *glp-1(e2141)*. These data suggest that the MML-1/MXL-2 transcriptional network is wired differently in the germline and the insulin longevity models.

Next, we manually interrogated the data to see whether genes that have been reported to contribute to *mml-1*-induced gonadal longevity were commonly regulated in *glp-1(e2141)* and *daf-2(e2141)* transcriptomes. We found that at least *mdl-1* and *fat-5* behaved similarly between both longevity models (**Figure 33D**) and confirmed that *fat-5* expression is significantly lower in the *daf-2(e1370) mml-1(ok849)* double mutant by qPCR analysis (**Figure 33E**). We have also found that MML-1 and MXL-2 regulate the transcription of multiple genes involved in fatty acid synthesis and desaturation in the *glp-1(e2141)* (Karalay et al., unpublished). To investigate whether MML-1 regulates these genes in the *daf-2(e2141)*, we manually interrogated the RNAseq data for the expression of these genes in the *daf-2(e1370) mml-1(ok849)* versus *daf-2(e1370)* transcriptome. We found that 11 of these transcripts were regulated similarly when comparing the *glp-1(e2141) mml-1(ok849)* versus *glp-1(e2141)* transcriptomes, five transcripts behaved oppositely, and five transcripts only showed regulation in the *daf-2(e1370)* background (**Figure 33F**). Collectively, these data indicate that MML-1 regulates distinct gene sets in the germline and insulin longevity mutants. However, at least a subset of the genes associated with longevity is commonly shared between both longevity models.

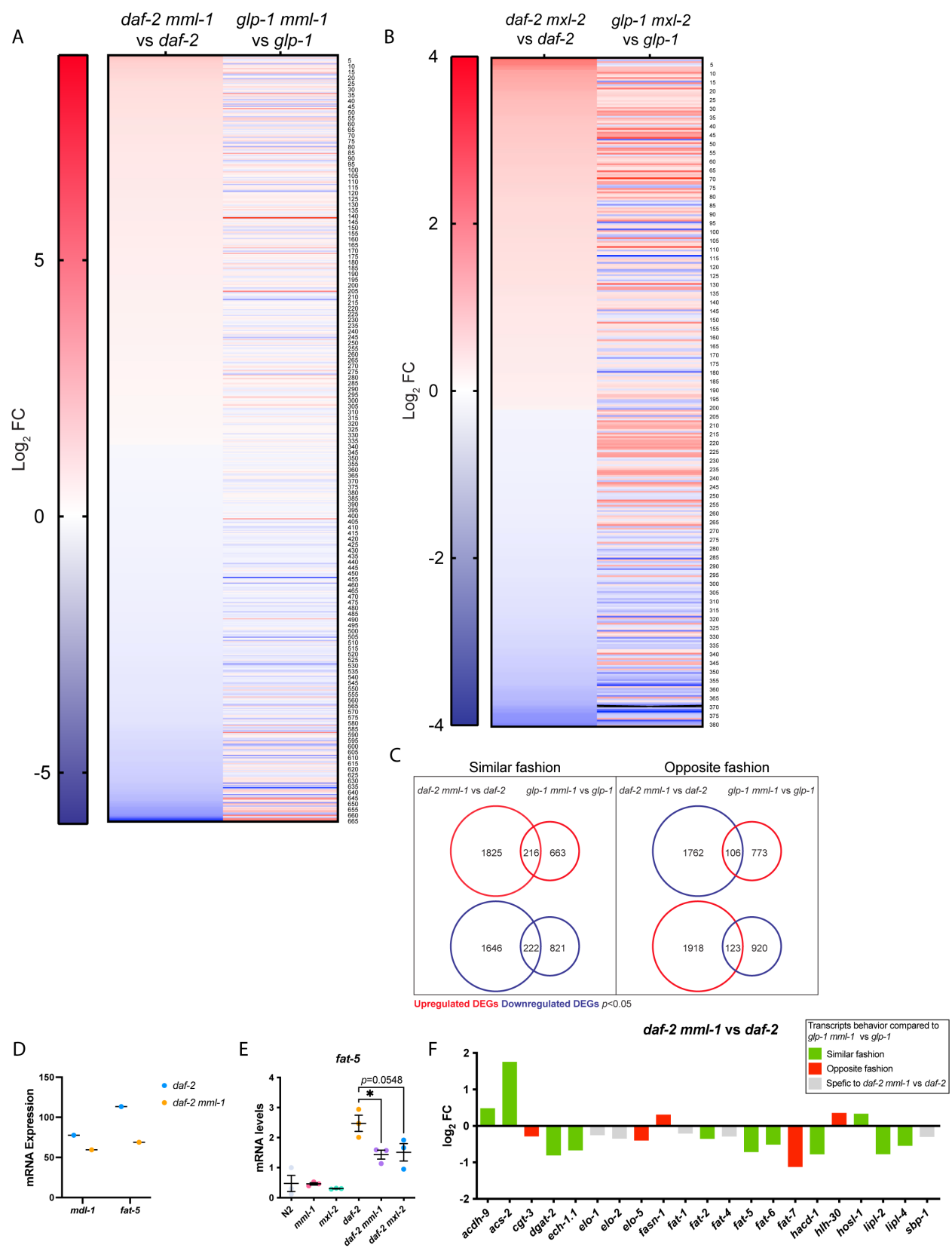
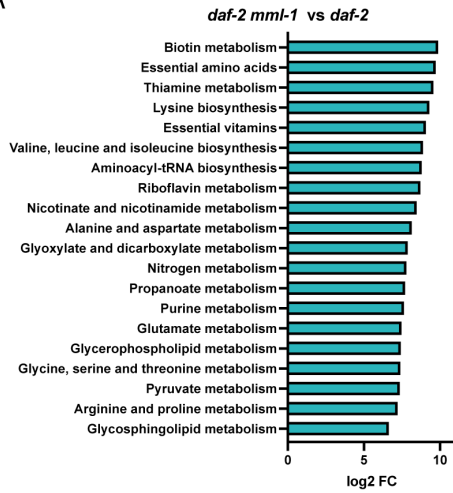


Figure 33. MML-1/MXL-2-dependent transcriptome reveals commonly regulated and preferentially regulated genes in the insulin and germline longevity pathways. **A.** Comparison between the *daf-2(e1370) mml-1(ok849)* versus *daf-2(e1370)* and the *glp-1(e2141) mml-1(ok849)* versus *glp-1(e2141)* DEGs. **B.** Comparison between the *daf-2(e1370) mxl-2(tm1516)* versus *daf-2(e1370)* and the *glp-1(e2141) mxl-2(tm1516)* versus *glp-1(e2141)* DEGs. **C.** Venn diagram shows the number of significantly changed DEGs (adj. $p < 0.05$) regulated by *mml-1* in the *daf-2(e1370)* and the *glp-1(e2141)* long-lived mutants. **D.** Expression level of *mdl-1* and *fat-5* from the RNAseq data ($p < 0.0001$). **E.** Relative gene expression of *fat-5* in young adult worms determined by qPCR (N=3). Statistical significance was calculated with a two-tailed *t*-test. **F.** Expression of fat metabolism genes from the *daf-2(e1370) mml-1(ok849)* versus *daf-2(e1370)* RNAseq data. Significantly regulated genes are shown as log₂ FC. The data was compared to the *glp-1(e2141) mml-1(ok849)* versus *glp-1(e2141)* transcriptomes and color-coded to depict whether the gene is regulated similarly or oppositely in both transcriptomes. **E** bars represent mean + SEM.

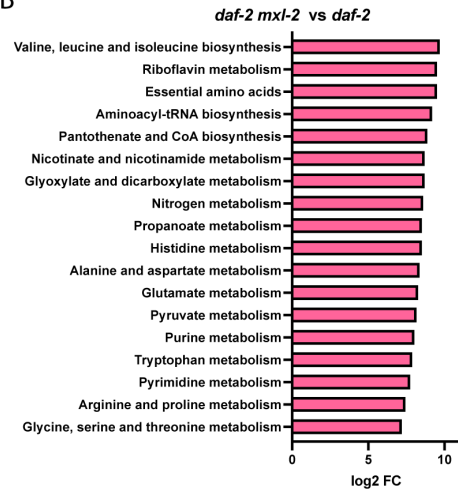
Insulin signaling and germline MML-1/MXL-2-dependent metabolomes

We performed mass spectrometry-based untargeted metabolomics to determine whether the effect of MML-1/MXL-2-dependent transcriptional network in the *daf-2(e1370)* and *glp-1(e2141)* results in changes in the metabolic profiles. We identified 45 and 30 metabolites that were significantly changed in the *daf-2(e1370) mml-1(ok849)* and *daf-2(e1370) mxl-2(tm1516)* mutants, respectively, compared to *daf-2(e2141)* (adj. $p < 0.05$) (**Figure 34A and B, Supplementary Table 9**). Pathway enrichment analysis revealed metabolites involved in amino acid, nitrogen, pyruvate, and purine metabolism in the *daf-2(e1370) mml-1(ok849)* versus *daf-2(e1370)* (**Figure 34C**). The *mxl-2*-dependent *daf-2(e1370)* metabolome showed similar pathways enriched (**Figure 34D**). Comparable with our transcriptomic data, we found metabolites commonly regulated by *mml-1* and *mxl-2*. However, we also found preferentially regulated metabolites in each mutant strain (**Figure 34E**). The 20 overlapping metabolites were regulated similarly by *mml-1(ok849)* and *mxl-2(tm1516)* in the *daf-2(e1370)*. Commonly regulated metabolites include the glycolysis intermediates glucose biphosphate, phosphoenolpyruvate, and TCA cycle intermediate citric acid. Taken together, these data indicate that MML-1 and MXL-2 share common metabolic signatures in insulin longevity.

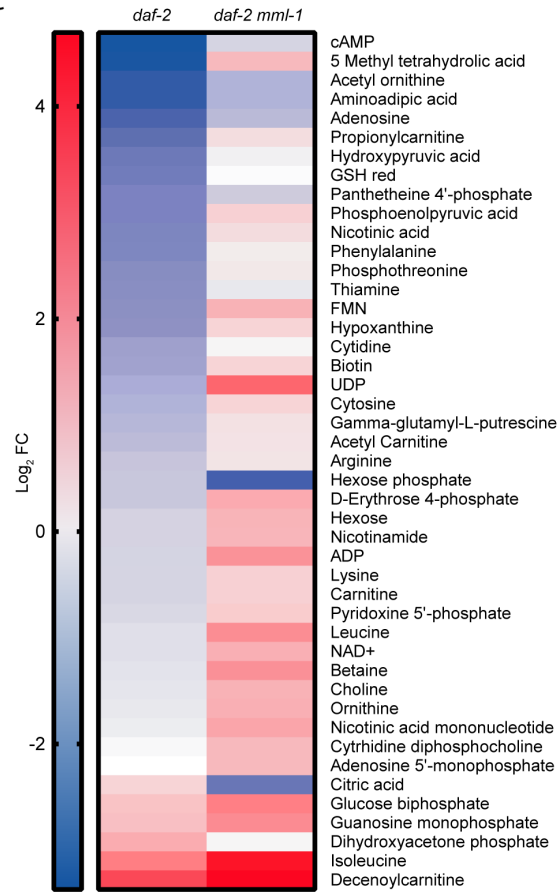
A



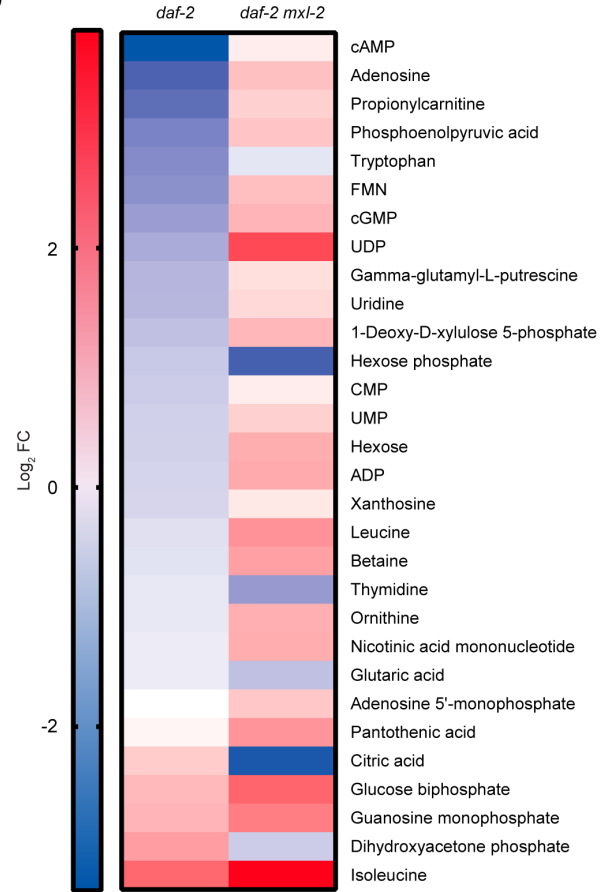
B



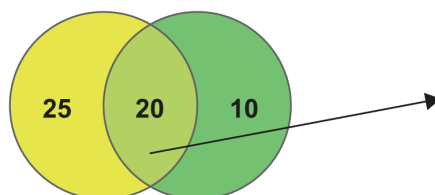
C



D



E

daf-2 mml-1 vs *daf-2**daf-2 mxl-2* vs *daf-2*

Adenosine	↑↑	Guanosine monophosphate	↑↑
Adenosine 5'-monophosphate	↑↑	Hexose	↑↑
ADP	↑↑	Hexose phosphate	↑↓
Betaine	↑↑	Isoleucine	↑↑
cAMP	↑↑	Leucine	↑↑
Citric acid	↓↓	Nicotinic acid mononucleotide	↑↑
Dihydroxyacetone phosphate	↓↓	Ornithine	↑↑
FMN	↑↑	Phosphoenolpyruvic acid	↑↑
Gamma-glutamyl-L-putrescine	↑↑	Propionylcarnitine	↑↑
Glucose biphosphate	↑↑	UDP	↑↑

Figure 34. MML-1/MXL-2-dependent metabolomic analysis reveals common regulation of metabolic pathways in insulin longevity. **A-B.** Untargeted metabolomic analysis of *daf-2(e1370)*, *daf-2(e1370) mml-1(ok849)* (**A**) and *daf-2(e1370) mxl-2(tm1516)* (**B**) at young adult stage (N=4). The heat map indicates the relative abundance of significantly changed metabolites compared to the wildtype average (adj. $p < 0.05$). **C-D.** Pathway enrichment analysis of *daf-2(e1370) mml-1(ok849)* versus *daf-2(e1370)* (**C**) and *daf-2(e1370) mxl-2(tm1516)* versus *daf-2(e1370)* (**D**). Only significantly changed metabolites were used with post hoc Benjamini-Hochberg correction for multiple comparisons. **E.** Venn Diagram with significantly changed metabolites comparing *daf-2(e1370) mml-1(ok849)* versus *daf-2(e1370)* and *daf-2(e1370) mxl-2(tm1516)* versus *daf-2(e1370)* data sets. On the right is the list with the 20 metabolites lying at the intersection of both data sets. Arrows indicate whether the metabolite is upregulated (up green arrow) or downregulated (down red arrow) in the double mutants compared to the single mutants.

We also performed untargeted metabolomics in the *glp-1(e2141)* longevity background. We found 18 and 14 metabolites differentially regulated in the *glp-1(e2141) mml-1(ok849)* and *glp-1(e2141) mxl-2(tm1516)*, respectively, compared to *glp-1(e2141)* (**Figure 35A and B, Supplementary Table 10**). We did not perform pathway enrichment analysis due to the small number of significantly changed metabolites in our data sets. However, we found the amino acids proline, tryptophan, glutamine, and methionine regulated and other glucose metabolism intermediates like glycerate biphosphate, 2-oxoglutarate, erythrose 4-phosphate, and citric acid. We found three metabolites commonly shared between both data sets that behaved similarly when comparing *mml-1*- and *mxl-2*-dependent changes of the *glp-1(e2141)* metabolome. At the same time, hexose phosphates were downregulated in the *glp-1(e2141) mml-1(ok849)* versus *glp-1(e2141)* and upregulated in the *glp-1(e2141) mxl-2(tm1516)* versus *glp-1(e2141)* metabolomics (**Figure 35C**). Next, we compared the *mml-1*-dependent metabolome in the *daf-2(e1370)* and *glp-1(e2141)*. We found ten metabolites shared between both data sets, some regulated differently depending on the longevity context, including aminoadipic acid, citric acid, hexose phosphate, and thiamine (**Figure 35D**). Collectively, these data suggest that MML-1/MXL-2 have common and specific metabolic fingerprints in different longevity contexts.

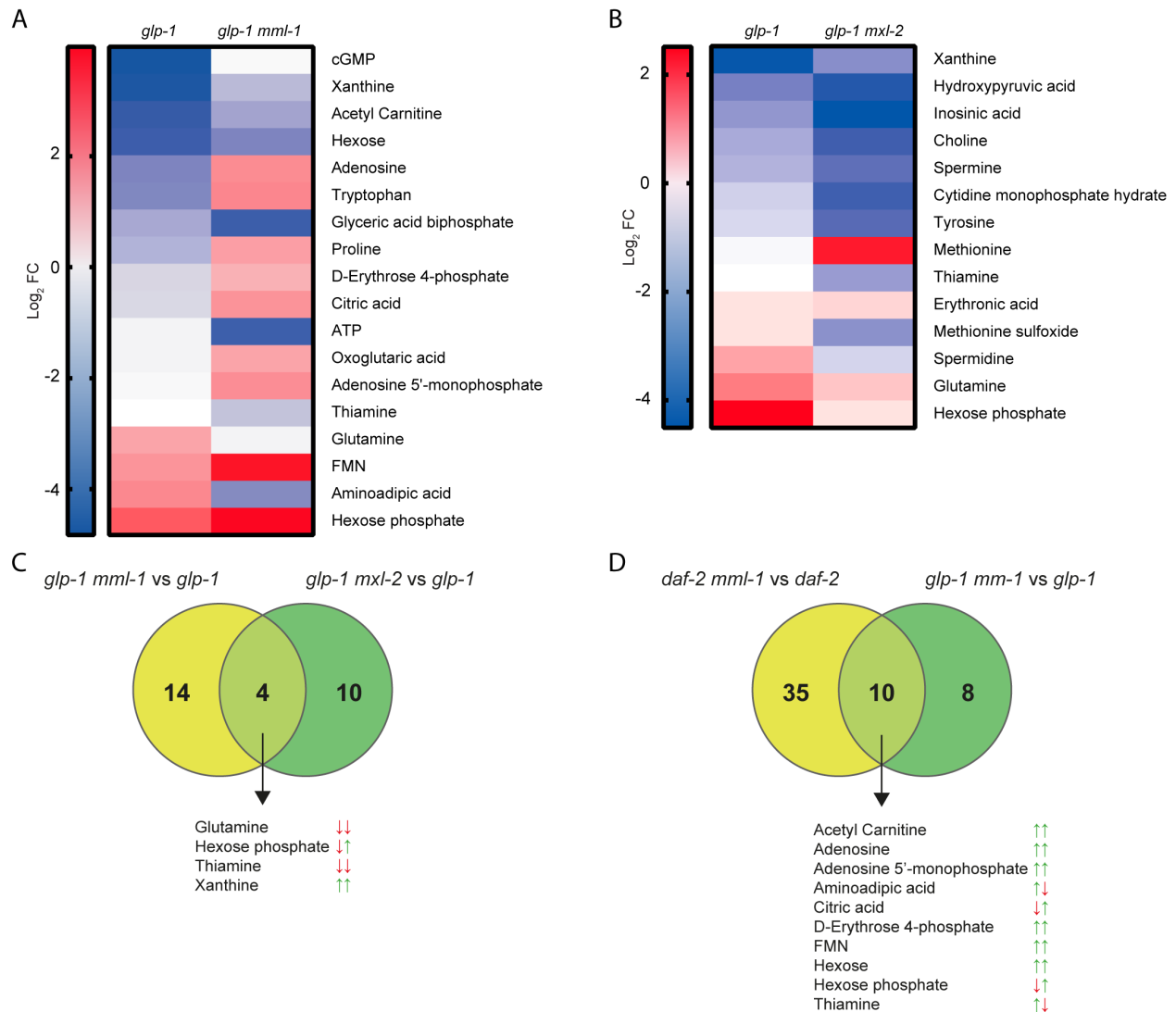


Figure 35. MML-1/MXL-2 metabolic fingerprints in distinct longevity contexts. A-B. Untargeted metabolomic analysis of *glp-1(e2141)*, *glp-1(e2141) mml-1(ok849)* (A) and *glp-1(e2141) mxl-2(tm1516)* (B) at young adult stage (N=4). The heat map indicates the relative abundance of significantly changed metabolites compared to the wildtype average (adj. $p < 0.05$). C. Venn Diagram with significantly changed metabolites comparing *glp-1(e2141) mml-1(ok849)* versus *glp-1(e2141)* and *glp-1(e2141) mxl-2(tm1516)* versus *glp-1(e2141)* data sets. D. Venn diagram with significantly changed metabolites comparing the *daf-2(e2141) mml-1(tm1516)* versus *daf-2(e2141)* and *glp-1(e2141) mml-1(ok849)* versus *glp-1(e2141)* data sets. Below, metabolites lying at the intersection of both data sets. Arrows indicate whether the metabolite is upregulated (up green arrow) or downregulated (down red arrow) in the double mutants compared to the single mutants.

VI. Discussion

Nutrient sensing and metabolism play a central role in modulating aging. Although much work has been done in identifying proteins involved in these processes, much work is needed to understand how organisms coordinate metabolic pathways and transcriptional responses. Here, we present novel mechanisms of carbohydrate and lipid metabolism regulating the transcription factor MML-1/Mondo. We observed that MML-1 senses multiple steps of glucose metabolism and found that hexokinases are upstream positive regulators of MML-1 function in *C. elegans* (**Figure 36**). On the one hand, we found that under *hvk-2* knockdown, MML-1 re-localizes to mitochondria and LD, abolishing the longevity of germline-less worms and mutants with reduced mitochondrial function. Moreover, we could rescue MML-1 function by decreasing the PPP and subunits of the OGDC independent of the G6P levels. On the other hand, we found that *hvk-1* knockdown decreased MML-1 function by upregulating mitochondrial β -oxidation. Thus, we found two metabolic branches that converge on MML-1 to trigger a transcriptional response and regulate longevity.

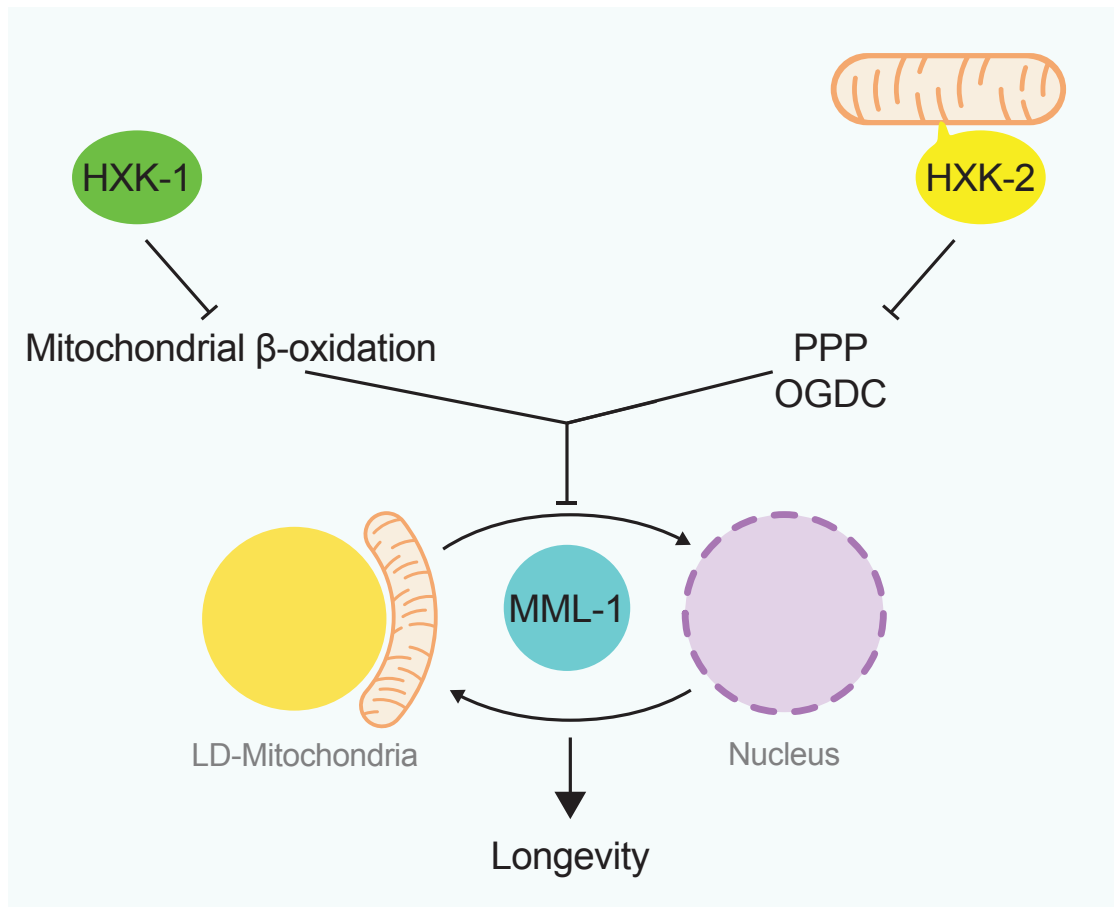


Figure 36. Working model of MML-1 regulation by hexokinases. MML-1 is positively regulated by HXK-1 and HXK-2 through different downstream mechanisms. Inhibition of the mitochondrial β -oxidation rescues MML-1 nuclear localization upon *hxx-1i*, while decreasing enzymes from the PPP and the OGDC of the TCA cycle rescues MML-1 localization upon *hxx-2i*. These upstream mechanisms regulate MML-1 subcellular localization between LD-mitochondria and the nucleus, which is required for the lifespan extension mediated by germ-line loss and reduced mitochondrial activity. Abbreviations: PPP, pentose phosphate pathway; LD, lipid droplet.

6.1 MML-1 senses multiple steps of glucose metabolism

Downregulation of pathways involved in insulin signaling, mTOR, mitochondrial activity, and germline signaling have been shown to regulate *C. elegans* metabolism and longevity (C. J. Kenyon, 2010). Although our understanding of how such pathways impact metabolism has increased over the last decades, the link between metabolism and transcriptional outputs in regulating lifespan has remained elusive. Our previous work described the basic helix-loop-helix (bHLH) transcription factors MML-1/MondoA/ChREBP and MXL-2/Mlx as vital metabolic

regulators towards which multiple longevity pathways converge (Nakamura et al., 2016). Our work here focuses on the upstream signals that modulate MML-1 function to illuminate the mechanistic connections between metabolism and longevity.

MondoA and ChREBP transcription factors have well-established central roles in glucose metabolism (Ma et al., 2006; Sans et al., 2006; Stoltzman et al., 2008; Yamashita et al., 2001). But whether and how glucose metabolic circuits affect Mondo regulation in a whole animal model is little explored. By performing a systematic RNAi-based targeted screen of enzymes involved in glucose anabolism and catabolism, we found that MML-1 senses multiple steps of glucose metabolism in the worm. Among the genes tested, we found MML-1 nuclear localization to be broadly sensitive to the downregulation of glycolytic enzymes, and the knockdown of hexokinase had the most profound effect. Hexokinase carries out the first step in glucose metabolism, the phosphorylation of glucose to form G6P, which can be shunted to multiple metabolic pathways, including glycolysis, the PPP, glycogenesis, and trehalose production. Our findings are consistent with previous work in cultured cells showing that MondoA localization is regulated by HKII, which is thought to stimulate nuclear localization via the production of G6P (Sans et al., 2006). Additionally, MondoA senses other phosphorylated hexoses, including allose and 3-*O*-methylglucose (Stoltzman et al., 2011).

Consistent with our genetic findings above, pharmacological inhibition of glycolysis by supplementation with 3-BrP and 2-DG suppressed MML-1 nuclear localization. In contrast to MML-1, MondoA has been shown to accumulate in the nucleus upon 2-DG in rat L6 cells (Stoltzman et al., 2008). A possible explanation for this difference is that our treatment represents a chronic exposure to 2-DG from development until adulthood, while the experiments in cells may reflect an acute response. Overall, 2-DG has been used as a glycolytic inhibitor because it can be phosphorylated by hexokinase to 2-DG 6-phosphate; however, it cannot be further metabolized in glycolysis. Further evidence shows that 2-DG not only functions as a catabolic inhibitor but can also be directed to the PPP or other pathways (Chi et al., 1987; Ralser et al., 2008).

Further, we found an important link between glycolysis and pyruvate metabolism regulating MML-1 localization. Under aerobic conditions, pyruvate is imported to the mitochondria and converted to acetyl-CoA to generate ATP and other reducing molecules. We found that downregulation of the mitochondria pyruvate carrier *mpc-1* and the pyruvate dehydrogenase complex (**Supplementary Table 4**) also decreased MML-1 nuclear localization

and function. Interestingly, loss of *MPC1* in yeast has been shown to accumulate pyruvate, lower TCA cycle intermediates, and reduce chronological aging (Bricker et al., 2012; Orlandi et al., 2014). *MPC1* similarly regulates the disposition of glycolytic and TCA intermediates in flies and mammals (Bricker et al., 2012). Pyruvate can also enter the TCA cycle through pyruvate carboxylase PYC-1, which converts pyruvate to oxaloacetate. However, knockdown of *pyc-1* did not affect MML-1 localization in our hands (**Supplementary Table 4**), suggesting that MML-1 may sense the metabolism of pyruvate mainly through oxidative decarboxylation acetyl-CoA.

We also found that MML-1 responds strongly to alterations in the TCA cycle. The TCA cycle allows organisms to oxidize carbohydrates, fatty acids, and amino acids to provide energy and intermediates for the biosynthesis of macromolecules. Interestingly, the knockdown of two subunits of the OGDC, *ogdh-1* and *dld-1*, increased MML-1 nuclear localization and rescued the MML-1 transcriptional response upon *hxx-2i*. How exactly this complex regulates MML-1 remains unknown. The OGDC is a rate-limiting enzyme within the mitochondrial TCA cycle that decarboxylates 2-oxoglutarate to succinyl-CoA. It has been shown previously that supplementation of 2-oxoglutarate and knockdown of *ogdh-1* extends lifespan through inhibition of ATP synthase, decreasing oxygen consumption, and increasing autophagy in an mTOR-dependent manner (Chin et al., 2014). It would be interesting to test whether this lifespan extension requires MML-1 activity. Conceivably, the mitochondrial localization of MML-1 could help sense 2-oxoglutarate levels, and accumulation of this metabolite could signal translocation to the nucleus. However, in our hands, supplementation of 2-oxoglutarate failed to rescue MML-1 nuclear localization upon *hxx-2* knockdown (Vonolfen, 2020). We also supplemented all TCA cycle intermediates upon *hxx-2i* and could not rescue the MML-1 nuclear localization (Vonolfen, 2020), suggesting that other mechanisms may link MML-1 to the TCA cycle independent of the metabolite levels.

Another such possibility is glutaminolysis. Glutamine can be converted to glutamate and subsequently to 2-oxoglutarate during glutaminolysis and represents an important mechanism to replenish the TCA cycle under different metabolic challenges. In this case, OGDC plays a pivotal role in channeling anaplerotic reactions into the TCA cycle from glutamine and glutamate and other amino acids that can ultimately be converted to 2-oxoglutarate (*i.e.*, histidine, proline, and arginine) (Owen et al., 2002). Interestingly, increased glutamine-dependent anaplerosis has been shown to regulate MondoA activity in BxPC-3 cells (Kadige et al., 2009), though the molecular

mechanism remains unclear. Whether glutamine, glutamate supplementation, or knockdown of glutamate dehydrogenase can regulate MML-1 nuclear localization remains to be determined.

On the other hand, the TCA cycle can operate in reverse to restore TCA intermediate levels (Dalziel & Londesborough, 1968). Increased levels of 2-oxoglutarate due to inhibition of OGDH, or glutamine anaplerosis, can undergo reductive carboxylation by isocitrate dehydrogenase to produce isocitrate. After that, aconitase can convert isocitrate to citrate, which can be exported out of the mitochondria for *de novo* lipogenesis. MML-1 could help orchestrate the metabolic rewiring of the TCA cycle with the fatty acid metabolism transcriptional response. Notably, ChREBP has been shown to regulate many lipogenic enzymes, including acetyl-CoA carboxylase (ACC), the fatty acid synthase (FAS), and ATP-citrate lyase (ACLY) (Ishii et al., 2004; Postic et al., 2007). Accordingly, the MML-1 transcriptome shows clear regulation of several fatty acid metabolic enzymes (Nakamura et al., 2016) and promotes MUFAs production (Karalay, unpublished).

Also, within the TCA cycle, we observed that the knockdown of two subunits of the succinyl-CoA synthase (SCS), *succa-1* and *sucg-1*, stimulated MML-1 nuclear localization. The SCS is an enzyme that catalyzes the reversible reaction of succinyl-CoA to succinate, generating ATP or GTP and free CoA. The SCS is a heterodimeric enzyme composed of subunits α and β , the latter determining the substrate specificity for ADP or GDP (J. D. Johnson et al., 1998). *succa-1* is a homolog to the ADP-dependent SUCLA2, and *sucg-1* is the GDP-dependent SUCLG2. Knockdown of this enzyme decreases the levels of succinate, affecting multiple cellular processes, including DNA methylation and gene expression (Martínez-Reyes & Chandel, 2020). Also, perturbations in mitochondrial metabolism elicit activation of the mitochondrial unfolded protein response (UPR^{mt}) (Runkel et al., 2013; X. Wang et al., 2016; Yoneda et al., 2004). However, we only observed induction of the mitochondrial stress response chaperone *hsp-6* upon knockdown of the SCS α subunits *suc1-1* and *suc1-2*, but not for β subunits *succa-1* and *sucg-1*. Further, we did not observe any effect upon inhibition of Complex III and IV of the ETC in MML-1 nuclear localization, indicating that the regulation observed is not likely due to a general increase of UPR^{mt} *per se*, but something more specific.

Aside from their mitochondrial metabolic functions, recent studies have also revealed non-canonical roles for TCA cycle enzymes in the nucleus. Multiple enzymes involved in the TCA cycle, including all the subunits of OGDH and SCS, have been identified in nuclei in cells and mice embryos (Nagaraj et al., 2017; Y. Wang et al., 2017). It has been proposed that their activity

is coupled with chromatin regulation (Xujun Liu et al., 2021). OGDC has been reported to provide a local pool of succinyl-CoA destined for succinylation of histones in the nucleus (Y. Wang et al., 2017). Other metabolic enzymes like the pyruvate kinase M2, fumarase, and the pyruvate dehydrogenase complex have also been reported to localize in the nucleus and regulate transcription and DNA repair (Y. Jiang et al., 2015; Sutendra et al., 2014; Weiwei Yang et al., 2011). Speculatively, the involvement of these metabolic enzymes in epigenetic regulation may link directly to promoters of genes regulated by MML-1. In the future, it will be important to determine the epistatic relationship between HXK-2 and TCA enzyme knockdowns for their impact on longevity and elucidate the metabolic signals that activate MML-1.

We observed that PPP pathway enzymes also strongly influenced MML-1 nuclear localization and function. The PPP is a cytosolic pathway involved in the interconversion of sugars to generate precursors for the biosynthesis of lipids, amino acids, and nucleotides and maintain redox homeostasis. We found that knockdown of PPP components, PGDH *T25B9.9*, transketolase *tkt-1*, and transaldolase *tald-1*, enhanced MML-1 nuclear localization, increased the transcription of MML-1 target genes, and restored longevity to *glp-1(e2141)* animals under *hvk-2i*. The PPP is the primary source of NADPH, which plays a vital role in many cellular processes, including fatty acid, nucleotide, neurotransmitter, and cholesterol metabolism, and works as an essential reducing agent (Ju et al., 2020). We found that pharmacological inhibition with 6-AN of the two enzymes producing NADPH in the PPP increased MML-1 nuclear localization. We also found increased levels of NADPH and lower levels of G6P under *hvk-2* knockdown. Importantly, these observations suggest that residual G6P may be diverted to the PPP under low mitochondrial hexokinase and further imply that metabolites other than G6P could regulate MML-1 nuclear localization. Different metabolic pathways also produce NADPH, including the malic enzyme, cytosolic and mitochondrial isocitrate dehydrogenase, the mitochondrial inner membrane transhydrogenase, and the folate cycle through the methylenetetrahydrofolate dehydrogenase (MTHFD1/2). Whether these other pathways or NADPH itself also influence the regulation of MML-1 under *hvk-2* knockdown remains to be seen.

A major output of the PPP and NADPH metabolism is the production of lipids. Interestingly, we found that under *tkt-1* knockdown, fat levels decreased, and LDs were smaller in diameter, suggesting that reduction in LDs could signal MML-1 to translocate to the nucleus. Consistently, transaldolase *tald-1* knockdown has been shown to increase lifespan and decrease

intestinal fat levels in the worm through increased activity of adipose triglyceride lipase ATGL-1 (Bennett et al., 2017). This enzyme is involved in the metabolism of LD under starvation to mobilize stored fats for energy production (Jung Hyun Lee et al., 2014). Nonetheless, we found that global fat content did not strictly correlate with MML-1 nuclear localization among tested RNAi modulators (Vonolfen, 2020), though LD size was not examined. Future studies should address whether the PPP regulates MML-1 through LD size or other mechanisms.

6.2 Hexokinases regulate MML-1 through distinct downstream mechanisms

Interestingly, we found that although both *hxx-1* and *hxx-2* positively regulate MML-1 function, they do so through different mechanisms. We observed that inhibiting fatty acid β -oxidation is sufficient to rescue MML-1 nuclear localization under *hxx-1* knockdown, but not *hxx-2* knockdown. Conversely, decreasing the OGDC or the PPP rescued MML-1 localization under *hxx-2* knockdown independent of the G6P levels, but not *hxx-1* knockdown. How both hexokinases activate different metabolic pathways to regulate MML-1 remains unknown and could work at multiple levels (Table 1).

Table 1. Differences between HXK-1 and HXK-2 and knockdown of the isozymes.

	HXK-1/ <i>hxx-1i</i>	HXK-2/ <i>hxx-2i</i>
Tissue expression	Neurons, pharynx, gonadal sheath, coelomocytes	Hypodermis, muscle, intestine
Subcellular localization	Cytoplasm (?)	Mitochondria
G6P levels	Decreased	Decreased
Lifespan requirement	<i>isp-1</i> and partially for <i>glp-1</i>	<i>glp-1</i> and <i>isp-1</i>
Stress pathways	Unaffected	Increased <i>hsp-4</i>
Fat levels	Increased	Increased
β -oxidation	Increased in wildtype and <i>glp-1</i> . Increased <i>acs-2</i> .	Increased in <i>glp-1</i> Increased <i>acs-2</i>
NADPH/NAD ⁺	Unchanged	Increased
Downstream regulation of MML-1	Requires β -oxidation	Requires PPP and OGDC
mTOR signaling (LARS-1)	Unchanged	Increased in wildtype

First, there is evidence that differences in subcellular location of hexokinases may result in the compartmentalization of glucose metabolism, with channeling of G6P to different pathways (John et al., 2011; J. E. Wilson, 2003). Mitochondrial hexokinase has preferential access to ATP generated in the mitochondria and provides efficient glycolysis coupling with further pyruvate oxidation by the TCA cycle and oxidative phosphorylation (OXPHOS). We found that knockdown of the mitochondrial pyruvate carrier *mpc-1* had a similar effect in inhibiting MML-1 localization and function, suggesting that HXK-2 and MPC-1 regulate MML-1 by connecting glycolysis and oxidation of pyruvate in the mitochondria. Supporting this idea, inhibition of mitochondrial β -oxidation did not rescue MML-1 nuclear localization upon *mpc-1* knockdown, suggesting that MPC-1 may be downstream of the HXK-2 branch.

Furthermore, mammalian HKI and HKII have a dynamic localization, shuttling between the mitochondrial outer membrane and the cytoplasm (John et al., 2011). Both mammalian hexokinases have been reported to reversibly bind to mitochondria through their N-terminal sequence (Roberts et al., 2014) and via their interaction with VDAC1 (Lindén et al., 1982). This dual localization allows the cell to adapt to different metabolic requirements and maintain energetic balance. Under high levels of G6P, HKII shuttles from the mitochondria to the cytoplasm, causing cells to use glycogen as an energy source (John et al., 2011). The subcellular localization also plays other significant roles in different signaling pathways. For example, mitochondria-bound hexokinase has an anti-apoptotic effects (Gottlob et al., 2001), and increased N-acetylglucosamine upon pathogen exposure releases hexokinase from the mitochondria and activates innate immune responses (Wolf et al., 2016). Here we found that *C. elegans* HXK-2 is associated with mitochondria and that this localization is abolished by deletion of the first ten amino acids. However, we saw no effect upon *vdac-1* knockdown nor dynamic localization of HXK-2 between mitochondria and cytosol. Taken together, these observations suggest that the nematode has dedicated mitochondrial (HXK-2) and cytosolic (HXK-1 and HXK-3) hexokinases.

Second, we also found differences in the tissue expression of the different hexokinase isozymes of the nematode: HXK-1 was mainly found in the pharynx, neurons, gonadal sheath, and coelomocytes, while HXK-2 was present in the hypodermis, body wall muscle, and intestine. Consistently, RNAseq data from different tissues in *C. elegans* shows that *hxx-2* is the main isozyme in the body wall muscle and intestine. At the same time, *hxx-1* is the main one expressed in pharyngeal muscle and neurons (Hutter & Suh, 2016). This differential distribution could

explain how *hxx-1* and *hxx-2* differentially regulate MML-1 through β -oxidation and PPP/OGDC pathways. Notably, we scored MML-1 nuclear localization in the intestine for most experiments, where *hxx-2* but not *hxx-1* is expressed. In the future, it will be important to see whether *hxx-1* cell autonomously impacts *mml-1* nuclear localization within the same tissue, such as the pharynx.

In any case, our observation that HXX-1 affects intestinal MML-1 nuclear localization suggests cell non-autonomous signaling. What might be the nature of such cell non-autonomous signaling? One possibility is the sterol hormone signaling pathway, which acts in somatic reproductive tissue to regulate *glp-1(e2141)* longevity. Decreasing the activity of the nuclear hormone receptor DAF-12, or its ligands, dafachronic acids, abolishes the longevity of germlineless worms (Gerisch et al., 2001; Yamawaki et al., 2010). Interestingly, carbohydrate metabolism directly impacts the production of dafachronic acids as NADPH is required for the last step of dafachronic acid biosynthesis by DAF-9 (Motola et al., 2006; Penkov et al., 2015). Furthermore, DAF-9 is expressed in the somatic gonad (spermatheca) and XXX neurons in adult animals (Gerisch & Antebi, 2004). Conceivably, downregulation of hexokinase could affect the production of NADPH and dafachronic acids regulating DAF-12 activity, thereby affecting MML-1 function. It will be interesting to see whether dafachronic acid supplementation can rescue MML-1 nuclear localization upon *hxx-1i* or *hxx-2i*.

Recent evidence strengthens the idea that the nervous system plays a crucial role in integrating the metabolic status and systemic responses in a cell nonautonomous manner (Mutlu et al., 2020; Y. Zhang et al., 2019). Inhibition of the mTOR signaling pathway has been shown to extend lifespan in the evolutionary spectrum (Kennedy & Lamming, 2016), and recent work has shown that restoring *raga-1/RagA* or *rsk-1/S6K* in the nervous system is enough to entirely suppress the lifespan extension conferred by mutation of these mTOR signaling factors (Y. Zhang et al., 2019). In cells, HKII has been shown to shuttle from the mitochondria and directly interact with mTOR under glucose deprivation and inhibit its function resulting in an induction of autophagy (Roberts et al., 2014). This interaction is dependent on the mTOR signaling (TOS) motif present in HK-II required for binding to Raptor. Interestingly, this TOS motif (KDIDI) is conserved in the nematode HXX-1; however, HXX-2 and HXX-3 lack this sequence. It would be interesting to study whether the interaction between hexokinase and mTOR is conserved in *C. elegans* and whether decreasing the main neuronal hexokinase (*hxx-1*) would result in mTOR-dependent inhibition of MML-1. We found that genetic and pharmacological inhibition of mTOR

failed to rescue MML-1 nuclear localization under the mitochondrial *hxx-2* knockdown; however, we cannot exclude the possibility that mTOR signaling is part of the *hxx-1* branch. Because RNAi does not work efficiently in the nervous system, it will be important to address the role of *hxx-1* in this tissue using other approaches.

6.3 *MML-1 interactome suggests multifaceted communication between organelles and transcription*

Proteins tend to co-localize near their substrates to maximize specificity and regulate signaling pathways. In particular, MondoA was first reported to be associated with the mitochondria outer membrane in primary human SkMC cells through protein-protein interaction (Sans et al., 2006). We have previously shown that this localization is conserved in *C. elegans* (Nakamura et al., 2016). Mitochondria-bound MondoA has been proposed to have preferential access to newly synthesized G6P from HKII to coordinate metabolism and transcriptional response (Wilde et al., 2019). However, the identity of the mitochondrial factor tethering MondoA at the mitochondria has not been reported.

Our proteomics analysis of MML-1 immunoprecipitation showed enrichment with proteins from different cellular compartments, including mitochondria, ER, LD, and nucleolus, suggesting an important role of Mondo in integrating diverse organellar signals. Localization to mitochondria was particularly conspicuous. Surprisingly, some of the enriched proteins reside at the mitochondrial inner membrane, including two subunits of cytochrome c oxidase (Complex IV), CTC-2 and COX-6A, the mitochondrial pyruvate carrier MPC-1, and the malate/succinate transporter SLC-25A10. We also found two proteins that reside at the mitochondrial outer membrane, the acyl-CoA synthetase ACS-13 and the scaffold protein AKAP-1. Whether MondoA or MML-1 can be imported to mitochondria has not been reported. Our preliminary data using ACS-13 as a mitochondrial marker suggest that MML-1 could reside within the mitochondria of the hypodermis, perhaps explaining how MML-1 could interact with proteins from the inner membrane and matrix. Clearly, biochemical approaches are needed to confirm any location within mitochondria.

Multiple nuclear transcription factors are localized in the mitochondria, although dissecting their nuclear and mitochondrial function is challenging (Leigh-Brown et al., 2010). On the one hand, nuclear transcription factors have been shown to directly bind the mitochondrial genome to regulate transcription, like the cAMP response element-binding (CREB) protein (Marinov et al.,

2014). Interestingly, *mml-1(ok849)* loss-of-function mutants showed a decrease in all 12 mitochondrial-encoded genes compared to wildtype (Nakamura et al., 2016). However, this could be indirect by regulating the mitochondrial transcription factor TFAM or mitochondrial biogenesis (F. Li et al., 2005). On the other hand, transcription factors like p53 have been shown to translocate to the mitochondrial outer membrane under apoptotic signals to interact with Bcl-2 and promote membrane permeabilization and apoptosis (Marchenko et al., 2007). Future studies will help elucidate whether MML-1/MondoA mitochondrial localization regulates other cellular processes independent of its nuclear transcription function.

We used our proteomics data to test whether MML-1 potential interactors had a functional effect on its localization and activity. We found that *acs-13* knockdown resulted in an upregulation of MML-1 nuclear localization. ACS-13 is a homolog to long-chain acyl-CoA synthetase ACSL1, ACSL5, and ACSL6 in humans. ACSL activates fatty acids by converting them to fatty acyl-CoA that then can be used for other reactions, including TAG biosynthesis, or imported to mitochondria for fatty acid β -oxidation. Mitochondrial ACSL1 has been shown to couple fatty acyl-CoA production with mitochondrial β -oxidation through its interaction with VDAC1 and carnitine palmitoyltransferase CPT-1 (K. Lee et al., 2011; Young et al., 2019). Supporting this idea, ACSL1 is responsible for 90% of the total cardiac ACSL activity, and knockout mice have impaired cardiac fatty acid oxidation (Ellis et al., 2011). In *C. elegans*, mutations in *acs-13* result in increased PUFA-containing phospholipids (Ruiz et al., 2019); hence modulation of intracellular levels of fatty acids and acyl-CoA could result in regulation of transcription through MML-1. In line with this idea, knockdown of ACSL3 in rat primary hepatocytes has been shown to decrease lipogenic genes through downregulation of the ChREBP activity (Bu et al., 2009), suggesting the activity of lipid metabolic enzymes could impinge on this transcription factor to regulate lipid metabolism gene expression. Whether MML-1 could directly sense lipid species or is regulated through protein-protein interaction remains unknown.

The A-kinase anchoring protein AKAP1 functions as a scaffold protein in the mitochondrial surface for multiple substrates, including the protein kinase A (PKA) (Felicciello et al., 2001). D-AKAP1 has also been proposed to tether PKA on the surface of LD in adipose tissue to regulate fat metabolism (D. Bridges et al., 2006). PKA is one of the primary kinases involved in regulating lipolysis by phosphorylating hormone-sensitive lipases (HSL) and perilipin to increase TAG breakdown into free fatty acids (Fain & Garcia Sainz, 1983; Pidoux et al., 2011).

PKA has been shown to phosphorylate ChREBP directly and block its nuclear import, decreasing the glucose-dependent L-PK transcription (T. Kawaguchi et al., 2001). Using algorithms for predicting potential phosphorylation sites of MML-1 in *C. elegans* (Blom et al., 1999, 2004), we found that S739 could be a substrate for PKA (score 0.709). Interestingly, this residue was found to be phosphorylated in a large scale *in vivo* phosphoproteome (Zielinska et al., 2009), suggesting that MML-1 interaction with AKAP could facilitate the PKA-dependent phosphorylation in the nematode and disrupting this interaction could promote MML-1 nuclear localization and activity.

AMP-activated protein kinase (AMPK) is another crucial player in energy homeostasis. AMPK is activated by a high AMP/ATP ratio and functions as a master regulator involved in multiple pathways, including lipid metabolism. AMPK has been shown to phosphorylate the mitochondrial AKAP1 in rat L6 myoblasts to increase mitochondrial β -oxidation and respiration (Hoffman et al., 2015). Interestingly, supplementation of 5-aminoimidazole-4-carboxamide-1-D-ribo-furanoside (AICAR), a specific AMPK activator that mimics AMP, inhibited the glucose-dependent activation of L-PK by ChREBP (Da Silva Xavier et al., 2000). Later it was shown that AMPK directly phosphorylates ChREBP under a high-fat diet in hepatocytes inhibiting its transcriptional function and blocking glycolysis and lipogenesis (Takumi Kawaguchi et al., 2002). Whether MML-1 is phosphorylated by AMPK is unknown in *C. elegans*. Consistently, we found that knockout of the AMPK α subunits *aak-1* and *aak-2* significantly increased MML-1 nuclear localization in an HXK-2-dependent manner, thus suggesting that AMPK inhibits MML-1.

We also found that vitellogenins were among the most enriched proteins co-immunoprecipitated with MML-1. These are among the most highly expressed genes in the nematode (M. F. Perez & Lehner, 2019); hence they could be an overrepresentation due to their abundance. However, vitellogenins have been found in multiple proteomics experiments associated with LD. It has been suggested that this interaction could assist the recruitment of lipids during the yolk production (Vrablik et al., 2015; P. Zhang et al., 2012). Thus, the localization of MML-1 with LD may facilitate the interaction between this transcription factor and vitellogenins.

LD represents the main lipid storage in cells to balance metabolism and energy demands. These organelles are essential for many signaling pathways and are required for survival during fasting by mobilizing lipids for energy production. In *C. elegans*, LDs are mainly localized in the intestine and hypodermis and are composed almost exclusively of TAG (Vrablik et al., 2015). We found two of the most abundant LD proteins, PLIN-1 and DHS-3, enriched in the MML-1

interactome. Interestingly, we found that MML-1 colocalizes with LD *in vivo* in the intestine. MondoA was previously seen in large-scale proteomics associated with LD (Krahmer et al., 2018). Recently, it was shown that MondoA and Mlx localized with LD through amphipathic helices in the C-terminus in SUM159 cells (Mejhert et al., 2020). The researchers proposed a model in which MondoA/Mlx colocalization with LD inhibits its transcriptional activity limiting glucose-dependent transcription. As MondoA has also been shown to localize with mitochondria, it would be interesting to understand the role of this organelle in regulating MondoA association with LD. Indeed, mitochondria and LD physically interact with one another to regulate metabolism (Boutant et al., 2017). Although the proteins involved in these contact sites are just beginning to be uncovered, both PLIN1/PLIN-1 and ACSL1/ACS-13 have been proposed to tether mitochondria and LD (Gordaliza-Alaguero et al., 2019).

Mitochondria bound to LD facilitate the coordination of TAG metabolism and fatty acid oxidation. For example, lipases (*e.g.*, ATGL) in the LDs break down TAG to release free fatty acids that can be activated in the mitochondria outer membrane by ACSL1 to fatty acyl-CoA. This acyl-CoA can be imported to the mitochondria for β -oxidation. We propose a model in which MML-1 interacts with specific mitochondria associated with LD to orchestrate a transcriptional response depending on the fuel utilization. Under normal conditions, glucose stimulates MML-1 translocation to the nucleus to activate the transcription of glycolytic enzymes. In contrast, upon blockage of glycolysis (*e.g.*, hexokinase knockdown), the cell utilizes fatty acids to produce ATP, re-localizing and inhibiting MML-1 at the mitochondria associated with LD.

6.4 MML-1 and MXL-2 regulate downstream processes independently

MML-1 and MXL-2 have been described to work in a complex to activate gene transcription (Grove et al., 2009; Pickett et al., 2007). Previously, we found that *mml-1(ok849)* and *mxl-2(tm1516)* mutants had independent effects, for example, *mml-1(ok849)* being required for *isp-1(qm150)* longevity and not *mxl-2(tm1516)* (Nakamura et al., 2016). Supporting this idea, we found that *mml-1(ok849)* and *mxl-2(tm1516)* in the *daf-2(e1370)* had different effects in the transcriptome and metabolome, suggesting that they may participate in other complexes independently of each other, in contrast to their mammalian counterparts that are obligate partners (Billin et al., 2000). In terms of metabolism, we found that all the metabolites regulated in common

by *mml-1* and *mxl-2* exhibited a similar trend, suggesting that their significant difference is mainly in transcriptional regulation.

Loss-of-function of *mml-1(ok849)* in the *daf-2(e1370)* mutant resulted in a more robust regulation of genes compared to *mxl-2(tm1516)* and PCA analysis of the RNAseq data distinctively separated *daf-2(e1370) mxl-2(tm1516)* and *daf-2(e1370) mml-1(ok849)* transcriptomes. MML-1 downstream targets in *daf-2(e1370)* were mainly genes involved in development, growth, and reproduction, while MXL-2 regulated genes were primarily involved in metabolism and immune response. We also found a significant number of genes upregulated in *mml-1(ok849)* and *mxl-2(tm1516)* mutants, supporting the idea that they may also play an important role in the repression of gene expression. For example, MondoA has been shown to recruit histone deacetylases (HDAC) to the promoter of TXNIP to repress its transcription in glutamine anaplerosis (Kadige et al., 2009), highlighting the idea that these factors can work as both transcriptional activators and repressors dependent on their interactions with co-activators or co-repressors at different promoters.

6.5 MML-1/MXL-2 transcriptional network wiring in distinct longevity signals

Long-lived insulin signaling and germline-less mutants result in extensive remodeling of metabolism and converge on similar factors, like the requirement of DAF-16 and MML-1/MXL-2 for the lifespan extension (Berman & Kenyon, 2006; D. W. Johnson et al., 2014; C. Kenyon et al., 1993). Indeed, MML-1 and MXL-2 play an intricate role in regulating multiple longevity pathways longevity (Nakamura et al., 2016). Our current work suggests that although these transcription factors are convergent factors for longevity, the mechanism by which they are activated may be context-dependent. For example, we found that hexokinases are a positive regulator of MML-1 nuclear localization in germline loss and impaired mitochondrial function longevity pathways, but not for the reduced insulin signaling longevity. We also found differences in the downstream targets regulated by MML-1 and MXL-2 in the *daf-2(e1370)* and *glp-1(e2141)* mutants, indicating that MML-1/MXL-2 have distinct effects in both longevity models.

Insulin signaling deficient worms shift their metabolism towards the accumulation of carbohydrates and lipids. *daf-2(e1370)* mutants show a DAF-16-dependent increase in *de novo* fatty acid synthesis (C. L. Perez & Van Gilst, 2008) and elevated levels of trehalose (Y. Honda et al., 2010). *daf-2* and *glp-1* mutants display increased intestinal lipid accumulation (Kimura et al.,

1997; O'Rourke et al., 2009). We have found that MML-1/MXL-2 regulate fatty acid metabolism through the expression of fatty acid synthase (*fasn-1*), fatty acid desaturases (*fat-2*, *fat-5*, *fat-6*), lipolytic genes (*dgat-2*, *hosl-1*, *lipl-2*), and mitochondrial β -oxidation enzymes (*acs-2*, *acdh-9*, *ech-1*, *hacd-1*) in the *glp-1(e2141)* mutant (Karalay et al., unpublished). Interestingly, in our RNAseq data, we found that *mml-1* had a similar effect in increasing the expression of *acdh-9* and *acs-2* and decreasing the expression of fatty acid desaturases in the *daf-2(e1370)*, suggesting overlapping functions of MML-1 in the germline and insulin longevity models for regulating fat metabolism.

On the other hand, insulin signaling and germline regulate metabolism and longevity through different mechanisms. Different metabolic enzymes are differentially regulated in both longevity models. For example, *hxx-1* and *hxx-3* are decreased at the transcript level in *daf-2* mutants compared to wildtype (Fuchs et al., 2010; Shaw et al., 2007), while only *hxx-1* is decreased in *glp-1(e2141)* mutants compared to wildtype (Nakamura et al., 2016). There are also differences between *daf-2(e1370)* and *glp-1(e2141)* mutants at the metabolite level. For example, *daf-2(e1370)* had a more substantial effect in regulating many intermediates of the folate cycle than *glp-1(e2141)* (Annibal et al., 2021). Interestingly, *glp-1(e2141)* mutants exhibited elevated steady-state levels of hexose phosphates, while *daf-2(e2141)* mutants had lower levels, perhaps explaining the differences in susceptibility of MML-1 nuclear localization to hexokinase knockdown. These mutants also differ in downstream pathways regulating longevity. *glp-1(e2141)* mutants, but not *daf-2(e1370)*, require intestinal autophagy for the lifespan extension (Chang et al., 2017). Future work understanding the overlapping and specific mechanisms regulating metabolism and longevity will help us elucidate how is MML-1/MXL-2 transcriptional network is rewired in a context-dependent manner.

6.6 Scientific advancement and limitations of the study

In this work, we focused on studying one of the major transcription factors that regulate energy homeostasis. We show the interplay between glucose metabolism and fatty acid oxidation in regulating the basic helix-loop-helix transcription factor MML-1. We propose novel mechanisms that regulate this transcription factor independent of G6P levels, which have been presented as the primary activator for MondoA in cells. We also demonstrate that MML-1 has a complex interaction with different organelles that could facilitate the transmission of information

between the cytoplasm and the nucleus. Our data also expands our knowledge of the MML-1/MXL-2 transcriptional network in the insulin signaling pathway, indicating that context-specific signals activate this transcription factor in different longevity pathways. Our work lays the groundwork for understanding how organisms integrate compartmentalization of organellar metabolism and transcription.

Although *C. elegans* has proven to be a powerful model organism for studying aging and metabolism, future work should focus on the evolutionary conservation of our findings in cell culture and vertebrate models. The Myc/Mondo transcriptional network in *C. elegans* is simpler than in mammals, where many more factors arose during evolution due to gene duplication and divergence (Jones, 2004). This presents a challenge as functions described in *C. elegans* may be conserved but in different proteins in vertebrates.

Members of the Myc superfamily of transcription factors differ in their tissue-specific expression and binding partners to regulate different downstream targets (Billin et al., 2000; Carroll et al., 2018; Yamashita et al., 2001). In this work, we focused mainly on the localization of MML-1 in the intestine, as this tissue plays a vital role in regulating metabolism and longevity. However, there is a growing body of evidence underlining the importance of tissue communication in regulating metabolism and stress responses (Berendzen et al., 2016; Weir et al., 2017). Future work will help elucidate the tissue-specific requirements of the hexokinase and MML-1 axis for lifespan extension and metabolism.

Glucose metabolism is essential during development, and loss of function mutations in many glucose metabolizing enzymes are embryonic lethal. To overcome this, we used RNAi, as it has proven to be a powerful tool for performing genetic screens. However, the knockdown efficiency of genes can be different between tissues, like the nervous system, and result in incomplete protein depletion. Using alternative methods to deplete proteins (*e.g.*, auxin-inducible degradation) could help study required proteins during development and our understanding of dynamic cellular processes.

VII. Future Perspective

7.1 *Validation of MML-1 protein-protein interactions*

MondoA has been shown to be localized at the mitochondrial outer membrane through protein-protein interaction (Sans et al., 2006); however, the identity of the mitochondrial interactor has not been elucidated. In this work, we immunoprecipitated MML-1 in different genetic backgrounds and found multiple proteins from different cellular compartments co-enriched with this transcription factor. In particular, the mitochondrial proteins MPC-1 and ACS-13, and the LD proteins PLIN-1 and DHS-3 are co-enriched with MML-1. Our next focus is on the validation of these candidates through biochemical approaches. Currently, we have cloned *mml-1* and some of the candidates in vectors for mammalian expression. We will do heterologous expression of *C. elegans* proteins in HEK293T cells to conduct co-immunoprecipitation of MML-1 with the candidates. Alternatively, we could use the yeast-two-hybrid system to confirm their physical interaction. This system has been used in *C. elegans* to map the dimerization network of bHLH transcription factors (Grove et al., 2009). We are also interested in studying whether the mammalian orthologs of these proteins physically interact. For this, we are optimizing immunoprecipitations of endogenous MondoA in HEK293T. We will test whether MondoA physically interacts with MPC-1, ACSL-1, and PLIN-1.

7.2 *Tissue-specific requirement of hexokinases for MML-1 regulation*

We found that *C. elegans* hexokinases are differentially expressed in multiple tissues. HXK-1 was mainly found in neurons, gonadal sheath, pharynx, and coelomocytes. Moreover, we monitored MML-1 nuclear localization in the intestine, suggesting that HXK-1 may regulate MML-1 in a cell nonautonomous manner. To better understand this mechanism, we will develop different models to study the tissue-specific requirements of hexokinase for MML-1 transcriptional activity. One option is using the *sid-1(qt9)* strain for tissue-specific RNAi knockdown. *sid-1* encodes for a transmembrane protein that allows dsRNA to enter the cell (Winston et al., 2002); thus, *sid-1(qt9)* mutants are refractive to systemic RNAi. Rescue of the *sid-1* gene under specific promoters will allow us to knock down hexokinases in the desired tissue. This system has been used to study the function of different proteins in a tissue-specific manner in *C. elegans* (Chang et al., 2017; Melo & Ruvkun, 2012).

Another method that has been proven to be useful for transient inactivation of proteins is auxin-inducible degradation (AID). This requires adding a 44 amino acid degron tag to the protein of interest and expressing the *Arabidopsis* ubiquitin ligase TIR1 in the desired tissue (Nishimura et al., 2009). When the hormone auxin is added, it stimulates the interaction between TIR1 and the protein tagged with the degron sequencing, triggering ubiquitination and degradation by the proteasome. Multiple lines have been generated in *C. elegans* to allow tissue-specific degradation of proteins by adding auxin (Divekar et al., 2021).

The AID system will also allow us to study the temporal effects of glucose metabolism. All our knockdown experiments were performed by growing the worms on the RNAi plates egg on. However, whether hexokinases are required for MML-1 activity and longevity in different stages during development remains elusive. Auxin supplementation can result in protein degradation in minutes (Divekar et al., 2021), does provide a great advantage to knockdown hexokinases in different larval stages or adult on and monitor MML-1 function. This will give us insight into whether rewiring glucose metabolism during development exerts long-term responses that affect lifespan.

We can use these systems to inactivate hexokinases in a tissue specific-manner and monitor MML-1 function. Specifically, we will test whether knockdown of the hexokinases in neurons, hypodermis, intestine, germline, and muscle influence MML-1 nuclear accumulation and expression of downstream targets. Furthermore, we can determine the tissue-specific requirements of the hexokinases for *glp-1(e2141)* and *isp-1(qm150)* longevity. This will be important for future studies focusing on the endocrine regulation of glucose metabolism and transcriptional responses.

Interestingly, we found that *hxx-2i*, but not *hxx-1i*, increased NADPH levels quantified in whole animal extracts. However, this observation could be due to the more restricted expression of *hxx-1* compared to *hxx-2*; hence changes in metabolite levels on specific tissues will be obscured by overall organismal levels. Thus, we could use metabolic sensors to quantify the intracellular levels of NADPH *in vivo*. Tao and colleagues have developed a genetically encoded NADPH fluorescent sensor (iNap) that facilitates monitoring NADPH levels in cultured cells and zebrafish larvae (T. Li et al., 2022; Tao et al., 2017). We could introduce this reporter under tissue-specific promoters in *C. elegans* to test whether NADPH pools are altered in specific tissues upon hexokinase knockdown. This would be very helpful, for example, to better understand whether hexokinases regulate the steroid signaling and thus affect MML-1 activity. Particularly, NADPH

is required to synthesize dafachronic acids mediated by DAF-9, which is expressed in the somatic gonad (spermatheca) and XXX neurons in adult animals (Gerisch & Antebi, 2004). We can also study the effect of hexokinase knockdown on DAF-9 activity by analyzing the production of dafachronic acids and dauer formation and determining whether the transcription factors DAF-12 and MML-1 are epistatic.

7.3 Glucose flux analysis

We observed that the different hexokinase isozymes differ in their subcellular localization. The subcellular localization of the hexokinase has been linked to the fate of G6P metabolism (John et al., 2011). Mitochondrial hexokinase is mainly committed to coupling glucose phosphorylation and further oxidation by glycolysis, while cytosolic hexokinase mainly links G6P to anabolic reactions. We showed that HXK-2 is the *C. elegans* mitochondrial hexokinase, while HXK-1 and HXK-3 are cytosolic. Our current hypothesis is that G6P generated by HXK-2 is oxidized through glycolysis thus promoting MML-1 nuclear localization. By downregulating *hxx-2* via RNAi, G6P will be used in other pathways, including the PPP. Consistently, we found increased levels of NADPH under *hxx-2i*. To prove this hypothesis, we are currently optimizing $^{13}\text{C}_6$ -glucose tracing metabolomics in worms with *hxx-1* and *hxx-2* knockdowns to measure the incorporation and kinetics of $^{13}\text{C}_6$ -glucose through glycolysis, PPP, and TCA cycle (**Figure 37**). We expect to gain insights into how glucose metabolism is rewired upon hexokinase isozyme-specific knockdown in an *in vivo* organism.

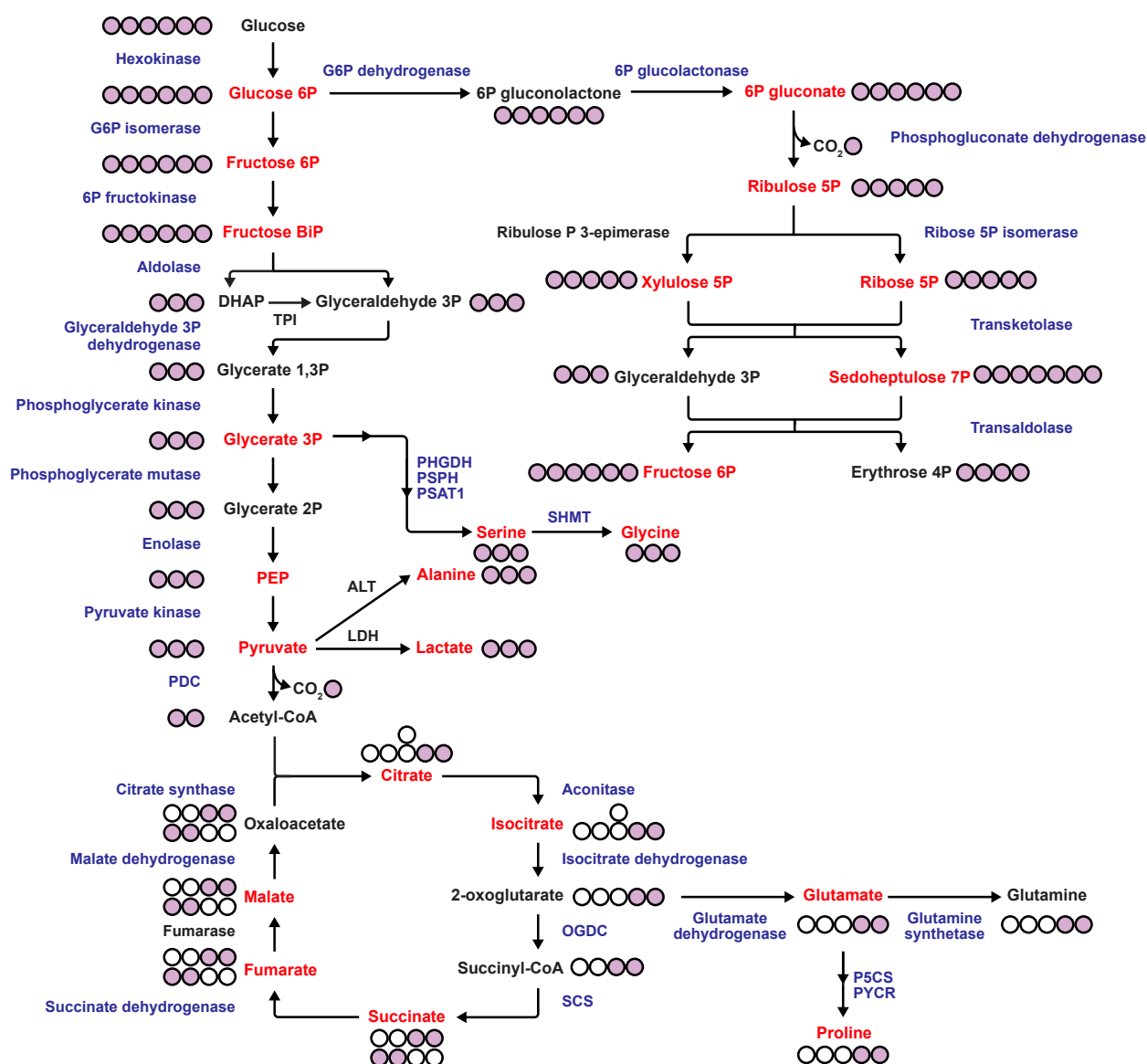


Figure 37. ¹³C₆-glucose flux analysis. Schematic representation of glucose flux analysis with fully labeled ¹³C₆-glucose. In red are all the metabolites that we were able to identify in our preliminary metabolomics data of worms fed with ¹³C₆-glucose. In blue are the enzymes involved in the metabolism of glucose. Abbreviations: G6P, glucose 6-phosphate; DHAP, dihydroxyacetone phosphate; TPI, triosephosphate isomerase; PEP, phosphoenolpyruvate; PDC, pyruvate dehydrogenase complex; OGDC, oxoglutarate dehydrogenase complex; SCS, succinyl CoA synthase; ALT, alanine transaminase; LDH, lactate dehydrogenase; PHGDH, phosphoglycerate dehydrogenase; PSPH, phosphoserine phosphatase; PSAT1, phosphoserine aminotransferase 1; SHMT, serine methyltransferase; P5CS, P5C synthase; PYCR, P5C reductase.

7.4 MML-1 regulation by metabolites

Protein-metabolite interactions are largely understudied. Most of the work on MondoA/ChREBP regulation by nutrients has been performed in cell culture, and inferences of their function are based on the correlation between specific nutrient levels and activity of the transcription factor (*e.g.*, nuclear localization, DNA binding, transcription of downstream targets). AMP, β -hydroxybutyrate, and acetoacetate were shown to directly bind to the ChREBP/14-3-3 protein complex and stabilize the interaction and retention in the cytoplasm, although none of these molecules allosterically bind to the individual proteins (Nakagawa et al., 2013; Sato et al., 2016). On the other hand, G6P has been suggested to bind to MondoA/ChREBP but has not been demonstrated experimentally (Peterson et al., 2010).

Thus, we would like to elucidate whether MML-1 can directly bind metabolites and, if so, which one(s). One untargeted approach would be to do affinity purification coupled with mass spectrometry. First, we will use our MML-1::3xFLAG CRISPR line to immunoprecipitate MML-1 to obtain native complexes. Next, metabolites are extracted and separated into either polar or hydrophobic phases and analyzed by ultra-performance liquid chromatography-mass spectrometry (Luzarowski et al., 2018). This will allow us to identify novel metabolites co-eluting with MML-1.

As targeted approaches, we could use isothermal titration calorimetry (ITC), differential protease-sensitivity assay, and intrinsic tryptophan fluorescence (ITF) to study the protein-ligand interaction. These methods have been used previously, for example, to demonstrate the interaction of the transcription factor NHR-80 and oleoylethanolamide (Folick et al., 2015). ITC is a label-free technique based on the principle that interaction between proteins and ligands releases or absorbs heat. Thus, ITC allows us to measure the thermodynamic changes produced by the interacting compounds and gives us information about the affinity constant K_a . The differential protease-sensitivity assay by chymotrypsin digestion is based on the idea that protein-ligand complexes are resistant to proteolytic degradation (Piazza et al., 2018). Finally, ITF is based on the capacity of tryptophan to emit intrinsic fluorescence that is measurable by fluorescence spectroscopy (Ghisaidoobe & Chung, 2014). If the tryptophan residue is involved in the interaction of the protein with the ligand, changes in the residue microenvironment alter the tryptophan fluorescence spectrum (Akbar et al., 2016; Vivian & Callis, 2001). MML-1 contains 15 tryptophan residues, three of which are in the N-terminus, the predicted ligand-binding site, and are conserved in ChREBP and MondoA. These methods could help elucidate whether MML-1 directly interacts

with metabolites, like glucose/G6P, other glucose-derived intermediates, hexose phosphates, NADPH, and lipids.

7.5 MML-1 implications in organellar communication

We found that the two most abundant LD proteins, PLIN-1 and DHS-3, were enriched in our MML-1 IP. Furthermore, we observed co-localization of MML-1 with LD in the *C. elegans* intestine. Recently, MondoA, ChREBP, and Mlx were shown to bind to LD in cell culture (Mejhert et al., 2020). However, whether MML-1/MondoA interact with LD to coordinate metabolism and transcription remains largely unknown. We found that upon *tkt-1* knockdown, LDs were smaller and MML-1 was translocated to the nucleus. Thus, we will test whether LD size and metabolism regulate MML-1 function (**Figure 38**). First, we will inhibit LD droplet synthesis and expansion by knocking down enzymes involved in TAG biosynthesis, including the acyl-CoA synthetase ACS-22 and the diacylglycerol acyltransferase DGAT-2 (Xu et al., 2012), and quantify MML-1 nuclear accumulation. We expect increased nuclear localization if MML-1 is negatively regulated by LD synthesis. Next, we will test whether the increased LD metabolism under *tkt-1* knockdown (Bennett et al., 2017) is required for MML-1 nuclear accumulation. For this, we will inhibit the major lipase, ATGL-1, required for LD consumption under PPP knockdown and test whether MML-1 nuclear localization is changed. In case decreased LD under *tkt-1i* signals MML-1 to the nucleus, we expect to abolish this by inhibiting *atgl-1*. These experiments will help us understand whether the PPP regulates MML-1 through the LD.

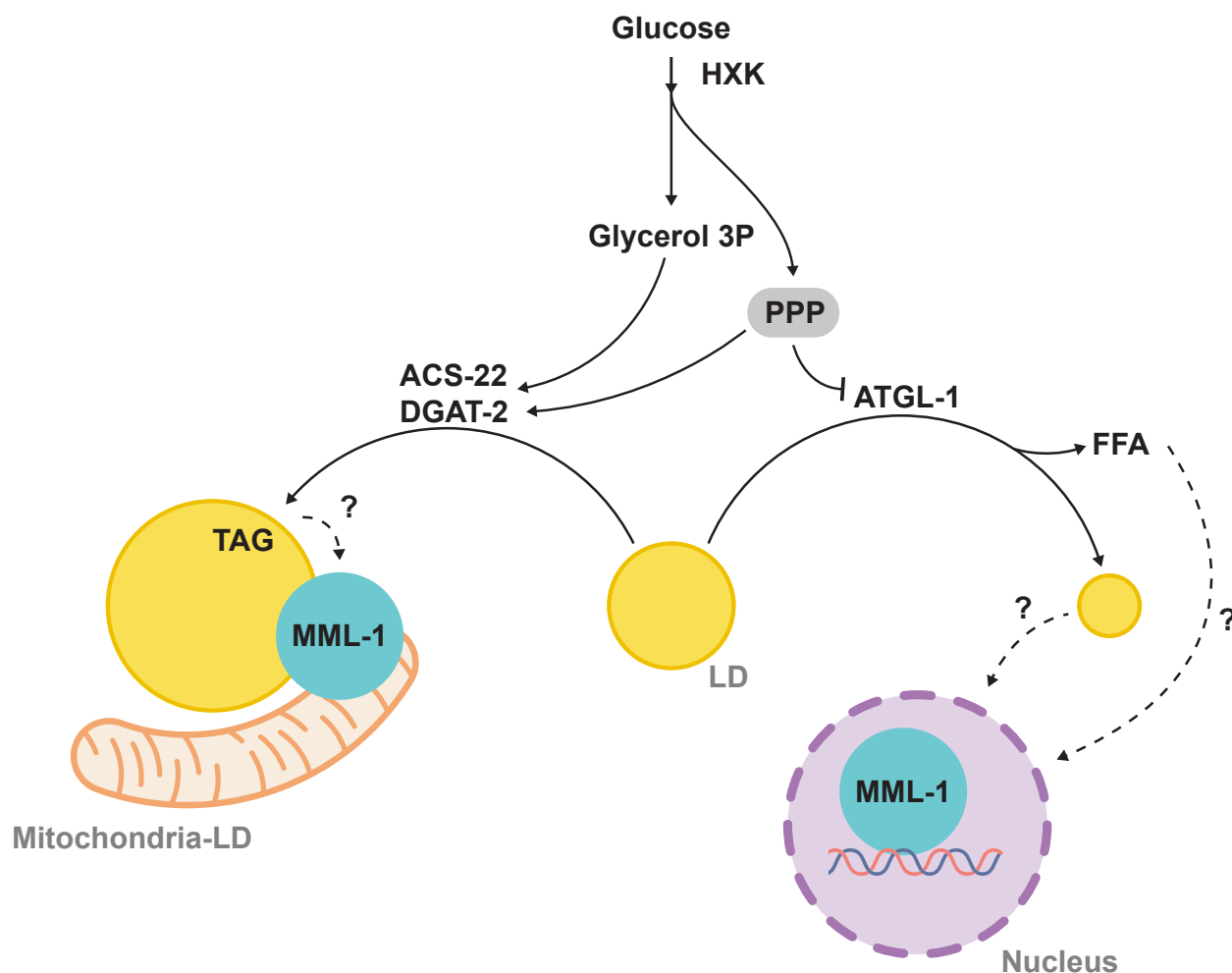


Figure 38. Regulation of MML-1 by LD metabolism. The current hypothesis of MML-1 regulation by LD metabolism. Under conditions where TAG glycerol synthesis is favored, MML-1 is retained at the LD-mitochondria. Upon fasting or nutrient depletion, LD are consumed to release free fatty acids, and MML-1 translocates to the nucleus to exert transcriptional response. The pathways are simplified for clarity. LD, lipid droplet; TAG, triacylglycerol; PPP, pentose phosphate pathway; FFA, free fatty acids.

MML-1 could be sensing specific ratios of saturated and unsaturated fatty acids. To test this hypothesis, we will quantify both classes of lipids under *hxx-1*, *hxx-2*, and *tkl-1* single and double knockdowns to see whether MML-1 nuclear localization correlates with the levels of these fatty acids. If we observe a correlation, we will do dietary supplementation of different saturated fatty acids, MUFAs, and PUFAs under hexokinase knockdown to test whether we can rescue MML-1 localization and function. Performing untargeted lipidomics will also give us insight into the lipid composition and species changed under hexokinase knockdown, and test whether

supplementation or decrease, by genetically reducing the enzymes involved in the biosynthesis and processing, of these lipids can rescue MML-1 function.

We found that MML-1 co-enriched with proteins from the inner mitochondrial membrane and matrix. Whether MondoA or MML-1 can be imported to the mitochondria has not been reported. Interestingly, we observed MML-1::GFP signal inside the mitochondria in the hypodermis of L4 worms. Thus, we would like to test whether MML-1 can be imported into mitochondria. We will use tissue-specific mitochondrial reporters to isolate mitochondria from specific cell types and do fractionation analysis of the mitochondrial compartments to test whether MML-1 is imported into the mitochondria (Ahier et al., 2018). MML-1 lacks a canonical mitochondrial targeting sequence; thus, it will be interesting to see whether an association with any chaperone could mediate this translocation.

7.6 *MML-1 crosstalk with the nucleolus*

The nucleolus plays an important role in lifespan regulation and has been established as a hallmark of aging (Tiku et al., 2017). Interestingly, we observed that MML-1 localizes with the nucleolus in different tissues. Specifically, we observed that MML-1 is enriched in the perinucleolar area upon *tkl-1* knockdown in intestinal nuclei (**Figure 39A, B, and C**). This region is enriched with RNA-binding proteins involved in rDNA transcription, RNA processing, and splicing (Pollock & Huang, 2009). We also observed MML-1 in discrete foci inside the nucleolus under standard growing conditions in the hypodermis and the intestine (**Figure 39D**). Moreover, we found two nucleolar proteins, ZK430.7 and BYN-1, enriched in the MML-1 IP, and knockdown of both proteins increased MML-1 nuclear localization. ZK430.7 is an ortholog of the human DCAF13, which is an important component of the rRNA-processing complex (J. Zhang et al., 2019). BYN-1 is an ortholog of the human bystin, a protein localized both in the cytoplasm and the nucleolus where it regulates ribosome biogenesis through the production of the 40S subunit (Miyoshi et al., 2007). To address whether MML-1 plays a role in nucleolar function, we would like to measure the effects of *mml-1(ok849)* loss-of-function mutant on rRNA processing. We will use qPCR probes for the rRNA precursors of the 18S and 26S rRNA. We could also do Northern blot analysis or fluorescent *in situ* hybridization (FISH) with antisense oligonucleotide probes to recognize the rRNA precursors.

Previous work showed that *mml-1(ok849)* increased nucleolar size in *glp-1(e2141)* and fibrillar/FIB-1 levels; however, the rRNA levels were not changed (Beck, 2017). However, we have only observed MML-1 perinucleolar enrichment upon *tkt-1*. Other candidates that increased MML-1 nuclear accumulation, like *ogdh-1* and *glp-1(e2141)*, did not show the same phenotype. Thus, MML-1 may play a role in nucleolar function under specific conditions. Transketolase knockdown could affect the ribose 5-phosphate pools, thus affecting RNA synthesis. It would be interesting to test whether *tkt-1* knockdown affects nucleolar morphology and function (e.g., nucleolar size, FIB-1 levels, rRNA processing) and whether these are dependent on MML-1. Moreover, it would be interesting to see whether nucleolar stress (e.g., supplementation of Actinomycin D) regulates MML-1 nuclear or nucleolar localization. MML-1 could directly bind to the rDNA loci to regulate its transcription. Chromatin immunoprecipitation (ChIP) sequencing will be helpful to determine whether MML-1 can bind rDNA loci upon *tkt-1* knockdown.

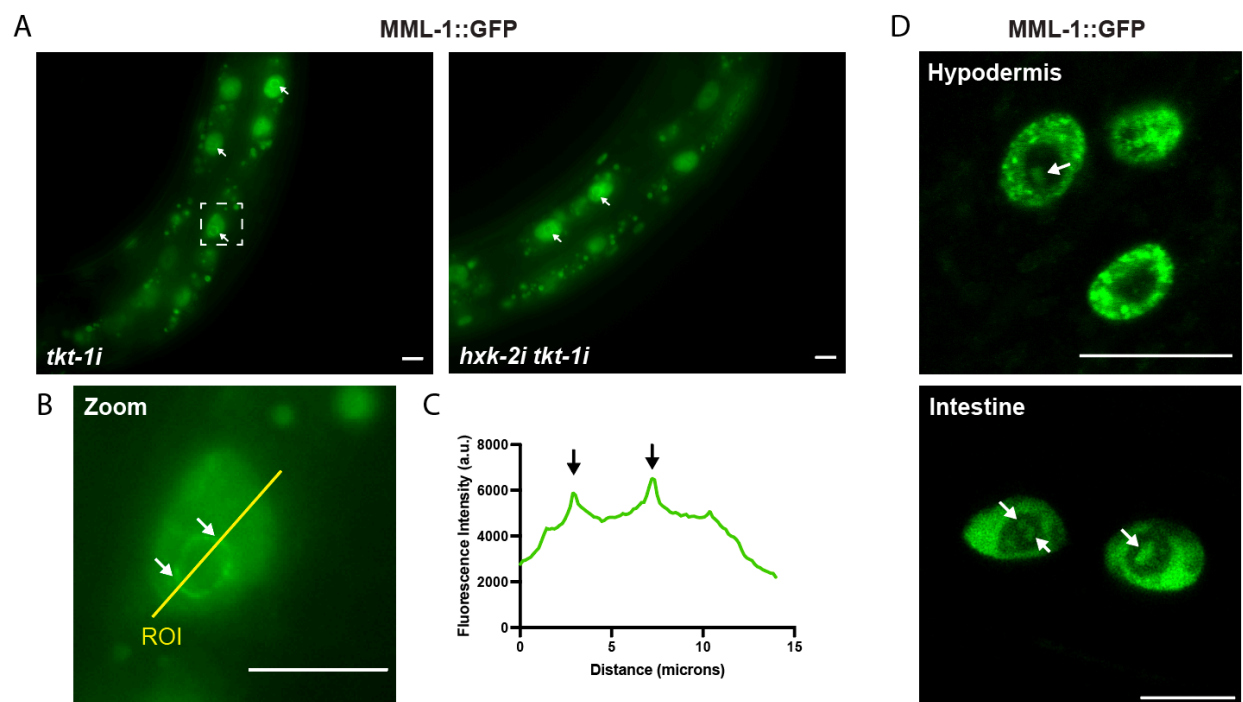


Figure 39. MML-1 colocalizes with the nucleolus. A-C. MML-1::GFP nuclear localization upon *tkt-1* and *tkt-1 hxx-2* double knockdown in intestinal cells of day one adult worms. White arrows mark the perinucleolar accumulation of MML-1. B. Magnification of one nucleus. C. The intensity plot of the ROI from B. The arrows indicate the peaks corresponding to the enrichment of MML-1 in the perinucleolar area. D. MML-1::GFP is found in foci inside the nucleolus (white arrows). Top, nuclei from hypodermal cells of L4 worms. Bottom, nuclei from intestinal cells of day one adult worms. Scale bars represent 10 μ m.

VIII. Materials and Methods

8.1 *C. elegans* husbandry

8.1.1 *Worm growth and maintenance*

C. elegans worm strains were grown and maintained on nematode growth medium (NGM) plates seeded with *E. coli* OP50 strain as the primary food source. Worms were grown at 20 °C unless stated otherwise. *glp-1(e2141)* strains were maintained at 15 °C. All worm strains are listed in **Supplementary Table 1**. To synchronize worm populations, adult worms were transferred to NGM plates with OP50 or RNAi-expressing bacteria and let to lay eggs for 4 to 6 h at 20 °C. For experiments that included *glp-1(e2141)* strain, egg lays were performed at 15 °C, and the eggs were upshifted to 25 °C for 52 to 56 h to induce the germline-less phenotype. After *glp-1* induction, worms were downshifted to 20 °C until the day of analysis or collection.

Worms were bleached to remove any microbial contamination or to synchronize the population. Animals were collected in M9 buffer, transferred to 15 mL conical tubes, and washed three times with M9 buffer. 5 and 10 mL of cold bleaching solution were added for 6 and 10 cm plates, respectively. After vortexing for 5 min at RT, the bleaching solution was removed, and worms were washed three times with M9 buffer. Eggs were resuspended in 200 µL of M9 buffer and transferred to seeded NGM plates. All media, buffers, and solutions are reported in **Supplementary Table 3**.

8.1.2 *Genotyping*

Worms were collected in single worm lysis buffer and incubated for 60 min at 60 °C, followed by 15 min at 95 °C. The lysate was used for PCR amplification of the region of interest using DreamTaq Green DNA Polymerase (ThermoFisher Scientific) according to the manufacturer's instructions. Annealing temperatures were determined using the T_m Calculator by ThermoFisher Scientific (Allawi & Santalucia, 1997). See **Supplementary Table 2** for the primer list. PCR products were analyzed by agarose gel electrophoresis and purified with QIAquick PCR Purification Kit (Qiagen). Sequencing was outsourced using the Mix2Seq Kit from Eurofins Genomics.

8.1.3 RNAi treatment

The NGM media for RNAi knockdown was supplemented with 1 mM Isopropyl β -1-D-thiogalactopyranoside (IPTG) and ampicillin (100 μ g/mL). The plates were seeded with the RNAi-expressing *E. coli* HT115 (DE3) strain to knock down specific genes. These strains are transformed with the L4440 vector, which expresses siRNA under the control of the IPTG-inducible promoter and come from the Ahringer and Vidal libraries (Kamath & Ahringer, 2003; Rual et al., 2004), or cloned for this work. All bacterial clones were confirmed by Sanger sequencing. Bacteria containing luciferase RNAi cloned into the L4440 vector were used as controls. Worms were grown on RNAi plates egg on in all the experiments.

8.2 *C. elegans* characterization

8.2.1 Demographic analysis

Lifespan analyses were conducted by synchronizing worms by egg lay as described above. All animals were kept at 20 °C egg on, or transferred to 20 °C at day one of adulthood for the experiments including *glp-1(e2141)*. More than 120 worms were used per strain/condition with 20-30 worms per 6 cm plate. Worms were transferred every other day to fresh plates until they stopped laying eggs and scored every time they were transferred. Animals with internal hatching and vulva protrusions were censored from the analysis. All lifespans were performed by blinding the genotypes/RNAi. Demographic parameters like mean, median, and maximum lifespan were calculated and plotted using GraphPad Prism 9 software.

8.2.2 Oxygen consumption rate measurements

Oxygen consumption rates (OCR) measurements in *C. elegans* were based on (Koopman et al., 2016). Worms were synchronized by egg lay, as mentioned above. The day before the experiment, the sensor cartridge was calibrated with 200 μ L of the Seahorse Bioscience XF96 calibrant solution, pH 7.4 (Agilent), and incubated overnight at 37 °C in a chamber without CO₂. On the day of the experiment, 10 to 15 adult worms were hand-picked and transferred to a Seahorse XF96 Cell Culture Microplate (Agilent) with 200 μ L of M9 buffer. OCR was measured using the Seahorse XFe96 Analyzer (Agilent). Basal oxygen consumption was measured five times, followed by injection of FCCP (final well concentration 10 μ M) and measured nine times, then injection of sodium azide (final well concentration 40 mM) and measured four times. The

experiment was prepared as described before to measure mitochondrial fatty acid β -oxidation. Basal oxygen consumption, followed by injection of Etomoxir (final well concentration 500 μ M) and finally injection of sodium azide (final well concentration 40 mM), all measured five times. OCR was normalized to the number of worms with six technical replicates.

8.2.3 Genome editing

Genome editing with CRISPR/Cas9 was outsourced to SunyBiotech (China). PHX808 *hvk-1*, PHX799 *hvk-2*, PHX851 *hvk-3*, PHX2987 *acs-13*, PHX2950 *mpc-1*, and PHX2050 *lars-1* were tagged with mKate2 in the C-terminus right before the stop codon. PHX2337 d10 *hvk-2* was generated from PHX799 by deleting the coding sequence corresponding to the first ten amino acid residues after the initial ATG. PHX997 *mml-1* was tagged with a 3xFLAG tag with a glycine linker in the C-terminus before the stop codon. PHX1524 *lmp-1* was tagged with mKate2 with a GA linker in the C-terminus before the stop codon.

8.2.4 Motility assay

Worm motility was assessed by placing >20 worms in a drop of M9 buffer and recorded for 30 sec using the Leica M80 Binocular Microscope equipped with the Leica MC170 HD camera. Videos were analyzed to count the thrashing of each worm and reported as the body bends per 30 sec.

8.2.5 Body measurements and pharyngeal pumping rates

Worms were imaged or recorded using the Leica stereo microscope MDG41 equipped with Leica DFC3000G monochrome camera with a 6.3X magnification. For measuring the body length and area, >20 worms were transferred to a drop of sodium azide 50 mM, imaged, and analyzed in Fiji imaging software. To measure the pharyngeal pumping rates, worms were transferred to a new plate, acclimated on the plates without a lid for 10 min, and then recorded for 30 sec. Videos were analyzed to count each animal's pharyngeal pumping and reported as pumping per 30 sec.

8.3 Molecular Biology

8.3.1 *Molecular cloning*

Plasmids were constructed by classical cloning or Gibson Assembly. Restriction enzymes from NEB were used according to the manufacturer's instructions. Custom primers were designed with SnapGene v.5.3.2 and NEBuilder Assembly Tool v.2.5.4 (**Supplementary Table 2**). For classical cloning, digested plasmids and amplicons were ligated using the T4 DNA Ligase according to the manufacturer's instructions (New England Biolabs). For Gibson Assembly, digested plasmid and amplicon were assembled using NEBuilder HiFi DNA Assembly Master Mix (New England Biolabs) according to the manufacturer's instructions.

Plasmids were transformed into *E. coli* DH5 α (Life Technologies) strain using the heat shock protocol and plated on LB media supplemented with ampicillin. Colony PCR was conducted to determine positive colonies as a primary screen, and candidates were chosen to purify the plasmid using the QIAprep Miniprep Kit (Qiagen) according to the manufacturer's instructions. Sanger sequencing of the plasmids was outsourced to Eurofins Genomics.

8.3.2 *RNA extraction*

Before RNA extraction, all the working stations and materials were cleaned with RNAzap solution to remove traces of RNase. All samples were kept on ice at every step. Worms were synchronized by egg lay for 4 h and collected once they reached the young adult stage in 15 mL conical tubes. Worms were washed three times with M9 buffer, snap-frozen in liquid nitrogen, and stored at -80 °C until extraction. The worm pellet was subjected to 4 cycles of freeze and thaw with liquid nitrogen and a water bath at ~37 °C. To lyse the worms, 200 μ L of 1.0 mm Zirconia/Silica beads (FisherScientific) were added and transferred to the TissueLyser LT (Qiagen) for 30 min, full speed at 4 °C. Samples were incubated for 5 min at RT. After, 200 μ L chloroform was added and centrifuged at 12,000 g for 15 min at 4 °C. The top aqueous phase was transferred to a new 1.5 mL tube and mixed with 200 μ L of ethanol. The RNA purification was performed using the RNeasy Mini Kit (Qiagen) according to the manufacturer's instructions. The concentration and purity of the RNA samples were quantified using the NanoPhotometer NP80 spectrophotometer (Implen).

8.3.3 *RT-qPCR*

cDNA was prepared after extracting total RNA from young adult worms using the iScript cDNA Synthesis Kit (BioRad) according to the manufacturer's instructions. Primers, cDNA, and Power SYBR Green Master Mix (Applied Biosystems) were transferred to a 384-well plate using the JANUS automated workstation (PerkinElmer) with four technical replicates per genotype/gene. The reaction was quantified using the ViiA 7 Real-Time PCR system machine (Applied Biosystems). *cdc-42* was used as an endogenous control for the quantification. The complete primer sequences are in **Supplementary Table 2**.

8.3.4 *RNA sequencing*

Worms were synchronized by egg lay for 4 h. Young adults were collected from one full 10 cm NGM plate, washed three times with M9 buffer, and resuspended in 700 μ L of QIAzol reagent (Qiagen). The worm pellet was snap-frozen in liquid nitrogen and stored at -80 °C until the extraction day. RNA was extracted as described previously. The RNA libraries, including polyA enrichment, were prepared by the Max Planck-Genome-Centre Cologne (MP-GC) from the Max Planck Institute for Plant Breeding Research. Sequencing was performed on HiSeq3000 of 150 bp single reads for a total of 37.6 Mio (5.62 Gigabases) reads.

The raw reads were mapped to the reference genome WBcel235 (Ensemble build 89) using hisat2 v2.1.0 (D. Kim et al., 2015). samtools was used to convert SAM to BAM files, selecting only mapped reads and sorting the alignments by position (H. Li et al., 2009). Guided transcript assembly of known and potential new transcripts was performed with StringTie v.1.3.4d (Pertea et al., 2016). Cufflinks' cuffmerge v.2.2.1 was used to create a consensus transcriptome across all the samples, cuffquant v.2.2.1 was used to count transcriptome abundance for each sample, and cuffdiff v.2.2.1 was used to calculate differential gene expression as pairwise comparisons (Trapnell et al., 2013). Enrichment analysis for GO terms was performed using the DAVID bioinformatics resources database. aDiff from the python package AGEpy was used to do functional enrichment of the differentially expressed genes for each comparison (Metge et al., 2018).

8.4 Biochemistry

8.4.1 Protein extraction and Western blot analysis

Worms were harvested from a mixed population or synchronized by egg lay or bleaching with M9 buffer and washed three times. The worm pellet was snap-frozen in liquid nitrogen and stored at -80 °C until extraction. The pellet was resuspended in liquid lysis buffer supplemented with cOmplete ULTRA EDTA-free protease inhibitors (Roche) and PhosSTOP phosphatase inhibitors (Roche) and sonicated with Bioruptor Plus (Diagenode S.A.) coupled to Minichiller 300 (Huber) for 15 cycles of 30 sec sonication, 30 sec rest at 4 °C. The total protein extract was cleared by spinning down at 20,817 g for 10 min at 4 °C. Supernatant was transferred to a new tube, and protein was quantified using Pierce BCA Protein Assay Kit (ThermoFisher Scientific) according to the manufacturer's instructions. Equal amounts of protein were mixed with 4X loading sample buffer containing DTT 50 mM and boiled at 95 °C for 10 min. Samples were loaded onto an SDS-PAGE PERCENTAGE gel (BioRad), and proteins were then transferred onto a nitrocellulose membrane (BioRad) using the Trans-Blot Turbo Transfer System (BioRad). Membranes were blocked for 1 h at RT with 5% milk in TBST. Primary and secondary antibodies (**Table 2**) were diluted in 5% bovine serum albumin (BSA) in TBST and incubated for 2-18 h at 4 °C. The membranes were washed three times with TBST for 10 min at RT in-between incubation with the antibodies and after the secondary. The signals were detected using Western Lightning Plus-ECL, Enhanced Chemiluminescence Substrate (PerkinElmer), and imaged in the ChemiDoc MP Imaging System with Image Lab software (BioRad).

Table 2. List of antibodies.

Antibody	Vendor	Cat. Number	Dilution
RFP Tag Polyclonal Antibody	ThermoFisher Scientific	R10367	1:1000
Monoclonal ANTI-FLAG M2, Clone M2	Sigma Aldrich	F1804	1:1000
Anti-beta Actin antibody	Abcam	Ab8224	1:1000
Phospho-AMPK α (Thr172) (40H9)	CST	2535	1:1000
Anti-rabbit IgG (H+L)	Invitrogen	G21234	1:5000
Anti-mouse IgG	Invitrogen	G21040	1:5000

8.4.2 Immunoprecipitation

Worms were collected from a mixed population or synchronized by bleaching for experiments including *glp-1(e2141)* from twenty 10 cm plates, transferred into 15 mL conical tubes with M9 buffer and washed three times. Worms were snap-frozen in liquid nitrogen and stored at -80 °C until extraction. The worm pellet was resuspended in lysis buffer supplemented with cOmplete ULTRA EDTA-free protease inhibitors (Roche) and PhosSTOP phosphatase inhibitors (Roche). Worms were sonicated with Bioruptor Plus (Diagenode S.A.) coupled to Minichiller 300 (Huber) for 30 cycles of 30 sec sonication, 30 sec rest at 4 °C. The total extract was cleared by spinning down at 20,817 g for 15 min at 4 °C. Supernatant was transferred to a new tube, and protein was quantified using Pierce BCA Protein Assay Kit (ThermoFisher Scientific) according to the manufacturer's instructions.

The Anti-FLAG M2 magnetic beads (Sigma) were resuspended and equilibrated with TBST buffer. A total of 7 mg of total protein extract in 800 µL was mixed with the magnetic beads and incubated overnight at 4 °C. The next day, the supernatant was removed and stored for WB analysis. The beads were washed 3 times with 1 mL of cold washing buffer #1 (Tris/HCl, pH 7.4 20 mM, NaCl 300 mM, EDTA 1 mM, NP-50 0.5%), and 3 times with 1 mL of cold washing buffer #2 (Tris/HCl, pH 7.4 20 mM, NaCl 300 mM, EDTA 1 mM). In the last wash, 500 µL of washing buffer #2 was added, and 100 µL were stored for WB analysis.

To elute samples for mass spectrometry, 100 µL of elution buffer (Trypsin 5 ng/µL, Tris/HCl, pH 7.5 50 mM, Tris(2-carboxyethyl)phosphine (TCEP) 1 mM, Chloroacetamide (CAA) 5 mM) were added and incubated 30 min at RT. The supernatant was transferred to a new 0.5 mL tube and incubated overnight at 37 °C. The next day, formic acid was added to a final concentration of 1% to stop the digestion. Peptides were stored at -20 °C until purification.

The peptides were cleaned and purified with StageTip. A 30 µg C18-SD tip was hydrated with 200 µL of methanol, followed by 200 µL of 40% acetonitrile (ACN)/0.1% formic acid (FA). 200 µL of 0.1% FA were added to equilibrate the C18-SD. The digested peptides were dissolved in 0.1% FA and added to the C18-SD and washed once with 0.1% FA. To elute the peptides, 80

μL of 40% ACN/0.1% FA was added, and elutes were collected in 0.5 μL tubes and dried in centrifugal vacuum Concentrator Plus (Eppendorf) for 45 min at 45 °C.

8.4.3 Proteomics

8.4.3.1 LC-MS/MS analysis

Peptides were separated on a 25 cm, 75 μm internal diameter PicoFrit analytical column (New Objective) packed with 1.9 μm ReproSil-Pur 120 C18-AQ media (Dr. Maisch) using an EASY-nLC 1200 (ThermoFisher Scientific). The column was maintained at 50 °C. Buffer A and B were 0.1% FA in water and 0.1% FA in 80% CAN, respectively. Peptides were separated on a segmented gradient from 6 to 31% buffer B for 57 min and from 31 to 44% buffer B for 5 min at 250 nl/min. Eluting peptides were analyzed on an Orbitrap Fusion Tribrid mass spectrometer (ThermoFisher Scientific). Peptide precursor m/z measurements were carried out at 60,000 resolution in the 350 to 1,500 m/z range. The most intense precursors with charge states from 2 to 7 were selected for HCD fragmentation using 27% normalized collision energy. The cycle time was set to 1 sec. The m/z values of the peptide fragments were measured at a resolution of 50,000 using an AGC target of 2e5 and 86 ms maximum injection time. Upon fragmentation, precursors were put on a dynamic exclusion list for 45 sec.

8.4.3.2 Protein identification and quantification

The raw data were analyzed with MaxQuant v.1.6.1.0 (Cox & Mann, 2008). Peptide fragmentation spectra were searched against the canonical and isoform sequences of the *C. elegans* reference proteome (proteome ID UP000001940, downloaded December 2018 from UniProt). Methionine oxidation and protein N-terminal acetylation were set as variable modifications; cysteine carbamidomethylation was set as fixed modification. The digestion parameters were set to “specific” and “Trypsin/P”. The minimum number of peptides and razor peptides for protein identification was 1; the minimum number of unique peptides was 0. Protein identification was performed at a peptide spectrum match and protein false discovery rate of 0.01. The “second peptide” option was on. Successful identification was transferred between the different raw files using the “Match between runs” option. Label-free quantification (LFQ) (Cox et al., 2014) was performed using an LFQ minimum ratio count of 2. LFQ intensities were filtered for at least two valid values in at least one group and imputed from a normal distribution with a width of 0.3 and

a downshift of 1.8. Differential expression analysis was performed using *limma* package v.3.34.9 (Ritchie et al., 2015) in R v.3.4.3 (R Core Team, 2017).

8.4.4 Metabolomics

8.4.4.1 Sample preparation

Worms were synchronized by egg lay and harvested at day one of adulthood after washing with M9 buffer three times to remove bacteria. Worm pellets were split into three Eppendorf tubes, one for each omics, and flash-frozen with liquid nitrogen before storing at -80 °C. Four biological replicates were collected in independent experiments, and the following processing was conducted in parallel for each omics analysis. For metabolomics, worm pellets were homogenized using the TissueLyser LT (Qiagen) for 30 min at 4 °C. Protein concentration was determined using a BCA kit. A volume of worm lysate, which corresponds to 150 µg of proteins for each sample, was subjected to Bligh and Dyer extraction (chloroform:methanol 2:1) for 1 h at 4 °C, as previously reported (Annibal et al., 2021). Samples were centrifuged at maximum speed for 5 min at 4 °C, and the supernatant was transferred into a new tube for drying. Before LC injections samples, were reconstituted in 10% aqueous ACN.

8.4.4.2 Untargeted metabolomics and analysis

Analytes were separated using a UHPLC system (Vanquish, ThermoFisher Scientific) coupled to an HRAM mass spectrometer (Q-Exactive Plus, ThermoFischer Scientific) as previously reported (Annibal et al., 2021). Briefly, 2 µL of the sample extracts were injected into an X Select HSS T3 XP column, 100 Å, 2.5 µm, 2.1 mm x 100 mm (Waters), using a binary system A water with 0.1% FA, B: ACN with 0.1% FA with a flow rate of 0.1 mL/min and the column temperature was kept at 30 °C. Gradient elution was conducted as follow: isocratic step at 0.1% eluent B for 0.3 min, gradient increased up to 2% eluent B in 2 min, then increased up to 30% eluent B in 6 min and to 95% eluent B in 7 min, isocratic step at 95% eluent B for 2 min. Gradient decreased to 0.1% eluent B in 3 min and was held at 0.1% eluent B for 5 min. Mass spectra were recorded from 100-800 m/z at a mass resolution of 70,000 at m/z 400 in both positive and negative ion mode using data-dependent acquisition (Top 3, dynamic exclusion list 10 sec). Tandem mass spectra were acquired by performing CID (isolation 1.5 u, stepped collision energy 20 and 80 NCE). MS data analysis was performed using Xcalibur software 4.0. Using Trace finder 4.1,

quantification was performed using genesis detection algorithm, nearest RT, S/N threshold 8, min peak height (S/N) equal to 3, peak S/N cutoff 2.00, valley rise 2%, valley S/N 1.10. Metabolite search was performed using Compound discoverer 2.0 and m/z Cloud as an online database, considering precursor ions with a deviation > 5 ppm, 0.3 min maximum retention time shift, minimum peak intensity 100,000, intensity tolerance 10, FT fragment mass tolerance 0.0025 Da, group covariance [%] less than 30, *p*-value less than 0.05 and area Max greater or equal to 10,000. Metabolites were correctly identified when at least two specific fragments were found in the MS2 spectra. Because of the high mass accuracy >3 ppm, predicted elemental compositions of the unknown features were submitted to another online database such as Chempider (<http://www.chemspider.com/>), HMDB (<http://www.hmdb.org/>), KEGG (<http://www.genome.jp/kegg/>), METLIN (<http://metlin.scripps.edu/>). Raw data were also analyzed using XCMS online (<https://xcmsonline.scripps.edu>).

8.4.5 G6P and NADP⁺/NADPH measurements

G6P and NADP⁺/NADPH were measured from total worm extracts using the Glucose-6-Phosphate Assay Kit (Sigma MAK014) and the NADP/NADPH-Glo Assay (Promega G9081), respectively, following the manufacturer's instructions. *glp-1(e2141)* strains were used to avoid signals from the germline. Briefly, worms were synchronized as mentioned previously, collected in a 15 mL conical tube, and washed three times with M9 buffer. Worms were snap-frozen in liquid nitrogen and sonicated using the Bioruptor Plus (Diagenode S.A.) coupled to Minichiller 300 (Huber) for 15 cycles of 30 sec sonication, 30 sec rest at 4 °C. Worms' extracts were cleared by centrifugation at 20,817 g for 15 min at 4 °C. Samples were always kept on ice. As mentioned previously, part of the samples was used to quantify protein, and the rest was used to quantify the metabolites.

For G6P colorimetric detection, samples were run in technical duplicates in a 96-well plate. The standard curve was made using the G6P Standard solution provided by diluting with ddH₂O to generate 0 (blank), 2, 4, 6, 8, and 10 nmol/well standards. Samples were combined with the reaction mix in each well and mixed for 30 min at RT, protecting the plate from the light. The absorbance was measured at 450 nm using the POLARstar OMEGA Plate Reader with Luminescence (BGM Labtech). For the analysis, all samples were corrected for the background. The standard curve was generated with the appropriate values obtained by the standards mentioned

previously, and the amount of G6P in each sample was calculated with the standard curve. Values were normalized to protein levels.

For the NADP⁺/NADPH bioluminescent assay, samples were run in technical duplicates in a 96-well plate. 50 µL of worm lysis in M9 buffer were incubated with 50 µL base solution with 1% DTAB. Samples were split into two: one to measure NADP⁺ and the other to measure NADPH. Samples were incubated with or without 25 µL 0.4 N of HCl to measure NADP⁺ or NADPH, respectively, at 60 °C for 15 min, and then the plate was equilibrated for 10 min at RT. Next, 25 µL of Trizma base were added to each well of acid-treated samples to neutralize the acid and 50 µL of HCl/Trizma solution to each well of base-treated samples. An equal amount of the NADP/NADPH-Glo Detection Reagent was added to each well and mixed at RT for 30 min by protecting the plate from the light. The luminescence was recorded using the POLARstar OMEGA Plate Reader with Luminescence (BGM Labtech). Samples were corrected to background luminescence. The relative luminescent units were standardized to the protein concentration.

8.5 Microscopy

8.5.1 *Staining and preparation of slides*

All dyes were added to the bacterial lawn, incubated egg on, and protected from the light until the day of imaging. Final solutions were made by diluting in M9 buffer. MitoTracker Deep Red FM (ThermoFisher Scientific) was resuspended in 100 µL of DMSO to make a 919.82 µM stock. The final concentration used was 500 nM of MitoTracker Deep Red. LipiBlue (Dojindo) was resuspended in 100 µL of DMSO to make a 100 µM stock. The final concentration used was 1 µM. C1-BODIPY-C12 500/510 (ThermoFisher Scientific) was dissolved in DMSO to make a 5 mM stock. The final concentration used was 1 µM. Worms were mounted on a slide with a 5% agarose pad using sodium azide 50 mM. Levamisole 20 mM was used as an anesthetic to image mitochondria.

8.5.2 *Brightfield and fluorescent imaging*

Brightfield and fluorescent images with higher resolution were acquired using the Zeiss Axio Imager Z1 Fluorescent Microscope equipped with the Digital Microscope Camera Axio Cam Mono 506 and the IcC5 true color camera. For fluorescent microscopy, the microscope used a

Colibri 7 LED Light Source and the filters sets GFP (Set 38 HE), TR (Set 45), and TL. The software used was Zeiss Zen v2.3.69.1017.

Brightfield and fluorescent images were also acquired with the Leica stereo microscope MDG41 equipped with Leica DFC3000G monochrome camera. The microscope was equipped with the Leica EL6000 external light source. The software used was the Leica Application Suite X v3.7.5.24914.

Nuclear localization of MML-1::GFP, HLH-30::GFP, DAF-16::GFP, and MDL-1::GFP was quantified in intestinal cells from day one adult worms. Worms anesthetized with sodium azide 40 mM. At least, 20 worms were imaged per genotype/condition. Quantification of the transcription factor nuclear localization was performed by manually selecting each nucleus and calculating the pixel intensity per area. The same area was used to calculate the cytosolic and background signal. Values were corrected by background subtraction. Nuclear localization was calculated by dividing the nuclear signal from the cytosolic signal.

8.5.3 Confocal Imaging

Confocal images were acquired with Leica TCS SP8 confocal microscope equipped with white light laser and a 63X 1.4 NA oil objective. The microscope was also equipped with HyD detectors for fluorescent images and a PMT detector for the bright field. The LAS X Life Science software was used to acquire images and 3D reconstruction. When multiple fluorescent proteins or dyes were imaged, sequential scanning was used to reduce bleed-through of the signal from one channel to another. All images used for colocalization analysis were deconvoluted with the installed LIGHTNING package to optimize the images and reduce background noise.

8.6 Statistical analysis

The results are presented as mean + SD or SEM, as indicated in the figure legends. The number of biological replicates is shown in the figure legends as “N”, while the number of worms is presented as “n”. Before comparing groups, the data were tested for Gaussian distribution using the Kolmogorov-Smirnov normality test with Dallal-Wilkinson-Lilliefors *p*-value. For normally distributed data, unpaired *t*-test with Welch’s correction or one-way ANOVA with Brown-Forsythe and Welch’s corrections were calculated in GraphPad Prism 9 (GraphPad software). For lifespan analysis, *p*-values were calculated using Log-rank (Mantel-Cox) test. Statistical data from

all the lifespans are included in **Supplementary Table 5**. Statistical significance for qPCR experiments was calculated with two-tailed *t*-test. For colocalization analysis, Costes' randomization was performed to determine statistical significance. For RNAseq data, GO terms enrichment analysis was performed using Fisher's test. Significance levels are ns = not significant $p>0.05$, * $p<0.05$, ** $p<0.01$, *** $p<0.001$, **** $p<0.0001$.

8.7 Software

Image analysis was performed using open-source Fiji package software. Additional JACoP (Bolte & Cordelières, 2006) plugin was used for colocalization analysis. Densitometry analyses were performed using GelAnalyzer v.19.1. Graphs were generated in GraphPad Prism 9 and using custom R scripts. Images were designed in Adobe Illustrator and BioRender.

IX. Supplementary Tables

Supplementary Table 1. Worm strains used for this work.

Name	Genotype	Short Name	Source
	N2 (Bristol)	N2/wildtype	CGC
AA4402	<i>glp-1(e2141) III</i>	<i>glp-1</i>	CGC
AA4714	<i>isp-1(qm150) IV</i>	<i>isp-1</i>	CGC
CB1370	<i>daf-2(e1370) III</i>	<i>daf-2</i>	CGC
YB84	<i>aak-1(tm1944) III</i>	<i>aak-1</i>	CGC
YB83	<i>aak-2(ok524) X</i>	<i>aak-2</i>	CGC
YB146	<i>aak-1(tm1944) III; aak-2(ok524) X</i>	<i>aak-1; aak-2</i>	CGC
AA3472	<i>dhIs989[mml-1a::GFP, myo-2p::mCherry]</i>	MML-1::GFP	1
AA3428	<i>wgIs198[mml-1::TY1::EGFP::3xFLAG(92C12) + unc-119(+)]</i>		1
AA3809	<i>dhIs989[mml-1a::GFP, myo-2p::mCherry]; glp-1(e2141) III</i>		This work
AA4775	<i>dhIs989[mml-1a::GFP, myo-2p::mCherry]; daf-2(e1370) III</i>		This work
AA5257	<i>dhIs989[mml-1a::GFP, myo-2p::mCherry]; isp-1(qm150) IV</i>		This work
AA5289	<i>dhIs989[mml-1a::GFP, myo-2p::mCherry]; aak-1(tm1944) III</i>		This work
AA5290	<i>dhIs989[mml-1a::GFP, myo-2p::mCherry]; aak-2(ok524) X</i>		This work
AA5302	<i>dhIs989[mml-1a::GFP, myo-2p::mCherry]; aak-1(tm1944) III; aak-2(ok524)</i>		This work
MAH235	<i>sqIs19[hllh-30p::hllh-30::GFP + rol-6(su1006)]</i>	HLH-30::GFP	CGC
AA3572	<i>glp-1(e2141ts) III; sqIs19[hllh-30p::hllh-30::GFP + rol-6(su1006)]</i>		1
TJ356	<i>zIs356[daf-16p::daf-16::GFP; rol-6] IV</i>	DAF-16::GFP	CGC
AA949	<i>daf-2(e1370) III; zIs356[daf-16p::daf-16::GFP; rol-6] IV</i>		V. Rottiers
PHX808	<i>hxx-1(syb808) I</i>	HXX-1::mKate2	This work
PHX799	<i>hxx-2(syb799) I</i>	HXX-2::mKate2	This work
PHX851	<i>hxx-3(syb851) IV</i>	HXX-3::mKate2	This work
PHX2337	<i>hxx-2(syb799 syb2337)</i>	d10 HXX-2::mKate2	This work
PHX1524	<i>lmp-1(syb1524) X</i>	LMP-1::mKate2	This work
PHX2987	<i>acs-13(syb2987) I</i>	ACS-13::mKate2	This work

PHX2950	<i>mpc-1(syb2950) III</i>	MPC-1::mKate2	This work
AA3972	<i>dhEx461[myo-3p::mitochondrial signal sequence::gfp, coel::rfp]</i>	mitoGFP	CGC
OJ3437	<i>vjIs148[Pges-1::tomm-20::mCherry]</i>	TOMM-20::mCherry	CGC
SJZ204	<i>foxSi37[ges-1p::tomm-20::mKate2::HA::tbb-2 3' UTR] I</i>	TOMM-20::mKate2	CGC
AA4917	<i>hxx-2(syb799); dhEx461[myo-3p::mitochondrial signal sequence::gfp, coel::rfp]</i>		This work
AA5340	<i>hxx-2(syb799 syb2337) I; dhEx461[myo-3p::mitochondrial signal sequence::gfp, coel::rfp]</i>		This work
PHX2050	<i>lars-1(syb2050) III</i>	LARS-1::mKate2	This work
AA5184	<i>glp-1(e2141) III, lars-1(syb2050) III</i>		This work
SJ4100	<i>zcls13 [hsp-6p::GFP] V</i>	<i>hsp-6p::GFP</i>	CGC
SJ4005	<i>zcls4 [hsp-4p::GFP] V</i>	<i>hsp-4p::GFP</i>	CGC
CL2070	<i>dvIs70 [hsp-16.2p::GFP + rol-6(su1006)]</i>	<i>hsp-16.2p::GFP</i>	CGC
AA4912	<i>dhIs989[mml-1a::GFP, myo-2p::mCherry]; hxx-2(syb799) I</i>		This work
AA5026	<i>dhIs989[mml-1a::GFP, myo-2p::mCherry]; vjIs148[Pges-1::tomm-20::mCherry]</i>		This work
AA5174	<i>dhIs989[mml-1a::GFP, myo-2p::mCherry]; foxSi37[ges-1p::tomm-20::mKate2::HA::tbb-2 3' UTR] I</i>		This work
AA5147	<i>dhIs989[mml-1a::GFP, myo-2p::mCherry]; lmp-1(syb1524) X</i>		This work
OP106	<i>unc-119(ed3) III; wgIs106[mdl-1::TY1::EGFP::3xFLAG + unc-119(+)]</i>	MDL-1::GFP	CGC
AA3773	<i>glp-1(e2141) III; wgIs106[mdl-1::TY1::EGFP::3xFLAG + unc-119(+)]</i>		1
PHX997	<i>mml-1(syb997) III</i>	MML-1::3xFLAG	This work
AA4965	<i>mml-1(syb997); glp-1(e1340)</i>		This work
AA4947	<i>mml-1(syb997); daf-2(e1370)</i>		This work
WBM170	<i>wbmEx57[acs-2p::GFP + rol-6(su1006)]</i>	<i>acs-2p::GFP</i>	CGC
LIU1	<i>ldrIs1 [dhs-3p::dhs-3::GFP + unc-76(+)]</i>	DHS-3::GFP	CGC
LIU2	<i>ldrIs2 [plin-1::plin-1::mCherry + unc-76(+)]</i>	PLIN-1::GFP	CGC
AA5185	<i>dhIs989[mml-1a::GFP, myo-2p::mCherry]; mpc-1(syb2950) III</i>		This work
AA5186	<i>dhIs989[mml-1a::GFP, myo-2p::mCherry]; acs-13(syb2987) I</i>		This work

¹ (Nakamura et al., 2016)

Supplementary Table 2. Oligonucleotides.

Name	Sequence	Used for
mml-1(ok849r) geno F	GTCTTCACAACCACAGTATGCCA	Genotyping
mml-1(ok849r) geno R	TTCTGCTAGATAACTTACCACC	Genotyping
mxl-2(tm1516) geno F	TTGGTTGGCTGACAAATTTCAAT	Genotyping
mxl-2(tm1516) geno R	GCCGGACGGCTCGGCGAGCTCCC	Genotyping
hxx-1 qPCR 1 FW	ACAAAACGGAATCGCCACAG	qPCR
hxx-1 qPCR 1 RV	ACAAGACGTTGGCATGCTTC	qPCR
hxx-2 qPCR 3 FW	ACATTGCCAAAGCTCTGTGC	qPCR
hxx-2 qPCR 3 RV	TGATCGCAGGGATACGAGAAAG	qPCR
hxx-3 qPCR 3 FW	AAAAGCTCGCGGTTACGATC	qPCR
hxx-3 qPCR 3 RV	CGTCGACTTCCCGATCAAATTG	qPCR
L4440 seq fw	AGCGAGTCAGTGAGCGAG	Sequencing
L4440 seq rv	TGTAAAACGACGGCCAGT	Sequencing
mml-1 FLAG fw	TTCGCATCGTCTGTAGCAGG	Genotyping
mml-1 FLAG RV	TGGCAACATGAAAGGGACTGA	Genotyping
mml-1 seq C-terminus fw	TAGCAGGAGACTCGTCGTCA	Genotyping
mml-1 seq C-terminus rv	TGGCAACATGAAAGGGACTGA	Genotyping
hxx-1 seq C-terminus fw	GATGGATCTGGACGTGGAGC	Genotyping
hxx-1 seq C-terminus rv	TTTGTTCCTAAGTGTGGGCGG	Genotyping
hxx-2 seq C-terminus fw	GCGAGCACAAAAGATCTCGG	Genotyping
hxx-2 seq C-terminus rv	AGTCTTTCAGGCTTTCAGGC	Genotyping
hxx-3 seq C-terminus fw	AGGAAGTTGTCAAGGAGCCG	Genotyping
hxx-3 seq C-terminus rv	GGGTTATGGCGGGGAAAACA	Genotyping
hxx-3 NotI fw 2	TAAGCAGCGGCCGCGCCAGTGTGCACAAAGGAAA	Cloning into L4440
hxx-3 HindIII rv2	TGCTTAAAGCTTCGGCTCCTTGACAACTTCCT	Cloning into L4440
mml-1 qPCR fw	CCGCTTGCGAGTACACTTTTG	qPCR
mml-1 qPCR rv	CGGCTCGGCGAGAATG	qPCR
mdl-1 qPCR fw	CTGCTCTCCTTCCGCCAAT	qPCR
mdl-1 qPCR rv	ATGAGTGCAAGGCGAATGG	qPCR
fat-5 qPCR fw	GGTCGGACTATATCAGCTTGTG	qPCR
fat-5 qPCR rv	CATGAGAGGGTGGCTTTGTAG	qPCR
lgg-2 qPCR fw	CTGCAAATTCCTAGTACCCGAG	qPCR
lgg-2 qPCR rv	CATAGAATTTGACACCATTGAGC	qPCR
swt-1 qPCR fw	TGTCCAGCTCGCCCTCTT	qPCR
swt-1 qPCR rv	TTCTAACGGGCTCTTCTCATTCTC	qPCR
cdc-42 qPCR fw	CTGCTGGACAGGAAGATTACG	qPCR

cdc-42 qPCR rv	CTCGGACATTCTCGAATGAAG	qPCR
isp-1(qm150) seq fw	ACGGTTAGGATAGGACTGAACTT	Genotyping
isp-1(qm150) seq rv	TCCAGAAGGAAAAACAAAGACA	Genotyping
hlh-30 seq C-terminus fw	CGCTCATCCATCACCACACT	Genotyping
hlh-30 seq C-terminus rv	ACTTGGAACGGGCAAATGTA	Genotyping
lmp-1 seq C-terminus fw	TGGTTGTGCTCGTCGGATAC	Genotyping
lmp-1 seq C-terminus rv	TGCACAACATTGCAACAGAGG	Genotyping
lars-1 seq C-terminus fw	TGTCCGACGCAGACATTTTC	Genotyping
lars-1 seq C-terminus rv	AGCTGAAATAGGGATTTCGGGT	Genotyping
mpc-1 SacI fw	CGGACGAGCTCATGTCTCGAGTTATATCAA	Cloning of into L4440
mpc-1 XbaI rv	GCCAGTCTAGATCAATGTGCCTTGCTGATC	Cloning of into L4440
mpc-1 SacII fw	GGTCACCGCGGATGTCTCGAGTTATATCAA	Cloning of into L4440
tomm-20::mKate2::HA fw	CATGGAGGGAACCGTCAACA	Genotyping
tomm-20::mKate2::HA rv	TGATACGCTCAAGACGACGG	Genotyping
hxx-2 N-terminus seq fw	TGACAATTTGTGTGTGCCCC	Genotyping
hxx-2 N-terminus seq rv	CCATTTTTGCCAGCGGAGTC	Genotyping
acs-13::mKate2 fw	GAAGAGCTGTGCAACAACGA	Genotyping
acs-13::mKate2 rv	AAATGGGAACAAGCCGATGA	Genotyping
mpc-1::mKate2 fw	TCAGCTCGGTCGATTTGTGA	Genotyping
mpc-1::mKate2 rv	CGCTAGTTACGGTTTTCTTCG	Genotyping
fln-2 fw	CATTCACTCCGGACGGCGCTGGTGAATT	Genotyping
fln-2 rv	AACGGATGCTGATCTCAAGTTC	Genotyping
aak-1(tm1944) fw	TTGTTTCGCGTCCAGAAGAAGA	Genotyping
aak-1(tm1944) rv	AGTTTCCCTTTCTTCGCTCAC	Genotyping
aak-2(ok524) fw	TCTTCCGCCATCCGCATATC	Genotyping
aak-2(ok524) rv	TCAAATGGCAGGGTTCCACA	Genotyping

Supplementary Table 3. Media, buffers, and solutions.

1. Nematode Growth Media (NGM)

NaCl	0.3% (w/v) (51.3 mM)
Bacto Peptone	0.25% (w/v)
Bacto Agar	1.7% (w/v)
KPO ₄ (Stock 1 M)	25 mM
Cholesterol (Stock 5 mg/mL)	5 µg/mL
MgSO ₄ (Stock 1 M)	1 mM
CaCl (Stock 1 M)	1 mM

Dissolve in ddH₂O and autoclave. Add the cholesterol, MgSO₄ and CaCl after autoclaving.

2. Luria-Bertani (LBH) media

NaCl	0.5% (w/v) (85.55 mM)
Bacto Yeast Extract	0.5% (w/v)
Tryptone	1% (w/v)

Dissolve in in ddH₂O and autoclave.

3. Luria-Bertani (LBH) media plates with ampicillin

NaCl	0.5% (w/v) (85.55 mM)
Bacto Yeast Extract	0.5% (w/v)
Tryptone	1% (w/v)
Bacto Agar	1.5% (w/v)
NaOH (Stock 1 M)	1 mM
Ampicillin (Stock 50 mg/mL)	100 µg/mL

Dissolve in in ddH₂O and autoclave. Add the ampicillin after autoclaving.

4. M9 buffer

NaCl	0.5% (w/v) (85.55 mM)
Na ₂ HPO ₄	42.26 mM
KH ₂ PO ₄	22.04 mM
MgSO ₄ (Stock 1 M)	1 mM

Dissolve in ddH₂O and autoclave. Add the MgSO₄ after autoclaving.

5. S-basal

NaCl	100 mM
K ₂ HPO ₄	5.74 mM
KH ₂ PO ₄	44.09 mM
Cholesterol (Stock 5 mg/mL)	5 µg/mL

Dissolve in water and autoclave. Add the cholesterol after autoclaving.

6. Bleaching solution

NaClO (Stock 6%)	1.8%
KOH (Stock 5 N)	0.75 N

Dissolve in ddH₂O and keep at 4 °C in an amber bottle.

7. Single worm lysis buffer

Tris pH 8.3	10 mM
KCl	50 mM
MgCl ₂	2.5 mM
Tween-20	0.45% (v/v)
Triton X-100	0.45% (v/v)
Proteinase K (NEB)	1 mg/mL

Dissolve in ddH₂O.

8. TBST buffer

Tris base	24.77 mM
NaCl	137 mM
KCl	2.68 mM
Tween-20	0.05%

Dissolve in ddH₂O and adjust the pH to 7.4.

9. Lysis buffer (for protein extraction)

Tris/HCl, pH 7.4	50 mM
NaCl	150 mM
EDTA	1 mM
NP-40	0.5% (v/v)

Dissolve in ddH₂O and store at 4 °C. Add protease and phosphatase inhibitors before using.

10. SDS-PAGE running buffer

Tris base	24.77 mM
Glycine	192 mM
SDS	3.47 mM
Dissolve in ddH ₂ O.	

11. Transfer buffer

Trans-Blot Turbo 5x Transfer	200 mL
Buffer (BioRad)	
Ethanol	200 mL
ddH ₂ O	600 mL

Supplementary Table 4. RNAi screen of glucose metabolism genes and MML-1 nuclear localization.

Gene	Gene ID	Pathway	MML-1 NL ¹	SD	<i>p</i> (t-test)	Sig.
<i>fgt-1</i>	H17B01.1	Glucose metabolism	0.406	0.135	<0.0001	****
<i>hxx-1</i>	F14B4.2	Glycolysis	0.368	0.062	<0.0001	****
<i>hxx-2</i>	H25P06.1	Glycolysis	0.207	0.057	<0.0001	****
<i>hxx-3</i>	Y77E11A.1	Glycolysis	0.713	0.210	<0.0001	****
<i>gpi-1</i>	Y87G2A.8	Glycolysis	0.459	0.073	<0.0001	****
<i>pfk-1.1</i>	Y71H10A.1	Glycolysis	0.498	0.182	<0.0001	****
<i>pfk-1.2</i>	C50F4.2	Glycolysis	1.018	0.757	0.9106	ns
<i>pfk-1.1</i>	Y110A7A.6	Glycolysis	0.704	0.164	<0.0001	****
<i>pfk-1.2</i>	K02B2.1	Glycolysis	0.711	0.230	<0.0001	****
<i>aldo-1</i>	T05D4.1	Glycolysis	0.465	0.105	<0.0001	****
<i>aldo-2</i>	F01F1.12	Glycolysis	0.487	0.114	<0.0001	****
<i>tpi-1</i>	Y17G7B.7	Glycolysis	0.481	0.073	<0.0001	****
<i>gpd-1</i>	T09F3.3	Glycolysis	-	-	-	-
<i>gpd-2</i>	K10B3.8	Glycolysis	0.811	0.162	<0.0001	****
<i>gpd-3</i>	K10B3.7	Glycolysis	1.227	0.528	0.0002	***
<i>gpd-4</i>	F33H1.2	Glycolysis	0.571	0.137	<0.0001	****
<i>pgk-1</i>	T03F1.3	Glycolysis	0.487	0.082	<0.0001	****
<i>ipgm-1</i>	F57B10.3	Glycolysis	0.471	0.083	<0.0001	****
<i>enol-1</i>	T21B10.2	Glycolysis	0.541	0.129	<0.0001	****
<i>pyk-1</i>	F25H5.3	Glycolysis	0.568	0.176	<0.0001	****
<i>pyk-2</i>	ZK593.1	Glycolysis	0.640	0.495	0.0015	**
<i>pdha-1</i>	T05H10.6	Pyruvate oxidation	0.649	0.207	<0.0001	****
<i>pdhb-1</i>	C04C3.3	Pyruvate oxidation	0.656	0.197	<0.0001	****
<i>dlat-1</i>	F23B12.5	Pyruvate oxidation	0.837	0.283	0.0055	**
<i>dlat-2</i>	C30H6.7	Pyruvate oxidation	0.634	0.157	<0.0001	****
<i>pyc-1</i>	D2023.2	Pyruvate metabolism	0.960	0.379	0.5653	ns

<i>ldh-1</i>	F13D12.2	Pyruvate metabolism	0.390	0.105	<0.0001	****
<i>pdhk-2</i>	ZK370.5	Pyruvate metabolism	0.836	0.248	0.0034	**
<i>cts-1</i>	T20G5.2	TCA Cycle	0.794	0.218	0.0158	*
<i>aco-1</i>	ZK455.1	TCA Cycle	0.627	0.208	<0.0001	****
<i>aco-2</i>	F54H12.1	TCA Cycle	0.760	0.206	<0.0001	****
<i>idh-1</i>	F59B8.2	TCA Cycle	0.490	0.156	<0.0001	****
<i>idh-2</i>	C34F6.8	TCA Cycle	0.828	0.217	0.0025	**
<i>ogdh-1</i>	T22B11.5	TCA Cycle	1.190	0.398	0.0371	*
<i>dld-1</i>	LLC1.3	TCA Cycle	1.587	0.531	<0.0001	****
<i>dlst-1</i>	W02F12.5	TCA Cycle	0.947	0.418	0.5486	ns
<i>sucl-1</i>	C05G5.4	TCA Cycle	0.632	0.154	<0.0001	****
<i>sucl-2</i>	F23H11.3	TCA Cycle	0.695	0.190	<0.0001	****
<i>suca-1</i>	F47B10.1	TCA Cycle	1.057	0.528	<0.0001	****
<i>sucg-1</i>	C50F7.4	TCA Cycle	1.791	0.603	0.0197	*
<i>sdha-1</i>	C03G5.1	TCA Cycle	1.145	0.352	0.0292	*
<i>sdha-2</i>	C34B2.7	TCA Cycle	0.485	0.086	<0.0001	****
<i>sdhb-1</i>	F42A8.2	TCA Cycle	0.621	0.161	<0.0001	****
<i>sdhd-1</i>	F33A8.5	TCA Cycle	0.468	0.075	<0.0001	****
<i>mev-1</i>	T07C4.7	TCA Cycle	0.957	0.338	0.4659	ns
<i>fum-1</i>	H14A12.2	TCA Cycle	0.514	0.117	<0.0001	****
<i>mdh-1</i>	F46E10.10	TCA Cycle	0.474	0.071	<0.0001	****
<i>mdh-2</i>	F20H11.3	TCA Cycle	0.610	0.199	<0.0001	****
<i>gspd-1</i>	B0035.5	PPP	0.874	0.189	0.0989	ns
<i>Y57G11C.3</i>	Y57G11C.3	PPP	0.454	0.087	<0.0001	****
<i>F26D11.1</i>	F26D11.1	PPP	0.468	0.171	<0.0001	****
<i>T25B9.9</i>	T25B9.9	PPP	1.693	0.658	<0.0001	****
<i>F08F8.7</i>	F08F8.7	PPP	0.837	0.356	0.0983	ns
<i>rpia-1</i>	B0280.3	PPP	0.469	0.108	<0.0001	****
<i>R151.2</i>	R151.2	PPP	0.845	0.221	0.0149	*
<i>F07A11.5</i>	F07A11.5	PPP	0.851	0.206	0.0043	**
<i>tkl-1</i>	F01G10.1	PPP	2.032	0.743	<0.0001	****
<i>tald-1</i>	Y24D9A.8	PPP	1.053	0.413	0.4774	ns
<i>F09E5.3</i>	F09E5.3	PPP	0.861	0.279	0.0723	ns
<i>Y43F4B.5</i>	Y43F4B.5	PPP /Gluconeogenesis	0.659	0.160	<0.0001	****
<i>R05F9.6</i>	R05F9.6	PPP /Gluconeogenesis	0.896	0.320	0.1852	ns
<i>gfat-1</i>	F07A11.2	Hexosamine Pathway	0.798	0.254	0.0190	**
<i>gfat-2</i>	F22B3.4	Hexosamine Pathway	0.520	0.095	<0.0001	****
<i>T03F6.3</i>	T03F6.3	Hexosamine Pathway	0.453	0.081	<0.0001	****
<i>gna-1</i>	B0024.12	Hexosamine Pathway	0.566	0.221	<0.0001	****
<i>gna-2</i>	T23G11.2	Hexosamine Pathway	0.521	0.147	<0.0001	****
<i>F59B2.3</i>	F59B2.3	Hexosamine Pathway	0.419	0.074	<0.0001	****
<i>F21D5.1</i>	F21D5.1	Hexosamine Pathway	-	-	-	-
<i>C36A4.4</i>	C36A4.4	Hexosamine Pathway	1.036	0.346	0.5555	ns
<i>chs-1</i>	T25G3.2	Hexosamine Pathway	-	-	-	-
<i>chs-2</i>	F48A11.1	Hexosamine Pathway	-	-	-	-
<i>gale-1</i>	C47B2.6	Hexosamine Pathway	0.636	0.196	<0.0001	****

<i>tre-1</i>	F57B10.7	Gluconeogenesis	0.643	0.171	<0.0001	****
<i>tre-2</i>	T05A12.2	Gluconeogenesis	0.529	0.107	<0.0001	****
<i>tre-3</i>	W05E10.4	Gluconeogenesis	-	-	-	-
<i>tre-5</i>	C23H3.7	Gluconeogenesis	-	-	-	-
<i>pck-1</i>	W05G11.6	Gluconeogenesis	0.549	0.109	<0.0001	****
<i>pck-2</i>	R11A5.4	Gluconeogenesis	-	-	-	-
<i>pck-3</i>	H04M03.1	Gluconeogenesis	0.672	0.213	<0.0001	****
<i>gsk-3</i>	Y18D10A.5	Glycogenesis	0.502	0.089	<0.0001	****
<i>rml-1</i>	K08E3.5	Glycogenesis	0.700	0.220	<0.0001	****
<i>T04A8.7</i>	T04A8.7	Glycogenesis	0.820	0.240	0.0133	*
<i>gyg-1</i>	F56B6.4	Glycogenesis	0.653	0.151	<0.0001	****
<i>gyg-2</i>	T25E12.5	Glycogenesis	-	-	-	-
<i>gsy-1</i>	Y46G5A.31	Glycogenesis	0.502	0.073	<0.0001	****
<i>agl-1</i>	R06A4.8	Glycogenolysis	0.785	0.295	0.0010	**
<i>pygl-1</i>	T22F3.3	Glycogenolysis	0.848	0.337	0.0675	ns
<i>tps-1</i>	ZK54.2	Trehalose Pathway	0.610	0.230	<0.0001	****
<i>tps-2</i>	F19H8.1	Trehalose Pathway	0.874	0.296	0.0572	ns
<i>gob-1</i>	H13N06.3	Trehalose Pathway	0.569	0.164	<0.0001	****

¹MML-1::GFP nuclear localization relative to *luci* control. Mean was calculated from at least 2 independent biological replicates. PPP, Pentose phosphate pathway.

Supplementary Table 5. Demographic analysis.

Biological Replicate	Genotype/Treatment	Population	Median (days)	<i>p</i> value	Compared to
BR1	N2; <i>luci</i>	87/100	14		
	N2; <i>hxx-1i</i>	66/100	16	ns	N2; <i>luci</i>
	N2; <i>hxx-2i</i>	76/100	15	ns	N2; <i>luci</i>
	N2; <i>mml-1i</i>	72/100	14	ns	N2; <i>luci</i>
	<i>glp-1</i> ; <i>luci</i>	76/100	30	53% <0.0001	N2; <i>luci</i>
	<i>glp-1</i> ; <i>hxx-1i</i>	73/100	22	27% 0.041	<i>glp-1</i> ; <i>luci</i>
	<i>glp-1</i> ; <i>hxx-2i</i>	81/100	14	ns	<i>glp-1</i> ; <i>luci</i>
	<i>glp-1</i> ; <i>mml-1i</i>	63/100	19	37% 0.034	<i>glp-1</i> ; <i>luci</i>
BR2	N2; <i>luci</i>	73/120	16		
	N2; <i>hxx-1i</i>	76/120	14	ns	N2; <i>luci</i>
	N2; <i>hxx-2i</i>	93/120	17	ns	N2; <i>luci</i>
	N2; <i>mml-1i</i>	67/112	13	ns	N2; <i>luci</i>
	<i>glp-1</i> ; <i>luci</i>	101/120	33	52% <0.0001	N2; <i>luci</i>
	<i>glp-1</i> ; <i>hxx-1i</i>	84/120	19	42% 0.011	<i>glp-1</i> ; <i>luci</i>
	<i>glp-1</i> ; <i>hxx-2i</i>	79/120	17	48% <0.0001	<i>glp-1</i> ; <i>luci</i>

	<i>glp-1; mml-1i</i>	73/120	14	58%	<0.0001	<i>glp-1; luci</i>
BR1	N2; <i>luci</i>	68/120	16			
	N2; <i>hxx-1i</i>	71/120	15		ns	N2; <i>luci</i>
	N2; <i>hxx-2i</i>	77/120	13		ns	N2; <i>luci</i>
	N2; <i>mml-1i</i>	66/120	16		ns	N2; <i>luci</i>
	<i>isp-1; luci</i>	91/150	28	43%	<0.0001	N2; <i>luci</i>
	<i>isp-1; hxx-1i</i>	103/150	19	32%	<0.0001	<i>isp-1; luci</i>
	<i>isp-1; hxx-2i</i>	114/150	18	36%	<0.0001	<i>isp-1; luci</i>
	<i>isp-1; mml-1i</i>	88/150	16	43%	<0.0001	<i>isp-1; luci</i>
BR2	N2; <i>luci</i>	78/120	15			
	N2; <i>hxx-1i</i>	83/120	16		ns	N2; <i>luci</i>
	N2; <i>hxx-2i</i>	74/120	16		ns	N2; <i>luci</i>
	N2; <i>mml-1i</i>	57/120	13		ns	N2; <i>luci</i>
	<i>isp-1; luci</i>	78/150	31	52%	<0.0001	N2; <i>luci</i>
	<i>isp-1; hxx-1i</i>	88/150	17	45%	<0.0001	<i>isp-1; luci</i>
	<i>isp-1; hxx-2i</i>	93/123	14	55%	<0.0001	<i>isp-1; luci</i>
	<i>isp-1; mml-1i</i>	103/150	17	45%	<0.0001	<i>isp-1; luci</i>
BR1	N2; <i>luci</i>	83/120	19			
	N2; <i>hxx-1i</i>	93/120	17	11%	0.003	N2; <i>luci</i>
	N2; <i>hxx-2i</i>	85/120	19		ns	N2; <i>luci</i>
	N2; <i>mml-1i</i>	71/120	17	11%	0.0004	N2; <i>luci</i>
	N2; <i>daf-16i</i>	66/120	17	11%	<0.0001	N2; <i>luci</i>
	<i>daf-2; luci</i>	89/113	39	51%	<0.0001	N2; <i>luci</i>
	<i>daf-2; hxx-1i</i>	74/120	39		ns	<i>daf-2; luci</i>
	<i>daf-2; hxx-2i</i>	75/120	38		ns	<i>daf-2; luci</i>
	<i>daf-2; mml-1i</i>	65/120	20	49%	<0.0001	<i>daf-2; luci</i>
	<i>daf-2; daf-16i</i>	76/120	16	59%	<0.0001	<i>daf-2; luci</i>
BR2	N2; <i>luci</i>	95/120	16			
	N2; <i>hxx-1i</i>	85/120	17		ns	N2; <i>luci</i>
	N2; <i>hxx-2i</i>	100/120	14		ns	N2; <i>luci</i>
	N2; <i>mml-1i</i>	74/120	14		ns	N2; <i>luci</i>
	<i>daf-2; luci</i>	103/120	42	62%	<0.0001	N2; <i>luci</i>
	<i>daf-2; hxx-1i</i>	70/120	40		ns	<i>daf-2; luci</i>
	<i>daf-2; hxx-2i</i>	83/120	42		ns	<i>daf-2; luci</i>
	<i>daf-2; mml-1i</i>	88/120	13	69%	<0.0001	<i>daf-2; luci</i>

BR1	N2; <i>luci</i>	76/120	15			
	N2; <i>hxx-2i luci</i>	83/120	13	ns		N2; <i>luci</i>
	N2; <i>T25B9.9i luci</i>	94/120	15	ns		N2; <i>luci</i>
	N2; <i>T25B9.9i hxx-2i</i>	83/103	15	ns		N2; <i>luci</i>
	N2; <i>tkt-1i luci</i>	85/120	18	20%	0.007	N2; <i>luci</i>
	N2; <i>tkt-1i hxx-2i</i>	91/120	18	20%	0.009	N2; <i>luci</i>
	<i>glp-1; luci</i>	105/120	28	87%	<0.0001	N2; <i>luci</i>
	<i>glp-1; hxx-2i luci</i>	67/103	16	75%	<0.0001	<i>glp-1; luci</i>
	<i>glp-1; T25B9.9i luci</i>	75/120	29	ns		<i>glp-1; luci</i>
	<i>glp-1; T25B9.9i hxx-2i</i>	86/120	24	ns		<i>glp-1; luci</i>
	<i>glp-1; tkt-1i luci</i>	79/120	27	ns		<i>glp-1; luci</i>
	<i>glp-1; tkt-1i hxx-2i</i>	91/120	29	ns		<i>glp-1; luci</i>
BR2	N2; <i>luci</i>	104/120	14			
	N2; <i>hxx-2i luci</i>	88/120	16	ns		N2; <i>luci</i>
	N2; <i>T25B9.9i luci</i>	89/120	15	ns		N2; <i>luci</i>
	N2; <i>T25B9.9i hxx-2i</i>	71/120	14	ns		N2; <i>luci</i>
	N2; <i>tkt-1i luci</i>	94/120	17	21%	0.046	N2; <i>luci</i>
	N2; <i>tkt-1i hxx-2i</i>	96/120	18	29%	0.039	N2; <i>luci</i>
	<i>glp-1; luci</i>	100/120	27	48%	<0.0001	N2; <i>luci</i>
	<i>glp-1; hxx-2i luci</i>	66/120	15	44%	<0.0001	<i>glp-1; luci</i>
	<i>glp-1; T25B9.9i luci</i>	88/120	26	ns		<i>glp-1; luci</i>
	<i>glp-1; T25B9.9i hxx-2i</i>	75/120	26	ns		<i>glp-1; luci</i>
	<i>glp-1; tkt-1i luci</i>	80/120	29	ns		<i>glp-1; luci</i>
	<i>glp-1; tkt-1i hxx-2i</i>	95/120	30	ns		<i>glp-1; luci</i>

p-values were calculated using Log-rank (Mantel-Cox) test. Worms with internal hatching, dried from escaping the plates, or had vulva protrusions were censored from the analysis.

Supplementary Table 6. Top 50 enriched candidates of MML-1::3xFLAG IP in wildtype and *glp-1(e2141)*

Protein	log FC <i>mml-1::3xFLAG</i> / N2	Protein	logFC <i>glp-1; mml-1::3xFLAG</i> / N2
MML-1	7.09	VIT-1	8.13
VIT-4	3.86	VIT-4	7.38
VIT-1	3.62	CLEC-1	7.21
CLEC-1	3.48	VIT-3	6.35
CTC-2	3.42	MML-1	6.12
MPC-1	3.31	DHS-26	6.00
FAR-2	3.22	ACOX-1.2	5.54
VIT-3	3.17	T22B7.7	5.47
MXL-2	3.08	T21F4.1	4.91
PLIN-1; MDT-28	3.00	ULE-1	4.71
ACOX-1.2	2.97	DHS-20	4.64
F32A11.1, W09H1.3	2.83	F55H12.4	4.61
F23B12.7	2.77	UGT-22	4.60
K10C3.5	2.75	FAR-2	4.52
CEY-2	2.71	VIT-5	4.48
PQN-22	2.62	DHS-3	4.43
ACS-13	2.57	CTC-2	4.41
C43H6.4	2.54	F38B6.4	4.17
T21F4.1	2.50	PYR-1	4.16
C56G2.1/C56G2.2	2.49	C30G12.2	4.13
LET-767	2.48	OSM-11	3.97
UGT-22	2.42	LBP-3	3.87
F44E5.1	2.36	TAG-147	3.85
BYN-1	2.35	PPAT-1	3.80
UGT-62	2.34	T01B11.2	3.79
TAG-174	2.25	DOD-23	3.74
RME-2	2.20	ZK177.8	3.72
UGT-46	2.20	VIT-2	3.72
F56G4.6	2.18	PMP-1	3.71
KDP-1	2.12	PGP-6;PGP-7	3.71
RPL-38	2.09	LEC-6	3.56

LIN-35	2.06	LYS-7	3.55
CEY-3	2.06	VIT-6	3.49
ZK430.7	2.04	CDR-6	3.35
MLC-5	2.02	C39D10.7	3.30
IFET-1	1.98	Y105C5B.5	3.23
ACDH-1	1.97	Y82E9BR.14	3.21
DPY-18	1.96	TTR-45	3.19
PYR-1	1.96	C42D4.1	3.17
PQN-59	1.95	ZK632.9	3.12
XPO-1	1.95	LET-767	3.11
SMG-2	1.88	MPC-1	3.05
HPO-34	1.87	Y69H2.3	3.05
FNTA-1	1.87	GST-10	3.01
ELO-1	1.86	CKC-1	2.81
F22D6.2	1.86	Y80D3A.9	2.81
AOS-1	1.83	D1086.3	2.80
HCP-1	1.83	C28G1.6	2.79
RMD-1	1.81	SLC-25A10	2.78
TALD-1	1.81	ZK813.3	2.77

These experiments include the enrichment of candidates from 3 independent biological replicates.

Supplementary Table 7. Statistical analysis of RNAi screen for MML-1 nuclear localization.

Dunnett's multiple comparisons test	Mean Diff	Summary	Adjusted <i>p</i> -value	Mammalian homologs
<i>luci</i> vs. <i>acs-13i</i>	-1.015	****	<0.0001	ACSL5
<i>luci</i> vs. <i>ugt-46i</i>	-0.7745	****	<0.0001	UGT2B28
<i>luci</i> vs. <i>pyr-1i</i>	-0.7617	****	<0.0001	CAD
<i>luci</i> vs. <i>ZK430.7i</i>	-0.641	****	<0.0001	DCAF13
<i>luci</i> vs. <i>akap-1i</i>	-0.6281	****	<0.0001	AKAP-1
<i>luci</i> vs. <i>plin-1i</i>	-0.5977	****	<0.0001	N/S
<i>luci</i> vs. <i>ifet-1i</i>	-0.5951	****	<0.0001	EIF4ENIF1
<i>luci</i> vs. <i>byn-1i</i>	-0.5923	****	<0.0001	BYSL
<i>luci</i> vs. <i>rpl-38i</i>	-0.3442	****	<0.0001	RPL38
<i>luci</i> vs. <i>pqn-59i</i>	-0.08797	ns	0.9982	UBAP2
<i>luci</i> vs. <i>lin-35i</i>	0.002717	ns	>0.9999	RBL1
<i>luci</i> vs. <i>C43H6.4i</i>	0.005264	ns	>0.9999	N/S

<i>luci</i> vs. <i>hcp-1i</i>	0.01037	ns	0.9999	N/S
<i>luci</i> vs. <i>acox-1.2i</i>	0.05275	ns	0.9992	ACOX1
<i>luci</i> vs. <i>smg-2i</i>	0.05317	ns	0.9994	UPF1
<i>luci</i> vs. <i>K10C3.5i</i>	0.07915	ns	0.9988	EFL1
<i>luci</i> vs. <i>vit-3i</i>	0.111	ns	0.9846	N/S
<i>luci</i> vs. <i>F32A11.1i</i>	0.1184	ns	0.9392	C3orf33
<i>luci</i> vs. <i>tald-1i</i>	0.1202	ns	0.8884	TALDO1
<i>luci</i> vs. <i>T21F4.1i</i>	0.1351	ns	0.8813	ARG1, ARG2
<i>luci</i> vs. <i>vit-1i</i>	0.1664	ns	0.6904	N/S
<i>luci</i> vs. <i>aos-1i</i>	0.1983	ns	0.2093	Sae1
<i>luci</i> vs. <i>ugt-62i</i>	0.2242	ns	0.2325	UGT1A6
<i>luci</i> vs. <i>fnta-1i</i>	0.2283	ns	0.1619	FNTA
<i>luci</i> vs. <i>F56G4.6i</i>	0.2291	ns	0.1146	N/S
<i>luci</i> vs. <i>W09H1.3i</i>	0.2355	ns	0.0759	C3orf33
<i>luci</i> vs. <i>F44E5.1i</i>	0.2423	ns	0.0626	N/S
<i>luci</i> vs. <i>clcc-1i</i>	0.2475	ns	0.0813	N/S
<i>luci</i> vs. <i>F22D6.2i</i>	0.2548	*	0.0202	ZFAND5
<i>luci</i> vs. <i>let-767i</i>	0.2561	**	0.0031	HSD17B12
<i>luci</i> vs. <i>far-2i</i>	0.2597	ns	0.0504	N/S
<i>luci</i> vs. <i>ugt-22i</i>	0.2674	*	0.0208	UGT1A5
<i>luci</i> vs. <i>rmd-1i</i>	0.2869	*	0.0136	RMDN3
<i>luci</i> vs. <i>cey-2i</i>	0.2961	*	0.0183	YBX1
<i>luci</i> vs. <i>cey-3i</i>	0.3012	*	0.0443	YBX1
<i>luci</i> vs. <i>acd-1i</i>	0.3095	**	0.0053	ACADSB
<i>luci</i> vs. <i>hpo-34i</i>	0.3239	***	0.0001	N/S
<i>luci</i> vs. <i>elo-1i</i>	0.3288	**	0.0034	ELOVL3
<i>luci</i> vs. <i>mxl-2i</i>	0.3372	**	0.0074	Mlx
<i>luci</i> vs. <i>F23B12.7i</i>	0.352	**	0.0011	CEBPZ
<i>luci</i> vs. <i>mpc-1i</i>	0.4603	****	<0.0001	MPC1

MML-1::GFP nuclear localization from *luci* control was compared to the indicated RNAi. Mean was calculated from the mean difference of three independent biological replicates. Mean difference was calculated as Mean (*luci*) – Mean (RNAi). Data from (Vonolfen, 2020).

Supplementary Table 8. Top 50 enriched candidates of MML-1::3xFLAG IP *daf-2(e1370)*.

Protein	logFC <i>daf-2; mml-1::3xFLAG</i> / <i>daf-2</i>
ACER-1	4.58
MML-1	3.973
CTL-1	2.54
ACLY-1	2.331
DIG-1	2.286
ATP-1	2.077
F02A9.10	2.015
CDC-5L	2.01
GST-1	1.829
MSRA-1	1.592
SACY-1	1.522
F49E2.5	1.491
C18B2.5	1.398
PYK-1	1.393
T09F3.2	1.379
ABCE-1	1.359
HIM-4	1.358
ZC434.8	1.355
GSPD-1	1.294
F27D4.1	1.288
M05D6.2	1.278
HPHD-1	1.274
NPP-7	1.266
PRDX-3	1.254
MUP-4	1.253
SCB-1	1.242
IFO-1	1.227
WAH-1	1.218
F46H5.7	1.21
PDE-6	1.201
COX-5B	1.178
F39B2.3	1.159
NMY-2	1.145

PQN-87	1.089
ATP-3	1.079
T27F2.1	1.074
MCCC-1	1.07
ALH-13	1.066
C39D10.8	1.04
C39D10.7	1.032
RARS-1	1.027
PGL-1	1.002
DHS-28	0.987
CDC-48.2	0.978
GLN-1	0.962
RSP-3	0.945
VHA-12	0.936
UNC-115	0.934
VAB-10	0.932
MXL-1	0.916

These experiments include the enrichment of candidates from 3 independent biological replicates.

Supplementary Table 9. Metabolomics from *daf-2(e1370) mml-1(ok849)* and *daf-2(e1370) mxl-2(tm1516)* mutants compared to *daf-2(e1370)*.

Metabolites	FC(<i>daf-2</i> <i>mml-1/daf-2</i>)	FC(<i>daf-2</i> <i>mxl-2/daf-2</i>)	p(<i>daf-2</i> <i>mml-1/daf-2</i>)	p(<i>daf-2</i> <i>mxl-2/daf-2</i>)	fdr(<i>daf-2</i> <i>mml-1/daf-2</i>)	fdr(<i>daf-2</i> <i>mxl-2/daf-2</i>)
1-Deoxy-D-xylulose 5-phosphate	0.432	0.350	0.136	0.010	0.309	0.058
5 Methyltetrahydrofolic acid	0.056	0.087	0.001	0.070	0.019	0.197
Acetyl Carnitine	0.487	1.002	0.028	0.989	0.117	0.989
Acetyl Ornithine	0.313	0.443	0.004	0.079	0.045	0.219
Adenine	0.923	0.967	0.584	0.912	0.756	0.966
Adenosine	0.400	0.142	0.015	0.000	0.079	0.005
Adenosine 5'-monophosphate	0.494	0.641	0.000	0.008	0.008	0.055
Adenyl succinic acid	0.631	0.414	0.361	0.204	0.574	0.385
ADP	0.225	0.357	0.005	0.038	0.047	0.141
Aminoadipic acid	0.307	0.442	0.004	0.094	0.046	0.244
Arginine	0.535	0.611	0.011	0.089	0.063	0.241
Betaine	0.248	0.361	0.000	0.024	0.005	0.106
Biotin	0.329	0.380	0.007	0.068	0.054	0.193

cAMP	0.129	0.087	0.004	0.002	0.047	0.032
Carnitine	0.336	0.439	0.009	0.136	0.055	0.309
Carnosine	0.553	0.426	0.402	0.120	0.621	0.285
cCMP	0.072	0.079	0.174	0.113	0.367	0.275
cGMP	0.300	0.247	0.118	0.006	0.281	0.052
Choline	0.388	0.482	0.005	0.085	0.048	0.234
Citric acid	4.930	11.483	0.001	0.000	0.019	0.005
Citrulline	1.247	1.396	0.624	0.478	0.783	0.696
CMP	0.698	0.637	0.228	0.034	0.412	0.135
Coenzyme A	0.778	0.768	0.430	0.225	0.645	0.412
Cystathionine	1.031	0.954	0.935	0.917	0.966	0.966
Cythidine diphosphocholine	0.482	0.606	0.008	0.136	0.054	0.309
Cytidine	0.445	0.482	0.043	0.127	0.152	0.296
Cytosine	0.371	0.435	0.002	0.056	0.036	0.174
Decenoylcarnitine	0.361	0.455	0.010	0.058	0.061	0.176
D-Erythrose 4-phosphate	0.279	0.447	0.003	0.070	0.045	0.197
Dihydroxyacetone phosphate	2.225	3.386	0.007	0.001	0.054	0.019
Dopaquinone	0.842	0.907	0.571	0.744	0.752	0.876
Erythronic acid	1.060	1.928	0.871	0.183	0.941	0.378
FAD	0.376	0.756	0.055	0.635	0.173	0.790
FMN	0.188	0.244	0.000	0.005	0.011	0.047
Gamma-glutamyl-L-putrescine	0.455	0.459	0.004	0.009	0.047	0.057
Glucosamine phosphate	0.485	0.482	0.186	0.055	0.378	0.173
Glucose biphosphate	0.408	0.394	0.016	0.030	0.081	0.122
Glutaric acid	1.283	1.425	0.062	0.025	0.185	0.111
GSH ox	0.346	0.453	0.063	0.226	0.185	0.412
GSH red	0.328	0.438	0.006	0.100	0.052	0.252
Guanine	0.868	0.673	0.779	0.485	0.893	0.700
Guanosine	0.901	0.668	0.489	0.200	0.700	0.385
Guanosine monophosphate	0.505	0.547	0.010	0.035	0.060	0.136
Hexanoyl carnitine	1.020	0.973	0.879	0.809	0.947	0.915
Hexose	0.343	0.371	0.002	0.008	0.031	0.055
Hexose phosphate	3.059	2.981	0.007	0.006	0.054	0.052
Hydroxypyruvic acid	0.338	0.348	0.009	0.074	0.055	0.206
Hypoxanthine	0.279	0.269	0.028	0.094	0.117	0.244
IMP	0.890	1.685	0.805	0.345	0.915	0.554
Inosine	0.518	0.532	0.095	0.093	0.246	0.244
Inosinic acid	0.902	0.574	0.853	0.270	0.933	0.466
Isoleucine	0.235	0.317	0.000	0.043	0.013	0.152

Leucine	0.229	0.303	0.000	0.016	0.010	0.081
Lysine	0.488	0.603	0.008	0.151	0.054	0.334
N-Acetyl-D-glucosamine	1.007	1.227	0.978	0.468	0.980	0.689
NAD+	0.362	0.447	0.021	0.229	0.097	0.412
Nicotinamide	0.352	0.443	0.009	0.061	0.057	0.184
Nicotinic acid	0.272	0.338	0.007	0.087	0.054	0.235
Nicotinic acid mononucleotide	0.348	0.446	0.006	0.049	0.052	0.161
Ornithine	0.389	0.445	0.004	0.018	0.045	0.088
Oxoglutaric acid	0.702	0.724	0.348	0.299	0.555	0.503
Pantetheine 4'-phosphate	0.507	0.447	0.043	0.058	0.152	0.176
Pantethine	0.595	0.512	0.244	0.244	0.427	0.427
Pantothenic acid	0.443	0.412	0.202	0.048	0.385	0.161
Phenylalanine	0.320	0.338	0.006	0.067	0.052	0.193
Phosphoenolpyruvic acid	0.232	0.225	0.005	0.001	0.048	0.019
Phosphothreonine	0.333	0.447	0.021	0.178	0.097	0.373
Proline	1.149	0.859	0.701	0.739	0.843	0.875
Propionylcarnitine	0.209	0.194	0.036	0.019	0.136	0.090
Pyridoxine 5'-phosphate	0.476	0.607	0.015	0.136	0.081	0.309
Thiamine	0.457	0.475	0.028	0.180	0.117	0.375
Thymidine	1.292	1.960	0.435	0.046	0.648	0.157
Trehalose_phosphate	0.972	0.845	0.935	0.655	0.966	0.805
Tryptophan	0.474	0.455	0.147	0.012	0.327	0.068
UDP	0.082	0.086	0.044	0.001	0.155	0.019
UMP	0.542	0.511	0.141	0.013	0.316	0.074
Uric acid	0.614	0.484	0.397	0.162	0.615	0.348
Uridine	0.520	0.447	0.189	0.022	0.380	0.100
Uridine diphosphate-N-acetylglucosamine	0.520	0.328	0.415	0.124	0.632	0.290
Xanthosine	0.767	0.660	0.245	0.009	0.427	0.057

These are the pulled data from 4 independent biological replicates.

Supplementary Table 10. Metabolomics from *glp-1(e2141)* *mml-1(ok849)* and *glp-1(e2141)* *mxl-2(tm1516)* mutants compared to *glp-1(e2141)*.

Metabolites	FC(<i>glp-1</i> <i>mml-1/glp-1</i>)	FC(<i>glp-1</i> <i>mxl-2/glp-1</i>)	p(<i>glp-1</i> <i>mml-1/glp-1</i>)	p(<i>glp-1</i> <i>mxl-2/glp-1</i>)	fdr(<i>glp-1</i> <i>mml-1/glp-1</i>)	fdr(<i>glp-1</i> <i>mxl-2/glp-1</i>)
Oxoglutaric acid	0.402	1.047	0.000	0.789	0.004	0.906
Acetyl Carnitine	0.235	1.023	0.008	0.963	0.073	0.996
N-Acetyl-D-glucosamine	2.001	1.677	0.249	0.306	0.518	0.568
Acetyl Ornithine	2.470	2.498	0.281	0.339	0.552	0.583

N acetyl spermidine	7.300	7.143	0.242	0.245	0.517	0.517
Adenine	0.764	1.176	0.634	0.752	0.818	0.885
Adenosine	0.079	0.046	0.050	0.080	0.238	0.324
Adenyl succininc acid	1.930	1.567	0.212	0.101	0.498	0.354
ADP	1.393	0.384	0.657	0.190	0.839	0.487
Aminoadipic acid	11.776	1.785	0.004	0.177	0.057	0.471
Adenosine 5'-monophosphate	0.327	1.613	0.001	0.310	0.035	0.571
Arginine	1.896	1.140	0.628	0.909	0.818	0.976
ATP	8.701	1.158	0.000	0.107	0.004	0.354
Biotin	0.278	0.389	0.101	0.277	0.354	0.550
Carnitine	1.577	2.322	0.473	0.172	0.679	0.467
Carnosine	15.936	17.867	0.339	0.336	0.583	0.583
CDP-Ethanolamine	4.070	1.129	0.129	0.800	0.396	0.916
cGMP	0.034	0.679	0.000	0.462	0.004	0.668
Choline	1.782	3.420	0.257	0.040	0.522	0.215
Citric acid	0.252	0.507	0.013	0.199	0.115	0.496
Coenzyme A	0.694	0.766	0.489	0.619	0.691	0.808
Cytidine monophosphate hydrate	3.226	5.118	0.072	0.036	0.306	0.205
Cytidine	2.633	5.544	0.527	0.404	0.728	0.632
Cytosine	0.604	0.851	0.316	0.715	0.572	0.857
Decenoylcarnitine	0.812	1.220	0.519	0.701	0.722	0.853
Deoxyadenosine	0.276	1.611	0.379	0.295	0.621	0.561
1-Deoxy-D-xylulose 5-phosphate	0.631	0.822	0.682	0.805	0.848	0.916
Deoxyguanosine	0.348	0.415	0.153	0.273	0.441	0.545
D-Erythrose 4-phosphate	0.343	2.124	0.006	0.331	0.065	0.582
Dihydroxyacetone phosphate	0.401	0.215	0.168	0.211	0.463	0.498
Dopaquinone	0.815	1.139	0.690	0.784	0.852	0.904
Erythronic acid	0.929	0.922	0.131	0.006	0.397	0.065
FAD	1.879	2.276	0.439	0.344	0.654	0.590
FMN	0.214	0.442	0.035	0.428	0.204	0.646
Fumarate/Malate	0.214	0.328	0.254	0.474	0.520	0.679
Glucosamine phosphate	1.783	2.417	0.413	0.235	0.635	0.510
Glucose biphosphate	1.072	0.436	0.949	0.552	0.992	0.748
Glutamic acid	0.968	1.187	0.954	0.708	0.993	0.853
Glutamine	2.513	1.687	0.006	0.021	0.062	0.141
Glutaric acid	0.625	0.557	0.447	0.332	0.659	0.582
Glyceric acid biphosphate	3.931	1.751	0.001	0.249	0.033	0.518
Guanosine monophosphate	2.689	3.298	0.077	0.079	0.322	0.324
GSH ox	1.246	0.296	0.738	0.177	0.877	0.471

GSH red	0.938	1.219	0.862	0.605	0.948	0.796
Guanine	0.901	1.413	0.859	0.505	0.948	0.706
Guanosine	0.411	1.008	0.389	0.992	0.621	0.998
Hexose	0.070	0.405	0.000	0.244	0.000	0.517
Hexose phosphate	0.364	5.010	0.001	0.027	0.034	0.171
Hydroxy deoxy guanosine	0.623	0.743	0.456	0.606	0.666	0.796
Hydroxypyruvic acid	2.001	3.206	0.176	0.033	0.471	0.201
IMP	0.351	0.363	0.114	0.207	0.363	0.498
Inosine	0.993	2.153	0.985	0.106	0.998	0.354
Inosinic acid	2.680	7.426	0.193	0.046	0.488	0.230
Leucine	2.086	2.129	0.217	0.200	0.499	0.496
Methionine	0.203	0.207	0.083	0.034	0.332	0.201
Methionine sulfoxide	2.116	3.734	0.088	0.017	0.340	0.134
Methylguanosine	0.166	0.359	0.051	0.084	0.242	0.333
5 Methyltetrahydrofolic acid	3.137	2.102	0.210	0.319	0.498	0.576
N Acetyl putresceine	0.776	1.425	0.449	0.216	0.659	0.499
N Acetyl-D-glucosamine	1.375	1.283	0.180	0.460	0.473	0.667
Nicotinamide	2.608	3.575	0.288	0.220	0.552	0.499
Pantethine	2.749	2.704	0.188	0.194	0.487	0.488
Pantetheine 4'-phosphate	1.170	1.737	0.819	0.421	0.925	0.642
Pantothenic acid	2.015	2.824	0.374	0.208	0.619	0.498
Phenylalanine	2.431	6.178	0.234	0.062	0.510	0.276
Phosphoenolpyruvic acid	0.337	0.595	0.245	0.448	0.517	0.659
Proline	0.183	0.252	0.037	0.104	0.205	0.354
Purine	0.816	0.989	0.630	0.977	0.818	0.998
Pyridoxine 5'-phosphate	0.670	1.171	0.543	0.668	0.739	0.842
Ribose/xylulose phosphate	0.481	0.535	0.226	0.301	0.504	0.565
S-Adenosylmethionine	0.752	0.317	0.490	0.147	0.691	0.425
Spermidine	2.115	2.477	0.107	0.041	0.354	0.215
Spermine	1.597	2.538	0.347	0.049	0.591	0.237
Thiamine	1.409	0.729	0.284	0.526	0.552	0.728
Threonine	1.405	1.449	0.595	0.557	0.792	0.750
Thiamine	1.844	2.850	0.001	0.000	0.030	0.007
Thymidine	1.109	1.003	0.783	0.993	0.904	0.998
Trehalose phosphate	0.612	0.338	0.391	0.218	0.621	0.499
Tryptophan	0.078	0.036	0.028	0.165	0.177	0.461
Tyrosine	2.693	4.161	0.080	0.019	0.324	0.138
UDP	1.309	2.263	0.682	0.307	0.848	0.569
Uracil	0.867	1.768	0.826	0.220	0.928	0.499
Uric acid	1.794	2.092	0.360	0.259	0.606	0.525

Valine	1.046	1.932	0.942	0.228	0.992	0.505
Xanthine	0.111	0.179	0.003	0.001	0.046	0.018
Xanthosine	0.470	6.637	0.556	0.105	0.750	0.354
Xanthosine Phosphate	0.894	4.597	0.906	0.163	0.975	0.457

These are the pulled data from 4 independent biological replicates.

X. Acknowledgments

Special thanks:

To my supervisor Dr. Adam Antebi.

To my mentor Dr. Özlem Karalay.

To the technicians of the A-Team (present and past) Katrin Wollenweber, Rosa Warner, Anna Lührke, Christian Latza, Nadine Hochhard, Nadine Henn, Anna Weber, and Maria Henn.

To the administrative members of the A-Team, Dr. Birgit Gerisch, Dr. Orsolya Symmons, and Dr. Christoph Geisen.

To the best friends I met through science, Dr. Jennifer Mak, Dr. Alex Zaufel, Dr. Victoria Eugenia Martínez Miguel, (soon to be Dr.) Eugen Ballhysa, (soon to be Dr.) Tonantzi Sandoval Silva, Dr. Rebecca Tharyan, Dr. Chiara Calabrese, Dr. Till Popkes-van Oepen, Dr. Miriam Popkes (and baby Finn Jonah), (soon to be Dr.) Tim Nonninger, and Dr. Pablo Rivera Mejías.

To all the members of the A-Team (present and past), especially Dr. Roberto Ripa and Dr. Andrea Annibal.

To the Cologne Graduate School of Ageing Research coordinators, especially Dr. Daniela Morick and Jenni Ostermann.

To the Bioinformatics Core Facility, especially Dr. Jorge Boucas and Dr. Franziska Metge.

To the FACS & Imaging Core Facility, especially Dr. Christian Kukat and Marcel Kirchner.

To the Proteomics Core Facility, especially Dr. Ilian Atanassov and Dr. Xinping Li.

To the Metabolomics Core Facility, especially Dr. Patrick Giavalisco.

To the Thesis Committee Members, Dr. Thomas Langer, Dr. Thorsten Hoppe, Dr. Nirmal Robinson, and Dr. Jan Riemer and Dr. Filipe Cabreiro for evaluating my thesis.

Special thanks to two master's students I had the privilege to supervise, Maximilian Vonolfen and Marjana Ndoci.

XI. Work contributions

This work had the support of multiple people and core facilities at different stages of the project, including conceptualization, training and assistance, analysis, and conducting experiments. The conceptualization of the experiments and initial training was supported by Dr. Adam Antebi and Dr. Özlem Karalay. The sequencing of the bacterial clones was performed with Maria Braun and Nadine Hochhard. Katrin Wollenweber, Maximilian Vonolfen, and Marjana Ndoci gave technical assistance in multiple experiments presented here. The RNAseq was conducted by the Max Planck Genome-Center Cologne, part of the Max Planck Institute for Plant Breeding Research, and analyzed by the Bioinformatics Core Facility of the Max Planck Institute for Biology of Ageing (MPI AGE). Confocal imaging training was provided by the FACS & Imaging Core Facility of the MPI AGE. The processing of the samples for immunoprecipitation was assisted by Maximilian Vonolfen and analyzed by the Proteomics Core Facility of the MPI AGE. The metabolomic analysis was performed in collaboration with Dr. Andrea Annibal and Christian Latza.

XII. References

- Ahier, A., Dai, C. Y., Tweedie, A., Bezawork-Geleta, A., Kirmes, I., & Zuryn, S. (2018). Affinity purification of cell-specific mitochondria from whole animals resolves patterns of genetic mosaicism. *Nature Cell Biology*, 20(3), 352–360. <https://doi.org/10.1038/s41556-017-0023-x>
- Akbar, S. M. D., Sreeramulu, K., & Sharma, H. C. (2016). Tryptophan fluorescence quenching as a binding assay to monitor protein conformation changes in the membrane of intact mitochondria. *Journal of Bioenergetics and Biomembranes*, 48(3), 241–247. <https://doi.org/10.1007/s10863-016-9653-0>
- Albert, P. S., & Riddle, D. L. (1988). Mutants of *Caenorhabditis elegans* that form dauer-like larvae. *Developmental Biology*, 126(2), 270–293. [https://doi.org/10.1016/0012-1606\(88\)90138-8](https://doi.org/10.1016/0012-1606(88)90138-8)
- Allawi, H. T., & Santalucia, J. (1997). Thermodynamics and NMR of internal G·T mismatches in DNA. *Biochemistry*, 36(34), 10581–10594. <https://doi.org/10.1021/bi962590c>
- Alpatov, W. W. (1930). Experimental studies on the duration of life. XIII. The influence of different feeding during the larval and imaginal stages on the duration of life of the imago of *Drosophila melanogaster*. *The American Naturalist*, 64(690), 37–55. <https://doi.org/https://doi.org/10.1086/280297>
- Anisimov, V. N., Berstein, L. M., Egormin, P. A., Piskunova, T. S., Popovich, I. G., Zabezhinski, M. A., Tyndyk, M. L., Yurova, M. V., Kovalenko, I. G., Poroshina, T. E., & Semchenko, A. V. (2008). Metformin slows down aging and extends life span of female SHR mice. *Cell Cycle*, 7(17), 2769–2773. <https://doi.org/10.4161/cc.7.17.6625>
- Annibal, A., Tharyan, R. G., Schonewolff, M. F., Tam, H., Latza, C., Auler, M. M. K., & Antebi, A. (2021). Regulation of the one carbon folate cycle as a shared metabolic signature of longevity. *Nature Communications*, 12(1), 1–14. <https://doi.org/10.1038/s41467-021-23856-9>
- Apfeld, J., & Kenyon, C. (1998). Cell nonautonomy of *C. elegans* daf-2 function in the regulation of diapause and life span. *Cell*, 95(2), 199–210. [https://doi.org/10.1016/S0092-8674\(00\)81751-1](https://doi.org/10.1016/S0092-8674(00)81751-1)
- Apfeld, J., O'Connor, G., McDonagh, T., DiStefano, P. S., & Curtis, R. (2004). The AMP-activated protein kinase AAK-2 links energy levels and insulin-like signals to lifespan in *C.*

- C. elegans*. *Genes and Development*, 18(24), 3004–3009. <https://doi.org/10.1101/gad.1255404>
- Arantes-Oliveira, N., Apfeld, J., Dillin, A., & Kenyon, C. (2002). Regulation of life-span by germ-line stem cells in *Caenorhabditis elegans*. *Science*, 295(5554), 502–505. <https://doi.org/10.1126/science.1065768>
- Arden, C., Tudhope, S. J., Petrie, J. L., Al-Oanzi, Z. H., Cullen, K. S., Lange, A. J., Towle, H. C., & Agius, L. (2012). Fructose 2, 6-bisphosphate is essential for glucose-regulated gene transcription of glucose-6-phosphatase and other ChREBP target genes in hepatocytes. *Biochemical Journal*, 443(1), 111–123. <https://doi.org/10.1042/BJ20111280>
- Atherton, H. J., Gulston, M. K., Bailey, N. J., Cheng, K. K., Zhang, W., Clarke, K., & Griffin, J. L. (2009). Metabolomics of the interaction between PPAR- α and age in the PPAR- α -null mouse. *Molecular Systems Biology*, 5(259), 1–10. <https://doi.org/10.1038/msb.2009.18>
- Avery, L. (1993). The genetics of feeding in *Caenorhabditis elegans*. *Genetics*, 133(4), 897–917. <https://doi.org/10.1093/genetics/133.4.897>
- Ayer, D. E., Kretzner, L., & Eisenman, R. N. (1993). Mad: A heterodimeric partner for Max that antagonizes Myc transcriptional activity. *Cell*, 72(2), 211–222. [https://doi.org/10.1016/0092-8674\(93\)90661-9](https://doi.org/10.1016/0092-8674(93)90661-9)
- B. Friedman, D., & E. Johnson, T. (1988). A Mutation in the age-1 Gene in *Caenorhabditis elegans* Lengthens Life and Reduces Hermaphrodite Fertility. *Genetics*, 118(1), 75–86. <https://www.genetics.org/content/genetics/118/1/75.full.pdf>
- Barak, Y., Nelson, M. C., Ong, E. S., Jones, Y. Z., Ruiz-Lozano, P., Chien, K. R., Koder, A., & Evans, R. M. (1999). PPAR γ is required for placental, cardiac, and adipose tissue development. *Molecular Cell*, 4(4), 585–595. [https://doi.org/10.1016/S1097-2765\(00\)80209-9](https://doi.org/10.1016/S1097-2765(00)80209-9)
- Baur, J. A., Pearson, K. J., Price, N. L., Jamieson, H. A., Lerin, C., Kalra, A., Prabhu, V. V., Allard, J. S., Lopez-Lluch, G., Lewis, K., Pistell, P. J., Poosala, S., Becker, K. G., Boss, O., Gwinn, D., Wang, M., Ramaswamy, S., Fishbein, K. W., Spencer, R. G., ... Sinclair, D. A. (2006). Resveratrol improves health and survival of mice on a high-calorie diet. *Nature*, 444(2), 337–342.
- Beck, N. (2017). *Transcriptional Networks Regulating Nucleolar Function*. University of Cologne.
- Belenky, P., Racette, F. G., Bogan, K. L., McClure, J. M., Smith, J. S., & Brenner, C. (2007).

- Nicotinamide Riboside Promotes Sir2 Silencing and Extends Lifespan via Nrk and Urh1/Pnp1/Meu1 Pathways to NAD⁺. *Cell*, 129(3), 473–484.
<https://doi.org/10.1016/j.cell.2007.03.024>
- Benador, I. Y., Veliova, M., Mahdavian, K., Petcherski, A., Wikstrom, J. D., Assali, E. A., Acín-Pérez, R., Shum, M., Oliveira, M. F., Cinti, S., Sztalryd, C., Barshop, W. D., Wohlschlegel, J. A., Corkey, B. E., Liesa, M., & Shirihai, O. S. (2018). Mitochondria Bound to Lipid Droplets Have Unique Bioenergetics, Composition, and Dynamics that Support Lipid Droplet Expansion. *Cell Metabolism*, 27(4), 869-885.e6.
<https://doi.org/10.1016/j.cmet.2018.03.003>
- Benhamed, F., Denechaud, P. D., Lemoine, M., Robichon, C., Moldes, M., Bertrand-Michel, J., Ratzl, V., Serfaty, L., Housset, C., Capeau, J., Girard, J., Guillou, H., & Postic, C. (2012). The lipogenic transcription factor ChREBP dissociates hepatic steatosis from insulin resistance in mice and humans. *Journal of Clinical Investigation*, 122(6), 2176–2194.
<https://doi.org/10.1172/JCI41636>
- Bennett, C. F., Kwon, J. J., Chen, C., Russell, J., Acosta, K., Burnaevskiy, N., Crane, M. M., Bitto, A., Vander Wende, H., Simko, M., Pineda, V., Rossner, R., Wasko, B. M., Choi, H., Chen, S., Park, S., Jafari, G., Sands, B., Perez Olsen, C., ... Kaeberlein, M. (2017). Transaldolase inhibition impairs mitochondrial respiration and induces a starvation-like longevity response in *Caenorhabditis elegans*. In *PLoS Genetics* (Vol. 13, Issue 3).
<https://doi.org/10.1371/journal.pgen.1006695>
- Bennett, C. F., Vander Wende, H., Simko, M., Klum, S., Barfield, S., Choi, H., Pineda, V. V., & Kaeberlein, M. (2014). Activation of the mitochondrial unfolded protein response does not predict longevity in *Caenorhabditis elegans*. *Nature Communications*, 5, 1–10.
<https://doi.org/10.1038/ncomms4483>
- Berdichevsky, A., Viswanathan, M., Horvitz, H. R., & Guarente, L. (2006). C. elegans SIR-2.1 Interacts with 14-3-3 Proteins to Activate DAF-16 and Extend Life Span. *Cell*, 125(6), 1165–1177. <https://doi.org/10.1016/j.cell.2006.04.036>
- Berendzen, K. M., Durieux, J., Shao, L. W., Tian, Y., Kim, H. eui, Wolff, S., Liu, Y., & Dillin, A. (2016). Neuroendocrine Coordination of Mitochondrial Stress Signaling and Proteostasis. *Cell*, 166(6), 1553-1563.e10. <https://doi.org/10.1016/j.cell.2016.08.042>
- Berlenga, J. J., Santoyo, J., & De Haro, C. (1999). Characterization of a mammalian homolog of

- the GCN2 eukaryotic initiation factor 2 α kinase. *European Journal of Biochemistry*, 265(2), 754–762. <https://doi.org/10.1046/j.1432-1327.1999.00780.x>
- Berman, J. R., & Kenyon, C. (2006). Germ-cell loss extends *C. elegans* life span through regulation of DAF-16 by kri-1 and lipophilic-hormone signaling. *Cell*, 124(5), 1055–1068. <https://doi.org/10.1016/j.cell.2006.01.039>
- Billin, A. N., & Ayer, D. E. (2006). The Mlx network: Evidence for a parallel max-like transcriptional network that regulates energy metabolism. *Current Topics in Microbiology and Immunology*, 302, 255–278. https://doi.org/10.1007/3-540-32952-8_10
- Billin, A. N., Eilers, A. L., Coulter, K. L., Logan, J. S., & Ayer, D. E. (2000). MondoA, a Novel Basic Helix-Loop-Helix–Leucine Zipper Transcriptional Activator That Constitutes a Positive Branch of a Max-Like Network. *Molecular and Cellular Biology*, 20(23), 8845–8854. <https://doi.org/10.1128/mcb.20.23.8845-8854.2000>
- Billin, A. N., Eilers, A. L., Queva, C., & Ayer, D. E. (1999). Mlx, a novel Max-like BHLHZip protein that interacts with the max network of transcription factors. *Journal of Biological Chemistry*, 274(51), 36344–36350. <https://doi.org/10.1074/jbc.274.51.36344>
- Bishop, N. A., & Guarente, L. (2007). Two neurons mediate diet-restriction-induced longevity in *C. elegans*. *Nature*, 447(7144), 545–549. <https://doi.org/10.1038/nature05904>
- Bjedov, I., Toivonen, J. M., Kerr, F., Slack, C., Jacobson, J., Foley, A., & Partridge, L. (2010). Mechanisms of Life Span Extension by Rapamycin in the Fruit Fly *Drosophila melanogaster*. *Cell Metabolism*, 11(1), 35–46. <https://doi.org/10.1016/j.cmet.2009.11.010>
- Blackwell, T. K., Kretzner, L., Blackwood, E. M., Eisenman, R. N., & Weintraub, H. (1990). Sequence-specific DNA binding by the c-Myc protein. *Science*, 250(494), 1149–1151. <https://doi.org/10.1126/science.2251503>
- Blagosklonny, M. V. (2017). From rapalogs to anti-aging formula. *Oncotarget*, 8(22), 35492–35507. <https://doi.org/10.18632/oncotarget.18033>
- Blom, N., Gammeltoft, S., & Brunak, S. (1999). Sequence and structure-based prediction of eukaryotic protein phosphorylation sites. *Journal of Molecular Biology*, 294(5), 1351–1362. <https://doi.org/10.1006/jmbi.1999.3310>
- Blom, N., Sicheritz-Pontén, T., Gupta, R., Gammeltoft, S., & Brunak, S. (2004). Prediction of post-translational glycosylation and phosphorylation of proteins from the amino acid sequence. *Proteomics*, 4(6), 1633–1649. <https://doi.org/10.1002/pmic.200300771>

- Blüher, M., Kahn, B. B., & Kahn, C. R. (2003). Extended Longevity in Mice lacking insulin signal receptor.pdf. *Curr. Opin. Neurobiol*, 299(January), 2000–2002.
www.sciencemag.org/cgi/content/full/299/5606/568/
- Blüher, M., Michael, M. D., Peroni, O. D., Ueki, K., Carter, N., Kahn, B. B., & Kahn, C. R. (2002). Adipose tissue selective insulin receptor knockout protects against obesity and obesity-related glucose intolerance. *Developmental Cell*, 3(1), 25–38.
[https://doi.org/10.1016/S1534-5807\(02\)00199-5](https://doi.org/10.1016/S1534-5807(02)00199-5)
- Bolte, S., & Cordelières, F. P. (2006). A guided tour into subcellular colocalization analysis in light microscopy. *Journal of Microscopy*, 224(3), 213–232. <https://doi.org/10.1111/j.1365-2818.2006.01706.x>
- Bonfils, G., Jaquenoud, M., Bontron, S., Ostrowicz, C., Ungermann, C., & De Virgilio, C. (2012). Leucyl-tRNA Synthetase Controls TORC1 via the EGO Complex. *Molecular Cell*, 46(1), 105–110. <https://doi.org/10.1016/j.molcel.2012.02.009>
- Boutant, M., Kulkarni, S. S., Joffraud, M., Ratajczak, J., Valera-Alberni, M., Combe, R., Zorzano, A., & Cantó, C. (2017). Mfn2 is critical for brown adipose tissue thermogenic function. *The EMBO Journal*, 36(11), 1543–1558.
<https://doi.org/10.15252/embj.201694914>
- Brenner, S. (1974). The genetics of *Caenorhabditis elegans*. *Genetics*, 77(1), 71–94.
<https://doi.org/10.1093/genetics/77.1.71>.
- Bricambert, J., Miranda, J., Benhamed, F., Girard, J., Postic, C., & Dentin, R. (2010). Salt-inducible kinase 2 links transcriptional coactivator p300 phosphorylation to the prevention of ChREBP-dependent hepatic steatosis in mice. *Journal of Clinical Investigation*, 120(12), 4316–4331. <https://doi.org/10.1172/JCI41624>
- Bricker, D. K., Taylor, E. B., Schell, J. C., Orsak, T., Boutron, A., Chen, Y.-C., Cox, J. E., Cardon, C. M., Van Vranken, J. G., Dephoure, N., Redin, C., Boudina, S., Gygi, S. P., Brivet, M., Thummel, C. S., & Rutter, J. (2012). A Mitochondrial Pyruvate Carrier Required for Pyruvate Uptake in Yeast, *Drosophila*, and Humans. *Science*, 337(July), 96–100. <https://doi.org/10.1126/science.1218099>
- Bridges, D., MacDonald, J. A., Wadzinski, B., & Moorhead, G. B. G. (2006). Identification and characterization of D-AKAP1 as a major adipocyte PKA and PP1 binding protein. *Biochemical and Biophysical Research Communications*, 346(1), 351–357.

<https://doi.org/10.1016/j.bbrc.2006.05.138>

- Bridges, H. R., Jones, A. J. Y., Pollak, M. N., & Hirst, J. (2014). Effects of metformin and other biguanides on oxidative phosphorylation in mitochondria. *Biochemical Journal*, 462(3), 475–487. <https://doi.org/10.1042/BJ20140620>
- Brown, A. J., Sun, L., Feramisco, J. D., Brown, M. S., & Goldstein, J. L. (2002). Cholesterol Addition to ER Membranes Alters Conformation of SCAP, the SREBP Escort Protein that Regulates Cholesterol Metabolism exogenous cholesterol for growth (Rawson et al The opposite phenotype, sterol resistance, occurs in cells with either of two p. *Molecular Cell*, 10, 237–245.
- Brown, M. S., & Goldstein, J. L. (1997). The SREBP pathway: Regulation of cholesterol metabolism by proteolysis of a membrane-bound transcription factor. *Cell*, 89(3), 331–340. [https://doi.org/10.1016/S0092-8674\(00\)80213-5](https://doi.org/10.1016/S0092-8674(00)80213-5)
- Bryk, B., Hahn, K., Cohen, S. M., & Teleman, A. A. (2010). MAP4K3 regulates body size and metabolism in *Drosophila*. *Developmental Biology*, 344(1), 150–157. <https://doi.org/10.1016/j.ydbio.2010.04.027>
- Bu, S. Y., Mashek, M. T., & Mashek, D. G. (2009). Suppression of long chain acyl-CoA synthetase 3 decreases hepatic de Novo fatty acid synthesis through decreased transcriptional activity. *Journal of Biological Chemistry*, 284(44), 30474–30483. <https://doi.org/10.1074/jbc.M109.036665>
- Burger, O., Baudisch, A., & Vaupel, J. W. (2012). Human mortality improvement in evolutionary context. *Proceedings of the National Academy of Sciences of the United States of America*, 109(44), 18210–18214. <https://doi.org/10.1073/pnas.1215627109>
- Burkewitz, K., Zhang, Y., & Mair, W. B. (2014). AMPK at the nexus of energetics and aging. *Cell Metabolism*, 20(1), 10–25. <https://doi.org/10.1016/j.cmet.2014.03.002>
- Byfield, M. P., Murray, J. T., & Backer, J. M. (2005). hVps34 is a nutrient-regulated lipid kinase required for activation of p70 S6 kinase. *Journal of Biological Chemistry*, 280(38), 33076–33082. <https://doi.org/10.1074/jbc.M507201200>
- Cabreiro, F., Au, C., Leung, K. Y., Vergara-Irigaray, N., Cochemé, H. M., Noori, T., Weinkove, D., Schuster, E., Greene, N. D. E., & Gems, D. (2013). Metformin retards aging in *C. elegans* by altering microbial folate and methionine metabolism. *Cell*, 153(1), 228–239. <https://doi.org/10.1016/j.cell.2013.02.035>

- Campbell, J. M., Bellman, S. M., Stephenson, M. D., & Lisy, K. (2017). Metformin reduces all-cause mortality and diseases of ageing independent of its effect on diabetes control: A systematic review and meta-analysis. *Ageing Research Reviews*, 40, 31–44.
<https://doi.org/10.1016/j.arr.2017.08.003>
- Campfield, L. A., Smith, F. J., Guisez, Y., Devos, R., & Burn, P. (1996). OB protein: A peripheral signal linking adiposity and central neural networks. *Appetite*, 26(3), 302.
<https://doi.org/10.1006/appe.1996.0024>
- Cargill, S. L., Carey, J. R., Müller, H. G., & Anderson, G. (2003). Age of ovary determines remaining life expectancy in old ovariectomized mice. *Aging Cell*, 2(3), 185–190.
<https://doi.org/10.1046/j.1474-9728.2003.00049.x>
- Carroll, P. A., Diolaiti, D., McFerrin, L., Gu, H., Djukovic, D., Du, J., Cheng, P. F., Anderson, S., Ulrich, M., Hurley, J. B., Raftery, D., Ayer, D. E., & Eisenman, R. N. (2015). Deregulated Myc Requires MondoA/Mlx for Metabolic Reprogramming and Tumorigenesis. *Cancer Cell*, 27(2), 271–285. <https://doi.org/10.1016/j.ccell.2014.11.024>
- Carroll, P. A., Freie, B. W., Mathsyaraja, H., & Eisenman, R. N. (2018). The MYC transcription factor network: balancing metabolism, proliferation and oncogenesis. *Frontiers of Medicine*, 12(4), 412–425. <https://doi.org/10.1007/s11684-018-0650-z>
- Castillo-Quan, J. I., Li, L., Kinghorn, K. J., Ivanov, D. K., Tain, L. S., Slack, C., Kerr, F., Nespital, T., Thornton, J. M., Hardy, J., Bjedov, I., & Partridge, L. (2016). Lithium Promotes Longevity through GSK3/NRF2-Dependent Hormesis. *Cell Reports*, 15(3), 638–650. <https://doi.org/10.1016/j.celrep.2016.03.041>
- Castillo-Quan, J. I., Tain, L. S., Kinghorn, K. J., Li, L., Grönke, S., Hinze, Y., Blackwell, T. K., Bjedov, I., & Partridge, L. (2019). A triple drug combination targeting components of the nutrient-sensing network maximizes longevity. *Proceedings of the National Academy of Sciences of the United States of America*, 116(42), 20817–20819.
<https://doi.org/10.1073/pnas.1913212116>
- Ceballos, A., Esse, R., & Grishok, A. (2021). The proline-rich domain of MML-1 is biologically important but not required for localization to target promoters. *MicroPublication Biology*.
<https://doi.org/10.17912/micropub.biology.000498>
- Chang, J. T., Kumsta, C., Hellman, A. B., Adams, L. M., & Hansen, M. (2017). Spatiotemporal regulation of autophagy during *Caenorhabditis elegans* aging. *ELife*, 6, 1–23.

- <https://doi.org/10.7554/eLife.18459>
- Chantranupong, L., Scaria, S. M., Saxton, R. A., Gygi, M. P., Shen, K., Wyant, G. A., Wang, T., Harper, J. W., Gygi, S. P., & Sabatini, D. M. (2016). The CASTOR Proteins Are Arginine Sensors for the mTORC1 Pathway. *Cell*, 165(1), 153–164. <https://doi.org/10.1016/j.cell.2016.02.035>
- Chantranupong, L., Wolfson, R. L., Orozco, J. M., Saxton, R. A., Scaria, S. M., Bar-Peled, L., Spooner, E., Isasa, M., Gygi, S. P., & Sabatini, D. M. (2014). The sestrins interact with gator2 to negatively regulate the amino-acid-sensing pathway upstream of mTORC1. *Cell Reports*, 9(1), 1–8. <https://doi.org/10.1016/j.celrep.2014.09.014>
- Chaudhari, S. N., & Kipreos, E. T. (2017). Increased mitochondrial fusion allows the survival of older animals in diverse C. Elegans longevity pathways. *Nature Communications*, 8(1). <https://doi.org/10.1038/s41467-017-00274-4>
- Chen, C., Liu, Y., Liu, Y., & Zheng, P. (2009). MTOR regulation and therapeutic rejuvenation of aging hematopoietic stem cells. *Science Signaling*, 2(98), 1–8. <https://doi.org/10.1126/scisignal.2000559>
- Chen, G., Kroemer, G., & Kepp, O. (2020). Mitophagy: An Emerging Role in Aging and Age-Associated Diseases. *Frontiers in Cell and Developmental Biology*, 8(March), 1–15. <https://doi.org/10.3389/fcell.2020.00200>
- Cheung, O., & Sanyal, A. J. (2009). Recent advances in nonalcoholic fatty liver disease. *Current Opinion in Gastroenterology*, 25(3), 230–237. <https://doi.org/10.1097/MOG.0b013e3283294a18>
- Chi, M. M. Y., Pusateri, M. E., Carter, J. G., Norris, B. J., McDougal, D. B., & Lowry, O. H. (1987). Enzymatic assays for 2-deoxyglucose and 2-deoxyglucose 6-phosphate. *Analytical Biochemistry*, 161(2), 508–513. [https://doi.org/10.1016/0003-2697\(87\)90481-7](https://doi.org/10.1016/0003-2697(87)90481-7)
- Chin, R. M., Fu, X., Pai, M. Y., Vergnes, L., Hwang, H., Deng, G., Diep, S., Lomenick, B., Meli, V. S., Monsalve, G. C., Hu, E., Whelan, S. A., Wang, J. X., Jung, G., Solis, G. M., Fazlollahi, F., Kaweeteerawat, C., Quach, A., Nili, M., ... Huang, J. (2014). The metabolite α -ketoglutarate extends lifespan by inhibiting ATP synthase and TOR. *Nature*, 510(7505), 397–401. <https://doi.org/10.1038/nature13264>
- Christensen, K., Doblhammer, G., Rau, R., & Vaupel, J. W. (2009). Ageing populations: the challenges ahead. *The Lancet*, 374(9696), 1196–1208. <https://doi.org/10.1016/S0140->

- Clancy, D. J., Gems, D., Harshman, L. G., Oldham, S., Stocker, H., Hafen, E., Leivers, S. J., & Partridge, L. (2001). Extension of life-span by loss of CHICO, a *Drosophila* insulin receptor substrate protein. *Science*, 292(5514), 104–106. <https://doi.org/10.1126/science.1057991>
- Colman, R. J., Anderson, R. M., Johnson, S. C., Kastman, E. K., Kosmatka, K. J., Beasley, T. M., Allison, D. B., Cruzen, C., Simmons, H. A., Kemnitz, J. W., & Weindruch, R. (2009). Caloric restriction delays disease onset and mortality in Rhesus monkeys. *Science*, 325(5937), 201–204. <https://doi.org/10.1126/science.1173635>
- Colman, R. J., Mark Beasley, T., Allison, D. B., & Weindruch, R. (2012). Skeletal effects of long-term caloric restriction in rhesus monkeys. *Age*, 34(5), 1133–1143. <https://doi.org/10.1007/s11357-011-9354-x>
- Consortium, C. elegans S. (1998). Genome Sequence of the Nematode *C. elegans*: A Platform for Investigating Biology. *Science*, 282(5396), 2012–2018. <https://doi.org/10.1126/science.282.5396.2012>
- Copeland, J. M., Cho, J., Lo, T., Hur, J. H., Bahadorani, S., Arabyan, T., Rabie, J., Soh, J., & Walker, D. W. (2009). Extension of *Drosophila* Life Span by RNAi of the Mitochondrial Respiratory Chain. *Current Biology*, 19(19), 1591–1598. <https://doi.org/10.1016/j.cub.2009.08.016>
- Corradetti, M. N., Inoki, K., Bardeesy, N., DePinho, R. A., & Guan, K. L. (2019). Corrigendum: Regulation of the TSC pathway by LKB1: evidence of a molecular link between tuberous sclerosis complex and Peutz-Jeghers syndrome (*Genes & Development*, (2004) 18, (1533-1538)). *Genes and Development*, 33(7–8), 477. <https://doi.org/10.1101/gad.324970.119>
- Cox, J., Hein, M. Y., Lubner, C. A., Paron, I., Nagaraj, N., & Mann, M. (2014). Accurate proteome-wide label-free quantification by delayed normalization and maximal peptide ratio extraction, termed MaxLFQ. *Molecular and Cellular Proteomics*, 13(9), 2513–2526. <https://doi.org/10.1074/mcp.M113.031591>
- Cox, J., & Mann, M. (2008). MaxQuant enables high peptide identification rates, individualized p.p.b.-range mass accuracies and proteome-wide protein quantification. *Nature Biotechnology*, 26(12), 1367–1372. <https://doi.org/10.1038/nbt.1511>
- Curtis, R., O'Connor, G., & DiStefano, P. S. (2006). Aging networks in *Caenorhabditis elegans*: AMP-activated protein kinase (*aak-2*) links multiple aging and metabolism pathways. *Aging*

- Cell*, 5(2), 119–126. <https://doi.org/10.1111/j.1474-9726.2006.00205.x>
- Da Silva Xavier, G., Leclerc, I., Salt, I. P., Doiron, B., Hardie, D. G., Kahn, A., & Rutter, G. A. (2000). Role of AMP-activated protein kinase in the regulation by glucose of islet beta cell gene expression. *Proceedings of the National Academy of Sciences of the United States of America*, 97(8), 4023–4028. <https://doi.org/10.1073/pnas.97.8.4023>
- Dagon, Y., Hur, E., Zheng, B., Wellenstein, K., Cantley, L. C., & Kahn, B. B. (2012). P70S6 kinase phosphorylates AMPK on serine 491 to mediate leptin's effect on food intake. *Cell Metabolism*, 16(1), 104–112. <https://doi.org/10.1016/j.cmet.2012.05.010>
- Dall, K. B., & Færgeman, N. J. (2019). Metabolic regulation of lifespan from a C. Elegans perspective. *Genes and Nutrition*, 14(1), 1–12. <https://doi.org/10.1186/s12263-019-0650-x>
- Dalziel, K., & Londesborough, J. C. (1968). The mechanisms of reductive carboxylation reactions: Carbon dioxide or bicarbonate as substrate of nicotinamide-adenine dinucleotide phosphate-linked isocitrate dehydrogenase and malic enzyme. *The Biochemical Journal*, 110(2), 223–230. <https://doi.org/10.1042/bj1100223>
- Davies, M. N., O'Callaghan, B. L., & Towle, H. C. (2008). Glucose activates ChREBP by increasing its rate of nuclear entry and relieving repression of its transcriptional activity. *Journal of Biological Chemistry*, 283(35), 24029–24038. <https://doi.org/10.1074/jbc.M801539200>
- Davies, M. N., O'Callaghan, B. L., & Towle, H. C. (2010). Activation and repression of glucose-stimulated ChREBP requires the concerted action of multiple domains within the MondoA conserved region. *American Journal of Physiology - Endocrinology and Metabolism*, 299(4), 665–674. <https://doi.org/10.1152/ajpendo.00349.2010>
- De Luis, O., Valero, M. C., & Pérez Jurado, L. A. (2000). WBSCR14, a putative transcription factor gene deleted in Williams-Beuren syndrome: Complete characterisation of the human gene and the mouse ortholog. *European Journal of Human Genetics*, 8(3), 215–222. <https://doi.org/10.1038/sj.ejhg.5200435>
- Dell'Agnello, C., Leo, S., Agostino, A., Szabadkai, G., Tiveron, C. C., Zulian, A. A., Prella, A., Roubertoux, P., Rizzuto, R., & Zeviani, M. (2007). Increased longevity and refractoriness to Ca²⁺-dependent neurodegeneration in Surfl knockout mice. *Human Molecular Genetics*, 16(4), 431–444. <https://doi.org/10.1093/hmg/ddl477>
- Denechaud, P. D., Dentin, R., Girard, J., & Postic, C. (2008). Role of ChREBP in hepatic

- steatosis and insulin resistance. *FEBS Letters*, 582(1), 68–73.
<https://doi.org/10.1016/j.febslet.2007.07.084>
- Dentin, R., Benhamed, F., Pégrier, J. P., Foufelle, F., Viollet, B., Vaulont, S., Girard, J., & Postic, C. (2005). Polyunsaturated fatty acids suppress glycolytic and lipogenic genes through the inhibition of ChREBP nuclear protein translocation. *Journal of Clinical Investigation*, 115(10), 2843–2854. <https://doi.org/10.1172/JCI25256>
- Dentin, R., Pégrier, J. P., Benhamed, F., Foufelle, F., Ferré, P., Fauveau, V., Magnuson, M. A., Girard, J., & Postic, C. (2004). Hepatic Glucokinase Is Required for the Synergistic Action of ChREBP and SREBP-1c on Glycolytic and Lipogenic Gene Expression. *Journal of Biological Chemistry*, 279(19), 20314–20326. <https://doi.org/10.1074/jbc.M312475200>
- Dentin, R., Tomas-Cobos, L., Foufelle, F., Leopold, J., Girard, J., Postic, C., & Ferré, P. (2012). Glucose 6-phosphate, rather than xylulose 5-phosphate, is required for the activation of ChREBP in response to glucose in the liver. *Journal of Hepatology*, 56(1), 199–209. <https://doi.org/10.1016/j.jhep.2011.07.019>
- Deus, C. M., Yambire, K. F., Oliveira, P. J., & Raimundo, N. (2020). Mitochondria–Lysosome Crosstalk: From Physiology to Neurodegeneration. *Trends in Molecular Medicine*, 26(1), 71–88. <https://doi.org/10.1016/j.molmed.2019.10.009>
- Dillin, A., Hsu, A. L., Arantes-Oliveira, N., Lehrer-Graiwer, J., Hsin, H., Fraser, A. G., Kamath, R. S., Ahringer, J., & Kenyon, C. (2002). Rates of behavior and aging specified by mitochondrial function during development. *Science*, 298(5602), 2398–2401. <https://doi.org/10.1126/science.1077780>
- Divekar, N. S., Horton, H. E., & Wignall, S. M. (2021). Methods for Rapid Protein Depletion in *C. elegans* using Auxin-Inducible Degradation. *Current Protocols*, 1(2), 1–20. <https://doi.org/10.1002/cpz1.16>
- Durieux, J., Wolff, S., & Dillin, A. (2011). The cell-non-autonomous nature of electron transport chain-mediated longevity. *Cell*, 144(1), 79–91. <https://doi.org/10.1016/j.cell.2010.12.016>
- Duttaroy, A., Paul, A., Kundu, M., & Belton, A. (2003). A Sod2 Null Mutation Confers Severely Reduced Adult Life Span in *Drosophila*. *Genetics*, 165(4), 2295–2299. <https://doi.org/10.1093/genetics/165.4.2295>
- Düvel, K., Yecies, J. L., Menon, S., Raman, P., Lipovsky, A. I., Souza, A. L., Triantafellow, E., Ma, Q., Gorski, R., Cleaver, S., Vander Heiden, M. G., MacKeigan, J. P., Finan, P. M.,

- Clish, C. B., Murphy, L. O., & Manning, B. D. (2010). Activation of a metabolic gene regulatory network downstream of mTOR complex 1. *Molecular Cell*, 39(2), 171–183. <https://doi.org/10.1016/j.molcel.2010.06.022>
- Dyck, J. R. B., Kudo, N., Barr, A. J., Davies, S. P., Hardie, D. G., & Lopaschuk, G. D. (1999). Phosphorylation control of cardiac acetyl-CoA carboxylase by cAMP- dependent protein kinase and 5'-AMP activated protein kinase. *European Journal of Biochemistry*, 262(1), 184–190. <https://doi.org/10.1046/j.1432-1327.1999.00371.x>
- Egan, D. F., Shackelford, D. B., Mihaylova, M. M., Gelino, S., Kohnz, R. A., Mair, W., Vasquez, D. S., Joshi, A., Gwinn, D. M., Taylor, R., Asara, J. M., Fitzpatrick, J., Dillin, A., Viollet, B., Kundu, M., Hansen, M., & Shaw, R. J. (2011). Phosphorylation of ULK1 (hATG1) by AMP-activated protein kinase connects energy sensing to mitophagy. *Science*, 331(6016), 456–461. <https://doi.org/10.1126/science.1196371>
- Eilers, A. L., Sundwall, E., Lin, M., Sullivan, A. A., & Ayer, D. E. (2002). A Novel Heterodimerization Domain, CRM1, and 14-3-3 Control Subcellular Localization of the MondoA-Mlx Heterocomplex. *Molecular and Cellular Biology*, 22(24), 8514–8526. <https://doi.org/10.1128/mcb.22.24.8514-8526.2002>
- Eissing, L., Scherer, T., Tödter, K., Knippschild, U., Greve, J. W., Buurman, W. A., Pinnschmidt, H. O., Rensen, S. S., Wolf, A. M., Bartelt, A., Heeren, J., Buettner, C., & Scheja, L. (2013). De novo lipogenesis in human fat and liver is linked to ChREBP- β and metabolic health. *Nature Communications*, 4. <https://doi.org/10.1038/ncomms2537>
- Elchuri, S., Oberley, T. D., Qi, W., Eisenstein, R. S., Roberts, L. J., Van Remmen, H., Epstein, C. J., & Huang, T. T. (2005). CuZnSOD deficiency leads to persistent and widespread oxidative damage and hepatocarcinogenesis later in life. *Oncogene*, 24(3), 367–380. <https://doi.org/10.1038/sj.onc.1208207>
- Ellis, J. M., Mentock, S. M., DePetrillo, M. A., Koves, T. R., Sen, S., Watkins, S. M., Muoio, D. M., Cline, G. W., Taegtmeyer, H., Shulman, G. I., Willis, M. S., & Coleman, R. A. (2011). Mouse Cardiac Acyl Coenzyme A Synthetase 1 Deficiency Impairs Fatty Acid Oxidation and Induces Cardiac Hypertrophy. *Molecular and Cellular Biology*, 31(6), 1252–1262. <https://doi.org/10.1128/mcb.01085-10>
- Fahy, E., Subramaniam, S., Murphy, R. C., Nishijima, M., Raetz, C. R. H., Shimizu, T., Spener, F., Van Meer, G., Wakelam, M. J. O., & Dennis, E. A. (2009). Update of the LIPID MAPS

- comprehensive classification system for lipids. *Journal of Lipid Research*, 50(SUPPL.), 9–14. <https://doi.org/10.1194/jlr.R800095-JLR200>
- Fain, J. N., & Garcia Sainz, J. A. (1983). Adrenergic regulation of adipocyte metabolism. *Journal of Lipid Research*, 24(8), 945–966. [https://doi.org/10.1016/s0022-2275\(20\)37910-4](https://doi.org/10.1016/s0022-2275(20)37910-4)
- Fang, E. F., Scheibye-Knudsen, M., Brace, L. E., Kassahun, H., Sengupta, T., Nilsen, H., Mitchell, J. R., Croteau, D. L., & Bohr, V. A. (2014). Defective mitophagy in XPA via PARP-1 hyperactivation and NAD⁺/SIRT1 reduction. *Cell*, 157(4), 882–896. <https://doi.org/10.1016/j.cell.2014.03.026>
- Feliciello, A., Gottesman, M. E., & Avvedimento, E. V. (2001). The biological functions of A-kinase anchor proteins. *Journal of Molecular Biology*, 308(2), 99–114. <https://doi.org/10.1006/jmbi.2001.4585>
- Feng, J., Bussière, F., & Hekimi, S. (2001). Mitochondrial Electron Transport Is a Key Determinant of Life Span in *Caenorhabditis elegans*. *Developmental Cell*, 1(5), 633–644. [https://doi.org/10.1016/S1534-5807\(01\)00071-5](https://doi.org/10.1016/S1534-5807(01)00071-5)
- Feng, Y., Williams, B. G., Koumanov, F., Wolstenholme, A. J., & Holman, G. D. (2013). FGT-1 is the major glucose transporter in *C. elegans* and is central to aging pathways. *Biochemical Journal*, 456(2), 219–229. <https://doi.org/10.1042/BJ20131101>
- Fiorese, C. J., Schulz, A. M., Lin, Y. F., Rosin, N., Pellegrino, M. W., & Haynes, C. M. (2016). The Transcription Factor ATF5 Mediates a Mammalian Mitochondrial UPR. *Current Biology*, 26(15), 2037–2043. <https://doi.org/10.1016/j.cub.2016.06.002>
- Flachsbart, F., Caliebe, A., Kleindorp, R., Blanché, H., Von Eller-Eberstein, H., Nikolaus, S., Schreiber, S., & Nebel, A. (2009). Association of FOXO3A variation with human longevity confirmed in German centenarians. *Proceedings of the National Academy of Sciences of the United States of America*, 106(8), 2700–2705. <https://doi.org/10.1073/pnas.0809594106>
- Flatt, T., Min, K. J., D’Alterio, C., Villa-Cuesta, E., Cumbers, J., Lehmann, R., Jones, D. L., & Tatar, M. (2008). *Drosophila* germ-line modulation of insulin signaling and lifespan. *Proceedings of the National Academy of Sciences of the United States of America*, 105(17), 6368–6373. <https://doi.org/10.1073/pnas.0709128105>
- Folick, A., Oakley, H. D., Yu, Y., Armstrong, E. H., Kumari, M., Sanor, L., Moore, D. D., Ortlund, E. A., Zechner, R., & Wang, M. C. (2015). Lysosomal signaling molecules regulate longevity in *Caenorhabditis elegans*. *Science*, 347(6217), 83–86.

<https://doi.org/10.1126/science.1258857>

- Franceschi, C., Garagnani, P., Parini, P., Giuliani, C., & Santoro, A. (2018). Inflammaging: a new immune–metabolic viewpoint for age-related diseases. *Nature Reviews Endocrinology*, *14*(10), 576–590. <https://doi.org/10.1038/s41574-018-0059-4>
- Friedman, J. M., Leibel, R. L., Siegel, D. S., Walsh, J., & Bahary, N. (1991). Molecular mapping of the mouse ob mutation. *Genomics*, *11*(4), 1054–1062. [https://doi.org/10.1016/0888-7543\(91\)90032-A](https://doi.org/10.1016/0888-7543(91)90032-A)
- Fuchs, S., Bundy, J. G., Davies, S. K., Viney, J. M., Swire, J. S., & Leroi, A. M. (2010). A metabolic signature of long life in *Caenorhabditis elegans*. *BMC Biology*, *8*(14). <https://doi.org/10.1186/1741-7007-8-14>
- Fukasawa, M., Ge, Q., Wynn, R. M., Ishii, S., & Uyeda, K. (2010). Coordinate regulation/localization of the carbohydrate responsive binding protein (ChREBP) by two nuclear export signal sites: Discovery of a new leucine-rich nuclear export signal site. *Biochemical and Biophysical Research Communications*, *391*(2), 1166–1169. <https://doi.org/10.1016/j.bbrc.2009.11.115>
- Gallant, P., Shio, Y., Cheng, P. F., Parkhurst, S. M., & Eisenman, R. N. (1996). *Myc and Max homologs in Drosophila*. *274*(November), 523–528.
- Ganley, I. G., Lam, D. H., Wang, J., Ding, X., Chen, S., & Jiang, X. (2009). ULK1·ATG13·FIP200 complex mediates mTOR signaling and is essential for autophagy. *Journal of Biological Chemistry*, *284*(18), 12297–12305. <https://doi.org/10.1074/jbc.M900573200>
- Gao, J., Kim, H. M., Elia, A. E., Elledge, S. J., & Colaiácovo, M. P. (2015). NatB Domain-Containing CRA-1 Antagonizes Hydrolase ACER-1 Linking Acetyl-CoA Metabolism to the Initiation of Recombination during *C. elegans* Meiosis. *PLoS Genetics*, *11*(3), 1–28. <https://doi.org/10.1371/journal.pgen.1005029>
- Gasteiger, E., Hoogland, C., Gattiker, A., Duvaud, S., Wilkins, M. R., Appel, R. D., & Bairoch, A. (2005). Protein Identification and Analysis Tools on the ExPASy Server. In J. M. Walker (Ed.), *The Proteomics Protocols Handbook* (pp. 571–607). Humana Press. <https://doi.org/10.1385/1592598900>
- Ge, Q., Nakagawa, T., Max Wynn, R., Chook, Y. M., Miller, B. C., & Uyeda, K. (2011). Importin- α protein binding to a nuclear localization signal of carbohydrate response

- element-binding protein (ChREBP). *Journal of Biological Chemistry*, 286(32), 28119–28127. <https://doi.org/10.1074/jbc.M111.237016>
- Genuth, S. M. (1969). Hyperinsulinism in mice with genetically determined obesity. *Endocrinology*, 84(2), 386–391. <https://doi.org/10.1210/endo-84-2-386>
- Gerisch, B., & Antebi, A. (2004). Hormonal signals produced by DAF-9/cytochrome P450 regulate *C. elegans* dauer diapause in response to environmental cues. *Development*, 131(8), 1765–1776. <https://doi.org/10.1242/dev.01068>
- Gerisch, B., Rottiers, V., Li, D., Motola, D. L., Cummins, C. L., Lehrach, H., Mangelsdorf, D. J., & Antebi, A. (2007). A bile acid-like steroid modulates *Caenorhabditis elegans* lifespan through nuclear receptor signaling. *Proceedings of the National Academy of Sciences of the United States of America*, 104(12), 5014–5019. <https://doi.org/10.1073/pnas.0700847104>
- Gerisch, B., Weitzel, C., Kober-Eisermann, C., Rottiers, V., & Antebi, A. (2001). A Hormonal Signaling Pathway Influencing *C. elegans* Metabolism, Reproductive Development, and Life Span. *Developmental Cell*, 1(6), 841–851. [https://doi.org/10.1016/S1534-5807\(01\)00085-5](https://doi.org/10.1016/S1534-5807(01)00085-5)
- Ghisaidoobe, A. B. T., & Chung, S. J. (2014). Intrinsic tryptophan fluorescence in the detection and analysis of proteins: A focus on förster resonance energy transfer techniques. *International Journal of Molecular Sciences*, 15(12), 22518–22538. <https://doi.org/10.3390/ijms151222518>
- Giannakou, M. E., Goss, M., Jünger, M. A., Hafen, E., Leever, S. J., & Partridge, L. (2004). Long-lived *Drosophila* with over-expressed dFOXO in adult fat body. *Science*, 305(5682), 361. <https://doi.org/10.1126/science.1098219>
- Goberdhan, D. C. I., Wilson, C., & Harris, A. L. (2016). Amino Acid Sensing by mTORC1: Intracellular Transporters Mark the Spot. *Cell Metabolism*, 23(4), 580–589. <https://doi.org/10.1016/j.cmet.2016.03.013>
- Goodpaster, B. H., & Sparks, L. M. (2017). Metabolic Flexibility in Health and Disease. *Cell Metabolism*, 25(5), 1027–1036. <https://doi.org/10.1016/j.cmet.2017.04.015>
- Gordaliza-Alaguero, I., Cantó, C., & Zorzano, A. (2019). Metabolic implications of organelle–mitochondria communication. *EMBO Reports*, 20(9), 1–27. <https://doi.org/10.15252/embr.201947928>
- Gottlob, K., Majewski, N., Kennedy, S., Kandel, E., Robey, R. B., & Hay, N. (2001). Inhibition

- of early apoptotic events by Akt/PKB is dependent on the first committed step of glycolysis and mitochondrial hexokinase. *Genes and Development*, 15(11), 1406–1418.
<https://doi.org/10.1101/gad.889901>
- Goudeau, J., Bellemin, S., Toselli-Mollereau, E., Shamalnasab, M., Chen, Y., & Aguilaniu, H. (2011). Fatty acid desaturation links germ cell loss to longevity through NHR-80/HNF4 in *C. elegans*. *PLoS Biology*, 9(3). <https://doi.org/10.1371/journal.pbio.1000599>
- Gowans, G. J., Hawley, S. A., Ross, F. A., & Hardie, D. G. (2013). AMP is a true physiological regulator of amp-activated protein kinase by both allosteric activation and enhancing net phosphorylation. *Cell Metabolism*, 18(4), 556–566.
<https://doi.org/10.1016/j.cmet.2013.08.019>
- Granneman, J. G., Moore, H. P. H., Mottillo, E. P., Zhu, Z., & Zhou, L. (2011). Interactions of Perilipin-5 (Plin5) with adipose triglyceride lipase. *Journal of Biological Chemistry*, 286(7), 5126–5135. <https://doi.org/10.1074/jbc.M110.180711>
- Green, C. L., Lamming, D. W., & Fontana, L. (2021). Molecular mechanisms of dietary restriction promoting health and longevity. *Nature Reviews Molecular Cell Biology*, 0123456789. <https://doi.org/10.1038/s41580-021-00411-4>
- Greer, E. L., & Brunet, A. (2009). Different dietary restriction regimens extend lifespan by both independent and overlapping genetic pathways in *C. elegans*. *Aging Cell*, 8(2), 113–127.
<https://doi.org/10.1111/j.1474-9726.2009.00459.x>
- Greer, E. L., Dowlathshahi, D., Banko, M. R., Villen, J., Hoang, K., Blanchard, D., Gygi, S. P., & Brunet, A. (2007). An AMPK-FOXO Pathway Mediates Longevity Induced by a Novel Method of Dietary Restriction in *C. elegans*. *Current Biology*, 17(19), 1646–1656.
<https://doi.org/10.1016/j.cub.2007.08.047>
- Grove, C. A., De Masi, F., Barrasa, M. I., Newburger, D. E., Alkema, M. J., Bulyk, M. L., & Walhout, A. J. M. (2009). A Multiparameter Network Reveals Extensive Divergence between *C. elegans* bHLH Transcription Factors. *Cell*, 138(2), 314–327.
<https://doi.org/10.1016/j.cell.2009.04.058>
- Guinez, C., Filhoulaud, G., Rayah-Benhamed, F., Marmier, S., Dubuquoy, C., Dentin, R., Moldes, M., Burnol, A. F., Yang, X., Lefebvre, T., Girard, J., & Postic, C. (2011). O-GlcNAcylation increases ChREBP protein content and transcriptional activity in the liver. *Diabetes*, 60(5), 1399–1413. <https://doi.org/10.2337/db10-0452>

- Gwinn, D. M., Shackelford, D. B., Egan, D. F., Mihaylova, M. M., Mery, A., Vasquez, D. S., Turk, B. E., & Shaw, R. J. (2008). AMPK Phosphorylation of Raptor Mediates a Metabolic Checkpoint. *Molecular Cell*, 30(2), 214–226. <https://doi.org/10.1016/j.molcel.2008.03.003>
- Hamilton, B., Dong, Y., Shindo, M., Liu, W., Odell, I., Ruvkun, G., & Lee, S. S. (2005). A systematic RNAi screen for longevity genes in *C. elegans*. *Genes and Development*, 19(13), 1544–1555. <https://doi.org/10.1101/gad.1308205>
- Han, J. M., Jeong, S. J., Park, M. C., Kim, G., Kwon, N. H., Kim, H. K., Ha, S. H., Ryu, S. H., & Kim, S. (2012). Leucyl-tRNA synthetase is an intracellular leucine sensor for the mTORC1-signaling pathway. *Cell*, 149(2), 410–424. <https://doi.org/10.1016/j.cell.2012.02.044>
- Hansen, M., Chandra, A., Mitic, L. L., Onken, B., Driscoll, M., & Kenyon, C. (2008). A role for autophagy in the extension of lifespan by dietary restriction in *C. elegans*. *PLoS Genetics*, 4(2). <https://doi.org/10.1371/journal.pgen.0040024>
- Hardie, D. G., Ross, F. A., & Hawley, S. A. (2012). AMPK: A nutrient and energy sensor that maintains energy homeostasis. *Nature Reviews Molecular Cell Biology*, 13(4), 251–262. <https://doi.org/10.1038/nrm3311>
- Harman, D. (1956). Aging: A Theory on Free Radical Radiation Chemistry. *J. Gerontol.*, 11, 298–300.
- Harrison, D. E., Strong, R., Sharp, Z. D., Nelson, J. F., Astle, C. M., Flurkey, K., Nadon, N. L., Wilkinson, J. E., Frenkel, K., Carter, C. S., Pahor, M., Javors, M. A., Fernandez, E., & Miller, R. A. (2009). Rapamycin fed late in life extends lifespan in genetically heterogeneous mice. *Nature*, 460(7253), 392–395. <https://doi.org/10.1038/nature08221>
- Hassan, K., Bhalla, V., El Regal, M. E., & Hesham A-Kader, H. (2014). Nonalcoholic fatty liver disease: A comprehensive review of a growing epidemic. *World Journal of Gastroenterology*, 20(34), 12082–12101. <https://doi.org/10.3748/wjg.v20.i34.12082>
- Havula, E., & Hietakangas, V. (2012). Glucose sensing by ChREBP/MondoA-Mlx transcription factors. *Seminars in Cell and Developmental Biology*, 23(6), 640–647. <https://doi.org/10.1016/j.semcdb.2012.02.007>
- Hawley, S. A., Boudeau, J., Reid, J. L., Mustard, K. J., Udd, L., Mäkelä, T. P., Alessi, D. R., & Hardie, D. G. (2003). Complexes between the LKB1 tumor suppressor, STRAD α/β and MO25 α/β are upstream kinases in the AMP-activated protein kinase cascade. *Journal of Biology*, 2(4), 1–16.

- Hawley, S. A., Davison, M., Woods, A., Davies, S. P., Beri, R. K., Carling, D., & Hardie, D. G. (1996). Characterization of the AMP-activated protein kinase kinase from rat liver and identification of threonine 172 as the major site at which it phosphorylates AMP-activated protein kinase. *Journal of Biological Chemistry*, 271(44), 27879–27887. <https://doi.org/10.1074/jbc.271.44.27879>
- Herman, M. A., & Kahn, B. B. (2006). Glucose transport and sensing in the maintenance of glucose homeostasis and metabolic harmony. *Journal of Clinical Investigation*, 116(7), 1767–1775. <https://doi.org/10.1172/JCI29027>
- Herman, M. A., Peroni, O. D., Villoria, J., Schön, M. R., Abumrad, N. A., Blüher, M., Klein, S., & Kahn, B. B. (2012). A novel ChREBP isoform in adipose tissue regulates systemic glucose metabolism. *Nature*, 484(7394), 333–338. <https://doi.org/10.1038/nature10986>
- Herndon, L.A., Wolkow, C. A., Driscoll, M., & Hall, D. . (2018). Introduction to Aging in *C. elegans*. In Laura A. Herndon (Ed.), *WormAtlas*. <https://doi.org/doi:10.3908/wormatlas.8.4>
- Hevener, A. L., Olefsky, J. M., Reichart, D., Nguyen, M. T. A., Bandyopadhyay, G., Leung, H. Y., Watt, M. J., Benner, C., Febbraio, M. A., Nguyen, A. K., Folian, B., Subramaniam, S., Gonzalez, F. J., Glass, C. K., & Ricote, M. (2007). Macrophage PPAR γ is required for normal skeletal muscle and hepatic insulin sensitivity and full antidiabetic effects of thiazolidinediones. *Journal of Clinical Investigation*, 117(6), 1658–1669. <https://doi.org/10.1172/JCI31561>
- Hoffman, N. J., Parker, B. L., Chaudhuri, R., Fisher-Wellman, K. H., Kleinert, M., Humphrey, S. J., Yang, P., Holliday, M., Trefely, S., Fazakerley, D. J., Stöckli, J., Burchfield, J. G., Jensen, T. E., Jothi, R., Kiens, B., Wojtaszewski, J. F. P., Richter, E. A., & James, D. E. (2015). Global Phosphoproteomic Analysis of Human Skeletal Muscle Reveals a Network of Exercise-Regulated Kinases and AMPK Substrates. *Cell Metabolism*, 22(5), 922–935. <https://doi.org/10.1016/j.cmet.2015.09.001>
- Holz, M. K., Ballif, B. A., Gygi, S. P., & Blenis, J. (2005). mTOR and S6K1 mediate assembly of the translation preinitiation complex through dynamic protein interchange and ordered phosphorylation events. *Cell*, 123(4), 569–580. <https://doi.org/10.1016/j.cell.2005.10.024>
- Honda, S., Ishii, N., Suzuki, K., & Matsuo, M. (1993). Oxygen-dependent perturbation of life span and aging rate in the nematode. *Journals of Gerontology*, 48(2), 57–61. <https://doi.org/10.1093/geronj/48.2.B57>

- Honda, Y., Tanaka, M., & Honda, S. (2010). Trehalose extends longevity in the nematode *Caenorhabditis elegans*. *Aging Cell*, 9(4), 558–569. <https://doi.org/10.1111/j.1474-9726.2010.00582.x>
- Hosokawa, N., Hara, T., Kaizuka, T., Kishi, C., Takamura, A., Miura, Y., Iemura, S., Natsume, T., Takehana, K., Yamada, N., Guan, J.-L., Oshiro, N., & Mizushima, N. (2009). Nutrient-dependent mTORC1 association with the ULK1-Atg13-FIP200 complex required for autophagy. *Molecular Biology of the Cell*, 20, 1981–1991. <https://doi.org/10.1091/mbc.E08>
- Hosono, R., Nishimoto, S., & Kuno, S. (1989). Alterations of life span in the nematode *Caenorhabditis elegans* under monoxenic culture conditions. *Experimental Gerontology*, 24(3), 251–264. [https://doi.org/10.1016/0531-5565\(89\)90016-8](https://doi.org/10.1016/0531-5565(89)90016-8)
- Houthoofd, K., Braeckman, B. P., Johnson, T. E., & Vanfleteren, J. R. (2003). Life extension via dietary restriction is independent of the Ins/IGF-1 signalling pathway in *Caenorhabditis elegans*. In *Experimental Gerontology* (Vol. 38, Issue 9). [https://doi.org/10.1016/S0531-5565\(03\)00161-X](https://doi.org/10.1016/S0531-5565(03)00161-X)
- Howitz, K. T., Bitterman, K. J., Cohen, H. Y., Lamming, D. W., Lavu, S., Wood, J. G., Zipkin, R. E., Chung, P., Kisielewski, A., Zhang, L. L., Scherer, B., & Sinclair, D. A. (2003). Small molecule activators of sirtuins extend *Saccharomyces cerevisiae* lifespan. *Nature*, 425(6954), 191–196. <https://doi.org/10.1038/nature01960>
- Hsin, H., & Kenyon, C. (1999). *Signals from the reproductive system regulate the lifespan of C. elegans*. 399, 362–366. <https://doi.org/10.1038/20694>
- Hsu, A. L., Murphy, C. T., & Kenyon, C. (2003). Regulation of aging and age-related disease by DAF-16 and heat-shock factor. *Science*, 300(5622), 1142–1145. <https://doi.org/10.1126/science.1083701>
- Huang, Y., Li, Q., Tian, H., Yao, X., Bakina, O., Zhang, H., Lei, T., & Hu, F. (2020). MEK inhibitor trametinib attenuates neuroinflammation and cognitive deficits following traumatic brain injury in mice. *American Journal of Translational Research*, 12(10), 6351–6365.
- Hutter, H., & Suh, J. (2016). GExplore 1.4: An expanded web interface for queries on *Caenorhabditis elegans* protein and gene function. *Worm*, 5(4), e1234659. <https://doi.org/10.1080/21624054.2016.1234659>
- Hwang, A. B., Ryu, E. A., Artan, M., Chang, H. W., Kabir, M. H., Nam, H. J., Lee, D., Yang, J. S., Kim, S., Mair, W. B., Lee, C., Lee, S. S., & Lee, S. J. (2014). Feedback regulation via

- AMPK and HIF-1 mediates ROS-dependent longevity in *Caenorhabditis elegans*. *Proceedings of the National Academy of Sciences of the United States of America*, 111(42), E4458–E4467. <https://doi.org/10.1073/pnas.1411199111>
- Hwangbo, D. S., Garsham, B., Tu, M. P., Palmer, M., & Tatar, M. (2004). *Drosophila* dFOXO controls lifespan and regulates insulin signalling in brain and fat body. *Nature*, 429(6991), 562–566. <https://doi.org/10.1038/nature02549>
- Iizuka, K., Bruick, R. K., Liang, G., Horton, J. D., & Uyeda, K. (2004). Deficiency of carbohydrate response element-binding protein (ChREBP) reduces lipogenesis as well as glycolysis. *Proceedings of the National Academy of Sciences of the United States of America*, 101(19), 7281–7286. <https://doi.org/10.1073/pnas.0401516101>
- Iizuka, K., Miller, B., & Uyeda, K. (2006). Deficiency of carbohydrate-activated transcription factor ChREBP prevents obesity and improves plasma glucose control in leptin-deficient (ob/ob) mice. *American Journal of Physiology - Endocrinology and Metabolism*, 291(2), 358–364. <https://doi.org/10.1152/ajpendo.00027.2006>
- Iizuka, K., Takeda, J., & Horikawa, Y. (2008). Hepatic overexpression of dominant negative Mlx improves metabolic profile in diabetes-prone C57BL/6J mice. *Biochemical and Biophysical Research Communications*, 379(2), 499–504. <https://doi.org/10.1016/j.bbrc.2008.12.100>
- Imamura, M., Chang, B. H. J., Kohjima, M., Li, M., Hwang, B., Taegtmeier, H., Harris, R. A., & Chan, L. (2014). MondoA deficiency enhances sprint performance in mice. *Biochemical Journal*, 464, 35–48. <https://doi.org/10.1042/BJ20140530>
- Inoki, K., Zhu, T., & Guan, K.-L. (2003). TSC2 mediates cellular energy response to control cell growth and survival. *Cell*, 115(5), 577–5590.
- Ishii, S., Iizuka, K., Miller, B. C., & Uyeda, K. (2004). Carbohydrate response element binding protein directly promotes lipogenic enzyme gene transcription. *Proceedings of the National Academy of Sciences of the United States of America*, 101(44), 15597–15602. <https://doi.org/10.1073/pnas.0405238101>
- Itoh, Y., Kawamata, Y., Harada, M., Kobayashi, M., Fujii, R., Fukusumi, S., Ogi, K., Hosoya, M., Tanaka, Y., Uejima, H., Tanaka, H., Maruyama, M., Satoh, R., Okubo, S., Kizawa, H., Komatsu, H., Matsumura, F., Noguchi, Y., Shinohara, T., ... Fujino, M. (2003). Free fatty acids regulate insulin secretion from pancreatic β cells through GPR40. *Nature*, 422(6928), 173–176. <https://doi.org/10.1038/nature01478>

- Jacinto, E., Loewith, R., Schmidt, A., Lin, S., Rüegg, M. A., Hall, A., & Hall, M. N. (2004). Mammalian TOR complex 2 controls the actin cytoskeleton and is rapamycin insensitive. *Nature Cell Biology*, 6(11), 1122–1128. <https://doi.org/10.1038/ncb1183>
- Janowski, B. A., Willy, P. J., Devi, T. R., Falck, J. R., & Mangelsdorf, D. J. (1996). An oxysterol signalling pathway mediated by the nuclear receptor LXR α . *Nature*, 383, 728–731. <https://doi.org/10.1038/383728a0>
- Jeong, Y. S., Kim, D., Lee, Y. S., Kim, H. J., Han, J. Y., Im, S. S., Chong, H. K., Kwon, J. K., Cho, Y. H., Kim, W. K., Osborne, T. F., Horton, J. D., Jun, H. S., Ahn, Y. H., Ahn, S. M., & Cha, J. Y. (2011). Integrated expression profiling and Genome-Wide analysis of ChREBP targets reveals the dual role for ChREBP in Glucose-Regulated gene expression. *PLoS ONE*, 6(7). <https://doi.org/10.1371/journal.pone.0022544>
- Jia, K., & Levine, B. (2007). Autophagy is required for dietary restriction-mediated life span extension in *C. elegans*. *Autophagy*, 3(6), 597–599. <https://doi.org/10.4161/auto.4989>
- Jiang, H. C., Hsu, J. M., Yen, C. P., Chao, C. C., Chen, R. H., & Pan, C. L. (2015). Neural activity and CaMKII protect mitochondria from fragmentation in aging *Caenorhabditis elegans* neurons. *Proceedings of the National Academy of Sciences of the United States of America*, 112(28), 8768–8773. <https://doi.org/10.1073/pnas.1501831112>
- Jiang, Y., Qian, X., Shen, J., Wang, Y., Li, X., Liu, R., Xia, Y., Chen, Q., Peng, G., Lin, S. Y., & Lu, Z. (2015). Local generation of fumarate promotes DNA repair through inhibition of histone H3 demethylation. *Nature Cell Biology*, 17(9), 1158–1168. <https://doi.org/10.1038/ncb3209>
- John, S., Weiss, J. N., & Ribalet, B. (2011). Subcellular localization of hexokinases I and II directs the metabolic fate of glucose. *PLoS ONE*, 6(3). <https://doi.org/10.1371/journal.pone.0017674>
- Johnson, D. W., Llop, J. R., Farrell, S. F., Yuan, J., Stolzenburg, L. R., & Samuelson, A. V. (2014). The *Caenorhabditis elegans* Myc-Mondo/Mad Complexes Integrate Diverse Longevity Signals. *PLoS Genetics*, 10(4). <https://doi.org/10.1371/journal.pgen.1004278>
- Johnson, J. D., Mehus, J. G., Tews, K., Milavetz, B. I., & Lambeth, D. O. (1998). Genetic evidence for the expression of ATP- and GTP-specific succinyl- CoA synthetases in multicellular eucaryotes. *Journal of Biological Chemistry*, 273(42), 27580–27586. <https://doi.org/10.1074/jbc.273.42.27580>

- Johnson, S. C., Rabinovitch, P. S., & Kaeberlein, M. (2013). mTOR is a key modulator of ageing and age-related disease. *Nature*, 493(7432), 338–345. <https://doi.org/10.1038/nature11861>
- Johnson, T. E. (1990). Increased life-span of age-1 mutants in *Caenorhabditis elegans* and lower gompertz rate of aging. *Science*, 249(4971), 908–912. <https://doi.org/10.1126/science.2392681>
- Jones, S. (2004). An overview of the basic helix-loop-helix proteins. *Genome Biology*, 5(6). <https://doi.org/10.1186/gb-2004-5-6-226>
- Jørgensen, S. B., Nielsen, J. N., Birk, J. B., Olsen, G. S., Viollet, B., Andreelli, F., Schjerling, P., Vaulont, S., Hardie, D. G., Hansen, B. F., Richter, E. A., & Wojtaszewski, J. F. P. (2004). The α 2-5' AMP-activated protein kinase is a site 2 glycogen synthase kinase in skeletal muscle and is responsive to glucose loading. *Diabetes*, 53(12), 3074–3081. <https://doi.org/10.2337/diabetes.53.12.3074>
- Ju, H. Q., Lin, J. F., Tian, T., Xie, D., & Xu, R. H. (2020). NADPH homeostasis in cancer: functions, mechanisms and therapeutic implications. *Signal Transduction and Targeted Therapy*, 5(1), 1–12. <https://doi.org/10.1038/s41392-020-00326-0>
- Jung, C. H., Jun, C. B., Ro, S.-H., Kim, Y.-M., Otto, N. M., Cao, J., Kundu, M., & Kim, D.-H. (2009). ULK-Atg13-FIP200 Complexes Mediate mTOR Signaling to the Autophagy Machinery. *Molecular Biology of the Cell*, 20, 1992–2003. <https://doi.org/10.1091/mbc.E08>
- Kaadige, M. R., Looper, R. E., Kamalanaadhan, S., & Ayer, D. E. (2009). Glutamine-dependent anapleurosis dictates glucose uptake and cell growth by regulating MondoA transcriptional activity. *Proceedings of the National Academy of Sciences of the United States of America*, 106(35), 14878–14883. <https://doi.org/10.1073/pnas.0901221106>
- Kaadige, M. R., Yang, J., Wilde, B. R., & Ayer, D. E. (2015). MondoA-Mlx Transcriptional Activity Is Limited by mTOR-MondoA Interaction. *Molecular and Cellular Biology*, 35(1), 101–110. <https://doi.org/10.1128/mcb.00636-14>
- Kabashima, T., Kawaguchi, T., Wadzinski, B. E., & Uyeda, K. (2003). Xylulose 5-phosphate mediates glucose-induced lipogenesis by xylulose 5-phosphate-activated protein phosphatase in rat liver. *Proceedings of the National Academy of Sciences of the United States of America*, 100(9), 5107–5112. <https://doi.org/10.1073/pnas.0730817100>
- Kaeberlein, T. L., Smith, E. D., Tsuchiya, M., Welton, K. L., Thomas, J. H., Fields, S., Kennedy, B. K., & Kaeberlein, M. (2006). Lifespan extension in *Caenorhabditis elegans* by complete

- removal of food. *Aging Cell*, 5(6), 487–494. <https://doi.org/10.1111/j.1474-9726.2006.00238.x>
- Kamath, R. S., & Ahringer, J. (2003). Genome-wide RNAi screening in *Caenorhabditis elegans*. *Methods*, 30(4), 313–321. [https://doi.org/10.1016/S1046-2023\(03\)00050-1](https://doi.org/10.1016/S1046-2023(03)00050-1)
- Kapahi, P., Chen, D., Rogers, A. N., Katewa, S. D., Li, P. W. L., Thomas, E. L., & Kockel, L. (2010). With TOR, less is more: A key role for the conserved nutrient-sensing TOR pathway in aging. *Cell Metabolism*, 11(6), 453–465. <https://doi.org/10.1016/j.cmet.2010.05.001>
- Kathiresan, S., Melander, O., Guiducci, C., Surti, A., Burt, N. P., Rieder, M. J., Cooper, G. M., Roos, C., Voight, B. F., Havulinna, A. S., Wahlstrand, B., Hedner, T., Corella, D., Tai, E. S., Ordovas, J. M., Berglund, G., Vartiainen, E., Jousilahti, P., Hedblad, B., ... Orholm, M. (2008). Six new loci associated with blood low-density lipoprotein cholesterol, high-density lipoprotein cholesterol or triglycerides in humans. *Nature Genetics*, 40(2), 189–197. <https://doi.org/10.1038/ng.75>
- Kawaguchi, T., Takenoshita, M., Kabashima, T., & Uyeda, K. (2001). Glucose and cAMP regulate the L-type pyruvate kinase gene by phosphorylation/dephosphorylation of the carbohydrate response element binding protein. *Proceedings of the National Academy of Sciences of the United States of America*, 98(24), 13710–13715. <https://doi.org/10.1073/pnas.231370798>
- Kawaguchi, Takumi, Osatomi, K., Yamashita, H., Kabashima, T., & Uyeda, K. (2002). Mechanism for fatty acid “sparing” effect on glucose-induced transcription: Regulation of carbohydrate-responsive element-binding protein by AMP-activated protein kinase. *Journal of Biological Chemistry*, 277(6), 3829–3835. <https://doi.org/10.1074/jbc.M107895200>
- Kayser, E. B., Morgan, P. G., Hoppel, C. L., & Sedensky, M. M. (2001). Mitochondrial Expression and Function of GAS-1 in *Caenorhabditis elegans*. *Journal of Biological Chemistry*, 276(23), 20551–20558. <https://doi.org/10.1074/jbc.M011066200>
- Kelley, D. E., & Mandarino, L. J. (1990). Hyperglycemia normalizes insulin-stimulated skeletal muscle glucose oxidation and storage in noninsulin-dependent diabetes mellitus. *Journal of Clinical Investigation*, 86(6), 1999–2007. <https://doi.org/10.1172/JCI114935>
- Kelley, D. E., & Simoneau, J. A. (1994). Impaired free fatty acid utilization by skeletal muscle in non-insulin-dependent diabetes mellitus. *Journal of Clinical Investigation*, 94(6), 2349–

2356. <https://doi.org/10.1172/JCI117600>
- Kennedy, B. K., & Lamming, D. W. (2016). The Mechanistic Target of Rapamycin: The Grand ConducTOR of Metabolism and Aging. *Cell Metabolism*, 23(6), 990–1003.
<https://doi.org/10.1016/j.cmet.2016.05.009>
- Kenyon, C., Chang, J., Gensch, E., Rudner, A., & Tabtiang, R. (1993). A *C. elegans* mutant that lives twice as long as wild type. *Nature*, 366(6454), 461–464.
<https://doi.org/10.1038/366461a0>
- Kenyon, C. J. (2010). The genetics of ageing. *Nature*, 464(7288), 504–512.
<https://doi.org/10.1038/nature08980>
- Khan, M. H., Ligon, M., Hussey, L. R., Hufnal, B., Farber, R., Munkácsy, E., Rodriguez, A., Dillow, A., Kahlig, E., & Rea, S. L. (2013). TAF-4 is required for the life extension of *isp-1*, *clk-1* and *tpk-1* Mit mutants. *Aging*, 5(10), 741–758.
<https://doi.org/10.18632/aging.100604>
- Kim, D. H., Sarbassov, D. D., Ali, S. M., King, J. E., Latek, R. R., Erdjument-Bromage, H., Tempst, P., & Sabatini, D. M. (2002). mTOR interacts with raptor to form a nutrient-sensitive complex that signals to the cell growth machinery. *Cell*, 110(2), 163–175.
[https://doi.org/10.1016/S0092-8674\(02\)00808-5](https://doi.org/10.1016/S0092-8674(02)00808-5)
- Kim, D., Langmead, B., & Salzberg, S. L. (2015). HISAT: A fast spliced aligner with low memory requirements. *Nature Methods*, 12(4), 357–360.
<https://doi.org/10.1038/nmeth.3317>
- Kim, E., Goraksha-Hicks, P., Li, L., Neufeld, T. P., & Guan, K. L. (2008). Regulation of TORC1 by Rag GTPases in nutrient response. *Nature Cell Biology*, 10(8), 935–945.
<https://doi.org/10.1038/ncb1753>
- Kim, J., Kundu, M., Viollet, B., & Guan, K. L. (2011). AMPK and mTOR regulate autophagy through direct phosphorylation of Ulk1. *Nature Cell Biology*, 13(2), 132–141.
<https://doi.org/10.1038/ncb2152>
- Kim, S., Wong, Y. C., Gao, F., & Krainc, D. (2021). Dysregulation of mitochondria-lysosome contacts by GBA1 dysfunction in dopaminergic neuronal models of Parkinson’s disease. *Nature Communications*, 12(1). <https://doi.org/10.1038/s41467-021-22113-3>
- Kimura, K. D., Tissenbaum, H. A., Liu, Y., & Ruvkun, G. (1997). Daf-2, an insulin receptor-like gene that regulates longevity and diapause in *Caenorhabditis elegans*. *Science*, 277(5328),

- 942–946. <https://doi.org/10.1126/science.277.5328.942>
- Kitaoka, S., Morielli, A. D., & Zhao, F. Q. (2013). FGT-1 Is a Mammalian GLUT2-Like Facilitative Glucose Transporter in *Caenorhabditis elegans* Whose Malfunction Induces Fat Accumulation in Intestinal Cells. *PLoS ONE*, 8(6), 1–13. <https://doi.org/10.1371/journal.pone.0068475>
- Klass, M. R. (1977). Aging in the nematode *Caenorhabditis elegans*: Major biological and environmental factors influencing life span. *Mechanisms of Ageing and Development*, 6(C), 413–429. [https://doi.org/10.1016/0047-6374\(77\)90043-4](https://doi.org/10.1016/0047-6374(77)90043-4)
- Klass, M. R. (1983). A method for the isolation of longevity mutants in the nematode *Caenorhabditis elegans* and initial results. *Mechanisms of Ageing and Development*, 22(3–4), 279–286. [https://doi.org/10.1016/0047-6374\(83\)90082-9](https://doi.org/10.1016/0047-6374(83)90082-9)
- Kontis, V., Bennett, J. E., Mathers, C. D., Li, G., Foreman, K., & Ezzati, M. (2017). Future life expectancy in 35 industrialised countries: projections with a Bayesian model ensemble. *The Lancet*, 389(10076), 1323–1335. [https://doi.org/10.1016/S0140-6736\(16\)32381-9](https://doi.org/10.1016/S0140-6736(16)32381-9)
- Koo, S. H., Flechner, L., Qi, L., Zhang, X., Srean, R. A., Jeffries, S., Hedrick, S., Xu, W., Boussouar, F., Brindle, P., Takemori, H., & Montminy, M. (2005). The CREB coactivator TORC2 is a key regulator of fasting glucose metabolism. *Nature*, 437(7062), 1109–1114. <https://doi.org/10.1038/nature03967>
- Kooner, J. S., Chambers, J. C., Aguilar-Salinas, C. A., Hinds, D. A., Hyde, C. L., Warnes, G. R., Gómez Pérez, F. J., Frazer, K. A., Elliott, P., Scott, J., Milos, P. M., Cox, D. R., & Thompson, J. F. (2008). Genome-wide scan identifies variation in MLXIPL associated with plasma triglycerides. *Nature Genetics*, 40(2), 149–151. <https://doi.org/10.1038/ng.2007.61>
- Koopman, M., Michels, H., Dancy, B. M., Kamble, R., Mouchiroud, L., Auwerx, J., Nollen, E. A. A., & Houtkooper, R. H. (2016). A screening-based platform for the assessment of cellular respiration in *Caenorhabditis elegans*. *Nature Protocols*, 11(10), 1798–1816. <https://doi.org/10.1038/nprot.2016.106>
- Kopec, S. (1928). On the influence of intermittent starvation on the longevity of the imaginal stage of *Drosophila melanogaster*. *Journal of Experimental Biology*, 5(3), 204–211. <https://doi.org/https://doi.org/10.1242/jeb.5.3.204>
- Krahmer, N., Najafi, B., Schueder, F., Quagliarini, F., Steger, M., Seitz, S., Kasper, R., Salinas, F., Cox, J., Uhlenhaut, N. H., Walther, T. C., Jungmann, R., Zeigerer, A., Borner, G. H. H.,

- & Mann, M. (2018). Organellar Proteomics and Phospho-Proteomics Reveal Subcellular Reorganization in Diet-Induced Hepatic Steatosis. *Developmental Cell*, 47(2), 205–221.e7. <https://doi.org/10.1016/j.devcel.2018.09.017>
- Kursawe, R., Caprio, S., Giannini, C., Narayan, D., Lin, A., D’Adamo, E., Shaw, M., Pierpont, B., Cushman, S. W., & Shulman, G. I. (2013). Decreased transcription of ChREBP-a/b isoforms in abdominal subcutaneous adipose tissue of obese adolescents with prediabetes or early type 2 diabetes associations with insulin resistance and hyperglycemia. *Diabetes*, 62(3), 837–844. <https://doi.org/10.2337/db12-0889>
- Kyte, J., & Doolittle, R. F. (1982). A simple method for displaying the hydropathic character of a protein. *Journal of Molecular Biology*, 157(1), 105–132. [https://doi.org/10.1016/0022-2836\(82\)90515-0](https://doi.org/10.1016/0022-2836(82)90515-0)
- Lagouge, M., Argmann, C., Gerhart-Hines, Z., Meziane, H., Lerin, C., Daussin, F., Messadeq, N., Milne, J., Lambert, P., Elliott, P., Geny, B., Laakso, M., Puigserver, P., & Auwerx, J. (2006). Resveratrol Improves Mitochondrial Function and Protects against Metabolic Disease by Activating SIRT1 and PGC-1 α . *Cell*, 127(6), 1109–1122. <https://doi.org/10.1016/j.cell.2006.11.013>
- Lai, C. H., Chou, C. Y., Ch’ang, L. Y., Liu, C. S., & Lin, W. C. (2000). Identification of novel human genes evolutionarily conserved in *Caenorhabditis elegans* by comparative proteomics. *Genome Research*, 10(5), 703–713. <https://doi.org/10.1101/gr.10.5.703>
- Lakowski, B., & Hekimi, S. (1996). Determination of life-span in *Caenorhabditis elegans* by four clock genes. *Science*, 272(5264), 1010–1013. <https://doi.org/10.1126/science.272.5264.1010>
- Lakowski, B., & Hekimi, S. (1998). The genetics of caloric restriction in *Caenorhabditis elegans*. *Proceedings of the National Academy of Sciences of the United States of America*, 95, 13091–13096. <https://doi.org/10.1073/pnas.95.22.13091>
- Lamming, D. W., Ye, L., Sabatini, D. M., & Baur, J. A. (2013). Rapalogs and mTOR inhibitors as anti-aging therapeutics. *Journal of Clinical Investigation*, 123(3), 980–989. <https://doi.org/10.1172/JCI64099>
- Lapierre, L. R., De Magalhaes Filho, C. D., McQuary, P. R., Chu, C. C., Visvikis, O., Chang, J. T., Gelino, S., Ong, B., Davis, A. E., Irazoqui, J. E., Dillin, A., & Hansen, M. (2013). The TFEB orthologue HLH-30 regulates autophagy and modulates longevity in *Caenorhabditis*

- C. elegans*. *Nature Communications*, 4. <https://doi.org/10.1038/ncomms3267>
- Lapierre, L. R., Gelino, S., Meléndez, A., & Hansen, M. (2011). Autophagy and lipid metabolism coordinately modulate life span in germline-less *C. elegans*. *Current Biology*, 21(18), 1507–1514. <https://doi.org/10.1016/j.cub.2011.07.042>
- Lapierre, L. R., Meléndez, A., & Hansen, M. (2012). Autophagy links lipid metabolism to longevity in *C. elegans*. *Autophagy*, 8(1), 144–146. <https://doi.org/10.4161/auto.8.1.18722>
- Laplanche, M., & Sabatini, D. M. (2012). mTOR signaling in growth control and disease. *Cell*, 149(2), 274–293. <https://doi.org/10.1016/j.cell.2012.03.017>
- Leduc-Gaudet, J. P., Picard, M., Pelletier, F. S. J., Sgarbi, N., Auger, M. J., Vallée, J., Robitaille, R., St-Pierre, D. H., & Gouspillou, G. (2015). Mitochondrial morphology is altered in atrophied skeletal muscle of aged mice. *Oncotarget*, 6(20), 17923–17937. <https://doi.org/10.18632/oncotarget.4235>
- Lee, D., Jeong, D. E., Son, H. G., Yamaoka, Y., Kim, H., Seo, K., Khan, A. A., Roh, T. Y., Moon, D. W., Lee, Y., & Lee, S. J. V. (2015). SREBP and MDT-15 protect *C. Elegans* from glucose-induced accelerated aging by preventing accumulation of saturated fat. *Genes and Development*, 29(23), 2490–2503. <https://doi.org/10.1101/gad.266304.115>
- Lee, John H., Tecedor, L., Chen, Y. H., Monteys, A. M., Sowada, M. J., Thompson, L. M., & Davidson, B. L. (2015). Reinstating aberrant mTORC1 activity in huntington's disease mice improves disease phenotypes. *Neuron*, 85(2), 303–315. <https://doi.org/10.1016/j.neuron.2014.12.019>
- Lee, Jung Hyun, Kong, J., Jang, J. Y., Han, J. S., Ji, Y., Lee, J., & Kim, J. B. (2014). Lipid Droplet Protein LID-1 Mediates ATGL-1-Dependent Lipolysis during Fasting in *Caenorhabditis elegans*. *Molecular and Cellular Biology*, 34(22), 4165–4176. <https://doi.org/10.1128/mcb.00722-14>
- Lee, K., Kerner, J., & Hoppel, C. L. (2011). Mitochondrial carnitine palmitoyltransferase 1a (CPT1a) is part of an outer membrane fatty acid transfer complex. *Journal of Biological Chemistry*, 286(29), 25655–25662. <https://doi.org/10.1074/jbc.M111.228692>
- Lee, S. J., Hwang, A. B., & Kenyon, C. (2010). Inhibition of respiration extends *C. elegans* life span via reactive oxygen species that increase HIF-1 activity. *Current Biology*, 20(23), 2131–2136. <https://doi.org/10.1016/j.cub.2010.10.057>
- Lee, S. S., Lee, R. Y. N., Fraser, A. G., Kamath, R. S., Ahringer, J., & Ruvkun, G. (2003). A

- systematic RNAi screen identifies a critical role for mitochondria in *C. elegans* longevity. *Nature Genetics*, 33(1), 40–48. <https://doi.org/10.1038/ng1056>
- Lehtinen, M. K., Yuan, Z., Boag, P. R., Yang, Y., Villén, J., Becker, E. B. E., DiBacco, S., de la Iglesia, N., Gygi, S., Blackwell, T. K., & Bonni, A. (2006). A Conserved MST-FOXO Signaling Pathway Mediates Oxidative-Stress Responses and Extends Life Span. *Cell*, 125(5), 987–1001. <https://doi.org/10.1016/j.cell.2006.03.046>
- Leigh-Brown, S., Enriquez, J. A., & Odom, D. T. (2010). Nuclear transcription factors in mammalian mitochondria. *Genome Biology*, 11(7), 1–9. <https://doi.org/10.1186/gb-2010-11-7-215>
- Li, F., Wang, Y., Zeller, K. I., Potter, J. J., Wonsey, D. R., O'Donnell, K. A., Kim, J., Yustein, J. T., Lee, L. A., & Dang, C. V. (2005). Myc Stimulates Nuclearly Encoded Mitochondrial Genes and Mitochondrial Biogenesis. *Molecular and Cellular Biology*, 25(14), 6225–6234. <https://doi.org/10.1128/mcb.25.14.6225-6234.2005>
- Li, H., Handsaker, B., Wysoker, A., Fennell, T., Ruan, J., Homer, N., Marth, G., Abecasis, G., & Durbin, R. (2009). The Sequence Alignment/Map format and SAMtools. *Bioinformatics*, 25(16), 2078–2079. <https://doi.org/10.1093/bioinformatics/btp352>
- Li, T., Zou, Y., Liu, S., Yang, Y., Zhang, Z., & Zhao, Y. (2022). Monitoring NAD(H) and NADP(H) dynamics during organismal development with genetically encoded fluorescent biosensors. *Cell Regeneration*, 11(1), 1–11. <https://doi.org/10.1186/s13619-021-00105-4>
- Li, M. V., Chang, B., Imamura, M., Pongvarin, N., & Chan, L. (2006). Glucose-dependent transcriptional regulation by an evolutionarily conserved glucose-sensing module. *Diabetes*, 55(5), 1179–1189. <https://doi.org/10.2337/db05-0822>
- Li, Y., Xu, S., Mihaylova, M. M., Zheng, B., Hou, X., Jiang, B., Park, O., Luo, Z., Lefai, E., Shyy, J. Y. J., Gao, B., Wierzbicki, M., Verbeuren, T. J., Shaw, R. J., Cohen, R. A., & Zang, M. (2011). AMPK phosphorylates and inhibits SREBP activity to attenuate hepatic steatosis and atherosclerosis in diet-induced insulin-resistant mice. *Cell Metabolism*, 13(4), 376–388. <https://doi.org/10.1016/j.cmet.2011.03.009>
- Liberti, M. V., & Locasale, J. W. (2016). The Warburg Effect: How Does it Benefit Cancer Cells? *Trends in Biochemical Sciences*, 41(3), 211–218. <https://doi.org/10.1016/j.tibs.2015.12.001>
- Libina, N., Berman, J. R., & Kenyon, C. (2003). Tissue-specific activities of *C. elegans* DAF-16

- in the regulation of lifespan. *Cell*, 115, 489–502.
[https://doi.org/https://doi.org/10.1016/S0092-8674\(03\)00889-4](https://doi.org/https://doi.org/10.1016/S0092-8674(03)00889-4)
- Lin, X. X., Sen, I., Janssens, G. E., Zhou, X., Fonslow, B. R., Edgar, D., Stroustrup, N., Swoboda, P., Yates, J. R., Ruvkun, G., & Riedel, C. G. (2018). DAF-16/FOXO and HLH-30/TFEB function as combinatorial transcription factors to promote stress resistance and longevity. *Nature Communications*, 9(1). <https://doi.org/10.1038/s41467-018-06624-0>
- Lindén, M., Gellerfors, P., & Dean Nelson, B. (1982). Pore protein and the hexokinase-binding protein from the outer membrane of rat liver mitochondria are identical. *FEBS Letters*, 141(2), 189–192. [https://doi.org/10.1016/0014-5793\(82\)80044-6](https://doi.org/10.1016/0014-5793(82)80044-6)
- Liu, G. Y., & Sabatini, D. M. (2020). mTOR at the nexus of nutrition, growth, ageing and disease. *Nature Reviews Molecular Cell Biology*, 21(4), 183–203.
<https://doi.org/10.1038/s41580-019-0199-y>
- Liu, Xingxing, Jiang, N., Hughes, B., Bigras, E., Shoubbridge, E., & Hekimi, S. (2005). Evolutionary conservation of the clk-1-dependent mechanism of longevity: Loss of melk1 increases cellular fitness and lifespan in mice. *Genes and Development*, 19(20), 2424–2434.
<https://doi.org/10.1101/gad.1352905>
- Liu, Xujun, Si, W., He, L., Yang, J., Peng, Y., Ren, J., Liu, X., Jin, T., Yu, H., Zhang, Z., Cheng, X., Zhang, W., Xia, L., Huang, Y., Wang, Y., Liu, S., Shan, L., Zhang, Y., Yang, X., ... Shang, Y. (2021). The existence of a nonclassical TCA cycle in the nucleus that wires the metabolic-epigenetic circuitry. *Signal Transduction and Targeted Therapy*, 6(1), 1–18.
<https://doi.org/10.1038/s41392-021-00774-2>
- Loeb, J., & Northrop, J. H. (1916). Is there a temperature coefficient for the duration of life? *Proc Natl Acad Sci U S A*, 2(8), 456–457.
- Loeb, J., & Northrop, J. H. (1917). On the influence of food and temperature upon the duration of Life. *Journal of Biological Chemistry*, 32(1), 103–121. [https://doi.org/10.1016/s0021-9258\(18\)86663-7](https://doi.org/10.1016/s0021-9258(18)86663-7)
- López-Otín, C., Blasco, M. A., Partridge, L., Serrano, M., & Kroemer, G. (2013). The hallmarks of aging. *Cell*, 153(6), 1194. <https://doi.org/10.1016/j.cell.2013.05.039>
- Lourenco, C., Resette, D., Redel, C., Lin, P., MacDonald, A. S., Ciaccio, R., Kenney, T. M. G., Wei, Y., Andrews, D. W., Sunnerhagen, M., Arrowsmith, C. H., Raught, B., & Penn, L. Z. (2021). MYC protein interactors in gene transcription and cancer. *Nature Reviews Cancer*,

- 21(9), 579–591. <https://doi.org/10.1038/s41568-021-00367-9>
- Luzarowski, M., Wojciechowska, I., & Skirycz, A. (2018). 2 in 1: One-step affinity purification for the parallel analysis of protein-protein and protein-metabolite complexes. *Journal of Visualized Experiments*, 2018(138), 1–10. <https://doi.org/10.3791/57720>
- Ma, L., Robinson, L. N., & Towle, H. C. (2006). ChREBP·Mlx is the principal mediator of glucose-induced gene expression in the liver. *Journal of Biological Chemistry*, 281(39), 28721–28730. <https://doi.org/10.1074/jbc.M601576200>
- Mair, W., Morante, I., Rodrigues, A. P. C., Manning, G., Montminy, M., Shaw, R. J., & Dillin, A. (2011). Lifespan extension induced by AMPK and calcineurin is mediated by CRTCL1 and CREB. *Nature*, 470(7334), 404–408. <https://doi.org/10.1038/nature09706>
- Mannick, J. B., Del Giudice, G., Lattanzi, M., Valiante, N. M., Praestgaard, J., Huang, B., Lonetto, M. A., Maecker, H. T., Kovarik, J., Carson, S., Glass, D. J., & Klickstein, L. B. (2014). mTOR inhibition improves immune function in the elderly. *Science Translational Medicine*, 6(268), 268ra179. <https://doi.org/10.1126/scitranslmed.3009892>
- Marchenko, N. D., Wolff, S., Erster, S., Becker, K., & Moll, U. M. (2007). Monoubiquitylation promotes mitochondrial p53 translocation. *EMBO Journal*, 26(4), 923–934. <https://doi.org/10.1038/sj.emboj.7601560>
- Marchesini, G., Brizi, M., Bianchi, G., Tomassetti, S., Bugianesi, E., Lenzi, M., McCullough, A. J., Natale, S., Forlani, G., & Melchionda, N. (2001). Nonalcoholic fatty liver disease: A feature of the Metabolic syndrome. *Diabetes*, 50(August), 1844–1850. <https://doi.org/10.2337/diabetes.50.8.1844>
- Marinov, G. K., Wang, Y. E., Chan, D., & Wold, B. J. (2014). Evidence for site-specific occupancy of the mitochondrial genome by nuclear transcription factors. *PLoS ONE*, 9(1), 1–24. <https://doi.org/10.1371/journal.pone.0084713>
- Marsin, A. S., Bouzin, C., Bertrand, L., & Hue, L. (2002). The stimulation of glycolysis by hypoxia in activated monocytes is mediated by AMP-activated protein kinase and inducible 6-phosphofructo-2-kinase. *Journal of Biological Chemistry*, 277(34), 30778–30783. <https://doi.org/10.1074/jbc.M205213200>
- Martina, J. A., Chen, Y., Gucek, M., & Puertollano, R. (2012). MTORC1 functions as a transcriptional regulator of autophagy by preventing nuclear transport of TFEB. *Autophagy*, 8(6), 903–914. <https://doi.org/10.4161/auto.19653>

- Martinez-Jimenez, C. P., Kyrmizi, I., Cardot, P., Gonzalez, F. J., & Talianidis, I. (2010). Hepatocyte Nuclear Factor 4 α Coordinates a Transcription Factor Network Regulating Hepatic Fatty Acid Metabolism. *Molecular and Cellular Biology*, 30(3), 565–577. <https://doi.org/10.1128/mcb.00927-09>
- Martínez-Reyes, I., & Chandel, N. S. (2020). Mitochondrial TCA cycle metabolites control physiology and disease. *Nature Communications*, 11(1), 1–11. <https://doi.org/10.1038/s41467-019-13668-3>
- Martínez, D. E. (1998). Mortality patterns suggest lack of senescence in hydra. *Experimental Gerontology*, 33(3), 217–225. [https://doi.org/10.1016/S0531-5565\(97\)00113-7](https://doi.org/10.1016/S0531-5565(97)00113-7)
- Masini, D., Bonito-Oliva, A., Bertho, M., & Fisone, G. (2018). Inhibition of mTORC1 signaling reverts cognitive and affective deficits in a mouse model of Parkinson's disease. *Frontiers in Neurology*, 9(APR), 1–8. <https://doi.org/10.3389/fneur.2018.00208>
- Mason, J. B., Cargill, S. L., Anderson, G. B., & Carey, J. R. (2009). Transplantation of young ovaries to old mice increased life Span in transplant recipients. *Journals of Gerontology - Series A Biological Sciences and Medical Sciences*, 64(12), 1207–1211. <https://doi.org/10.1093/gerona/glp134>
- Massari, M. E., & Murre, C. (2000). *Helix-Loop-Helix Proteins: Regulators of Transcription in Eucaryotic*. 20(2), 429–440. <https://doi.org/10.1128/mcb.20.2.429-440.2000>
- Mattison, J. A., Roth, G. S., Mark Beasley, T., Tilmont, E. M., Handy, A. M., Herbert, R. L., Longo, D. L., Allison, D. B., Young, J. E., Bryant, M., Barnard, D., Ward, W. F., Qi, W., Ingram, D. K., & De Cabo, R. (2012). Impact of caloric restriction on health and survival in rhesus monkeys from the NIA study. *Nature*, 489(7415), 318–321. <https://doi.org/10.1038/nature11432>
- McCay, C. M., Crowell, M. F., & Maynard, L. A. (1935). The effect of retarded growth upon the length of life span and upon the ultimate body size. *The Journal of Nutrition*, 10(1), 63–79. <https://doi.org/https://doi.org/10.1093/jn/10.1.63>
- McColl, G., Killilea, D. W., Hubbard, A. E., Vantipalli, M. C., Melov, S., & Lithgow, G. J. (2008). Pharmacogenetic analysis of lithium-induced delayed aging in *Caenorhabditis elegans*. *Journal of Biological Chemistry*, 283(1), 350–357. <https://doi.org/10.1074/jbc.M705028200>
- McFerrin, L. G., & Atchley, W. R. (2011). Evolution of the max and MIX networks in animals.

- Genome Biology and Evolution*, 3(1), 915–937. <https://doi.org/10.1093/gbe/evr082>
- Mejhert, N., Kuruvilla, L., Gabriel, K. R., Elliott, S. D., Guie, M. A., Wang, H., Lai, Z. W., Lane, E. A., Christiano, R., Danial, N. N., Farese, R. V., & Walther, T. C. (2020). Partitioning of MLX-Family Transcription Factors to Lipid Droplets Regulates Metabolic Gene Expression. *Molecular Cell*, 77(6), 1251–1264.e9. <https://doi.org/10.1016/j.molcel.2020.01.014>
- Meléndez, A., Tallóczy, Z., Seaman, M., Eskelinen, E. L., Hall, D. H., & Levine, B. (2003). Autophagy genes are essential for dauer development and life-span extension in *C. elegans*. *Science*, 301(5638), 1387–1391. <https://doi.org/10.1126/science.1087782>
- Melo, J. A., & Ruvkun, G. (2012). Inactivation of conserved *C. elegans* genes engages pathogen- and xenobiotic-associated defenses. *Cell*, 149(2), 452–466. <https://doi.org/10.1016/j.cell.2012.02.050>
- Metge, F., Sehlke, R., & Boucas, J. (2018). AGEpy: A Python package for computational biology. *BioRxiv*, 3–7. <https://doi.org/10.1101/450890>
- Mihaylova, M. M., Vasquez, D. S., Ravnskjaer, K., Denechaud, P. D., Yu, R. T., Alvarez, J. G., Downes, M., Evans, R. M., Montminy, M., & Shaw, R. J. (2011). Class IIa histone deacetylases are hormone-activated regulators of FOXO and mammalian glucose homeostasis. *Cell*, 145(4), 607–621. <https://doi.org/10.1016/j.cell.2011.03.043>
- Miller, R. A., Harrison, D. E., Astle, C. M., Fernandez, E., Flurkey, K., Han, M., Javors, M. A., Li, X., Nadon, N. L., Nelson, J. F., Pletcher, S., Salmon, A. B., Sharp, Z. D., Van Roekel, S., Winkleman, L., & Strong, R. (2014). Rapamycin-mediated lifespan increase in mice is dose and sex dependent and metabolically distinct from dietary restriction. *Aging Cell*, 13(3), 468–477. <https://doi.org/10.1111/accel.12194>
- Mitchell, S. M. S., Gloyn, A. L., Owen, K. R., Hattersley, A. T., & Frayling, T. M. (2002). The role of the HNF4 α enhancer in type 2 diabetes variants of the HNF4 α enhancer are not a common cause of susceptibility to type 2 diabetes. *Molecular Genetics and Metabolism*, 76(2), 148–151. [https://doi.org/10.1016/S1096-7192\(02\)00027-6](https://doi.org/10.1016/S1096-7192(02)00027-6)
- Miyoshi, M., Okajima, T., Matsuda, T., Fukuda, M. N., & Nadano, D. (2007). Bystin in human cancer cells: Intracellular localization and function in ribosome biogenesis. *Biochemical Journal*, 404(3), 373–381. <https://doi.org/10.1042/BJ20061597>
- Mockett, R. J., Sohal, B. H., & Sohal, R. S. (2010). Expression of multiple copies of

- mitochondrially targeted catalase or genomic Mn superoxide dismutase transgenes does not extend the life span of *Drosophila melanogaster*. *Free Radical Biology and Medicine*, 49(12), 2028–2031. <https://doi.org/10.1016/j.freeradbiomed.2010.09.029>
- Momcilovic, M., Hong, S. P., & Carlson, M. (2006). Mammalian TAK1 activates Snf1 protein kinase in yeast and phosphorylates AMP-activated protein kinase in vitro. *Journal of Biological Chemistry*, 281(35), 25336–25343. <https://doi.org/10.1074/jbc.M604399200>
- Mörck, C., & Pilon, M. (2006). *C. elegans* feeding defective mutants have shorter body lengths and increased autophagy. *BMC Developmental Biology*, 6, 1–11. <https://doi.org/10.1186/1471-213X-6-39>
- Motola, D. L., Cummins, C. L., Rottiers, V., Sharma, K. K., Li, T., Li, Y., Suino-Powell, K., Xu, H. E., Auchus, R. J., Antebi, A., & Mangelsdorf, D. J. (2006). Identification of Ligands for DAF-12 that Govern Dauer Formation and Reproduction in *C. elegans*. *Cell*, 124(6), 1209–1223. <https://doi.org/10.1016/j.cell.2006.01.037>
- Mouchiroud, L., Houtkooper, R. H., Moullan, N., Katsyuba, E., Ryu, D., Cantó, C., Mottis, A., Jo, Y. S., Viswanathan, M., Schoonjans, K., Guarente, L., & Auwerx, J. (2013). The NAD⁺/sirtuin pathway modulates longevity through activation of mitochondrial UPR and FOXO signaling. *Cell*, 154(2), 430. <https://doi.org/10.1016/j.cell.2013.06.016>
- Murphy, C. T., McCarroll, S. A., Lieb, J. D., Bargmann, C. I., Kamath, R. S., Fraser, A., Ahringer, J., Li, H., & Kenyon, C. J. (2003). Genes that act downstream of DAF-16 to influence *C. elegans* lifespan. *Nature*, 424, 277–283. www.nature.com/nature
- Mutlu, A. S., Gao, S. M., Zhang, H., & Wang, M. C. (2020). Olfactory specificity regulates lipid metabolism through neuroendocrine signaling in *Caenorhabditis elegans*. *Nature Communications*, 11(1), 1–15. <https://doi.org/10.1038/s41467-020-15296-8>
- Nagaraj, R., Sharpley, M. S., Chi, F., Braas, D., Zhou, Y., Kim, R., Clark, A. T., & Banerjee, U. (2017). Nuclear Localization of Mitochondrial TCA Cycle Enzymes as a Critical Step in Mammalian Zygotic Genome Activation. *Cell*, 168(1–2), 210–223.e11. <https://doi.org/10.1016/j.cell.2016.12.026>
- Nakagawa, T., Ge, Q., Pawlosky, R., Wynn, R. M., Veech, R. L., & Uyeda, K. (2013). Metabolite regulation of nucleo-cytosolic trafficking of carbohydrate response element-binding protein (ChREBP): Role of ketone bodies. *Journal of Biological Chemistry*, 288(39), 28358–28367. <https://doi.org/10.1074/jbc.M113.498550>

- Nakamura, S., Karalay, Ö., Jäger, P. S., Horikawa, M., Klein, C., Nakamura, K., Latza, C., Templer, S. E., Dieterich, C., & Antebi, A. (2016). Mondo complexes regulate TFEB via TOR inhibition to promote longevity in response to gonadal signals. *Nature Communications*, 7. <https://doi.org/10.1038/ncomms10944>
- Nargund, A. M., Pellegrino, M. W., Fiorese, C. J., Baker, B. M., & Haynes, C. M. (2012). Mitochondrial import efficiency of ATSF-1 regulates mitochondrial UPR activation. *Science*, 337(August), 587–590.
- Navale, A. M., & Paranjape, A. N. (2016). Glucose transporters: physiological and pathological roles. *Biophysical Reviews*, 8(1), 5–9. <https://doi.org/10.1007/s12551-015-0186-2>
- Nespital, T., Neuhaus, B., Mesaros, A., Pahl, A., & Partridge, L. (2021). Lithium can mildly increase health during ageing but not lifespan in mice. *Aging Cell*, 20(10), 1–6. <https://doi.org/10.1111/accel.13479>
- Nguyen, T. B., Louie, S. M., Daniele, J. R., Tran, Q., Dillin, A., Zoncu, R., Nomura, D. K., & Olzmann, J. A. (2017). DGAT1-Dependent Lipid Droplet Biogenesis Protects Mitochondrial Function during Starvation-Induced Autophagy. *Developmental Cell*, 42(1), 9–21.e5. <https://doi.org/10.1016/j.devcel.2017.06.003>
- Nishimura, K., Fukagawa, T., Takisawa, H., Kakimoto, T., & Kanemaki, M. (2009). An auxin-based degron system for the rapid depletion of proteins in nonplant cells. *Nature Methods*, 6(12), 917–922. <https://doi.org/10.1038/nmeth.1401>
- North, B. J., Rosenberg, M. A., Jeganathan, K. B., Hafner, A. V., Michan, S., Dai, J., Baker, D. J., Cen, Y., Wu, L. E., Sauve, A. A., Van Deursen, J. M., Rosenzweig, A., & Sinclair, D. A. (2014). SIRT2 induces the checkpoint kinase BubR1 to increase lifespan. *The EMBO Journal*, 33(13), 1438–1453.
- O’Rourke, E. J., & Ruvkun, G. (2013). MXL-3 and HLH-30 transcriptionally link lipolysis and autophagy to nutrient availability. *Nature Cell Biology*, 15(6), 668–676. <https://doi.org/10.1038/ncb2741>
- O’Rourke, E. J., Soukas, A. A., Carr, C. E., & Ruvkun, G. (2009). C. elegans Major Fats Are Stored in Vesicles Distinct from Lysosome-Related Organelles. *Cell Metabolism*, 10(5), 430–435. <https://doi.org/10.1016/j.cmet.2009.10.002>
- Oakhill, J. S., Steel, R., Chen, Z. P., Scott, J. W., Ling, N., Tam, S., & Kemp, B. E. (2011). AMPK is a direct adenylate charge-regulated protein kinase. *Science*, 332(6036), 1433–

1435. <https://doi.org/10.1126/science.1200094>
- Oeppen, J., & Vaupel, J. W. (2002). Broken Limits to Life Expectancy. *Science*, 296(5570), 1029–1031.
- Ogg, S., & Ruvkun, G. (1998). *The C. elegans PTEN homolog, DAF-18, acts in the insulin receptor-like metabolic signaling pathway*. 2, 887–893.
- Oh, S. W., Mukhopadhyay, A., Svrzikapa, N., Jiang, F., Davis, R. J., & Tissenbaum, H. A. (2005). JNK regulates lifespan in *Caenorhabditis elegans* by modulating nuclear translocation of forkhead transcription factor/DAF-16. *Proceedings of the National Academy of Sciences of the United States of America*, 102(12), 4494–4499. <https://doi.org/10.1073/pnas.0500749102>
- Ojha, A., Ojha, U., Mohammed, R., Chandrashekar, A., & Ojha, H. (2019). Current perspective on the role of insulin and glucagon in the pathogenesis and treatment of type 2 diabetes mellitus. *Clinical Pharmacology: Advances and Applications*, 11, 57–65. <https://doi.org/10.2147/CPAA.S202614>
- Onken, B., & Driscoll, M. (2010). Metformin induces a dietary restriction-like state and the oxidative stress response to extend *C. elegans* healthspan via AMPK, LKB1, and SKN-1. *PLoS ONE*, 5(1). <https://doi.org/10.1371/journal.pone.0008758>
- Orlandi, I., Coppola, D. P., & Vai, M. (2014). Rewiring yeast acetate metabolism through *mpc1* loss of function leads to mitochondrial damage and decreases chronological lifespan. *Microbial Cell*, 1(12), 393–405. <https://doi.org/10.15698/mic2014.12.178>
- Owen, O. E., Kalhan, S. C., & Hanson, R. W. (2002). The key role of anaplerosis and cataplerosis for citric acid cycle function. *Journal of Biological Chemistry*, 277(34), 30409–30412. <https://doi.org/10.1074/jbc.R200006200>
- Paillusson, S., Stoica, R., Gomez-Suaga, P., Lau, D. H. W., Mueller, S., Miller, T., & Miller, C. J. (2016). There's Something Wrong with my MAM; the ER-Mitochondria Axis and Neurodegenerative Diseases. *Trends in Neurosciences*, 39(3), 146–157. <https://doi.org/10.1016/j.tins.2016.01.008>
- Panowski, S. H., Wolff, S., Aguilaniu, H., Durieux, J., & Dillin, A. (2007). PHA-4/Foxa mediates diet-restriction-induced longevity of *C. elegans*. *Nature*, 447(7144), 550–555. <https://doi.org/10.1038/nature05837>
- Park, S., Artan, M., Han, S. H., Park, H. E. H., Jung, Y., Hwan, A. B., Shin, W. S., Kim, K. T., &

- Lee, S. J. V. (2020). VRK-1 extends life span by activation of AMPK via phosphorylation. *Science Advances*, 6(27), 1–14. <https://doi.org/10.1126/sciadv.aaw7824>
- Passtoors, W. M., Beekman, M., Deelen, J., van der Breggen, R., Maier, A. B., Guigas, B., Derhovanessian, E., van Heemst, D., de Craen, A. J. M., Gunn, D. A., Pawelec, G., & Slagboom, P. E. (2013). Gene expression analysis of mTOR pathway: Association with human longevity. *Aging Cell*, 12(1), 24–31. <https://doi.org/10.1111/accel.12015>
- Pastorino, J. G., Shulga, N., & Hoek, J. B. (2002). Mitochondrial binding of hexokinase II inhibits Bax-induced cytochrome c release and apoptosis. *Journal of Biological Chemistry*, 277(9), 7610–7618. <https://doi.org/10.1074/jbc.M109950200>
- Pawlikowska, L., Hu, D., Huntsman, S., Sung, A., Chu, C., Chen, J., Joyner, A. H., Schork, N. J., Hsueh, W. C., Reiner, A. P., Psaty, B. M., Atzmon, G., Barzilai, N., Cummings, S. R., Browner, W. S., Kwok, P. Y., & Ziv, E. (2009). Association of common genetic variation in the insulin/IGF1 signaling pathway with human longevity. *Aging Cell*, 8(4), 460–472. <https://doi.org/10.1111/j.1474-9726.2009.00493.x>
- Pearl, R., & Parker, S. L. (1921). Experimental Studies on the Duration of Life. I. Introductory Discussion of the Duration of Life in *Drosophila*. *The American Naturalist*, 55(641), 481–509. <https://doi.org/https://doi.org/10.1086/279836>
- Penkov, S., Kaptan, D., Erkut, C., Sarov, M., Mende, F., & Kurzchalia, T. V. (2015). Integration of carbohydrate metabolism and redox state controls dauer larva formation in *Caenorhabditis elegans*. *Nature Communications*, 6. <https://doi.org/10.1038/ncomms9060>
- Perez, C. L., & Van Gilst, M. R. (2008). A ¹³C Isotope Labeling Strategy Reveals the Influence of Insulin Signaling on Lipogenesis in *C. elegans*. *Cell Metabolism*, 8(3), 266–274. <https://doi.org/10.1016/j.cmet.2008.08.007>
- Perez, M. F., & Lehner, B. (2019). Vitellogenins - Yolk Gene Function and Regulation in *Caenorhabditis elegans*. *Frontiers in Physiology*, 10(August). <https://doi.org/10.3389/fphys.2019.01067>
- Pertea, M., Kim, D., Pertea, G. M., Leek, J. T., & Salzberg, S. L. (2016). Transcript-level expression analysis of RNA-seq experiments with HISAT, StringTie and Ballgown. *Nature Protocols*, 11(9), 1650–1667. <https://doi.org/10.1038/nprot.2016.095>
- Peterson, C. W., Stoltzman, C. A., Sighinolfi, M. P., Han, K.-S., & Ayer, D. E. (2010). Glucose Controls Nuclear Accumulation, Promoter Binding, and Transcriptional Activity of the

- MondoA-Mlx Heterodimer. *Molecular and Cellular Biology*, 30(12), 2887–2895.
<https://doi.org/10.1128/mcb.01613-09>
- Peyrefitte, S., Kahn, D., & Haenlin, M. (2001). New members of the Drosophila Myc transcription factor subfamily revealed by a genome-wide examination for basic helix-loop-helix genes. *Mechanisms of Development*, 104(1–2), 99–104.
[https://doi.org/10.1016/S0925-4773\(01\)00360-4](https://doi.org/10.1016/S0925-4773(01)00360-4)
- Phillips, J. P., Campbell, S. D., Michaud, D., Charbonneau, M., & Hilliker, A. J. (1989). Null mutation of copper/zinc superoxide dismutase in Drosophila confers hypersensitivity to paraquat and reduced longevity. *Proceedings of the National Academy of Sciences of the United States of America*, 86(8), 2761–2765. <https://doi.org/10.1073/pnas.86.8.2761>
- Piazza, I., Kochanowski, K., Cappelletti, V., Fuhrer, T., Noor, E., Sauer, U., & Picotti, P. (2018). A Map of Protein-Metabolite Interactions Reveals Principles of Chemical Communication. *Cell*, 172(1–2), 358–372.e23. <https://doi.org/10.1016/j.cell.2017.12.006>
- Pickett, C. L., Breen, K. T., & Ayer, D. E. (2007). A C. elegans Myc-like network cooperates with semaphorin and Wnt signaling pathways to control cell migration. *Developmental Biology*, 310(2), 226–239. <https://doi.org/10.1016/j.ydbio.2007.07.034>
- Pidoux, G., Witezak, O., Jarnss, E., Myrvold, L., Urlaub, H., Stokka, A. J., Küntziger, T., & Taskén, K. (2011). Optic atrophy 1 is an A-kinase anchoring protein on lipid droplets that mediates adrenergic control of lipolysis. *EMBO Journal*, 30(21), 4371–4386.
<https://doi.org/10.1038/emboj.2011.365>
- Pollock, C., & Huang, S. (2009). The perinucleolar compartment. *Journal of Cellular Biochemistry*, 107(2), 189–193. <https://doi.org/10.1002/jcb.22107>
- Postic, C., Dentin, R., Denechaud, P. D., & Girard, J. (2007). ChREBP, a transcriptional regulator of glucose and lipid metabolism. *Annual Review of Nutrition*, 27, 179–192.
<https://doi.org/10.1146/annurev.nutr.27.061406.093618>
- Poungvarin, N., Chang, B., Imamura, M., Chen, J., Moolsuwan, K., Sae-Lee, C., Li, W., & Chan, L. (2015). Genome-wide analysis of ChREBP binding sites on male mouse liver and white adipose chromatin. *Endocrinology*, 156(6), 1982–1994. <https://doi.org/10.1210/en.2014-1666>
- Prendergast, G. C., Lawe, D., & Ziff, E. B. (1991). Association of Myn, the murine homolog of Max, with c-Myc stimulates methylation-sensitive DNA binding and ras cotransformation.

- Cell*, 65(3), 395–407. [https://doi.org/10.1016/0092-8674\(91\)90457-A](https://doi.org/10.1016/0092-8674(91)90457-A)
- R Core Team. (2017). *R: A language and environment for statistical computing* (3.4.3). R Foundation for Statistical Computing. <https://www.r-project.org/>
- Rajman, L., Chwalek, K., & Sinclair, D. A. (2018). Therapeutic Potential of NAD-Boosting Molecules: The In Vivo Evidence. *Cell Metabolism*, 27(3), 529–547. <https://doi.org/10.1016/j.cmet.2018.02.011>
- Ralser, M., Wamelink, M. M., Struys, E. A., Joppich, C., Krobitsch, S., Jakobs, C., & Lehrach, H. (2008). A catabolic block does not sufficiently explain how 2-deoxy-D-glucose inhibits cell growth. *Proceedings of the National Academy of Sciences of the United States of America*, 105(46), 17807–17811. <https://doi.org/10.1073/pnas.0803090105>
- Ramachandran, P. V., Savini, M., Folick, A. K., Hu, K., Masand, R., Graham, B. H., & Wang, M. C. (2019). Lysosomal Signaling Promotes Longevity by Adjusting Mitochondrial Activity. *Developmental Cell*, 48(5), 685-696.e5. <https://doi.org/10.1016/j.devcel.2018.12.022>
- Rambold, A. S., Cohen, S., & Lippincott-Schwartz, J. (2015). Fatty acid trafficking in starved cells: Regulation by lipid droplet lipolysis, autophagy, and mitochondrial fusion dynamics. *Developmental Cell*, 32(6), 678–692. <https://doi.org/10.1016/j.devcel.2015.01.029>
- Rambold, A. S., Kostecky, B., Elia, N., & Lippincott-Schwartz, J. (2011). Tubular network formation protects mitochondria from autophagosomal degradation during nutrient starvation. *Proceedings of the National Academy of Sciences of the United States of America*, 108(25), 10190–10195. <https://doi.org/10.1073/pnas.1107402108>
- Rana, A., Rera, M., & Walker, D. W. (2013). Parkin overexpression during aging reduces proteotoxicity, alters mitochondrial dynamics, and extends lifespan. *Proceedings of the National Academy of Sciences of the United States of America*, 110(21), 8638–8643. <https://doi.org/10.1073/pnas.1216197110>
- Rappuoli, R., Pizza, M., Del Giudice, G., & De Gregorio, E. (2014). Vaccines, new opportunities for a new society. *Proceedings of the National Academy of Sciences of the United States of America*, 111(34), 12288–12293. <https://doi.org/10.1073/pnas.1402981111>
- Ratnappan, R., Amrit, F. R. G., Chen, S. W., Gill, H., Holden, K., Ward, J., Yamamoto, K. R., Olsen, C. P., & Ghazi, A. (2014). Germline Signals Deploy NHR-49 to Modulate Fatty-Acid β -Oxidation and Desaturation in Somatic Tissues of *C. elegans*. *PLoS Genetics*,

- 10(12). <https://doi.org/10.1371/journal.pgen.1004829>
- Rea, S. L., Ventura, N., & Johnson, T. E. (2007). Relationship between mitochondrial electron transport chain dysfunction, development, and life extension in *Caenorhabditis elegans*. *PLoS Biology*, 5(10), 2312–2329. <https://doi.org/10.1371/journal.pbio.0050259>
- Rebsamen, M., Pochini, L., Stasyk, T., De Araújo, M. E. G., Galluccio, M., Kandasamy, R. K., Snijder, B., Fauster, A., Rudashevskaya, E. L., Bruckner, M., Scorzoni, S., Filipek, P. A., Huber, K. V. M., Bigenzahn, J. W., Heinz, L. X., Kraft, C., Bennett, K. L., Indiveri, C., Huber, L. A., & Superti-Furga, G. (2015). SLC38A9 is a component of the lysosomal amino acid sensing machinery that controls mTORC1. *Nature*, 519(7544), 477–481. <https://doi.org/10.1038/nature14107>
- Regan, J. C., Khericha, M., Dobson, A. J., Bolukbasi, E., Rattanavirotkul, N., & Partridge, L. (2016). Sex difference in pathology of the ageing gut mediates the greater response of female lifespan to dietary restriction. *ELife*, 5(FEBRUARY2016), 1–16. <https://doi.org/10.7554/eLife.10956>
- Riddle, D. L., Swanson, M. M., & Albert, P. S. (1981). Interacting genes in nematode dauer larva formation. *Nature*, 290(5808), 668–671. <https://doi.org/10.1038/290668a0>
- Rieusset, J. (2018). The role of endoplasmic reticulum-mitochondria contact sites in the control of glucose homeostasis: An update. *Cell Death and Disease*, 9(3), 1–12. <https://doi.org/10.1038/s41419-018-0416-1>
- Ritchie, M. E., Phipson, B., Wu, D., Hu, Y., Law, C. W., Shi, W., & Smyth, G. K. (2015). limma powers differential expression analyses for RNA-sequencing and microarray studies. *Nucleic Acids Research*, 43(7), e47. <https://doi.org/10.1093/nar/gkv007>
- Roberts, D. J., Tan-Sah, V. P., Ding, E. Y., Smith, J. M., & Miyamoto, S. (2014). Hexokinase-II Positively Regulates Glucose Starvation-Induced Autophagy through TORC1 Inhibition. *Molecular Cell*, 53(4), 521–533. <https://doi.org/10.1016/j.molcel.2013.12.019>
- Robida-Stubbs, S., Glover-Cutter, K., Lamming, D. W., Mizunuma, M., Narasimhan, S. D., Neumann-Haefelin, E., Sabatini, D. M., & Blackwell, T. K. (2012). TOR signaling and rapamycin influence longevity by regulating SKN-1/Nrf and DAF-16/FoxO. *Cell Metabolism*, 15(5), 713–724. <https://doi.org/10.1016/j.cmet.2012.04.007>
- Roczniak-Ferguson, A., Petit, C. S., Froehlich, F., Qian, S., Ky, J., Angarola, B., Walther, T. C., & Ferguson, S. M. (2012). The transcription factor TFEB links mTORC1 signaling to

- transcriptional control of lysosome homeostasis. *Science Signaling*, 5(228).
<https://doi.org/10.1126/scisignal.2002790>
- Rousakis, A., Vlassis, A., Vlanti, A., Patera, S., Thireos, G., & Syntichaki, P. (2013). The general control nonderepressible-2 kinase mediates stress response and longevity induced by target of rapamycin inactivation in *Caenorhabditis elegans*. *Aging Cell*, 12(5), 742–751.
<https://doi.org/10.1111/accel.12101>
- Rual, J. F., Ceron, J., Koreth, J., Hao, T., Nicot, A. S., Hirozane-Kishikawa, T., Vandenhaute, J., Orkin, S. H., Hill, D. E., van den Heuvel, S., & Vidal, M. (2004). Toward improving *Caenorhabditis elegans* phenome mapping with an ORFeome-based RNAi library. *Genome Research*, 14(10 B), 2162–2168. <https://doi.org/10.1101/gr.2505604>
- Ruiz, M., Bodhicharla, R., Ståhlman, M., Svensk, E., Busayavalasa, K., Palmgren, H., Ruhanen, H., Boren, J., & Pilon, M. (2019). Evolutionarily 1 conserved long-chain acyl-coa synthetases regulate membrane composition and fluidity. *ELife*, 8, 1–31.
<https://doi.org/10.7554/eLife.47733>
- Runkel, E. D., Liu, S., Baumeister, R., & Schulze, E. (2013). Surveillance-Activated Defenses Block the ROS-Induced Mitochondrial Unfolded Protein Response. *PLoS Genetics*, 9(3).
<https://doi.org/10.1371/journal.pgen.1003346>
- Sakamoto, K., & Holman, G. D. (2008). Emerging role for AS160/TBC1D4 and TBC1D1 in the regulation of GLUT4 traffic. *American Journal of Physiology - Endocrinology and Metabolism*, 295(1), 29–37. <https://doi.org/10.1152/ajpendo.90331.2008>
- Sakiyama, H., Wynn, R. M., Lee, W. R., Fukasawa, M., Mizuguchi, H., Gardner, K. H., Repa, J. J., & Uyeda, K. (2008). Regulation of nuclear import/export of carbohydrate response element-binding protein (ChREBP): Interaction of an α -helix of ChREBP with the 14-3-3 proteins and regulation by phosphorylation. *Journal of Biological Chemistry*, 283(36), 24899–24908. <https://doi.org/10.1074/jbc.M804308200>
- Sampath, H., Miyazaki, M., Dobrzyn, A., & Ntambi, J. M. (2007). Stearoyl-CoA desaturase-1 mediates the pro-lipogenic effects of dietary saturated fat. *Journal of Biological Chemistry*, 282(4), 2483–2493. <https://doi.org/10.1074/jbc.M610158200>
- Sancak, Y., Peterson, T. R., Shaul, Y. D., Lindquist, R. A., Thoreen, C. C., Bar-Peled, L., & Sabatini, D. M. (2008). The rag GTPases bind raptor and mediate amino acid signaling to mTORC1. *Science*, 320(5882), 1496–1501. <https://doi.org/10.1126/science.1157535>

- Sans, C. L., Satterwhite, D. J., Stoltzman, C. A., Breen, K. T., & Ayer, D. E. (2006). MondoA-Mlx Heterodimers Are Candidate Sensors of Cellular Energy Status: Mitochondrial Localization and Direct Regulation of Glycolysis. *Molecular and Cellular Biology*, 26(13), 4863–4871. <https://doi.org/10.1128/mcb.00657-05>
- Sarbassov, D. D., Ali, S. M., Kim, D.-H., Guertin, D. A., Latek, R. R., Erdjument-Bromage, H., Tempst, P., & Sabatini, D. M. (2004). Rictor, a novel binding partner of mTOR, defines a rapamycin-insensitive and raptor-independent pathway that regulates the cytoskeleton. *Current Biology*, 14, 1296–1302. [https://doi.org/https://doi.org/10.1016/j.cub.2004.06.054](https://doi.org/10.1016/j.cub.2004.06.054)
- Sato, S., Jung, H., Nakagawa, T., Pawlosky, R., Takeshima, T., Lee, W. R., Sakiyama, H., Laxman, S., Wynn, R. M., Tu, B. P., MacMillan, J. B., De Brabander, J. K., Veech, R. L., & Uyeda, K. (2016). Metabolite regulation of nuclear localization of carbohydrate-response element-binding protein (ChREBP): Role of amp as an allosteric inhibitor. *Journal of Biological Chemistry*, 291(20), 10515–10527. <https://doi.org/10.1074/jbc.M115.708982>
- Saxton, R. A., Knockenhauer, K. E., Wolfson, R. L., Chantranupong, L., Pacold, M. E., Wang, T., Schwartz, T. U., & Sabatini, D. M. (2016). Structural basis for leucine sensing by the Sestrin2-mTORC1 pathway. *Science*, 351(6268), 53–58. <https://doi.org/10.1126/science.aad2087>
- Scheckhuber, C. Q., Erjavec, N., Tinazli, A., Hamann, A., Nyström, T., & Osiewacz, H. D. (2007). Reducing mitochondrial fission results in increased life span and fitness of two fungal ageing models. *Nature Cell Biology*, 9(1), 99–105. <https://doi.org/10.1038/ncb1524>
- Schrepfer, E., & Scorrano, L. (2016). Mitofusins, from Mitochondria to Metabolism. *Molecular Cell*, 61(5), 683–694. <https://doi.org/10.1016/j.molcel.2016.02.022>
- Schulz, T. J., Zarse, K., Voigt, A., Urban, N., Birringer, M., & Ristow, M. (2007). Glucose Restriction Extends Caenorhabditis elegans Life Span by Inducing Mitochondrial Respiration and Increasing Oxidative Stress. *Cell Metabolism*, 6(4), 280–293. <https://doi.org/10.1016/j.cmet.2007.08.011>
- Schuster, E., McElwee, J. J., Tullet, J. M. A., Doonan, R., Matthijssens, F., Reece-Hoyes, J. S., Hope, I. A., Vanfleteren, J. R., Thornton, J. M., & Gems, D. (2010). DamID in C. elegans reveals longevity-associated targets of DAF-16/FoxO. *Molecular Systems Biology*, 6(399), 1–6. <https://doi.org/10.1038/msb.2010.54>
- Sebastián, D., Sorianello, E., Segalés, J., Irazoki, A., Ruiz-Bonilla, V., Sala, D., Planet, E.,

- Berenguer-Llargo, A., Muñoz, J. P., Sánchez-Feutrie, M., Plana, N., Hernández-Álvarez, M. I., Serrano, A. L., Palacín, M., & Zorzano, A. (2016). Mfn2 deficiency links age-related sarcopenia and impaired autophagy to activation of an adaptive mitophagy pathway. *The EMBO Journal*, 35(15), 1677–1693. <https://doi.org/10.15252/emboj.201593084>
- Selman, C., Lingard, S., Choudhury, A. I., Batterham, R. L., Claret, M., Clements, M., Ramadani, F., Okkenhaug, K., Schuster, E., Blanc, E., Piper, M. D., Al-Qassab, H., Speakman, J. R., Carmignac, D., Robinson, I. C. A., Thornton, J. M., Gems, D., Partridge, L., & Withers, D. J. (2008). Evidence for lifespan extension and delayed age-related biomarkers in insulin receptor substrate 1 null mice. *The FASEB Journal*, 22(3), 807–818. <https://doi.org/10.1096/fj.07-9261com>
- Senchuk, M. M., Dues, D. J., Schaar, C. E., Johnson, B. K., Madaj, Z. B., Bowman, M. J., Winn, M. E., & Van Raamsdonk, J. M. (2018). Activation of DAF-16/FOXO by reactive oxygen species contributes to longevity in long-lived mitochondrial mutants in *Caenorhabditis elegans*. *PLoS Genetics*, 14(3), 1–27. <https://doi.org/10.1371/journal.pgen.1007268>
- Senoo-Matsuda, N., Yasuda, K., Tsuda, M., Ohkubo, T., Yoshimura, S., Nakazawa, H., Hartman, P. S., & Ishii, N. (2001). A Defect in the Cytochrome b Large Subunit in Complex II Causes Both Superoxide Anion Overproduction and Abnormal Energy Metabolism in *Caenorhabditis elegans*. *Journal of Biological Chemistry*, 276(45), 41553–41558. <https://doi.org/10.1074/jbc.M104718200>
- Seo, K., Choi, E., Lee, D., Jeong, D. E., Jang, S. K., & Lee, S. J. (2013). Heat shock factor 1 mediates the longevity conferred by inhibition of TOR and insulin/IGF-1 signaling pathways in *C. elegans*. *Aging Cell*, 12(6), 1073–1081. <https://doi.org/10.1111/accel.12140>
- Settembre, C., Di Malta, C., Polito, V. A., Garcia, M., Vetrini, F., Erdin, S. U. S., Erdin, S. U. S., Huynh, T., Medina, D., Colella, P., Sardiello, M., Rubinsztein, D. C., & Ballabio, A. (2011). TFEB links autophagy to lysosomal biogenesis. *Science*, 332(6036), 1429–1433. <https://doi.org/10.1126/science.1204592.TFEB>
- Settembre, C., Zoncu, R., Medina, D. L., Vetrini, F., Erdin, S., Erdin, S., Huynh, T., Ferron, M., Karsenty, G., Vellard, M. C., Facchinetti, V., Sabatini, D. M., & Ballabio, A. (2012). A lysosome-to-nucleus signalling mechanism senses and regulates the lysosome via mTOR and TFEB. *EMBO Journal*, 31(5), 1095–1108. <https://doi.org/10.1038/emboj.2012.32>
- Sgrò, C. M., & Partridge, L. (1999). A delayed wave of death from reproduction in *Drosophila*.

- Science*, 286(5449), 2521–2524. <https://doi.org/10.1126/science.286.5449.2521>
- Shaw, W. M., Luo, S., Landis, J., Ashraf, J., & Murphy, C. T. (2007). The C. elegans TGF- β Dauer Pathway Regulates Longevity via Insulin Signaling. *Current Biology*, 17(19), 1635–1645. <https://doi.org/10.1016/j.cub.2007.08.058>
- Sheaffer, K. L., Updike, D. L., & Mango, S. E. (2008). The Target of Rapamycin Pathway Antagonizes pha-4/FoxA to Control Development and Aging. *Current Biology*, 18(18), 1355–1364. <https://doi.org/10.1016/j.cub.2008.07.097>
- Singh, P., & Irwin, D. M. (2016). Contrasting patterns in the evolution of vertebrate MLX Interacting Protein (MLXIP) and MLX Interacting Protein-Like (MLXIPL) genes. *PLoS ONE*, 11(2). <https://doi.org/10.1371/journal.pone.0149682>
- Slack, C., Alic, N., Foley, A., Cabecinha, M., Hoddinott, M. P., & Partridge, L. (2015). The Ras-Erk-ETS-Signaling Pathway Is a Drug Target for Longevity. *Cell*, 162(1), 72–83. <https://doi.org/10.1016/j.cell.2015.06.023>
- Smith, H. J., Sharma, A., & Mair, W. B. (2020). Metabolic Communication and Healthy Aging: Where Should We Focus Our Energy? *Developmental Cell*, 54(2), 196–211. <https://doi.org/10.1016/j.devcel.2020.06.011>
- Soare, A., Cangemi, R., Omodei, D., Holloszy, J. O., & Fontana, L. (2011). Long-term calorie restriction, but not endurance exercise, lowers core body temperature in humans. *Aging*, 3(4), 374–379. <https://doi.org/10.18632/aging.100280>
- Sonenberg, N., & Hinnebusch, A. G. (2009). Regulation of Translation Initiation in Eukaryotes: Mechanisms and Biological Targets. *Cell*, 136(4), 731–745. <https://doi.org/10.1016/j.cell.2009.01.042>
- Spilman, P., Podlitskaya, N., Hart, M. J., Debnath, J., Gorostiza, O., Bredesen, D., Richardson, A., Strong, R., & Galvan, V. (2010). Inhibition of mTOR by rapamycin abolishes cognitive deficits and reduces amyloid- β levels in a mouse model of alzheimer's disease. *PLoS ONE*, 5(4), 1–8. <https://doi.org/10.1371/journal.pone.0009979>
- Spoel, V. Der, Rozing, M. P., Duistermaat, J. J. H., Eline, P., Beekman, M., Craen, A. J. M. De, & Westendorp, R. G. J. (2015). Association analysis of insulin-like growth factor-1 axis parameters with survival and functional status in nonagenarians of the Leiden Longevity Study. 7(11), 956–963.
- Stadtman, E. R. (1992). Protein Oxidation and Aging. *Science*, 257(August), 1220–1224.

<https://doi.org/10.1126/science.1355616>

- Steinbaugh, M. J., Narasimhan, S. D., Robida-Stubbs, S., Moronetti Mazzeo, L. E., Dreyfuss, J. M., Hourihan, J. M., Raghavan, P., Operaña, T. N., Esmailie, R., & Blackwell, T. K. (2015). Lipid-mediated regulation of SKN-1/Nrf in response to germ cell absence. *ELife*, 4(JULY2015), 1–30. <https://doi.org/10.7554/eLife.07836>
- Steinkraus, K. A., Smith, E. D., Davis, C., Carr, D., Pendergrass, W. R., Sutphin, G. L., Kennedy, B. K., & Kaerberlein, M. (2008). Dietary restriction suppresses proteotoxicity and enhances longevity by an hsf-1-dependent mechanism in *Caenorhabditis elegans*. *Aging Cell*, 7(3), 394–404. <https://doi.org/10.1111/j.1474-9726.2008.00385.x>
- Stenesen, D., Suh, J. M., Seo, J., Yu, K., Lee, K. S., Kim, J. S., Min, K. J., & Graff, J. M. (2013). Adenosine nucleotide biosynthesis and AMPK regulate adult life span and mediate the longevity benefit of caloric restriction in flies. *Cell Metabolism*, 17(1), 101–112. <https://doi.org/10.1016/j.cmet.2012.12.006>
- Stoltzman, C. A., Kaadige, M. R., Peterson, C. W., & Ayer, D. E. (2011). MondoA senses non-glucose sugars: Regulation of thioredoxin-interacting protein (TXNIP) and the hexose transport curb. *Journal of Biological Chemistry*, 286(44), 38027–38034. <https://doi.org/10.1074/jbc.M111.275503>
- Stoltzman, C. A., Peterson, C. W., Breen, K. T., Muoio, D. M., Billin, A. N., & Ayer, D. E. (2008). Glucose sensing by MondoA: Mlx complexes: A role for hexokinases and direct regulation of thioredoxin-interacting protein expression. *Proceedings of the National Academy of Sciences of the United States of America*, 105(19), 6912–6917. <https://doi.org/10.1073/pnas.0712199105>
- Sui, D., & Wilson, J. E. (1997). Structural determinants for the intracellular localization of the isozymes of mammalian hexokinase: Intracellular localization of fusion constructs incorporating structural elements from the hexokinase isozymes and the green fluorescent protein. *Archives of Biochemistry and Biophysics*, 345(1), 111–125. <https://doi.org/10.1006/abbi.1997.0241>
- Sun, Jiayi, Shen, X., Liu, H., Lu, S., Peng, J., & Kuang, H. (2020). Caloric restriction in female reproduction: is it beneficial or detrimental? *Reproductive Biology and Endocrinology*, 13(1), 1–11. <https://doi.org/https://doi.org/10.1186/s12958-020-00681-1>
- Sun, Jingtao, & Tower, J. (1999). FLP Recombinase-Mediated Induction of Cu/Zn-Superoxide

- Dismutase Transgene Expression Can Extend the Life Span of Adult *Drosophila melanogaster* Flies . *Molecular and Cellular Biology*, 19(1), 216–228.
<https://doi.org/10.1128/mcb.19.1.216>
- Sutendra, G., Kinnaird, A., Dromparis, P., Paulin, R., Stenson, T. H., Haromy, A., Hashimoto, K., Zhang, N., Flaim, E., & Michelakis, E. D. (2014). A nuclear pyruvate dehydrogenase complex is important for the generation of Acetyl-CoA and histone acetylation. *Cell*, 158(1), 84–97. <https://doi.org/10.1016/j.cell.2014.04.046>
- Swindell, W. R. (2012). Dietary restriction in rats and mice: A meta-analysis and review of the evidence for genotype-dependent effects on lifespan. *Ageing Research Reviews*, 11(2), 254–270. <https://doi.org/10.1016/j.arr.2011.12.006>
- Tang, D., Tao, S., Chen, Z., Koliesnik, I. O., Calmes, P. G., Hoerr, V., Han, B., Gebert, N., Zörnig, M., Löffler, B., Morita, Y., & Rudolph, K. L. (2016). Dietary restriction improves repopulation but impairs lymphoid differentiation capacity of hematopoietic stem cells in early aging. *Journal of Experimental Medicine*, 213(4), 535–553.
<https://doi.org/10.1084/JEM.20151100>
- Tao, R., Zhao, Y., Chu, H., Wang, A., Zhu, J., Chen, X., Zou, Y., Shi, M., Liu, R., Su, N., Du, J., Zhou, H. M., Zhu, L., Qian, X., Liu, H., Loscalzo, J., & Yang, Y. (2017). Genetically encoded fluorescent sensors reveal dynamic regulation of NADPH metabolism. *Nature Methods*, 14(7), 720–728. <https://doi.org/10.1038/nmeth.4306>
- Taormina, G., Ferrante, F., Vieni, S., Grassi, N., Russo, A., & Mirisola, M. G. (2019). Longevity: Lesson from model organisms. *Genes*, 10(7).
<https://doi.org/10.3390/genes10070518>
- Tatenaka, Y., Kato, H., Ishiyama, M., Sasamoto, K., Shiga, M., Nishitoh, H., & Ueno, Y. (2019). Monitoring Lipid Droplet Dynamics in Living Cells by Using Fluorescent Probes. *Biochemistry*, 58(6), 499–503. <https://doi.org/10.1021/acs.biochem.8b01071>
- Tee, A. R., & Blenis, J. (2005). mTOR, translational control and human disease. *Seminars in Cell and Developmental Biology*, 16(1), 29–37.
<https://doi.org/10.1016/j.semcdb.2004.11.005>
- Tharyan, R. G., Annibal, A., Schiffer, I., Laboy, R., Atanassov, I., Weber, A. L., Gerisch, B., & Antebi, A. (2020). NFYB-1 regulates mitochondrial function and longevity via lysosomal prosaposin. *Nature Metabolism*, 2(5), 387–396. <https://doi.org/10.1038/s42255-020-0200-2>

- Tiku, V., Jain, C., Raz, Y., Nakamura, S., Heestand, B., Liu, W., Späth, M., Suchiman, H. E. D., Müller, R.-U., Slagboom, P. E., Partridge, L., & Antebi, A. (2017). Small nucleoli are a cellular hallmark of longevity. *Nature Communications*, 8(August).
<https://doi.org/10.1038/ncomms16083>
- Tissenbaum, H. A., & Guarente, L. (2002). Model organisms as a guide to mammalian aging. *Developmental Cell*, 2(1), 9–19. [https://doi.org/10.1016/S1534-5807\(01\)00098-3](https://doi.org/10.1016/S1534-5807(01)00098-3)
- Tomczyk, S., Fischer, K., Austad, S., & Galliot, B. (2015). Hydra, a powerful model for aging studies. *Invertebrate Reproduction and Development*, 59(2012), 11–16.
<https://doi.org/10.1080/07924259.2014.927805>
- Tong, X., Zhao, F., Mancuso, A., Gruber, J. J., & Thompson, C. B. (2009). The glucose-responsive transcription factor ChREBP contributes to glucose-dependent anabolic synthesis and cell proliferation. *Proceedings of the National Academy of Sciences of the United States of America*, 106(51), 21660–21665. <https://doi.org/10.1073/pnas.0911316106>
- Tóth, M. L., Sigmond, T., Borsos, É., Barna, J., Erdélyi, P., Takács-Vellai, K., Orosz, L., Kovács, A. L., Csikós, G., Sass, M., & Vellai, T. (2008). Longevity pathways converge on autophagy genes to regulate life span in *Caenorhabditis elegans*. *Autophagy*, 4(3), 330–338.
<https://doi.org/10.4161/auto.5618>
- Tower, J. (2017). Sex-Specific Gene Expression and Life Span Regulation. *Trends in Endocrinology and Metabolism*, 28(10), 735–747.
<https://doi.org/10.1016/j.tem.2017.07.002>
- Trapnell, C., Hendrickson, D. G., Sauvageau, M., Goff, L., Rinn, J. L., & Pachter, L. (2013). Differential analysis of gene regulation at transcript resolution with RNA-seq. *Nature Biotechnology*, 31(1), 46–53. <https://doi.org/10.1038/nbt.2450>
- Tsatsos, N. G., & Towle, H. C. (2006). Glucose activation of ChREBP in hepatocytes occurs via a two-step mechanism. *Biochemical and Biophysical Research Communications*, 340(2), 449–456. <https://doi.org/10.1016/j.bbrc.2005.12.029>
- Tsou, P., Zheng, B., Hsu, C. H., Sasaki, A. T., & Cantley, L. C. (2011). A fluorescent reporter of AMPK activity and cellular energy stress. *Cell Metabolism*, 13(4), 476–486.
<https://doi.org/10.1016/j.cmet.2011.03.006>
- Tsun, Z. Y., Bar-Peled, L., Chantranupong, L., Zoncu, R., Wang, T., Kim, C., Spooner, E., & Sabatini, D. M. (2013). The folliculin tumor suppressor is a GAP for the RagC/D GTPases

- that signal amino acid levels to mTORC1. *Molecular Cell*, 52(4), 495–505.
<https://doi.org/10.1016/j.molcel.2013.09.016>
- Tullet, J. M. A., Araiz, C., Sanders, M. J., Au, C., Benedetto, A., Papatheodorou, I., Clark, E., Schmeisser, K., Jones, D., Schuster, E. F., Thornton, J. M., & Gems, D. (2014). DAF-16/FoxO Directly Regulates an Atypical AMP-Activated Protein Kinase Gamma Isoform to Mediate the Effects of Insulin/IGF-1 Signaling on Aging in *Caenorhabditis elegans*. *PLoS Genetics*, 10(2). <https://doi.org/10.1371/journal.pgen.1004109>
- Vacca, M., Allison, M., Griffin, J. L., & Vidal-Puig, A. (2015). Fatty Acid and Glucose Sensors in Hepatic Lipid Metabolism: Implications in NAFLD. *Seminars in Liver Disease*, 35(3), 250–261. <https://doi.org/10.1055/s-0035-1562945>
- Valenzano, D. R., Aboobaker, A., Seluanov, A., & Gorbunova, V. (2017). Non-canonical aging model systems and why we need them. *The EMBO Journal*, 36(8), 959–963.
<https://doi.org/10.15252/embj.201796837>
- van den Berg, N., Rodríguez-Girondo, M., van Dijk, I. K., Mourits, R. J., Mandemakers, K., Janssens, A. A. P. O., Beekman, M., Smith, K. R., & Slagboom, P. E. (2019). Longevity defined as top 10% survivors and beyond is transmitted as a quantitative genetic trait. *Nature Communications*, 10(1). <https://doi.org/10.1038/s41467-018-07925-0>
- Van Gilst, M. R., Hadjivassiliou, H., & Yamamoto, K. R. (2005). A *Caenorhabditis elegans* nutrient response system partially dependent on nuclear receptor NHR-49. *Proceedings of the National Academy of Sciences of the United States of America*, 102(38), 13496–13501.
<https://doi.org/10.1073/pnas.0506234102>
- Van Raamsdonk, J. M., & Hekimi, S. (2009). Deletion of the mitochondrial superoxide dismutase sod-2 extends lifespan in *Caenorhabditis elegans*. *PLoS Genetics*, 5(2).
<https://doi.org/10.1371/journal.pgen.1000361>
- Van Raamsdonk, J. M., & Hekimi, S. (2012). Superoxide dismutase is dispensable for normal animal lifespan. *Proceedings of the National Academy of Sciences of the United States of America*, 109(15), 5785–5790. <https://doi.org/10.1073/pnas.1116158109>
- Varga, T., Czimmerer, Z., & Nagy, L. (2011). PPARs are a unique set of fatty acid regulated transcription factors controlling both lipid metabolism and inflammation. *Biochimica et Biophysica Acta - Molecular Basis of Disease*, 1812(8), 1007–1022.
<https://doi.org/10.1016/j.bbadis.2011.02.014>

- Vézina, C., Kudelski, A., & Sehgal, S. N. (1975). Rapamycin (AY-22,989), a new antifungal antibiotic. I. Taxonomy of the producing streptomycete and isolation of the active principle. *The Journal of Antibiotics*, 28(10), 721–726. <https://doi.org/10.7164/antibiotics.28.721>
- Vivian, J. T., & Callis, P. R. (2001). Mechanisms of tryptophan fluorescence shifts in proteins. *Biophysical Journal*, 80(5), 2093–2109. [https://doi.org/10.1016/S0006-3495\(01\)76183-8](https://doi.org/10.1016/S0006-3495(01)76183-8)
- Vonolfen, M. (2020). *Upstream Regulators of MML-1 / Mondo Nuclear Localization and Activity* (Issue October). University of Cologne.
- Vrablik, T. L., Petyuk, V. A., Larson, E. M., Smith, R. D., & Watts, J. L. (2015). Lipidomic and proteomic analysis of *Caenorhabditis elegans* lipid droplets and identification of ACS-4 as a lipid droplet-associated protein. *Biochimica et Biophysica Acta - Molecular and Cell Biology of Lipids*, 1851(10), 1337–1345. <https://doi.org/10.1016/j.bbalip.2015.06.004>
- Wai, T., & Langer, T. (2016). Mitochondrial Dynamics and Metabolic Regulation. *Trends in Endocrinology and Metabolism*, 27(2), 105–117. <https://doi.org/10.1016/j.tem.2015.12.001>
- Walter, L., Baruah, A., Chang, H. W., Pace, H. M., & Lee, S. S. (2011). The homeobox protein CEH-23 mediates prolonged longevity in response to impaired Mitochondrial Electron Transport Chain in *C. elegans*. *PLoS Biology*, 9(6). <https://doi.org/10.1371/journal.pbio.1001084>
- Wang, D., Malo, D., & Hekimi, S. (2010). Elevated Mitochondrial Reactive Oxygen Species Generation Affects the Immune Response via Hypoxia-Inducible Factor-1 α in Long-Lived Mcl1 +/– Mouse Mutants. *The Journal of Immunology*, 184(2), 582–590. <https://doi.org/10.4049/jimmunol.0902352>
- Wang, J., Ban, M. R., Zou, G. Y., Cao, H., Lin, T., Kennedy, B. A., Anand, S., Yusuf, S., Huff, M. W., Pollex, R. L., & Hegele, R. A. (2008). Polygenic determinants of severe hypertriglyceridemia. *Human Molecular Genetics*, 17(18), 2894–2899. <https://doi.org/10.1093/hmg/ddn188>
- Wang, M. C., O'Rourke, E. J., & Ruvkun, G. (2008). Fat metabolism links germline stem cells and longevity in *C. elegans*. *Science*, 322(5903), 957–960. <https://doi.org/10.1126/science.1162011>
- Wang, S., Tsun, Z. Y., Wolfson, R. L., Shen, K., Wyant, G. A., Plovanich, M. E., Yuan, E. D., Jones, T. D., Chantranupong, L., Comb, W., Wang, T., Bar-Peled, L., Zoncu, R., Straub, C., Kim, C., Park, J., Sabatini, B. L., & Sabatini, D. M. (2015). Lysosomal amino acid

- transporter SLC38A9 signals arginine sufficiency to mTORC1. *Science*, 347(6218), 188–194. <https://doi.org/10.1126/science.1257132>
- Wang, X., Pandey, A. K., Mulligan, M. K., Williams, E. G., Mozhui, K., Li, Z., Jovaisaite, V., Quarles, L. D., Xiao, Z., Huang, J., Capra, J. A., Chen, Z., Taylor, W. L., Bastarache, L., Niu, X., Pollard, K. S., Ciobanu, D. C., Reznik, A. O., Tishkov, A. V., ... Williams, R. W. (2016). Joint mouse-human phenome-wide association to test gene function and disease risk. *Nature Communications*, 7. <https://doi.org/10.1038/ncomms10464>
- Wang, Y., Guo, Y. R., Liu, K., Yin, Z., Liu, R., Xia, Y., Tan, L., Yang, P., Lee, J. H., Li, X. J., Hawke, D., Zheng, Y., Qian, X., Lyu, J., He, J., Xing, D., Tao, Y. J., & Lu, Z. (2017). KAT2A coupled with the α -KGDH complex acts as a histone H3 succinyltransferase. *Nature*, 552(7684), 273–277. <https://doi.org/10.1038/nature25003>
- Warburg, O. (1925). The metabolism of carcinoma cells. *The Journal of Cancer Research*, 9(1), 148–163. <https://doi.org/10.1158/jcr.1925.148>
- Wawryn, J., Krzepiřko, A., Myska, A., & Biliński, T. (1999). Deficiency in superoxide dismutases shortens life span of yeast cells. In *Acta Biochimica Polonica* (Vol. 46, Issue 2, pp. 249–253). https://doi.org/10.18388/abp.1999_4158
- Weir, H. J., Yao, P., Huynh, F. K., Escoubas, C. C., Goncalves, R. L., Burkewitz, K., Laboy, R., Hirschey, M. D., & Mair, W. B. (2017). Dietary Restriction and AMPK Increase Lifespan via Mitochondrial Network and Peroxisome Remodeling. *Cell Metabolism*, 26(6), 884–896.e5. <https://doi.org/10.1016/j.cmet.2017.09.024>
- Wilde, B. R., Ye, Z., Lim, T. Y., & Ayer, D. E. (2019). Cellular acidosis triggers human monooxygenase transcriptional activity by driving mitochondrial atp production. *ELife*, 8, 1–25. <https://doi.org/10.7554/eLife.40199>
- Willcox, B. J., Donlon, T. A., He, Q., Chen, R., Grove, J. S., Yano, K., Masaki, K. H., Willcox, D. C., Rodriguez, B., & Curb, J. D. (2008). FOXO3A genotype is strongly associated with human longevity. *Proceedings of the National Academy of Sciences of the United States of America*, 105(37), 13987–13992. <https://doi.org/10.1073/pnas.0801030105>
- Wilson, E. L., & Metzakopian, E. (2021). ER-mitochondria contact sites in neurodegeneration: genetic screening approaches to investigate novel disease mechanisms. *Cell Death and Differentiation*, 28(6), 1804–1821. <https://doi.org/10.1038/s41418-020-00705-8>
- Wilson, J. E. (2003). Isozymes of mammalian hexokinase: Structure, subcellular localization and

- metabolic function. *Journal of Experimental Biology*, 206(12), 2049–2057.
<https://doi.org/10.1242/jeb.00241>
- Winston, W. M., Molodowitch, C., & Hunter, C. P. (2002). Systemic RNAi in *C. elegans* requires the putative transmembrane protein SID-1. *Science*, 295(5564), 2456–2459.
<https://doi.org/10.1126/science.1068836>
- Wolf, A. J., Reyes, C. N., Liang, W., Becker, C., Shimada, K., Wheeler, M. L., Cho, H. C., Popescu, N. I., Coggeshall, K. M., Arditi, M., & Underhill, D. M. (2016). Hexokinase Is an Innate Immune Receptor for the Detection of Bacterial Peptidoglycan. *Cell*, 166(3), 624–636. <https://doi.org/10.1016/j.cell.2016.05.076>
- Wolkow, C. A., Muñoz, M. J., Riddle, D. L., & Ruvkun, G. (2002). Insulin receptor substrate and p55 orthologous adaptor proteins function in the *Caenorhabditis elegans* daf-2/insulin-like signaling pathway. *Journal of Biological Chemistry*, 277(51), 49591–49597.
<https://doi.org/10.1074/jbc.M207866200>
- Wood, J. G., Rogina, B., Lavu, S., Howitz, K., Helfand, S. L., Tatar, M., & Sinclair, D. (2004). Erratum: corrigendum: Sirtuin activators mimic caloric restriction and delay ageing in metazoans. *Nature*, 431(7004), 107–107. <https://doi.org/10.1038/nature02941>
- Woods, A., Dickerson, K., Heath, R., Hong, S. P., Momcilovic, M., Johnstone, S. R., Carlson, M., & Carling, D. (2005). Ca²⁺/calmodulin-dependent protein kinase kinase- β acts upstream of AMP-activated protein kinase in mammalian cells. *Cell Metabolism*, 2(1), 21–33. <https://doi.org/10.1016/j.cmet.2005.06.005>
- Woods, A., Williams, J. R., Muckett, P. J., Mayer, F. V., Liljevald, M., Bohlooly-Y, M., & Carling, D. (2017). Liver-Specific Activation of AMPK Prevents Steatosis on a High-Fructose Diet. *Cell Reports*, 18(13), 3043–3051.
<https://doi.org/10.1016/j.celrep.2017.03.011>
- Wu, J. J., Liu, J., Chen, E. B., Wang, J. J., Cao, L., Narayan, N., Fergusson, M. M., Rovira, I. I., Allen, M., Springer, D. A., Lago, C. U., Zhang, S., DuBois, W., Ward, T., deCabo, R., Gavrilova, O., Mock, B., & Finkel, T. (2013). Increased mammalian lifespan and a segmental and tissue-specific slowing of aging after genetic reduction of mTOR expression. *Cell Reports*, 4(5), 913–920. <https://doi.org/10.1016/j.celrep.2013.07.030>
- Wu, N., Zheng, B., Shaywitz, A., Dagon, Y., Tower, C., Bellinger, G., Shen, C. H., Wen, J., Asara, J., McGraw, T. E., Kahn, B. B., & Cantley, L. C. (2013). AMPK-Dependent

- Degradation of TXNIP upon Energy Stress Leads to Enhanced Glucose Uptake via GLUT1. *Molecular Cell*, 49(6), 1167–1175. <https://doi.org/10.1016/j.molcel.2013.01.035>
- Wu, S., Zhou, F., Zhang, Z., & Xing, D. (2011). Mitochondrial oxidative stress causes mitochondrial fragmentation via differential modulation of mitochondrial fission-fusion proteins. *FEBS Journal*, 278(6), 941–954. <https://doi.org/10.1111/j.1742-4658.2011.08010.x>
- Wu, Z., Senchuk, M. M., Dues, D. J., Johnson, B. K., Cooper, J. F., Lew, L., Machiela, E., Schaar, C. E., DeJonge, H., Blackwell, T. K., & Van Raamsdonk, J. M. (2018). Mitochondrial unfolded protein response transcription factor ATFS-1 promotes longevity in a long-lived mitochondrial mutant through activation of stress response pathways. *BMC Biology*, 16(1), 1–19. <https://doi.org/10.1186/s12915-018-0615-3>
- Xiao, B., Sanders, M. J., Underwood, E., Heath, R., Mayer, F. V., Carmena, D., Jing, C., Walker, P. A., Eccleston, J. F., Haire, L. F., Saiu, P., Howell, S. A., Aasland, R., Martin, S. R., Carling, D., & Gamblin, S. J. (2011). Structure of mammalian AMPK and its regulation by ADP. *Nature*, 472(7342), 230–233. <https://doi.org/10.1038/nature09932>
- Xu, N., Zhang, S. O., Cole, R. A., McKinney, S. A., Guo, F., Haas, J. T., Bobba, S., Farese, R. V., & Mak, H. Y. (2012). The FATP1-DGAT2 complex facilitates lipid droplet expansion at the ER-lipid droplet interface. *Journal of Cell Biology*, 198(5), 895–911. <https://doi.org/10.1083/jcb.201201139>
- Yamaguchi, T., Kakefuda, R., Tajima, N., Sowa, Y., & Sakai, T. (2011). Antitumor activities of JTP-74057 (GSK1120212), a novel MEK1/2 inhibitor, on colorectal cancer cell lines in vitro and in vivo. *International Journal of Oncology*, 39(1), 23–31. <https://doi.org/10.3892/ijo.2011.1015>
- Yamashita, H., Takenoshita, M., Sakurai, M., Bruick, R. K., Henzel, W. J., Shillinglaw, W., Arnot, D., & Uyeda, K. (2001). A glucose-responsive transcription factor that regulates carbohydrate metabolism in the liver. *Proceedings of the National Academy of Sciences of the United States of America*, 98(16), 9116–9121. <https://doi.org/10.1073/pnas.161284298>
- Yamawaki, T. M., Berman, J. R., Suchanek-Kavipurapu, M., McCormick, M., Gaglia, M. M., Lee, S. J., & Kenyon, C. (2010). The somatic reproductive tissues of *C. elegans* promote longevity through steroid hormone signaling. *PLoS Biology*, 8(8), 45–46. <https://doi.org/10.1371/journal.pbio.1000468>

- Yang, Weiwei, Xia, Y., Ji, H., Zheng, Y., Liang, J., Huang, W., Gao, X., Aldape, K., & Lu, Z. (2011). Nuclear PKM2 regulates β -catenin transactivation upon EGFR activation. *Nature*, 480(7375), 118–122. <https://doi.org/10.1038/nature10598>
- Yang, Wen, & Hekimi, S. (2010). Two modes of mitochondrial dysfunction lead independently to lifespan extension in *Caenorhabditis elegans*. *Aging Cell*, 9(3), 433–447. <https://doi.org/10.1111/j.1474-9726.2010.00571.x>
- Yang, X., Mudgett, J., Bou-About, G., Champy, M. F., Jacobs, H., Monassier, L., Pavlovic, G., Sorg, T., Herault, Y., Petit-Demoulière, B., Lu, K., Feng, W., Wang, H., Ma, L. J., Askew, R., Erion, M. D., Kelley, D. E., Myers, R. W., Li, C., & Guan, H. P. (2016). Physiological expression of *ampk γ 2RG* Mutation causes Wolff-Parkinson-White syndrome and induces kidney injury in mice. *Journal of Biological Chemistry*, 291(45), 23428–23439. <https://doi.org/10.1074/jbc.M116.738591>
- Yavari, A., Stocker, C. J., Ghaffari, S., Wargent, E. T., Steeples, V., Czibik, G., Pinter, K., Bellahcene, M., Woods, A., Martínez De Morentin, P. B., Cansell, C., Lam, B. Y. H., Chuster, A., Petkevicius, K., Nguyen-Tu, M. S., Martinez-Sanchez, A., Pullen, T. J., Oliver, P. L., Stockenhuber, A., ... Ashrafi, H. (2016). Chronic Activation of γ 2 AMPK Induces Obesity and Reduces β Cell Function. *Cell Metabolism*, 23(5), 821–836. <https://doi.org/10.1016/j.cmet.2016.04.003>
- Yoneda, T., Benedetti, C., Urano, F., Clark, S. G., Harding, H. P., & Ron, D. (2004). Compartment-specific perturbation of protein handling activates genes encoding mitochondrial chaperones. *Journal of Cell Science*, 117(18), 4055–4066. <https://doi.org/10.1242/jcs.01275>
- Young, P. A., Senkal, C. E., Suchanek, A. L., Grevenkoed, T. J., Lin, D. D., Zhao, L., Crunk, A. E., Klett, E. L., Füllekrug, J., Obeid, L. M., & Coleman, R. A. (2019). Long-chain acyl-CoA synthetase 1 interacts with key proteins that activate and direct fatty acids into niche hepatic pathways. *Journal of Biological Chemistry*, 293(43), 16724–16740. <https://doi.org/10.1074/jbc.RA118.004049>
- Yu, Y., Yoon, S. O., Poulogiannis, G., Yang, Q., Ma, X. M., Villén, J., Kubica, N., Hoffman, G. R., Cantley, L. C., Gygi, S. P., & Blenis, J. (2011). Phosphoproteomic analysis identifies Grb10 as an mTORC1 substrate that negatively regulates insulin signaling. *Science*, 332(6035), 1322–1326. <https://doi.org/10.1126/science.1199484>

- Yuan, X., Ta, T. C., Lin, M., Evans, J. R., Dong, Y., Bolotin, E., Sherman, M. A., Forman, B. M., & Sladek, F. M. (2009). Identification of an endogenous ligand bound to a native orphan nuclear receptor. *PLoS ONE*, 4(5). <https://doi.org/10.1371/journal.pone.0005609>
- Zarse, K., Terao, T., Tian, J., Iwata, N., Ishii, N., & Ristow, M. (2011). Low-dose lithium uptake promotes longevity in humans and metazoans. *European Journal of Nutrition*, 50(5), 387–389. <https://doi.org/10.1007/s00394-011-0171-x>
- Zhang, J., Zhang, Y. L., Zhao, L. W., Guo, J. X., Yu, J. L., Ji, S. Y., Cao, L. R., Zhang, S. Y., Shen, L., Ou, X. H., & Fan, H. Y. (2019). Mammalian nucleolar protein DCAF13 is essential for ovarian follicle maintenance and oocyte growth by mediating rRNA processing. *Cell Death and Differentiation*, 26(7), 1251–1266. <https://doi.org/10.1038/s41418-018-0203-7>
- Zhang, P., Na, H., Liu, Z., Zhang, S., Xue, P., Chen, Y., Pu, J., Peng, G., Huang, X., Yang, F., Xie, Z., Xu, T., Xu, P., Ou, G., Zhang, S. O., & Liu, P. (2012). Proteomic study and marker protein identification of *Caenorhabditis elegans* lipid droplets. *Molecular and Cellular Proteomics*, 11(8), 317–328. <https://doi.org/10.1074/mcp.M111.016345>
- Zhang, Y., Lanjuin, A., Chowdhury, S. R., Mistry, M., Silva-García, C. G., Weir, H. J., Chia-Lin, L., Escoubas, C. C., Tabakovic, E., & Mair, W. B. (2019). Neuronal TORC1 modulates longevity via ampk and cell nonautonomous regulation of mitochondrial dynamics in *C. Elegans*. *ELife*, 8, 1–24. <https://doi.org/10.7554/eLife.49158>
- Zheng, S., Chiu, H., Boudreau, J., Papanicolaou, T., Bendena, W., & Chin-Sang, I. (2019). A functional study of all 40 *Caenorhabditis elegans* insulin-like peptides. *Journal of Biological Chemistry*, 293(43), 16912–16922. <https://doi.org/10.1074/jbc.RA118.004542>
- Zielinska, D. F., Gnad, F., Jedrusik-Bode, M., Wiśniewski, J. R., & Mann, M. (2009). *Caenorhabditis elegans* has a phosphoproteome atypical for metazoans that is enriched in developmental and sex determination proteins. *Journal of Proteome Research*, 8(8), 4039–4049. <https://doi.org/10.1021/pr900384k>
- Zorzano, A., Liesa, M., & Palacín, M. (2009). Role of mitochondrial dynamics proteins in the pathophysiology of obesity and type 2 diabetes. *International Journal of Biochemistry and Cell Biology*, 41(10), 1846–1854. <https://doi.org/10.1016/j.biocel.2009.02.004>

XIII. Erklärung

Erklärung zur Dissertation gemäß der Promotionsordnung vom 12. März 2020

Diese Erklärung muss in der Dissertation enthalten sein.
(This version must be included in the doctoral thesis)

„Hiermit versichere ich an Eides statt, dass ich die vorliegende Dissertation selbstständig und ohne die Benutzung anderer als der angegebenen Hilfsmittel und Literatur angefertigt habe. Alle Stellen, die wörtlich oder sinngemäß aus veröffentlichten und nicht veröffentlichten Werken dem Wortlaut oder dem Sinn nach entnommen wurden, sind als solche kenntlich gemacht. Ich versichere an Eides statt, dass diese Dissertation noch keiner anderen Fakultät oder Universität zur Prüfung vorgelegen hat; dass sie - abgesehen von unten angegebenen Teilpublikationen und eingebundenen Artikeln und Manuskripten - noch nicht veröffentlicht worden ist sowie, dass ich eine Veröffentlichung der Dissertation vor Abschluss der Promotion nicht ohne Genehmigung des Promotionsausschusses vornehmen werde. Die Bestimmungen dieser Ordnung sind mir bekannt. Darüber hinaus erkläre ich hiermit, dass ich die Ordnung zur Sicherung guter wissenschaftlicher Praxis und zum Umgang mit wissenschaftlichem Fehlverhalten der Universität zu Köln gelesen und sie bei der Durchführung der Dissertation zugrundeliegenden Arbeiten und der schriftlich verfassten Dissertation beachtet habe und verpflichte mich hiermit, die dort genannten Vorgaben bei allen wissenschaftlichen Tätigkeiten zu beachten und umzusetzen. Ich versichere, dass die eingereichte elektronische Fassung der eingereichten Druckfassung vollständig entspricht.“

Teilpublikationen:

23.09.2021

Raymond Alexis Laboy Morales



Datum, Name und Unterschrift

XIV. Curriculum vitae

RAYMOND ALEXIS LABOY MORALES



Date of birth: July 23th, 1994
Country of birth: Puerto Rico
Nationality: American

Max Planck Institute for Biology of Ageing
Department of Molecular Genetics of Ageing
Joseph-Stelzmann-Str. 9b
50931 Cologne, Germany
rmorales@age.mpg.de
+49 (0) 221 37970 454

University Education

- 2016 - Present • **University of Cologne (UoC)** Cologne, Germany
Ph.D. in Genetics
- 2012 - 2016 • **Universidad Nacional Autónoma de México (UNAM)** Mexico City, Mexico
B.Sc. in Biology
- 2011 - 2012 • **University of Puerto Rico, Mayagüez Campus (UPRM)** Mayagüez, Puerto Rico
B.Sc. in Biology. Transferred to UNAM.

Research Experience

- 2016 - Present • **Max Planck Institute for Biology of Ageing**
Department of Molecular Genetics of Ageing
Graduate Researcher - “Role of Mondo/Myc complexes in lifespan regulation”
Advisor: Prof. Adam Antebi
- 2012 - 2016 • **Institute of Cellular Physiology, UNAM**
Department of Molecular Genetics
Undergraduate Researcher - “Role of the mitochondrial protein Slm35 during aging and stress response in *Saccharomyces cerevisiae*”
Advisor: Dr. Soledad Funes
- 2015 • **Harvard T.H. Chan School of Public Health**
Department of Genetics and Complex Diseases
Intern Researcher - “Relationship between mitochondrial dynamics and electron transport chain-mediated longevity in *Caenorhabditis elegans*”
Advisor: Dr. William B. Mair
- 2012 • **Institute of Cellular Physiology, UNAM**
Department of Molecular Genetics
Undergraduate Researcher - “Study of physical interactions between FtsY and SecY in *Escherichia coli*”
Advisor: Dr. Soledad Funes

Publications

- 2021 • Schiffer I, Gerisch B, Kawamura K, **Laboy R**, Hewitt J, Denzel MS, Mori MA, Vanapalli S, Shen Y, Symmons O & Antebi A. miR-1 coordinately regulates lysosomal v-ATPase and biogenesis to impact proteotoxicity and muscle function during aging. *eLife*, 10:e66768.
- 2020 • Tharyan RG, Annibal A, Schiffer I, **Laboy R**, Atanassov I, Weber AL, Gerisch B & Antebi A. NFYB-1 regulates mitochondrial function and longevity via lysosomal prosaposin. *Nat Metab*, 2(5):387-96.
- 2017 • Weir HJ, Yao P, Huynh FK, Escoubas CC, Goncalves RL, Burkewitz K, **Laboy R**, Hirschey MD & Mair WB. Dietary Restriction and AMPK Increase Lifespan via Mitochondrial Network and Peroxisome Remodeling. *Cell Metab*, 26(6):884-96.
- 2016 • Aguilar-López JL, **Laboy R**, Jaimes-Miranda F, Garay E, DeLuna A & Funes S. Slm35 links mitochondrial stress response and longevity through TOR signaling pathway. *Aging (Albany NY)*, 8(12):10.18632/aging.101093.

Book Chapter

- 2015 • Jaimes-Miranda F, Aguilar-López JL, **Laboy R** & Funes S. The cell proposes, the mitochondria disposes: stress, longevity and cell death. In: Butanda Ochoa A *et al.* Mensaje Bioquímico, Vol. XLII, 205-22, Depto de Bioquímica, Facultad de Medicina, UNAM. Cd. Universitaria, Mexico City, Mexico. *ISSN-0188-127X*.

Honors and Awards

- 2016-2019 • Ph.D. Research Fellowship - Cologne Graduate School of Ageing Research
Max Planck Institute and University of Cologne Excellence Cluster on Stress Responses in Aging-Associated Diseases (CECAD)
- 2016 • Honorable Mention for Bachelor's Thesis Defense
- 2016 • Scholarship - Dirección General de Asuntos del Personal Académico (DGAPA), UNAM
- 2015 • Intern Fellowship - Summer Internships in Biological Sciences in Public Health, Harvard T.H. Chan School of Public Health
- 2015 • Scholarship - Fundación Miguel Alemán A. C.

Scientific Meetings

- Oral • XIX National Meeting of the Bioenergetics and Biomembranes branch of the Mexican Society of Biochemistry at Guanajuato, Mexico (Nov 2015)
- V Congress of the Reactive Oxygen Species in Biology and Medicine Branch of the Mexican Society of Biochemistry at Morelos, Mexico (Mar 2015)
- Poster • Advances in Metabolic Communication at Rio de Janeiro, Brazil (Oct 2019)
- Mitochondrial Biology, Keystone Symposia on Molecular and Cellular Biology at Kyoto, Japan (Apr 2018)

Standard and Specialized Techniques

- Molecular Biology and Biochemistry
 - Recombinant DNA technology, CRISPR/Cas9 technology, RNA extraction, RT-qPCR
 - OCR (Seahorse XF Analyzers)
 - Protein purification, immunoprecipitation, immunoblotting, Phostag SDS-PAGE
- Microscopy
 - Fluorescence and confocal microscopy
 - Immunofluorescence
- Model Organisms and Cell Culture
 - Yeast genetics
 - *C. elegans* husbandry, genetics and demographic analyses
 - Mammalian cell lines maintenance
- Software
 - Fiji
 - GraphPad Prism, Microsoft Office
 - Adobe Illustrator, Photoshop, and Lightroom

Conference and Event Organization

- Initiator and co-organizer of the “Max Planck Digest” lecture series (2019 - Present)
- Co-organizer of the 7th Graduate Symposium of the Cologne Graduate School of Ageing Research (Oct 2018)
- Volunteer for the Max Planck Day at the MPI for Biology of Ageing (Sep 2018)

Research-related Responsibilities and Membership

- Ad-hoc reviewing for FEBS Journal
- Member of the Genetics Society of America
- Supervision of Master Thesis (M. Vonolfen & M. Ndoci)

Workshops and Research Training

- Scientific and Grant Writing (Bioscript, Cologne)
- Statistical Literacy (Science Craft, Cologne)
- Poster Design and PowerPoint Presentation (Bioscript, Vienna/Cologne)
- Adobe Illustrator Advance Course (Amselrehhase, Cologne)

Languages

- Bilingual
 - Spanish
 - English